UCRL-53188-82
Distribution Category UC-70

UCRL--53188-82

DE83 017548

Nuclear Waste-Form Risk Assessment for U.S. Defense Waste at Savannah River Plant. Annual Report, FY 1982

H. Cheung

L. L. Edwards

T. F. Harvey

Manuscript date: August 9, 1982

LAWRENCE LIVERMORE LABORATORY
University of California • Livermore, California • 94550

Available from: National Technical Information Service • U.S. Department of Commerce
5285 Port Royal Road • Springfield, VA 22161 • $13.00 per copy • (Microfiche $4.50)

Contents

Abstract 1
1. Introduction 1
Background 1
Technical Approach 2
Technical Results and Conclusions 3
References 6
2. Technical Approach 8
Introduction 8
Probabilistic Systems Assessment of Deep Geologic Repositories 10
References 33
3. Analytical Results 35
Basecase Repository—Uneventful Layered Salt 35
Alternative Waste Forms 39
Release Rates and Uncertainties 53
Point-Source and Extended-Source Repository Models 56
Comparison of MISER and Other Models 65
Sensitivity and Uncertainty Analyses 68
References 87
4. Technical Conclusions 89
Appendix A. Radioactivity vs Time 91
Appendix B. Results of Analyses 97

Nuclear Waste-Form Risk Assessment for U.S. Defense Waste at Savannah River Plant Annual Report FY 1982

Abstract

A network model was developed to simulate the hydrological flow and the transport of radionuclides from a deep geological repository to the biosphere subsequent to closure. By means of very efficient computational methods for solving the fundamental differential equations, a code was developed to treat in great detail the effects of waste form characteristics and of repository designs on the repository risks. It is possible to examine near field effects heretofore not attempted. Without sacrificing the essential details of description, the code can also be applied to perform probabilistic risk analyses to high confidence levels. Analytical results showed:

1) For waste form release rates greater than approximately 5×10^{-7}/yr, dose to man is insensitive to release rate and release rate uncertainty
2) Significant reduction in dose can be achieved through simple design modifications
3) A basalt repository generally does not perform as well as a salt repository
4) Disruptive events are relatively unimportant for repository safety.

1. Introduction

Background

Significant quantities of high-level nuclear waste have been generated in defense programs at the Savannah River Plant (SRP). The waste has been stored in aboveground storage tanks and will be incorporated into a solid host form suitable for permanent disposal in a deep geologic repository. The Department of Energy (DOE) has been sponsoring research and development on borosilicate glass, the reference waste form for SRP waste, and on potential alternative hosts such as SYNROC, coated particles, and others. The possible geologic media in which to construct the final repository might be bedded salt, basalt, or tuff. The choice of a suitable combination of solid form and geologic medium depends, in part, on the resulting risk of exposure to present and future generations. Savannah River Laboratory has been supporting the present work at the Lawrence Livermore National Laboratory (LLNL) to perform an assessment of risk for the storage of borosilicate glass and alternative waste forms containing SRP waste in deep geologic repositories. This, the third annual report, presents a discourse of our work on probabilistic risk assessment (PRA) of geologic nuclear waste repositories. A portion of this work was presented in the second annual report.[1] An abbreviated version of the work on PRA was given in an interim report.[2] In this report we present not only a combined and detailed discourse of the material appearing in the prior reports, but also new work accomplished more recently.

To immobilize the nuclear high-level defense wastes (HLW) for permanent disposal in a Federal Repository, Savannah River is developing a nuclear Defense Waste Processing Facility (DWPF). Borosilicate glass is the reference waste form and a crystalline ceramic form, SYNROC, is the primary alternative for the immobilization of SRP waste in the DWPF. The objective of our work is to provide timely, state-of-the-art scientific information on long-term risks of disposing of defense HLW in solid waste forms in geologic repositories. Technical data to satisfy the National Environmental Policy Act (NEPA) needs for an evaluation of the waste form alternatives require development of a model which predicts not only individual dose at the "accessible environment" but also population dose associated with an extensive water use system.

A final EIS has been published for the DWPF.[3] However, the final choice of the DWPF waste form was left open. To support the choice of a waste form for the DWPF, a technical data base of risks and costs of viable alternatives is needed. This document provides a risk assessment for the leading DWPF waste form, borosilicate glass, and for a waste form defined to have a lower release rate of radionuclides in layered salt and basalt.

Recently the regulatory and adjudication guidance on what constitutes an acceptable risk assessment procedure has tended toward the probabilistic approach. LLNL has developed substantial expertise in applying probabilistic risk analysis to nuclear waste disposal. We have compiled extensive probabilistic data bases for different media during the past five years. These data bases provide the means to predict realistically the biological impact of high-level nuclear waste disposal in various geological media, including bedded-salt and basalt. A number of studies using this expertise and data base, including sensitivity and uncertainty analyses on risks associated with high-level commercial wastes and spent fuel, have been made for both the DOE and the Nuclear Regulatory Commission (NRC).[4-8]

To satisfy NEPA requirements as currently perceived, we have chosen to provide state-of-the-art information as consistent as possible with existing national standards. The main standards guiding us in the development of our numerical results were the Nuclear Regulatory Commission's 10CFR20, 10CFR50, and draft 10CFR60, and the Environmental Protection Agency's draft 40CFR191.

Technical Approach

The most probable process for release of significant quantities of radionuclides to the human environment from a closed, deep geologic nuclear repository is leach of the waste form and ground water transport.[9] The process involves a scenario which allows ground water to contact the waste, leach the radionuclides, and transport them to the human environment. To provide a scientific analysis, we must deal not only with the complexity of the phenomena, but also with uncertainties inherent in the processes and in extrapolation of data over extended periods. Although it may introduce additional uncertainties, computer modeling is a necessary means to quantitatively forecast the behavior of radionuclides in repositories. At the outset of the program, we reviewed the available computer models. They range in degree of complexity from simple one-dimensional, single flow-path models to those involving highly detailed, three-dimensional, finite-difference and finite-element representations.*[10-22]

Because of convenience and availability, we initially selected the MACRO[23] codes developed at LLNL. These codes are based on the concept of a general model-management tool that systematically samples finite-probability representations of parameters to propagate uncertainty to the final results. The initial version, MACRO1, did not readily allow physical constraints and correlations, while the language features of its successor were much more general than we required. Further, its usage of conditional probability arrays in some cases of highly constrained and correlated systems could lead to an inordinate number of computations.

Recognizing the need for a physically consistent yet versatile model, we have developed the MISER code. It was written to efficiently study the effects of repository system design in a probabilistic framework in both the near-field and far-field. MISER is written in a modular fashion to allow rapid implementation of new or improved models. It is user-oriented, and extensive graphical output is generated. MISER computes dose to man at risk-sensitive observation points. Monte Carlo techniques are applied, where appropriate, to account for parameter uncertainties and correlations.

The MISER Model

The MISER model can be conceived of as a combination of four numerical submodels:

Waste Package Model. This model describes the radionuclides originally in the canister and their release as a function of time to the surrounding excavation. The original amount of radionuclides in a canister, a nonstochastic (certain) quantity in this analysis, is used to calculate the set of radionuclides as a function of time in the system. Thus, the total amount of radioactivity in the total system is certain. Its spacial distribution as a function of time is uncertain, however. Conservative assumptions were made in deriving a waste form release rate for the basecase analysis.

*No single, detailed code exists which couples all hydrological, chemical, transport, canister stress, corrosion, and other phenomena using either finite-difference or finite-element methodology.

Hydrology Model. This model consists of a defined network and parameters that describe the flow paths, the locations of the source canisters, and the locations of the monitor points. Under simplifying assumptions, we solve the steady state hydrology using D'Arcy's law and the conservation of water.

Transport Model. This computes the radionuclides transported as a function of time and position. Thousands of radionuclide flux pulses can be transported. These are accumulated over time and then converted to dose.

Biological Impact Models. To provide a spectrum of results compatible with today's regulations we emphasize two sets of results: an individual drinking from a well at the edge of the "accessible environment," which we call the Accessible-Environment-Individual (AEI) model, and a population dose model for the current Columbia River water-use system, the Columbia River population (CRP) model.

Monte Carlo Treatment. Our reported results of Monte Carlo uncertainty analyses are based on 100 random trials. To ensure that the results are relatively independent of the procedure we have compared results from 5 independent runs with 100 trials each, with 200 trials, and with 500 trials. In general we found that results agree within one or two bins of the discretized output space. That is, we believe 100 trials per computation give an adequate level of accuracy.

Correlations and Constraints. Although the physics does not dictate correlations and/or constraints on certain of the physical parameters, the measured data often show these properties. For example, measurements of permeability and effective porosity tend to show a strong relationship.[24] Or, the retardation factors of the actinides are typically greater than those of the fission products.[25]

Further, the selection of a layered medium model network is based on levels of different permeabilities. To ensure that the random selection of parameters reflects the proper ordering (e.g., aquifer permeability greater than that of an aquitard), we incorporate correlations by using a pairwise correlated selection procedure for normal and log-normal distributions.

Technical Results and Conclusions

Our approach is to focus on a "basecase" scenario, the uneventful (normal) bedded-salt scenario with a waste form which conservatively simulates the release from borosilicate glass, the reference waste form for the DWPF. We refer to this as the REFERENCE waste form. No credit is taken for chemical interactions with other parts of the engineered system and the geologic media, or for limited solubility of some waste elements. The basecase doses are compared with other doses from representative scenarios, including disruptive events, different waste package release rates, and different geologic media.

In general, we found median dose rates ("best-estimates") far below natural background radiation levels for individual doses and nearly trivial results for integrated population doses. The reduction of these small doses by using a lower waste package release rate, the ALTERNATIVE waste form, instead of the REFERENCE waste form is consequently small, even though the reduction factor at times was greater than an order of magnitude. Where the doses were large in the probabilistic analysis (i.e., at high confidence levels), the effect on dose of improving the waste form was small. This indicates that there are other mitigating factors which vitiate the influence of release rates when doses are high. Thus, where one would hope to gain the most from a better waste form, there seems to be little dependence on waste form durability.

Basecase

The generic layered-salt repository model includes general features of sedimentary basins containing bedded salt. It does not represent any particular basin. It is intended as a model with properties characteristic of a real basin which has had a moderate amount of exploration.

For the basecase individual dose we find:

- For the layered salt repository with REFERENCE waste form, our best-estimate of peak dose rate to an individual using a well located one mile downstream from a repository (i.e., the AEI dose) is about three orders of magnitude below the dose he would receive from background radiation. If the confidence level of the calculation is increased from 50 to 90%, then the AEI peak dose increases to 10 mrem/yr, still an order of magnitude below background. If, however, the individual is part of the Columbia River water-use system with an average diet of only contaminated food, he will receive approximately one ten-millionth of background radiation.
- Improving the waste form by changing to ALTERNATIVE reduces the peak dose obtained from a well one mile downstream over a factor of 10 for doses below the 70% confidence level.

Above the 90% confidence level, however, there is little or no improvement.

For the basecase population dose:

- Integrated population dose over the first million years results in only a 200 person-rem total dose, less than one tenth of the dose considered to lead to a single additional premature cancer for the 50% confidence level estimate. Increasing the confidence level from 50 to 90% increases the integrated population dose to 2000 person-rem.
- Improving the waste form by changing to ALTERNATIVE reduces by 190 person-rem in one million years the best-estimate integrated population dose calculated using REFERENCE.

Alternative Site

Another leading candidate medium for a defense waste repository is basalt. The basalt model is intended to include general features of flood basalt basins. It is not a simulation of any particular site, but has characteristics similar to those of a real site with moderate exploration.

- The basalt repository yields higher doses (by approximately a factor of 5–50) than the layered-salt repository for the integrated population dose and the peak individual dose one mile downstream. It was a better performer by about a factor of 10,000 than the layered-salt repository for the individual with his well above the repository, the limiting individual (LI) case, since more waste could migrate through the rock barriers in basalt, instead of up the well just downstream of the shafts. Including the bypass in the design reduced the well-above-repository dose to zero.
- Improving the waste form by changing to ALTERNATIVE reduces the basalt repository dose one mile from the repository by 1 mrem/yr and the integrated population dose by 50 person-rem.

Design Alternative

In cases where the waste form is assumed to dissolve fairly rapidly, repository design features could have a strong effect on near-field doses.[26] To analyze the possible effects of repository design on predicted doses, we have calculated the doses from a salt repository with an engineered hydraulic bypass which would provide a path beneath the repository, which is more permeable to the flow of ground water than the backfilled repository itself.

We found:

- The BYPASS increases containment time of the initial pulse from 7000 to about one million years when all parameters have median values. Also, using a full uncertainty study, at the 90% confidence level the BYPASS reduces the AEI dose by a factor of fifty.
- Using the improved waste form, ALTERNATIVE, does not improve the performance of the repository with BYPASS at the 50% confidence level. At the 90% confidence level it improves performance by 0.2 mrem/yr for AEI and 18 person-rem for integrated population dose.

Disruptive Events

To determine the magnitude of the hazard if future disruptive events occur, we have looked at events that are both sufficiently probable and also likely to lead to high doses. The risk from all the important scenarios can be incorporated into a single curve which provides a single probabilistic measure of performance.

Incorporating possible flaws or disruptive events into the analysis changed the best estimates of the peak individual dose rate by about a factor of three. This is a small change compared with the dose increase of a factor of 100 between the 50 and 90% confidence levels. This result implies that the major risk sensitivities in a permeable layered-salt system are due to the inability to measure and predict the geohydrologic processes of a given scenario, and not to the effects of disruptive events.

Alternative Criteria

No definitive standard criteria exist with which forecasts of the radiological consequences of high-level waste disposal can be unequivocally compared. For individual dose there are several locations in our model where forecasting the dose seems reasonable. We chose three different locations. The first dose is from a well just downstream from the shafts (LI); the second is a well one mile from the repository edge (AEI); and the third is an average individual who lives in the Columbia River water-use system (CRI). The calculated level of dose is several orders of magnitude between an individual who drinks water from a well located one mile downstream and an individual who obtains his water and food from the Columbia River water-use system. For comparison, the difference in dose between different waste forms is typically below a factor of 10. Our results indicate that great care should be taken in choosing the location at which the repository risks are to be measured, calculated, or regulated.

Waste Form Release Rate

Waste form release rates and their uncertainties (as represented by the median and geometric standard deviation of a lognormal distribution) are important parameters for the purpose of this report. We studied the effects of release rates and their uncertainties to see how improvements in waste form technology affect repository safety.

- The low-dose ends of the dose vs release rate curves are sensitive to both release rate and release rate uncertainty, but the high release rate ends of these curves (for 90% confidence levels) are insensitive to release rate and release rate uncertainty. This is true for release rates greater than approximately 5×10^{-7}/yr.
- The choice of waste form should be insensitive to uncertainty of waste form release rate. Where the doses are sensitive to uncertainty, the doses are orders of magnitude below background. Where the doses are significant fractions of background, they are insensitive to uncertainty.

Point-Source and Extended-Source Repository Models

We analyzed different point-source repository models to establish how the assumptions invoked in this commonly used model affect prediction of individual dose. Our results show that the assumptions in a point-source model are quite arbitrary and can lead to poor or misleading predictions of near-field individual doses. Also, predictions from point-source models of curies released to the near field must be considered very questionable. To adequately predict repository releases in the local vicinity will require more sophisticated models of the repository than point-source models.

We also compared the point-source model with extended-source models. We showed that the dose difference between a conservative point-source model and a detailed 1000-canister model is about two orders of magnitude. Besides these differences, the predicted radionuclide causing the peak dose is also different.

Sensitivity and Uncertainty Analyses

Using the 89-pathway network of the basecase salt repository, we studied the sensitivity of dose to both hydraulic gradient and to some numerical modeling choices. Over horizontal gradients from 10^{-6} and 10^{-2} m/m, both the LI and the AEI doses generally decrease linearly with horizontal gradient. The CRI dose, on the other hand, showed insensitivity over a wide range of the horizontal gradient. Over the range of 10^{-3} to 10^{-1} m/m, the impact of vertical hydraulic gradient is not nearly as important as horizontal gradient. Other sensitivity analyses were carried out to ensure that our results were not biased by the number of canisters used to represent the repository or by the assumed shape of the release pulse.

Calculated repository performance is sensitive to input and intermediate parameter values. Because of parameter uncertainties our input and results are represented by lognormal and lognormal-like distributions, respectively. To help to understand model sensitivities, we calculated the correlation of the logorithms of selected input and intermediate parameters with dose rates. The most significant correlations are the Group I dose rate, the peak dose rate time-of-arrival, and the Group II dose rate.

To establish the approximate precision of our results, we ran our basecase for five 100-trial runs. By combining results we obtained a 500-trial case. We found that mean values for the 100-trial cases fell within 10% of the 500-trial case. These calculations also allowed us to test the procedure of extrapolation to higher confidence levels by using a lognormal distribution. The results of extrapolation to 99% confidence level showed that such a procedure may be unrealistically conservative.

Comparison Study

As a step towards model verification we reviewed the current literature. In addition, we computed the release of ^{240}Pu and ^{236}U from a simple network, point-source repository as reported by Sandia.[18] We found excellent agreement between our MISER model and the Network Flow and Transport (NWFT) model. Sandia reported excellent agreement between the NWFT network model and the three-dimensional finite-difference model SWIFT; therefore, we may conclude that the MISER model also agrees with that finite-difference model.

Additional Comments

The results presented have been taken out of the context of the main body of this work. To provide proper perspective, two important points must be made.

The first point is that we have made many conservative assumptions in the analysis which bias our dose frequency distributions toward high doses. Two examples of important conservative assumptions follow.

The first example is our use of a convective flow model in layered salt. It is possible, in a well-chosen site, that convective flow in salt is zero.

Thus, under nonflawed conditions the transport of radionuclides to the human environment would require either a disruptive event or a Brownian diffusion. If a disruptive event occurs, then the doses obtained are similar to those obtained in convective flow calculations; however, in a probabilistic analysis, the probability of the disruptive event must be folded into the calculation. This leads to a smaller risk than predicted by the convective flow probabilistic risk calculation. If no disruptive event occurs, then calculations show very low peak dose rates. Thus, the convective flow method, with appropriately low permeabilities, will either be valid or lead to conservative results.[27]

The second example of an important modeling conservatism is that the release rate was calculated from leach rate obtained in laboratory experiments over short durations with high oxygen content in the water. Because the oxygen content in ground water is usually low, leading to much lower release rates, and because release rates for many radionuclides would likely be constrained by solubility limits, the release rates used in this analysis are believed to be upper bounds.

Many other important conservative assumptions have been made which are appropriately addressed in the main body of the text. Although it is impossible to quantify their effects on the final results, taken together they significantly raise our confidence that the systems studied are safe.

The second point is that the conclusions on the comparison of waste forms in this report do not necessarily scale to commercial waste repository size. The larger amounts of radioactivity in a full-scale, licensed HLW repository could lead to peak AEI doses which may be larger fractions of background radiation levels. Lower waste package release rates, under such circumstances, might have a greater effect in reducing the peak dose rates for the commercial repository. Alternatively the higher doses could be lowered as greater understanding of repository site, engineered barrier performance, and leaching phenomena allow some relaxation of the conservative assumptions used in this study.

Calculations for a larger HLW repository are recommended to assess what the effects of a high waste inventory distributed over a much larger repository area would be on the AEI dose. The effects on the population dose and dose to the average individual in the CRP system are expected to be unimportant because they are several orders of magnitude below background levels.

References

1. H. Cheung, L. L. Edwards, T. F. Harvey, D. D. Jackson, and M. A. Revelli, *Nuclear Waste-Form Risk Assessment for U.S. Defense Waste at Savannah River Plant: Annual Report FY 1981*, Lawrence Livermore National Laboratory, Livermore, Calif., UCRL-53188-81 (1981).
2. H. Cheung, L. Edwards, T. Harvey, and M. Revelli, *Postclosure Risks of Alternative SRP Nuclear Waste Forms in Geologic Repositories*, Lawrence Livermore National Laboratory, Livermore, Calif., UCRL-53269 (1982).
3. *Environmental Assessment of Waste Form Selection for SRP High-Level Waste*, compiled by W. G. Holmes, E. I. Dupont de Nemours & Co., Savannah River Laboratory (1982).
4. J. J. Cohen, et al., *Determination of Performance Criteria for High-Level Solidified Nuclear Waste*, Lawrence Livermore National Laboratory, Livermore, Calif., for U.S. Nuclear Regulatory Commission, NUREG-0279 (1977).
5. R. A. Heckman and T. Holdsworth, *A Probabilistic Safety Analysis for Solidified High-Level Nuclear Waste Management Systems: A Status Report*, Lawrence Livermore National Laboratory, Livermore, Calif., for U.S. Nuclear Regulatory Commission, NUREG/CR-0577 (1979).
6. R. A. Heckman, D. F. Towse, D. Isherwood, T. Harvey, and T. Holdsworth, *High-Level Waste Repository Site Suitability Study—Status Report*, Lawrence Livermore National Laboratory, Livermore, Calif., for U.S. Nuclear Regulatory Commission, NUREG/CR-0578 (1979).
7. W. G. Sutcliffe, K. G. Feller, N. K. Madsen, and G. D. Pollak, *Uncertainties and Sensitivities in the Performance of Geologic Nuclear Waste Isolation Systems*, Volumes I and II, Lawrence Livermore National Laboratory, Livermore, Calif., UCRL-53142 (1981), ONWI-352.

8. W. G. Sutcliffe, "Nuclear Waste Storage: Evaluating the Uncertainties," *Energy and Technology Review*, Lawrence Livermore National Laboratory, Livermore, Calif., May 1982.
9. "Report to the President," Interagency Review Group on Nuclear Waste Management, 1978, Washington, D. C. (1979).
10. B. I. Ross, et al., *NUTRAN: A Computer Model of Long-Term Hazards from Waste Repositories*, The Analytical Sciences Corporation, Reading, Mass. (1979).
11. W. V. De Mier, M. W. Cloninger, H. C. Burkholder, and P. S. Liddall, *GETOUT--A Computer Program for Predicting Radionuclide Decay Chain Transport Through Geologic Media*, Battelle Pacific Northwest Laboratory, Richland, Wash., PNL-2970 (1979).
12. B. J. Wood, "The Use of Simple Transport Equations to Estimate Waste Package Performance Requirements," *Waste Management '81*, American Nuclear Society, R. G. Post, Ed., vol. 2, pp. 911–947, 1981.
13. M. D. Hill and P. D. Grimwood, *Preliminary Assessment of the Radiological Protection Aspects of Disposal of High-Level Waste in Geologic Formations*, NRPD-469 (1978).
14. M. D. Hill, "The Effect of Variations in Parameter Values on the Predicted Radiological Consequences of Geologic Disposal of High-Level Waste," *Scientific Basis for Nuclear Waste Management*, vol. 2, p. 753, 1980.
15. M. O. Cloninger, C. R. Cole, and J. F. Washburn, *An Analysis of the Use of Engineered Barriers for Geologic Isolation of Spent Fuel in a Reference Salt Site Repository*, Battelle Pacific Northwest Laboratory, Richland, Wash., PNL-3356 (1980).
16. G. S. Barney and B. J. Wood, *Identification of Key Radionuclides in a Nuclear Waste Repository in Basalt*, Rockwell Hanford Operations, Richland, Wash., RHO-BWT-ST-9 (1980).
17. J. R. Raymond, F. W. Bond, C. R. Cole, R. W Nelson, A. E. Reisenauer, J. F. Washburn, N. A. Norman, P. A. Mote, and G. Segal, *Test Case Release Consequences Analysis for a Spent Fuel Repository in Bedded Salt*, Battelle Pacific Northwest Laboratory, Richland, Wash., PNL-2782 (1980).
18. J. E. Campbell et al., *Risk Methodology for Geologic Disposal of Radioactive Waste: The Network Flow and Transport (NWFT) Model*, Sandia National Laboratory, Albuquerque, New Mex., NUREG/CR-1190, SAND-79-1920, (1980).
19. A. M. Kaufman, L. L. Edwards, and W. J. O'Connell, "A Repository Post Sealing Risk Analysis Using MACRO," *Proceedings of the Waste Management Symposium, Tucson, Arizona, 1980* (The University of Arizona, College of Engineering, Tucson, Ariz., 1980), p. 109.
20. F. R. Kovar and T. L. Steinborn, *The Bedded Salt Report: A Compendium of Technical Issues and Analyses Pertaining to Siting of a Nuclear Waste Repository*, Lawrence Livermore National Laboratory, Livermore, Calif., NUREG/CR-1525, UCRL-52737 (1980).
21. T. G. Naymik, and L. D. Thorson, *Numerical Simulation of Transport in a Regional Groundwater Flow System*, Lawrence Livermore National Laboratory, Livermore, Calif., UCRL-52556 (1978).
22. R. T. Dillon, R. D. Lantz, and F. B. Pahwa, *Risk Methodology for Geologic Disposal of Radioactive Waste: The Sandia Waste Isolation Flow and Transport (SWIFT) Model*, Sandia Laboratories, Albuquerque, N. Mex., SAND 78-1267 (NUREG/CR-0424) (1978).
23. L. L. Edwards, *MACRO1: A Code to Test A Methodology for Analyzing Nuclear Waste Management Systems*, Lawrence Livermore National Laboratory, Livermore, Calif., UCRL-52736 (1979).
24. *Second Report: Development of Site Suitability Criteria for the High Level Waste Repository* for Lawrence Livermore National Laboratory, Golder Associates, Kirkland, Wash. (1977).
25. D. Isherwood, *Geoscience Data Base Handbook for Modeling a Nuclear Waste Repository*, Vol. 1, Lawrence Livermore National Laboratory, Livermore, Calif., UCRL-52719 (1980).
26. L. L. Edwards and T. F. Harvey, *A High-Level Waste-Repository Excavation Model and Limiting Individual Dose*, Lawrence Livermore National Laboratory, Livermore, Calif., UCRL-86849 (1981).
27. I. Remson, S. J. Dreiss, and A. G. Journel, "Radioactive-Waste Disposal—An Application of Predictive Geology," in *Predictive Geology with Emphasis on Nuclear Waste Disposal*, C. De Marsily and D. F. Merriam, Eds. (Pergamon Press, NY, 1982) pp. 25–32.

2. Technical Approach

Introduction

The most probable mechanism for release of significant quantities of radionuclides to the biosphere from a closed deep geologic nuclear repository is groundwater transport. The process involves events that allow groundwater to contact the waste, leach the radionuclides, and, subsequently, transport them to the biosphere.

Predicting doses to individuals who live near a nuclear waste repository requires careful modeling of the repository excavation, its backfill, and its effects on surrounding hydrologic conditions. The availability of waste to individuals always starts with a radionuclide release from one of many spatially separated canisters in a repository. The transport of waste from each canister to an individual can occur by many pathways. If an observer were able to follow the migration of the many waste pulses, he would see a system of pulses moving through various pathways at different times and, finally, arriving at the biosphere release point.

"To provide decision makers with technically complete information, evaluating the hazards associated with the disposal of high level radioactive wastes in deep geologic strata demands that we acknowledge the uncertainties implicit in our predictions. These uncertainties by no means invalidate the findings of waste-disposal studies, but only by properly accounting for the uncertainties can we assure that conclusions and forecasts will stand up to criticism."[1]

Not only are we faced with those uncertainties inherent in predicting the future and those associated with measurements of the present, but with the complexity of radionuclide transport in geologic media over long periods of time (at least 10^6 years). This complexity is such that simulation of the processes by computer modeling seems to be the most desirable means of analysis. However, mathematical computer models are still another source of uncertainty. How well do they actually model the processes? Answers to such questions are ascertained by exercising and validating the models.

The highly detailed, time-dependent, three-dimensional computer code required to properly couple all the processes—e.g., hydrology, meteorological recharge, heat conduction, waste-canister stress and corrosion, waste-package leaching, water chemistry, repository refill and repressurization, nuclide transport, sorption, etc.—is not only complex, but will be too costly to run for very many simulations. Furthermore, in some cases (e.g., leaching or sorption), the processes may not be understood well enough to warrant detailed models.

The development of a performance-assessment technology should occur in three stages:

1. The development of individual models.
2. The development of coupled models.
3. The integration of coupled models into a modeling system.

The U.S. Geological Survey recently proposed a policy of model development.

> "The procedure for developing and verifying individual models includes: (1) collecting laboratory and field observations of physical phenomena; (2) developing an empirical or theoretical working hypothesis; and (3) testing and verifying the working hypothesis. Details of the verification process vary greatly depending on the subject matter of the model. Far-field scenario analysis involves natural phenomena over long time periods; because such models are impossible to verify by direct observation, general agreement by peer review is necessary. In contrast, some models that are part of the near-field scenario analysis and the near-field consequence analysis can be verified by appropriate *in situ* tests. These tests may demonstrate the need for model modification and further observations of the physical system under different conditions from those used for model development.
>
> "The process of observation and model modification to predict these observations will continue until a reasonable demonstration that predictions and observations are in agreement has been achieved. Peer review of the various steps used in model verification, from the basic physics used in model formulation to the comparison of predicted and measured test results, should lead to model acceptance. In a few cases, it will be possible to verify radionuclide trans-

port models by comparison of simulated results with field data from natural ore bodies.

"The general procedure for developing and verifying coupled models follows a similar process. However, the verification of the coupled models is more difficult because conducting the tests and interpreting the experimental results are more difficult.

"The integration of the coupled models into a modeling system involves the development of an "executive" model which manages the interactions of the coupled models. The isolation system performance model cannot be verified because system behavior cannot be observed or tested over the time period of interest; however, data collected during the period of repository operation (approximately 40 years) will provide verification for much of the near-field analysis system."[2]

We recognize that such a computer model is highly desirable (perhaps necessary) to do best-estimate simulations of "real-world" measurements. However, we can obtain a great deal of understanding about bounding calculations, uncertainty, and sensitivity by using simpler models.[3-6] While these simpler models may be only qualitatively correct, relative measures of risk may be readily ascertained.

Our task is to investigate the post-closure consequences associated with emplacement of solidified forms of nuclear waste in mined geologic repositories. Realism requires judicious choice not only of the processes, but also of the level of detail of their description to be incorporated in the model. Selection of the processes strongly depends on the results required. The results required, in turn, are matters of national policy. In this work we have tried to bridge the scientific and policy needs by incorporating the processes necessary to obtain required, but conservative forecasts.

Figure 2-1 shows the many subsystems that contribute to post-closure performance. Individually, these subsystems can be modeled at several levels of detail (i.e., from detailed codes that reproduce experimental data to codes that model

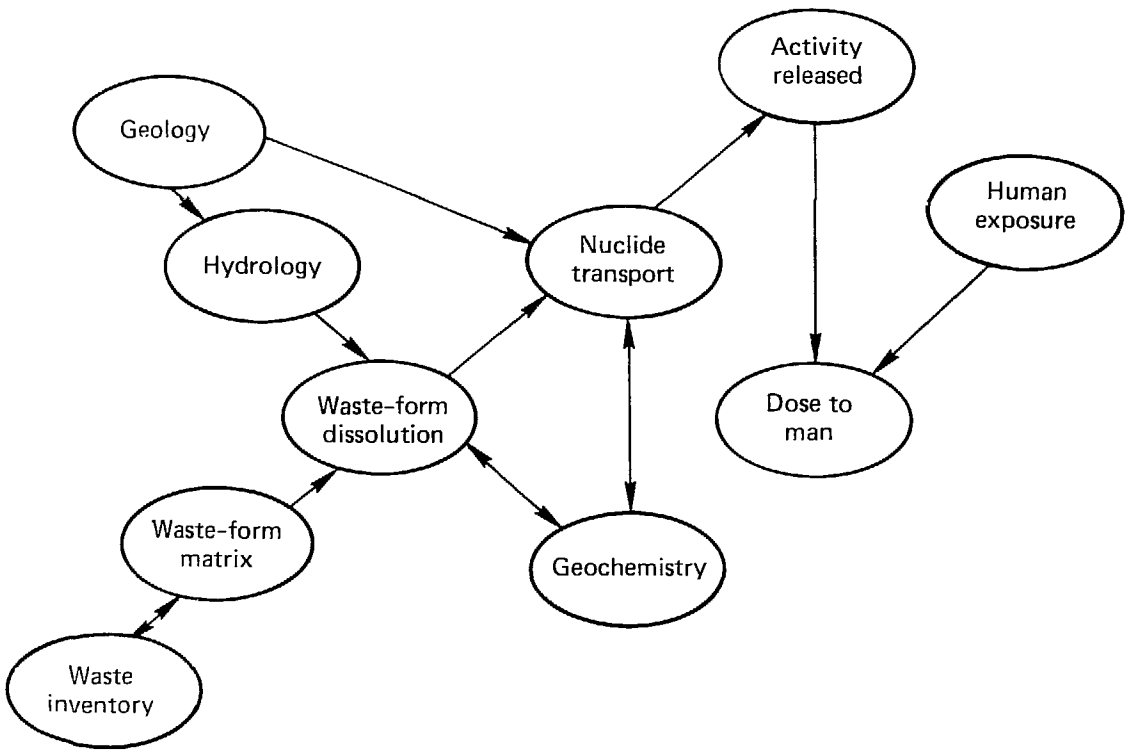

Figure 2-1. Elements that contribute to overall systems performance.

only dominant subsystem features). Each approach has relative merits for particular applications, and each should be pursued to ensure that the resulting analyses are, ultimately, in agreement.

The three-part LLNL approach has been: (1) to separate the system into physically distinct subsystems—waste-form package, repository site, regional aquifer, etc., (2) to identify and model the key features within each subsystem, and (3) to combine this understanding into an overall systems-level model to evaluate the performance of alternate waste forms in terms of radiological risk to man. The focus of the task was to calculate and assess the sensitivity of results to both individual input parameters and their uncertainties and then to quantify the resulting uncertainty associated with the consequences.

We have developed in the MISER[7] code a model that is versatile and physically consistent while providing needed results. It has been written to provide a computationally efficient means to study the effects of repository design features in a probabilistic framework in both the near field and far field. MISER is written in a modular fashion to allow rapid implementation of new or improved models. It is user-oriented and implements extensive graphical output. MISER solves a set of equations describing a network of 1-D streamtube pathways resulting in a consistent 3-D steady-state hydrology, traces "tree branches" of nuclide transport from numerous sources using a propagator approach, and computes dosage to man at risk-sensitive observation points. Monte Carlo techniques are applied, where appropriate, to account for parameter uncertainties and correlations. (See the subsection "Basecase Repository—Uneventful Layered Salt" for an illustrated discussion of results from a Monte Carlo calculation.)

Probabilistic Systems Assessment of Deep Geologic Repositories

This section begins with a general description of the physical scenario we are studying. Subsequently, we describe the MISER model in detail.

General Physical Scenario

Figure 2-2 is a side view of the general scenario we are studying. It does not depict a specific site, but represents a reasonable model with characteristic features of real basins. Before the underground facility is built, the regional pressure gradient has a hydraulic gradient from left to right and from bottom to top. The arrows approximate the directions of flow and water flows into the lower aquifer from the left. Some of this water migrates upward into the lower aquitard and traverses it* finally merging with water in the upper aquifer.

Excavation causes local perturbations to the regional flow-field, and the hydraulic pressure field around the excavation evolves from one associated with the undisturbed system to a new one consistent with the excavation features. Depending on the permeability and area of the tunnel, for example, more or less of the water will move along the tunnel and up the shaft. Thus, although the boundary conditions for the system remain essentially the same, local flow conditions in the repository can vary greatly because of mine design. Maximum deviations from the virginal flow conditions will occur when the repository storage area, tunnel, and shaft are highly permeable compared to the aquitard. This could be the case if the repository backfill is deteriorated or if large fracture zones are caused by excavation of drifts.

As indicated in Table 2-1, which gives the repository and media parameters at 1000 yr, the aquifers are considered to be sandstone with a typical sandstone permeability and effective porosity.[8] We have assumed that the deteriorated backfill will have the same permeability as the aquifers, but that its effective porosity will be an order of magnitude smaller. The effect is high volumetric flow rates and flow speeds for water in the tunnel and shaft.

*There are four concerns that cause us to use the more conservative convective flow calculation in layered salt. First, layered salt has layered interbeds of clay and shale. Second, laboratory measurements of layered salt permeability tend to have a measurable permeability at the beginning of the experiments. These permeabilities tend to become smaller as the experiments progress, until some lower bound of experimentally determined permeability is reached. We feel that this lower-bound is a conservative value appropriate for risk analysis. If the permeability of salt is experimentally pushed to substantially lower values, the diffusion-dominated model will become more appropriate. Third, every major site repository program has been surprised by unexpected water flows. Asse, WIPP, and Salt Vault have all suffered from unexpected water problems. There appears to be a very low probability of obtaining a truly "dry" salt repository site. Finally, undetected flaws or future disruptive events, which could lead to leaching and dispersal of radioactivity to the human environment appear to be conservatively approximated by a probabilistic calculation using a convective-flow model.

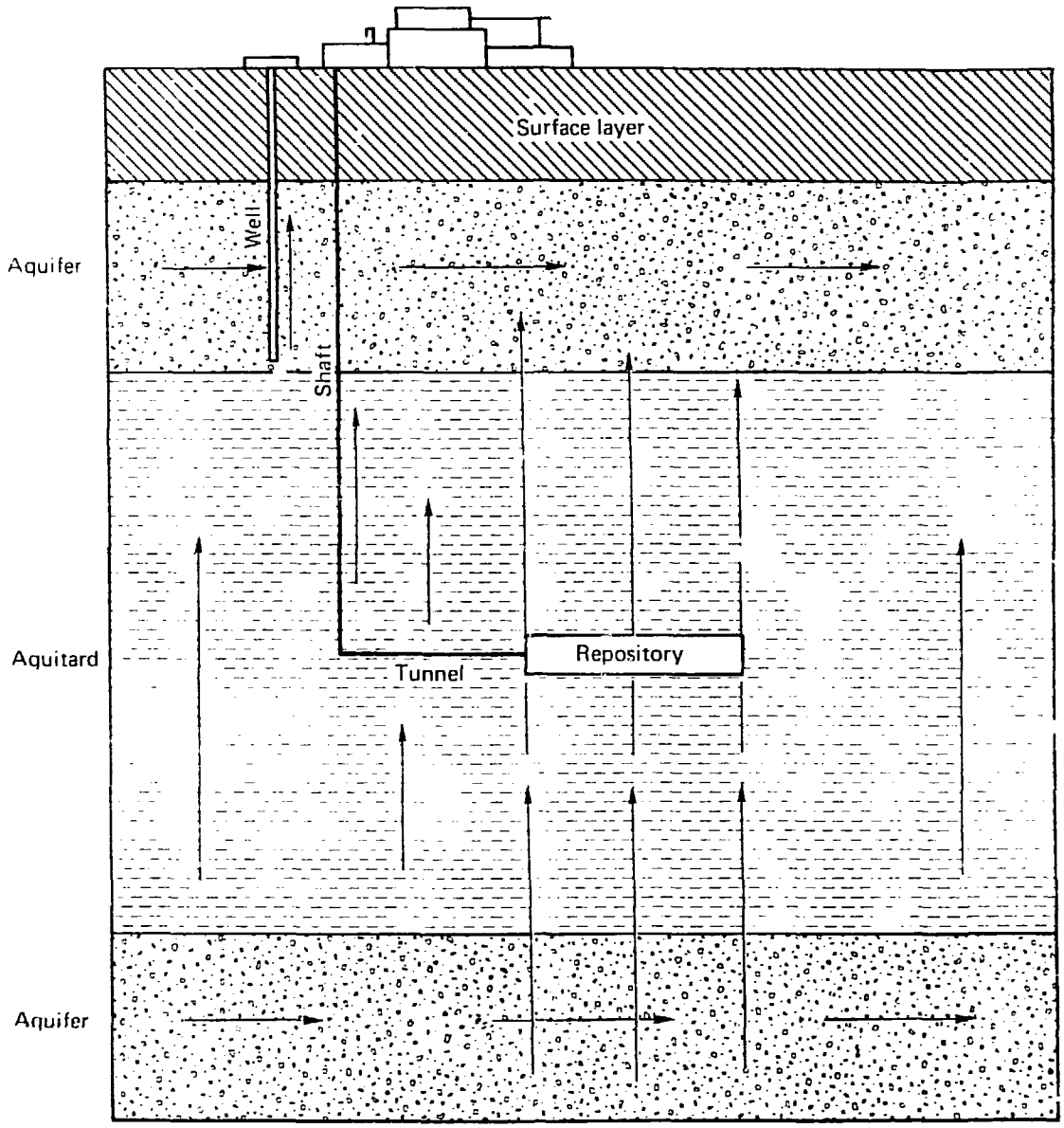

Figure 2-2. Side view of near-field features of high-level waste-repository excavation model (arrows approximate directions of flow).

Table 2-1. Hydrologic parameters – unflawed bedded salt.

	Permeability		Porosity	
	μ (cm/s)	σ	μ	σ
Sandstone/aquifer	6.3×10^{-4}	2.5	0.1	2.5
Shale/aquitard	10^{-7}	5.62	0.05	2.37
Salt/aquiclude	10^{-10}	10.0	0.01	3.16
Fracture zone/tunnels/shafts	10^{-6}	3.87	0.001	2.0

	μ	σ
Vertical gradient	0.01 m/m	2.0
Horizontal gradient	0.001 m/m	2.0
Dispersivity	50 m	2.5
Horz. perm. of salt (between storage rooms)	2×10^{-8} cm/s	10.0

	Group I		Group II		Group III	
	μ	σ	μ	σ	μ	σ
Retardation factor (along aquifer only)	1.	0.	10^2	3.87	10^4	3.87

Figure 2-3 illustrates the qualitative features of a MISER hydrology model. The repository model has both a main (operation) shaft and an air ventilation shaft upstream of the storage area. The storage area is modeled with 25 flow cells. The model is symmetric around the centerline location of the shafts and the main tunnel. The horizontal boundary conditions for the basecase scenario are head gradients that cause a regional flow from left to right, parallel to the tunnel.

To display the typical flow cell (shown by the cutaway in Fig. 2-3 and located near its geometric center), we have depicted the upper aquitard as being transparent.* The typical flow cell is shown to run from the top of the lower aquifer through the repository storage area to the bottom of the upper aquifer. The hatched strata are the upper and lower aquifers, and shaded areas 1, 2, and 3 are, respectively, the bottom of the lower aquitard, the top of the storage area, and the top of the upper aquitard.

For the typical cell, uncontaminated water flows from the left side of Fig. 2-3 through the lower aquifer to the cell. It is pushed by the vertical head gradient through Area 1 and up into the lower aquitard. Then it moves through the lower aquitard into the repository storage area where—if the canister has been breached—the leaching waste mixes with the passing water. The contaminated water is then split into three flow paths that move along orthogonal flow directions. The amount of water diverted into each flow path depends on the calculated pressure gradients in the repository. Part of the contaminated water moves parallel to the tunnel into the adjacent downstream flow cell. Another part moves toward the tunnel. Most of the water, however, moves into the upper aquitard barrier where, because of the barrier's permeability, the flow is very slow.

The hydrology scenario is a hypothetical, representative basin[9] with an excavation design[10,11] shown in Fig. 2-4. The numerical model includes a network of pathways defined by flow, parameters that define the flow paths, locations of the source canisters, and location of monitoring points. In the storage area, there are assumed to be 6500† canis-

*Figure 2-3 shows a 25-cell numerical model of the storage area. Where it can be shown numerically that the number of cells can be reduced, we actually run with fewer cells to lower computer costs. In our analysis in this report we have used a nine-cell model of the storage area. There are six (three when symmetry is employed) cells representing the waste storage rooms and three cells for the tunnels. Each cell has the equivalent of (1.08×10^3 canisters) worth of waste. We have numerically found that this number of canisters per cell can be represented by five numerical canisters spacially distributed throughout a waste-storage-room cell.

†Due to changes in waste immobilization plans at SRP, more or less than 6500 canisters may be emplaced in the repository. However, as long as the total amount of waste remains the same, doses are insensitive to the exact number of canisters.[12] For example, five canisters/cell for three cells produces essentially the same (slightly conservative) result as does 25 canisters/cell.

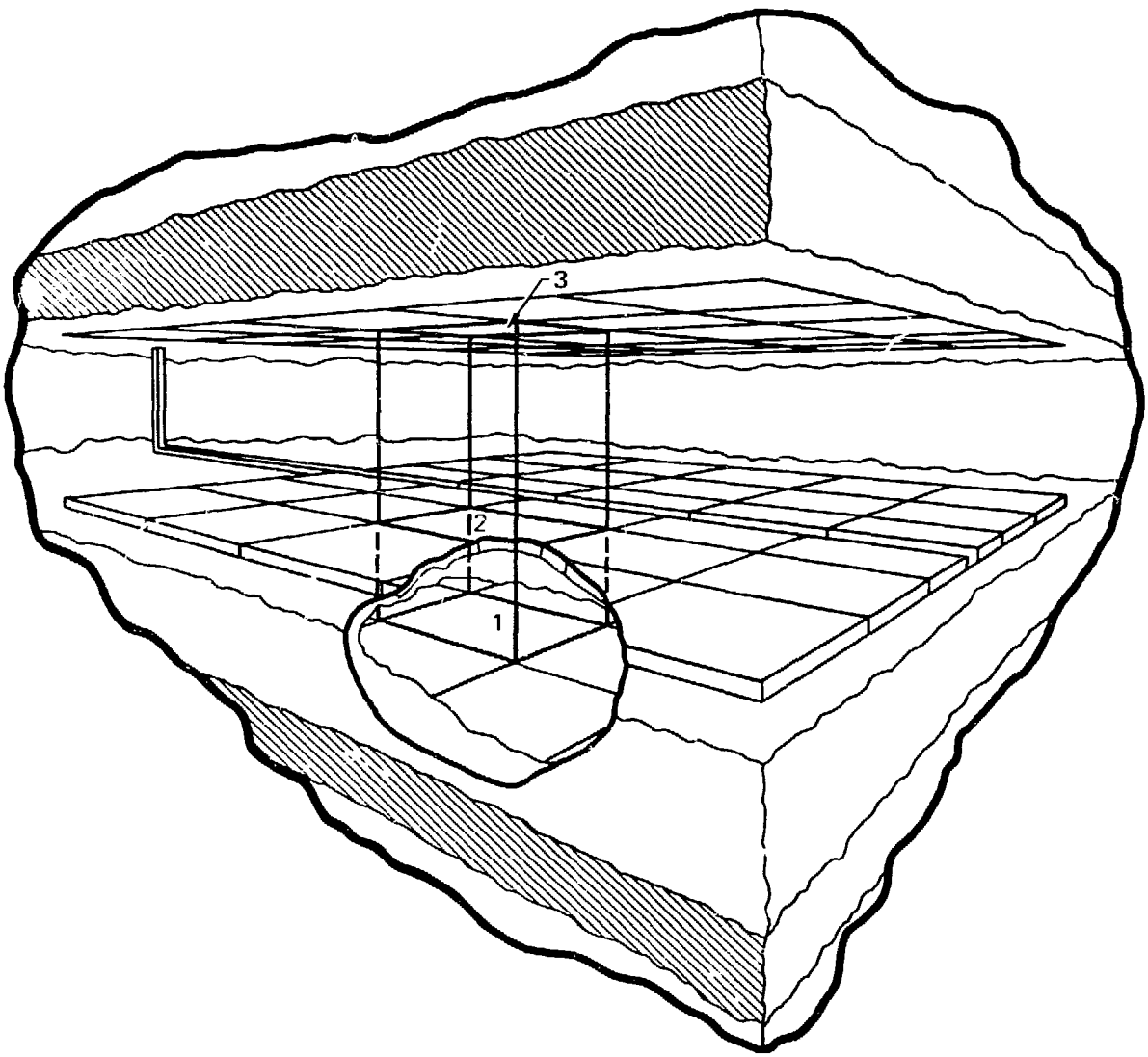

Figure 2-3. Two-shaft, 25-cell MISER model (typical flow cell is shown in cutaway).

ters of defense waste in tunnels containing two rows of canisters spaced 2.3 m apart. The canister pairs are separated by 2.3 m along the tunnels. The storage rooms are 5.5 m × 5.5 m in cross section. Tunnels connect the rooms to an access shaft and ventilation shaft. A fracture zone exists around the excavations. This is where the majority of the flow in the excavation occurs unless the backfill has deteriorated. Both the bedded salt basin and the basalt basin are layered. We also allow the model to incorporate an engineered bypass and major flaws, either undetected or caused by future disruptive events.

The fracture zone areas and their permeabilities are among the most uncertain parameters in the hydrological submodel. When disruptive events occur, additional hydrological pathways to the biosphere are created. Since disruptive events are extremely variable in their time and location of occurrence, our conservative approach is to choose a representative case at a bad location for the flaw and to have the event occur at an early time after closure. The probability of such a scenario occurring is calculated from a rate of occurrence over the policy-dictated time of interest, i.e., 10,000 yr.[13,14]

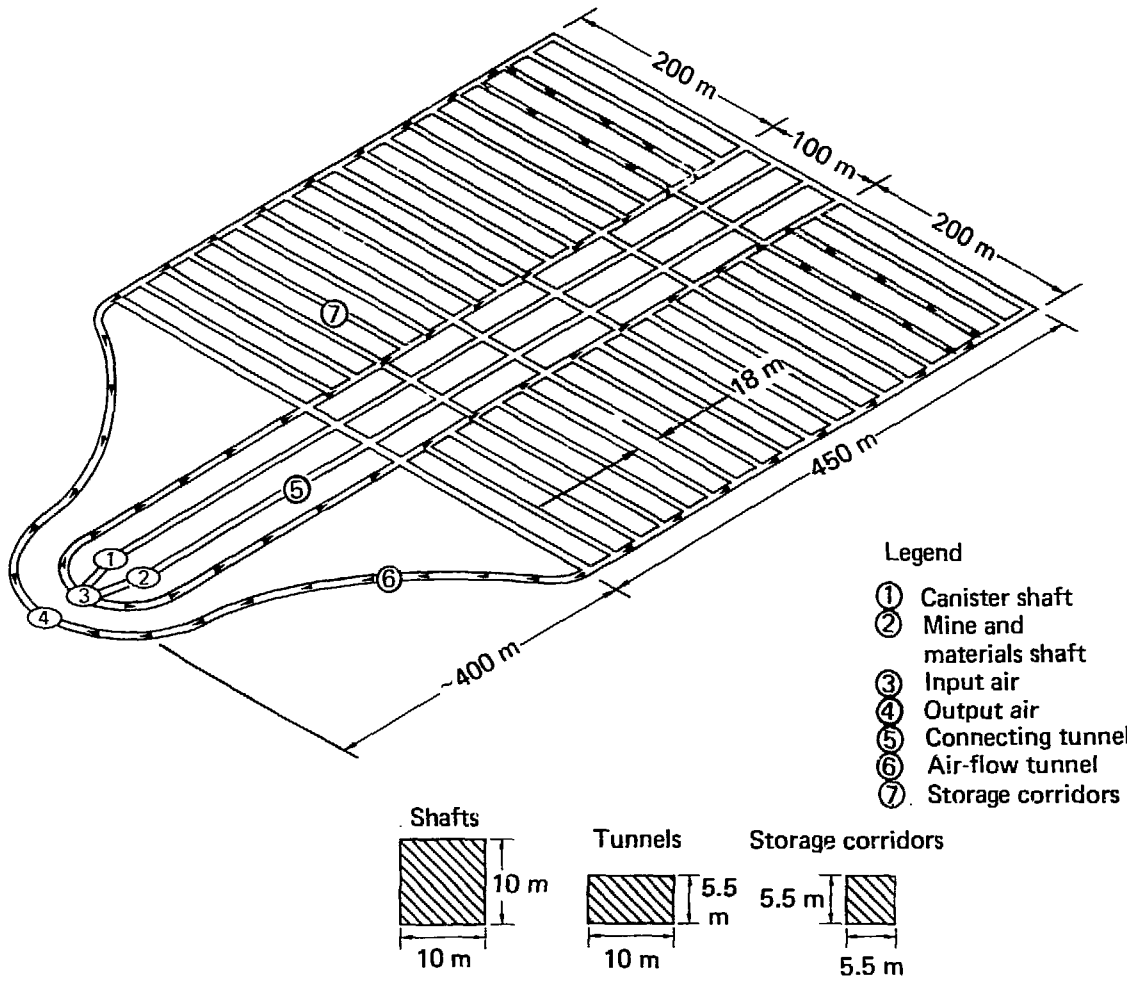

Figure 2-4. Layout of the mine design (storage rooms are orthogonal to the main tunnels, and those with ventilation are the ones currently being filled with waste; area of this design is at least several factors smaller than commercial waste repository designs).

We consider two well locations. The first is that for the limiting individual (LI) who drills a well directly on top of the repository 0.25 km downstream from the shafts. The second is a well 1.6 km (see Fig. 2.2) from the edge of the accessible environment. We refer to this as the accessible environment individual (AEI) case. A hydraulic connection to the upper aquifer is established by the fracture zone around the shaft or by a shaft seal that has failed completely by 1000 yr. Thus, water reaching the top of the shaft becomes a dispersing plume in the upper aquifer. This plume intersects the lower portion of the limiting individual's low-volume well. The well mixes water drawn from the aquifer and shaft thoroughly, diluting the contaminated water from the shaft plume with purer water from the aquifer. If the individual drinks wa :r from his well, he receives toxic radionuclides from three transport groups: (1) anion fission products, with no retardation, (2) cation fission products, which move 10 times slower than the anions, and (3) actinides, which move 100 times slower than the cations.* See Table 2-2.

*People drink water with as much as 3000 ppm of dissolved salt. (The standard for drinking water is 1000 ppm). Our well scenarios contain substantially less than 100 ppm dissolved salt since the upper aquifer is assumed to be fresh water. The salt contamination comes from salt-saturate d water flowing up the shafts.

Table 2-2. Radionuclides present in initial inventory.

Group I $B_I = 1$	^{99}Tc	^{129}I					
Group II $B_{II} = 10$	^{154}Eu ^{126}Sb ^{79}Se	^{151}Sm ^{90}Y	^{137}Cs ^{147}Pm	^{135}Cs ^{144}Ce	^{126}Sn ^{134}Cs	^{107}Pd ^{106}Ru	^{93}Zr ^{90}Sr
Group III $B_{III} = 100$	^{243}Am ^{235}U ^{227}Ac ^{223}Ra	^{241}Am ^{234}U ^{228}Ra ^{244}Cm	^{240}Pu ^{233}U ^{226}Ra ^{242}Cm	^{239}Pu ^{231}Pa ^{210}Po ^{241}Pu	^{238}Pu ^{232}Th ^{210}Pb ^{242m}Am	^{237}Pu ^{230}Th ^{225}Ac ^{242}Pu	^{238}U ^{229}Th ^{225}Ra ^{236}U

The MISER Model

The MISER computer code was written to provide a computationally efficient analysis tool for studies of radionuclide release from closed geologic nuclear waste repositories. Because its development drew heavily on previous modeling efforts at LLNL and elsewhere,[3–6] it is similar to previous models. By the same token, it has several significant differences.*

All of the referenced models have three basic assumptions:

1. Three-dimensional single-phase flow in a porous medium may be adequately approximated by a network of one-dimensional stream tubes.
2. Thermal energy, heat conduction, waste-canister stress, water chemistry and saturation, diffusion, and lateral dispersion may be neglected.
3. Flow is slow enough for instantaneous ion-exchange equilibrium to occur.

If one further assumes that the repository recharge is sufficiently fast, then a steady-state hydrology may be employed to decouple the hydrology and the nuclide transport.

The concept underlying the MISER code is that the user/analyst describes a general network of hydrologic flow paths with heads specified at boundary conditions (sources and sinks for flow). The user also specifies the radionuclide sources (beginnings of paths) and the risk-sensitive, nuclide-release observation points (ends of paths). Then the code traces "tree branches" of water flow from sources to sinks through all possible pathways before a subset of branches for nuclide transport is extracted from the full set.

*MACRO,[7] for example, systematically samples all values of finite-probability distributions representing problem parameters and variables which may lead to an inordinate number of calculations in a physically consistent system of constraints and correlations. MISER uses Monte Carlo techniques where appropriate. The modeling of MISER transport phenomena differs from that for either NUTRAN[4] or NWFT.[5]

The dimensions of the arrays are set by parameters, so the number of paths, branches, nuclide sources, and release points are, in theory, limited only by the size of the computer and the time available for computations.

The MISER model can be conceived as a combination of four numerical submodels that have been linked together. A "wrap-around" Monte Carlo methodology is applied to uncertainty analyses. Detailed descriptions of the numerical submodels follow.

Waste Package Submodel. The first submodel is the waste package. It describes the radionuclides originally in the canister and their release as a function of time to the surrounding excavation. The original amount of radionuclides in a canister, a nonstochastic (certain) quantity in this analysis, is then used to calculate the nonstochastic set of radionuclides as a function of time in the system. Thus, the amount of radioactivity in the total system is certain. The radionuclide locations as a function of time are uncertain, however.

The radioactive content of the defense waste contains 87 radionuclides[15] of which 53 are biologically significant and represent >99% of the activity. ORIGEN[16] (the ORNL Isotope Generation and Depletion Code) can be used to calculate decay of spent fuel or reprocessed defense waste vs time. The method of calculation and an example of ORIGEN output based on Savannah River Defense Waste Inventory are given in Appendix A. From ORIGEN output we obtain a table of activity (Ci) for each nuclide in the original inventory or produced by decay as a function of time. Figure 2-5 shows the radionuclide total activity vs time of one canister of defense HLW from Savannah River.[15] The dotted lines trace the groups, i.e., Group 1 (^{99}Tc, ^{129}I, ^{14}C), Group 2 (other fission products), and Group 3 (actinides). The solid line is the total activity.

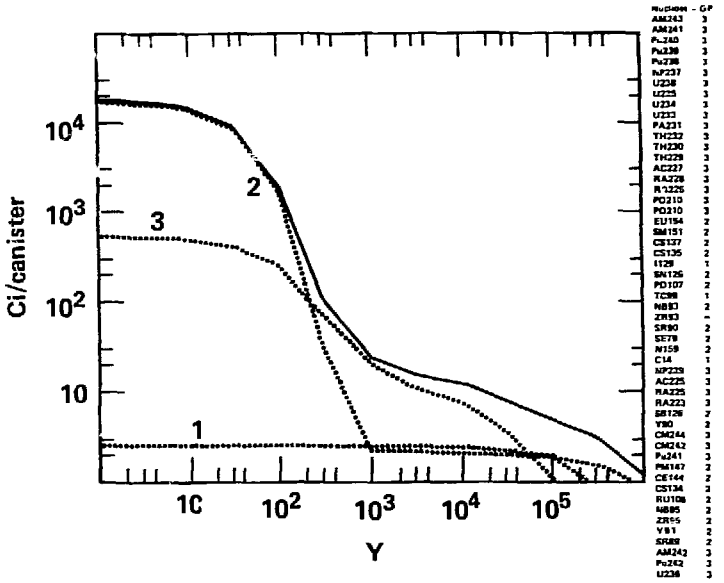

Figure 2-5. Savannah River Plant – high level defense waste inventory/canister, by groups.

Besides the reasonably well-known quantities of radionuclides vs time, the waste package model in MISER has two parameters with large uncertainties. These are the time of initial release of radioactivity from the package, (referred to here as the breach time) and the duration of the release (or the release time). For the release model, i.e., a model of the amount of radionuclide released as a function of time, any empirical results can be included in MISER by summing over unit pulses using a Green's-function approach. This will incur large computer costs. To avoid this we use a "Gaussian-like" release function. For example, the release functions for release times of 2×10^5 and 2×10^6 yr are shown in Fig. 2-6.

If we assume the waste release mechanism is Gaussian-like, we do not need to convolute the release function with a Green's function. We merely add the terms as though the release pulse were caused by an additional path at the beginning of the transport branch. We truncate our pulse and compute over M (≥ 20) time steps. Finally, these results are summed in the result space.

This numerical approach is orders of magnitude more efficient than other models doing similar process analyses. Also, we conservatively assume no solubility limits in this analysis by allowing all radionuclides to release at the same rate.

Our understanding of the release rate is limited at this time. The present values (obtained from characterizing these parameters in laboratory experiments) are limited by not knowing their *in situ* variability. To date, the variability of release rate for real waste at specific sites has not been determined in the measurements of these quantities. The best information available is sparse and difficult to generalize, but a general

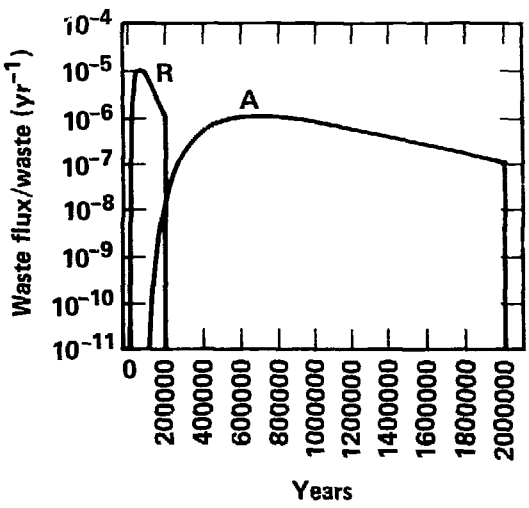

Figure 2-6. Median dissolution rates of canisters of REFERENCE (R) and ALTERNATIVE (A) waste forms (both canisters start leaching at time zero).

status report is presented here. We use as a baseline release rate, that rate at which a cracked borosilicate glass monolith might be leached based on initial laboratory tests. The actual release rate of the glass waste form in a repository may be lower than this value because of solubility limits and sorption properties of engineered barrier materials. Therefore, our baseline rate is a conservative upper bound of the release rate and is, therefore, suitable for use in radiological risk studies. If such an estimated release rate leads to acceptably low doses, a better level of release rate performance would then also lead to acceptably low doses.

These conservative estimates of waste package release rates[17] (which ignore solubility limits and the beneficial effects of engineered barrier materials) predict that the basecase borosilicate glass form (REFERENCE) will have median dissolution duration of about 2×10^5 yr in salt and 10^5 yr in basalt. Our alternative or improved waste form (ALTERNATIVE) is assumed to have a median release duration an order of magnitude better, but with larger uncertainty. The uncertainty on the release duration for the REFERENCE has been approximated by a geometric standard deviation of 10. For the ALTERNATIVE, a geometric standard deviation of 15 was used. For example, this means that about 68% of the time, values of ALTERNATIVE release duration will be chosen between 7×10^4 and 1.5×10^7 yr in the basalt case. Better understanding of the stability of waste forms and their environment could lead to substantial reduction in the number of high dose cases seen for individual doses.

The breach time, an insensitive parameter in the analysis, is taken to be the same for all canisters in the model for a given Monte Carlo trial. The median breach time is 1000 yr. The 98% interval is from 250 to 4000 yr. Previous sensitivity analyses indicate that the dose to humans is independent of breaching time after 1000 yr.[7]

Since the release rate parameters are not well understood, we have done a sensitivity study on the release rate to determine the effects of changing our best estimates and reducing the uncertainties of the release rate. These results are presented in the subsection "Release Rates and Uncertainties."

Hydrology Submodel. Under the simplifying assumptions of the preceding section, we solve the steady-state hydrology using D'Arcy's laws and conservation of water relationships. We assume a network of N paths, $N \geq 2$, and at least two boundary conditions.

The network of stream tubes are described by assuming that all flows are positive from the source(s) to sink(s) at which hydrologic heads are specified. Then, by interactive input, flows from each path to subsequent paths or boundary conditions are flagged in a "connector" matrix. The code then traces all "tree branches" from sources to sinks, producing a set of D'Arcy law equations.

$$\left\{ \sum_{n \mid \text{path } n \text{ is in branch } m} Q_n Z_n / K_n A_n = H_R^m - H_E^m : m = 1,2,\ldots,NB \right\} \quad (1)$$

where

NB = number of tree branches in the network
Q_n = D'Arcy flux
K_n = permeability
A_n = cross-sectional area
Z_n = path length
H_E^m = boundary head at exit of branch m
H_R^m = boundary head at root of branch m
n = path number.

The conservation of water at path junctions also produces a set of equations

$$\left\{ \sum_{i \mid \text{path } i \text{ flows to junction } m} Q_i = \sum_{j \mid \text{path } j \text{ flows from junction } m} Q_j \right\}, \quad (2)$$

where m=1, 2, ..., NJ; NJ = number of path junctions in the network. In general, NB + NJ $\geq$ N, where N is the number of paths (equal number of unknowns), but a linearly independent set of N equations can be chosen. We use the LLNL MATHLIB[18] routines to obtain a rapid solution of the NB + NJ equations for the unknowns Q_1, Q_2,...,Q_N. If any Q_N is computed to be negative, the code redefines the connector matrix and tree branches so all resulting flows are positive. An example will clarify the hydrology solution methodology. Suppose we wish to solve the 16-path network of Fig. 2-7. We assume boundary-condition heads so that $H_R^1 > H_E^1$, $H_R^2 > H_E^2$, $H_R^1 < H_R^2$, and $H_E^1 < H_E^2$, i.e., flow is generally upward and to the right, with the exception of path 8, which flows to the left.

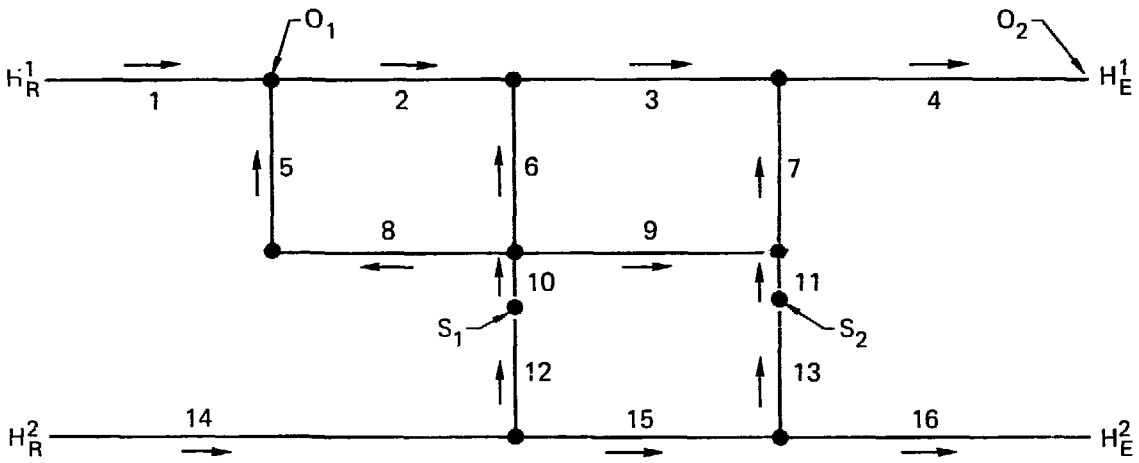

Figure 2-7. Sample hydrology network of stream-tube flow paths (arrows indicate assumed direction of flow; radionuclide sources are at S_1 and S_2, and risk-sensitive observation points are at O_1 and O_2).

The connector matrix is defined by the user input of

path 1 flow to 2
path 2 flow to 3
path 3 flow to 4
path 4 flow to B.C.
. .
. .
. .
path 10 flow to 8, 6, and 9
. .
. .
. .
path 16 flow to B.C.

The code then traces the branches

1 → 2 → 3 → 4
14 → 12 → 10 → 8 → 5 → 2 → 3 → 4
14 → 12 → 10 → 6 → 3 → 4
14 → 12 → 10 → 9 → 7 → 4
14 → 15 → 13 → 11 → 7 → 4
14 → 15 → 16

for a total of six branches, i.e., NB = 6.

There are 10 junctions, NJ = 10, in the network, resulting in the conservation equations

$$
\begin{aligned}
Q_1 + Q_5 &= Q_2 \\
Q_2 + Q_6 &= Q_3 \\
Q_3 + Q_7 &= Q_4 \\
Q_8 &= Q_5 \\
Q_{10} &= Q_8 + Q_6 + Q_9 \\
Q_9 + Q_{11} &= Q_7 \\
Q_{12} &= Q_{10} \\
Q_{13} &= Q_{11} \\
Q_{14} &= Q_{12} + Q_{15} \\
Q_{15} &= Q_{13} + Q_{16}
\end{aligned}
$$

The user supplies parameters for Z_n, K_n, and A_n, which may be uncertain; in that case, they are selected using the aforementioned Monte Carlo techniques. Then, letting $x_n = Z_n/K_nA_n$, the codes sets up the matrix equation

$$
\begin{bmatrix}
X_1 & X_2 & X_3 & X_4 & 0 & 0 & 0 & 0 & 0 & 0 & 0 & 0 & 0 & 0 & 0 & 0 \\
0 & X_2 & X_3 & X_4 & X_5 & 0 & 0 & X_8 & 0 & X_{10} & 0 & X_{12} & 0 & X_{14} & 0 & 0 \\
0 & 0 & X_3 & X_4 & 0 & X_6 & 0 & 0 & 0 & X_{10} & 0 & X_{12} & 0 & X_{14} & 0 & 0 \\
0 & 0 & 0 & X_4 & 0 & 0 & X_7 & 0 & X_9 & X_{10} & 0 & X_{12} & 0 & X_{14} & 0 & 0 \\
0 & 0 & 0 & X_4 & 0 & 0 & X_7 & 0 & 0 & 0 & X_{11} & 0 & X_{13} & X_{14} & X_{15} & 0 \\
0 & 0 & 0 & 0 & 0 & 0 & 0 & 0 & 0 & 0 & 0 & 0 & 0 & X_{14} & X_{15} & X_{16} \\
1 & -1 & 0 & 0 & 1 & 0 & 0 & 0 & 0 & 0 & 0 & 0 & 0 & 0 & 0 & 0 \\
0 & 1 & -1 & 0 & 0 & 1 & 0 & 0 & 0 & 0 & 0 & 0 & 0 & 0 & 0 & 0 \\
0 & 0 & 1 & -1 & 0 & 0 & 1 & 0 & 0 & 0 & 0 & 0 & 0 & 0 & 0 & 0 \\
0 & 0 & 0 & 0 & -1 & 0 & 0 & 1 & 0 & 0 & 0 & 0 & 0 & 0 & 0 & 0 \\
0 & 0 & 0 & 0 & 0 & -1 & 0 & -1 & -1 & 1 & 0 & 0 & 0 & 0 & 0 & 0 \\
0 & 0 & 0 & 0 & 0 & 0 & -1 & 0 & 1 & 0 & 1 & 0 & 0 & 0 & 0 & 0 \\
0 & 0 & 0 & 0 & 0 & 0 & 0 & 0 & 0 & -1 & 0 & 1 & 0 & 0 & 0 & 0 \\
0 & 0 & 0 & 0 & 0 & 0 & 0 & 0 & 0 & 0 & -1 & 0 & 1 & 0 & 0 & 0 \\
0 & 0 & 0 & 0 & 0 & 0 & 0 & 0 & 0 & 0 & 0 & -1 & 0 & 1 & -1 & 0 \\
0 & 0 & 0 & 0 & 0 & 0 & 0 & 0 & 0 & 0 & 0 & 0 & -1 & 0 & 1 & -1
\end{bmatrix}
\begin{bmatrix} Q_1 \\ Q_2 \\ Q_3 \\ Q_4 \\ Q_5 \\ Q_6 \\ Q_7 \\ Q_8 \\ Q_9 \\ Q_{10} \\ Q_{11} \\ Q_{12} \\ Q_{13} \\ Q_{14} \\ Q_{15} \\ Q_{16} \end{bmatrix}
=
\begin{bmatrix} H_R^1 - H_E^1 \\ H_R^1 - H_E^2 \\ H_R^1 - H_E^2 \\ H_R^1 - H_E^2 \\ H_R^1 - H_E^2 \\ H_R^2 - H_E^2 \\ 0 \\ 0 \\ 0 \\ 0 \\ 0 \\ 0 \\ 0 \\ 0 \\ 0 \\ 0 \end{bmatrix}
\qquad (3)
$$

which is solved for Q_n, n = 1, 16.

Suppose that the permeabilities were such that, in path 9, the resulting flow were negative. Then, the connector matrix and tree branches would be altered to reflect that the branch

14 — 12 — 10 — 9 — 7 — 4
becomes
14 — 15 — 13 — 11 — 9 — 6 — 3 — 4 and
14 — 15 — 13 — 11 — 9 — 8 — 5 — 2 — 3 — 4 .

The conservation laws are

$$Q_{11} = Q_9 + Q_7 \text{ (not } Q_9 + Q_{11} = Q_7)$$

and

$$Q_9 + Q_{10} = Q_6 + Q_8 \text{ (not } Q_{10} = Q_6 + Q_8 + Q_9) .$$

This gives us 17 equations and 16 unknowns. However, if we subtract row 3 from row 2 of the matrix, we get just the difference of the last two D'Arcy equations. Thus, a dependent set and one equation may be eliminated to produce a solution.*

The conservation laws are used to compute the water-split fractions, f_m, at each junction to complete the steady-state hydrology solution.

*MISER only eliminates equations, if necessary, for storage purposes. We actually solve m equations for n unknowns, m ≥ n, using the LLNL MATHLIB[18] routines.

The validity of this stream-tube approximation to a real three-dimensional hydrology should be checked using results from finite-element or finite-difference codes, as well as experimental data. Obviously, if the stream-tubes chosen are far from reality, the approximation will be poor. On the other hand, the size and expense of many computer runs almost precludes consideration of the three-dimensional codes for sensitivity and uncertainty analyses. Further, the uncertainties associated with the measurement and chemical properties of nuclide transport may overwhelm the hydrology model uncertainty.

Nuclide Transport Submodel

General Procedure. Our general procedure for transport of radionuclides is to extract from the set of hydrology tree branches that subset that leads from all nuclide sources to all risk-sensitive observation points. Then we apply the results of the waste-pipe calculus[19,20] to each series of paths in a branch to approximate the waste flux at the release points. The flux pulses are accumulated on a discretized time line, then converted to hazard or dose measures. The waste is assumed to split in the same fractions as the water at each junction in the network.

Radioactive decay is not used explicitly in our transport model. We first compute a flux of nuclide groups as a function of time. Then we use tabulated results from the ORIGEN isotope and depletion code[21] as multipliers in the dose/hazard calculations described below.

Using our example from the preceding section and assuming nuclide sources at S_1 and S_2, with observation points at O_1 and O_2, we select the branches

$10 \rightarrow 8 \rightarrow 5$ for S_1 to O_1

$10 \rightarrow 8 \rightarrow 5 \rightarrow 2 \rightarrow 3 \rightarrow 4$
$10 \rightarrow 6 \rightarrow 3 \rightarrow 4$
$10 \rightarrow 9 \rightarrow 7 \rightarrow 4$
} for S_1 to O_2

$11 \rightarrow 7 \rightarrow 4$ for S_2 to O_2.

Now an observer located at O_1, as a function of time, would see as many waste pulses as the number, N_1, of canisters with different release times or durations located at S_1. At O_2, he would see $3 \times N_1 + N_2$ pulses, where N_2 is the number of canisters at S_2. As the number of overlapping (in time) pulses increases, the exact form of each individual pulse becomes decreasingly important. See "Waste Release and Convolution Models" below.

Transport Green's Function. For completeness, and to delineate the assumptions and approximations, we extract from Refs. 19, 20, and 22 the derivation of our transport models.

One of the fundamental equations governing the transport and dispersion of ions in one-dimensional flow through porous media is

$$\frac{\partial m_r}{\partial t} + \frac{\partial C_r}{\partial t} + v\frac{\partial C_r}{\partial x} = \alpha v \frac{\partial^2 C_r}{\partial x^2} - \lambda_r C_r + \sum_{s \neq r} \lambda_s^r C_s - \lambda_r m_r + \sum_{s \neq r} \lambda_s^r m_s \quad , \quad (4)$$

where

- λ_r = radioactive decay constant of nuclide r (= ln 2/half-life)
- λ_s^r = production rate of nuclide r from decay of nuclide s
- v = interstitial water flow velocity (= Q/Aη, η is effective porosity)
- α = longitudinal dispersion constant
- m_r = amount of ion r sorbed on the solid per-unit volume
- C_r = concentration of nuclide r in the interstitial water
- x = spatial coordinate
- t = time.

We note that $v(\partial C_r/\partial x)$ is a simple advection and that $\alpha v(\partial^2 C_r/\partial x^2)$ is a hydrodynamic dispersion term. Diffusion and lateral dispersion have been neglected.

Assume that flow is slow enough for instantaneous ion-exchange equilibrium to result and that the ion-exchange absorption isotherm is linear. Then,

$$m_r = \frac{\rho}{\eta} K_d C_r \quad , \quad (5)$$

where

- ρ = bulk density
- η = effective porosity
- K_d = distribution coefficient.

Assume that the retardation factor, B_r, is the same for all nuclides in the same decay chain.*

Then,

$$B_r = 1 + \frac{\rho}{\eta} K_d$$

and

$$m_r = \frac{\rho}{\eta} K_d C_r = (B_r - 1) C_r \quad . \quad (6)$$

Substitution simplifies Eq. (4) to

$$B_r \frac{\partial C_r}{\partial t} + v\frac{\partial C_r}{\partial x} = \alpha v \frac{\partial^2 C_r}{\partial x^2} - B_r \lambda_r C_r + \sum_{s \neq r} B_s \lambda_s^r C_s^r \quad . \quad (7)$$

Assume that the dissolution rate for the waste form is the same for all nuclides in the same decay chain. Let $I_r(t)$ be the total amount of nuclide r at time t that was originally emplaced in the repository. Then the decay equation for I_r is given by:

$$\frac{\partial I_r}{\partial t} = -\lambda_r I_r + \sum_{s \neq r} \lambda_s^r I_s \quad . \quad (8)$$

Now let $c_r(x,t) = C_r(x,t)/I_r(t)$ be the concentration of nuclide r per unit inventory of waste, I_r. Then

*As we learn more about retardation factors, we recognize that this assumption needs to be reexamined.

$$\frac{\partial C_r}{\partial t} = I_r \frac{\partial c_r}{\partial t} + c_r \frac{\partial I_r}{\partial t}$$

$$= I_r \frac{\partial c_r}{\partial t} - c_r \left(\lambda_r I_r - \sum_{s \neq r} \lambda_s^r I_s \right)$$

and

$$\frac{\partial C_r}{\partial x} = I_r \frac{\partial c_r}{\partial x}, \frac{\partial^2 C_r}{\partial x^2} = I_r \frac{\partial^2 c_r}{\partial x^2} \quad ,$$

which, when substituted in Eq. (7), gives

$$B_r \frac{\partial c_r}{\partial t} + v \frac{\partial c_r}{\partial x} = \alpha v \frac{\partial^2 c_r}{\partial x^2} + \frac{1}{I_r} \sum_s \lambda_s^r I_s (B_s c_s - B_r c_r) \quad . \tag{9}$$

We have assumed that $B_r = B_s$ in the same decay chain. Thus, for nuclides in the same chain, we may factor B_r from the last term, apply uniqueness, and arrive at the fundamental equation

$$\frac{\partial c_r}{\partial t} + \frac{v}{B_r} \frac{\partial c_r}{\partial x} - \alpha \frac{v}{B_r} \frac{\partial^2 c_r}{\partial x^2} = 0 \quad , \tag{10}$$

where $c_r = c_r(x,t)$ is the concentration of nuclide r at spatial point x and time t per unit inventory of r at t.

A reasonable assumption is to place the nuclides in three groups based on retardations, dissolutions, and decay chains. They are

1. Anions (e.g., ^{99}Tc, ^{129}I, and ^{14}C).
2. Cations (other fission products).
3. Actinides.

To model the one-dimensional nuclide transport, we must solve (or approximate) Eq. (10) for reasonable boundary conditions over a series of paths within each tree branch.

Since boundary conditions are often more easily set with mass flux than with concentration, we note that if J(x,t) is the mass flux, then

$$J(x,t) = V(x,t) \left(c(x,t) - \alpha \frac{\partial c(x,t)}{\partial x} \right) \quad , \tag{11}$$

where V is the water volumetric flow rate. Differentiation and substitution in Eq. (10) gives the identical equation

$$\frac{\partial J_r}{\partial t} + \frac{v}{B_r} \frac{\partial J_r}{\partial x} - \alpha \frac{v}{B_r} \frac{\partial^2 J_r}{\partial x^2} = 0 \quad , \tag{12}$$

in terms of nuclide mass flux per unit inventory.

We will drop the subscript r for the rest of this discussion, keeping in mind that the equations apply to nuclides in the same decay chain or (approximately) in the same retardation group.

Let us assume the initial and boundary conditions

J(x,0) = 0, no nuclides are present initially.

J(0,t) = δ(t), unit impulse input at one end.

J(x,t) $\rightarrow$ 0 as x $\rightarrow \infty$ (semi-infinite path).

The semi-infinite path assumption has been investigated by Oston.[23] Generally, results obtained by the semi-infinite path assumption fall between those of his "slug-flow" and "diffusion" boundary condition assumptions. In reality, we have none of the above. However, as the path length z becomes large compared to the dispersion constant α, results coalesce. If $z/\alpha > 10$, the results are almost indistinguishable.

The solution for unit impulse is a Green's function and has the form

$$J(x,t) = G(x,t)$$

$$= \frac{x}{\left(\frac{4\pi v \alpha t^3}{B} \right)^{1/2}} \exp \left[- \frac{(x - \frac{v}{B} t)^2}{4\alpha \frac{v}{B} t} \right] \quad . \tag{13}$$

For a path length of z, let us write

$\tau = \frac{zB}{v}$ as the mean transit time for a pulse

and

$\sigma = \left(\frac{2\alpha}{z} \right)^{1/2} \tau$ as the dispersive spread of the pulse about the mean.

Then the Green's function becomes

$$G(\tau,\sigma;t) = \frac{1}{(2\pi)^{1/2}\sigma} \left(\frac{\tau}{t} \right)^{3/2} \exp \left[- \frac{(t-\tau)^2 \tau}{2\sigma^2 t} \right] \quad . \tag{14}$$

If the path has flux input at x=0, given by S(t), then, by the convolution theorem, the output flux, $J(\sigma,\tau;t)$, at x=z is

$$J(\sigma,\tau;t) = \int_0^t S(t') \, G(\sigma,\tau;t-t') \, dt' \quad . \tag{15}$$

In Ref. 19, the Laplace transform theory is applied to show that for a series sequence of paths,

n=1, 2, ..., N, the transform of $J(\sigma,\tau;t)$ is a product of transforms, e.g.,

$$\overline{J(\sigma,\tau;s)} = \prod_{n=1}^{N} \overline{G(\sigma_n,\tau_n;s)}\ \overline{S(s)} \quad , \tag{16}$$

where

$$\overline{G(\sigma_n,\tau_n;s)} = \int_0^\infty e^{-st}\, G(\sigma_n,\tau_n;t)\, dt \quad ,$$

and

$$\overline{S(s)} = \int_0^\infty e^{-st}\, S(t)\, dt \quad ,$$

where S(t) is the initial source function, and the mean time and width parameters add as follows:

$$\left.\begin{aligned} \tau &= \sum_{n=1}^{N} \tau_n + \tau_0 \\ \sigma^2 &= \sum_{n=1}^{N} \sigma_n^2 + \sigma_0^2 \end{aligned}\right\} \quad . \tag{17}$$

τ_0 and σ_0 are the mean and variance of the source function.

We are interested in the final mass transfer function $J(\sigma,\tau;t)$ at the end of a series of paths that is either the inverse Laplace transform of Eq. (16) or a convolution integral in time, e.g., for two paths,

$$J(\sigma,\tau;t) = \int_0^t dt'' \int_0^{t''} G(\sigma_2,\tau_2;t-t'') \times G(\sigma_1,\tau_1;\, t''-t')\, S(t')\, dt' \quad .$$

Reference 19 suggests that the inverse transform may be obtained by the method of steepest descent. In either case, computation time will be costly; therefore, we chose to use approximate methods.

O'Connell's extensions to the waste-pipe calculus[20] shows that if we assume (1) that the flow-path network is a single-series path and (2) that the source term is narrow in width and drops off more quickly for high times t, compared to the overall (convoluted) Green's function, then

$$J(\sigma,\tau;t) \approx G(\sigma,\tau;t) \quad ,$$

which is Eq. (14), with σ and τ as defined by Eq. (17).

As indicated in Ref. 20, this approximation has the same first and second moments as the exact function within our assumptions.* We note that the approximation is still valid if assumption (2) does not hold, but we must perform the convolution integral.

The MISER code traces nuclide flows through the tree branches from nuclide sources to risk-sensitive observation points so that each branch is a series of sequential network paths. The appropriate fraction is computed based on water-flow fractions. The approximate Green's function is then convoluted with the source function and resulting flux accumulated on a discretized time line.

To account for the spatial separation of canisters within each waste "source cell," we choose the network such that the first path leaving the source represents a storage room. Then for each retardation group, r, we compute the single path transit time, τ_r. For each of N canisters located at the source we then choose a first path transit time, $\tau_{r,n}$, n = 1, 2, ..., N by a random number selection from the interval $[0, \tau_r]$. This procedure implies that a canister has equal probability of being placed at any distance along the first network path leading away from a nuclide source point.

Further work needs to be done to validate transport models, particularly with respect to the near-field effects of repository design, placement of waste, and waste dissolution and release.

Waste Release and Convolution Models. It is obvious from discussions of chemical modeling (Ref. 7) that waste dissolution and release is a major area of modeling uncertainty. MISER currently models the release as a step or Gaussian (or Gaussian-like) function; however, these may be limiting cases with reality somewhere between.

---

*One might observe that the Gaussian function,

$$g(\sigma,\tau;t) = \frac{1}{(2\pi)^{1/2}\sigma} \exp\left[-\frac{(t-\tau)^2}{2\sigma^2}\right] ,$$

also has the same first and second moments. In a system of many overlapping pulses, the exact form of the pulse is washed out and either of the above may also produce reasonable approximations. In the probabilistic analysis, even a flat transport pulse with step release gives a reasonable approximation (see under "Selected Sensitivity Analysis" in Sec. 3). Since we are interested particularly in near-field scenarios, further studies in this area are necessary, particularly in the cases of $z/\alpha < 10$.

For step-function release, we assume that, for each nuclide group r, the waste has a constant dissolution rate beginning at time TC and lasting for a period TD_r; that is,

$$S_r(t) = \begin{cases} 0 \text{ for } t < TC \text{ and } t > (TC + TD_r) \\ \dfrac{\tilde{I}_r}{TD_r} \text{ for } TC \le t \le (TC + TD_r) \end{cases} \quad (18)$$

where $\tilde{I}_r$ is the path-fractional reduced inventory of group r and TC is a time that reflects the age of the waste at time of emplacement added to the time at which the canister is assumed to have breached because of corrosion.

We use the approximate Green's function of Eq. (14) and evaluate the convolution integral of Eq. (15). In this case, an analytical solution exists in terms of error functions. Further, if t is very large compared to the dissolution time, the step function may be approximated as a delta function. Then

$$J_r(\sigma_r,\tau_r;t) = \begin{cases} 0 \text{ if } t \le TC \\ \dfrac{\tilde{I}_r\tau_r}{TD_r}\varphi(\beta,\gamma) \text{ if } TC \le t < (TC + TD_r) \\ \dfrac{\tilde{I}_r\tau_r}{TD_r}\left|\varphi(\beta,\gamma) - \varphi\left(\beta,\gamma - \dfrac{TD_r}{\tau_r}\right)\right| \\ \quad \text{if } (TC + TD_r) < t < 10^3\, TD_r \\ \tilde{I}_r\, G(\tau_r,\sigma_r;t) \text{ if } 10^3\, TD_r \le t \end{cases}$$

where $\gamma = t/\tau_r$, $\beta = \sigma_r/\tau_r$, and

$$\varphi(\beta,\gamma) = \frac{1}{2}\left\{\exp\left(\frac{2}{\beta^2}\right)\operatorname{erfc}\left[\frac{\gamma^2+1}{(2\beta)^{1/2}\gamma^{3/2}}\right] - \operatorname{erfc}\left[\frac{\gamma^2-1}{(2\beta)^{1/2}\gamma^{3/2}}\right]\right\} \quad , \quad (19)$$

and erfc is the complementary error function.

Since we are going to accumulate the sums of many waste pulses on a discretized time line, we must produce, in a finite number of steps, a reasonable approximation of the flux for the MISER computer model. Further, the dose/hazard curves may vary rapidly in time so that the peak dose does not necessarily occur at the time of peak flux.

If we differentiate the Green's function, we find that the peak occurs at time

$$\hat{t}_r = \frac{\tau_r}{2} - 3\left(\frac{\sigma_r}{\tau_r}\right)^2 + \left\{9\left(\frac{\sigma_r}{\tau_r}\right)^4 + 4\right\}^{1/2} \quad .$$

Let $J_r = J_r(\sigma_r,\tau_r;t_r)$. Then we determine truncation limits by successive evaluations, using $0.9^m\,\hat{t}_r$ and $1.1^m\,\hat{t}_r$, m=1, 2,... to find $\underline{m}$ and $\bar{m}$ so that

$$J_r(\sigma_r,\tau_r;0.9^{\underline{m}}\hat{t}_r) < \epsilon\,\hat{J}_r < J_r(\sigma_r,\tau_r;0.9^{\underline{m}-1}\hat{t}_r)$$

and

$$J_r(\sigma_r,\tau_r;1.1^{\bar{m}-1}\hat{t}_r) < \epsilon\,\hat{J}_r < J_r(\sigma_r,\tau_r;1.1^{\bar{m}}\hat{t}_r) \quad ,$$

where ϵ is an arbitrary parameter (e.g., $\epsilon \simeq 10^{-10}$).

The time range of interest is then set to

$$\underline{t} = 0.9^{\underline{m}}\,\hat{t}_r + TC$$

$$\bar{\tau} = 1.1^{\bar{m}}\,\hat{t}_r + TC + TD_r \quad .$$

The leading portion is evaluated over $\underline{M}$ ($\approx$20) time steps with $\Delta t = (\bar{t}-\underline{t})/(\underline{M}-1)$, $t_1 = \underline{t}$, $t_m = t_{m-1} + \Delta t$, m=2,3,..., $\underline{M}$. The remaining time $\bar{t}$ to $\bar{\tau}$ is subdivided using the algorithms

$$N = \max\left\{\left(\left[\frac{TD_r}{\sigma_r}\right] + 1\right)\underline{M}\,\underline{N},\ 1000 - \underline{M}\right\} \quad ,$$

where $[TD_r/\sigma_r]$ is the integer part of TD_r/σ_r and $\underline{N}$ ($\approx$4) is a parameter.

If $N\,\Delta t \ge \bar{\tau} - \bar{t}$, set $\delta t = (\bar{\tau}-\bar{t})/(N-1)$ and R=1; otherwise, set $\delta t = \Delta t$ and let $R = 1.01^j$, where $j = \min\{1, 2, 3,...\}$ such that

$$\bar{\tau} - \bar{t} \le \Delta t\,(R^{N-1} - 1)/(R-1) \quad ,$$

i.e., R is the ratio that is a minimum integral power of 1.01 to produce a geometric progression of time steps to span the time of interest in N steps. Then we compute $J_r(\sigma_r,\tau_r;t_j)$ by Eq. (19) for

$$t_1 = \underline{t}$$
$$t_j = t_{j-1} + \Delta t \text{ for } j=2, ..., \underline{M}, \text{ and}$$
$$t_j = t_{j-1} + \delta t\, R^{j-1},\ j = \underline{M}+1,...,M+N \quad .$$

Finally, if the discretized output time line is given by T_i, i=1,2...,I, we integral average the $J_r(\sigma_r,\tau_r;t_j)$ to produce values to add to the existing waste flux.* That is,

*An option exists in MISER to move the time of peak flux, $\hat{t}$, to the nearest discretized output time T_i. In this case, the t_j are all shifted by the amount $T_i - \hat{t}$. Since we are primarily interested in peak doses, this shift helps compensate for sharp pulses that might otherwise be lost in the discretized output time line.

$$J_r^k(T_i) = \sum_{\text{[all branches leading to observation point k]}} J_r^k(\sigma_r, \tau_r; T_i) \qquad (20)$$

is the resulting flux of nuclide group r at observation point k.

If we assume that the waste release mechanism is "Gaussian-like," we could model the release as the Green's function, Eq. (14). In this case, we set $\sigma_r = TD_r/4$ and $\tau_r = TC + (TD_r/2)$ and merely add the terms as though the release were an additional path in the branch. We truncate $J_k(\sigma_r, \tau_r; t)$ at $\tau_r \pm 2\,\sigma_r$ and compute over $\underline{M}$ (≈ 20) time steps. Finally, we sum these results as in Eq. (20).

The second model is much more computationally efficient because the tabular values for the error function do not enter. That is, the convolution integral need not be evaluated. However, we must remember that, in both cases, we are using only the approximate Green's function, which may not be valid if $\tau/\sigma < 10$.

Figure 2-8A displays the set of pulses arriving at a well 237 m downstream of the main shaft. The pulses originate from three waste cells with five "cans" per cell. The transport pulses travel up either the air shaft or the main shaft. Groups 2 and 3 are retarded in the upper aquifer. Figure 2-8B shows the group-by-group summation of the pulses (dotted lines) and the total of all groups (solid line). Our studies have shown that the envelope of waste flux Fig. 2-8B, is essentially insensitive to the exact shape of individual pulses. Gaussian or Gaussian-like pulses convoluted with step-function releases produce essentially the same envelope.

Biological Impact Submodel. The fourth submodel describes the biological impact. To provide a spectrum of results compatible with today's regulations, we use two models: a dose model for an individual drinking water from a well and a population dose model for the current Columbia River water use system—the Columbia River Population (CRP) model.

In general, the calculation of potential hazard or dose to man at any time, t, after release may be approximated by two pieces of information: (1) The value of the release function $J_r(t)$ in appropriate units of mass flow per year for nuclide type r, and (2) a hazard or dose function, $H_r(t)$, based on percent of inventory, toxicity, population, water use, and other human-related factors for nuclide type r, as indicated earlier under the waste package model.

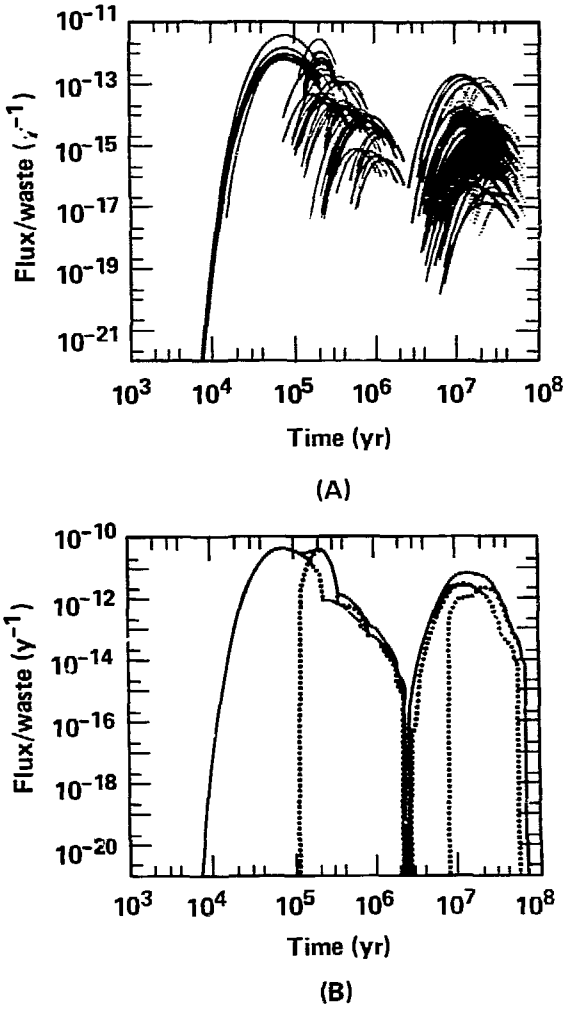

Figure 2-8. Pulses and their summation, which arrive at well above repository: (A) Gaussian-like flux pulses, which arrive vs time; (B) group-by-group (dotted lines) and total summation (solid line) of flux vs time.

The potential hazard or dose rate, D(t), is calculated by

$$D(t) = \sum_r J_r(t)\, H_r(t) \qquad (21)$$

in appropriate units, e.g., in curies, rems, or relative units per year. The peak dose is then given by

$$\hat{D} = \max_t |D(t)| \quad ,$$

occurring at time $\hat{t}$, and the total dose is given by

$$\underline{D} = \int_0^{\infty} D(t)dt \quad .$$

In the preceding section, we showed the calculation of the release functions $J_r^k(T_i)$ for nuclide group r at observation point k on the discretized output time line, T_i.

In MISER, the discretized time line is user defined by

$$T_i = T_1\, 10^{(i-1)/m},\ i = 1, 2, ..., I \quad ,$$

where T_1 is the user-specified minimum time of interest. If $\overline{T}$ is the user-specified maximum time of interest, then I is computed so that $T_{I-1} \leq \overline{T} < T_I$. The number of points per decade, m, is also user specified.

In the case of Monte Carlo calculations, the hazard/dose measures are discretized in the same manner, e.g., we have

$$\hat{D}_j = \hat{D}_1\, 10^{(j-1)/m},\ j=1, 2, ..., I \quad .$$

The outcome of each trial results in $\hat{D}$ and $\hat{t}$ for peak dose and time of peak. Then the counter for the bin (i,j) is incremented when

$$\hat{D}_{j-1/2} \leq \hat{D} < \hat{D}_{j+1/2}$$

and

$$T_{i-1/2} \leq \hat{t} < T_{i+1/2} \quad ,$$

where $x_{i+1/2} = x_1 10^{(2i-1)/2m}$ for x = D or T. Results that fall outside the range of interest are also counted.

MISER currently allows for estimation of potential hazard or dose in the three models discussed in the following sections.

BIODOSE Dose-To-Man Model. Human doses will depend on the movement of waste to wells or surface waters, the concentration in the ecosystem, human diets and living habits, and the biochemistry of the waste nuclides in the human body. These factors are modeled in the BIODOSE code[4,22,24] to produce a set of tables $H_r(t_j)$ for use in Eq. (21) in the manner described previously. In this case, the results are in rem or man-rem. The following discussion is essentially that from Ref. 4.

Environmental assessment of future releases requires consideration of the cycling of long-lived radionuclides in the biosphere and the possibility of local buildup and concentration. Because of vast uncertainty about future conditions, the basis of model predictions for times far into the future must be defined carefully. The basic philosophy of BIODOSE is to provide tools that can be used to evaluate the consequences of radionuclide release under conditions not too far removed from those experienced today.

Transport in surface water systems is calculated using a compartment or box model. Because the release of waste is expected to occur over long time periods, the surface water system is assumed to be in dynamic equilibrium with the input flow of the waste. This simplification allows one to calculate the doses per unit input flow of waste independent of the waste release function.

The transport model computes the concentrations of each radionuclide in soil, sediment, and water systems. The model is composed of compartments for each system and assumes uniform mixing within each compartment. The following dynamic processes, which affect concentration, are considered: dilution by mixing, diffusion between sediment and water, sedimentation, man's removal of water and food products, ion exchange, biogeochemical processes, and radioactive decay. The potential for accumulating radionuclides in the topsoil because of the irrigation of crop lands is also modeled. The complexity of this model is limited by the accuracy with which the transfer coefficients between compartments can be modeled.

The concentrations calculated for the sediment, topsoil, and water subsystems are used with a simple ecosystem model to give radionuclide dose rates to man. Doses are assumed to be received by ingestion and external exposure. The ingestion pathways modeled are drinking water, aquatic foods, irrigated crops, and farm animals. External exposure to both the water subsystems and the topsoil is considered. The pathways considered are summarized in Fig. 2-9.

Doses for individuals and populations are computed as a function of living habits and usage. Although estimates for the local demography are not possible far into the future, reasonable limits to potential population exposure can be developed. For example, the population dose from the aquatic food pathway depends on the net harvest, not on the size of the local population. Similarly, the vegetable and animal pathways depend primarily on the irrigation rate. Since these pathways are dominant, the potential population dose from a river system is relatively independent of the lo-

Table 2-3. Columbia River base-case calculation of potential dose to a worst-situated individual with an average diet and lifestyle (rem) for ^{129}I and ^{99}Tc (Group 1): SRP glass waste (curies/canister).[15]

time	body equiv	body	gi - lli	thyroid	bone	liver	lung	kidney	skin
0.	1.616e-06	9.218e-08	9.941e-06	5.989e-13	2.849e-07	3.845e-07	6.989e-13	5.589e-13	1.182e-12
1.0	1.604e-06	8.553e-08	1.036e-05	6.119e-13	2.134e-07	3.172e-07	6.119e-13	6.119e-13	1.224e-12
3.0	1.604e-06	8.553e-08	1.036e-05	6.119e-13	2.134e-07	3.172e-07	6.119e-13	6.119e-13	1.224e-12
10.	1.603e-06	8.553e-08	1.036e-05	6.119e-13	2.134e-07	3.172e-07	6.119e-13	6.119e-13	1.224e-12
30.	1.603e-06	8.553e-08	1.036e-05	6.118e-13	2.134e-07	3.172e-07	6.118e-13	6.118e-13	1.224e-12
1.00e+02	1.603e-06	8.551e-08	1.035e-05	6.117e-13	2.134e-07	3.171e-07	6.117e-13	6.117e-13	1.223e-12
3.00e+02	1.602e-06	8.545e-08	1.035e-05	6.113e-13	2.132e-07	3.169e-07	6.113e-13	6.113e-13	1.223e-12
1.00e+03	1.578e-06	8.526e-08	1.032e-05	6.099e-13	2.127e-07	3.162e-07	6.099e-13	6.099e-13	1.220e-12
3.00e+03	1.567e-06	8.470e-08	1.026e-05	6.059e-13	2.114e-07	3.141e-07	6.059e-13	6.059e-13	1.212e-12
1.00e+04	1.038e-06	8.283e-08	1.003e-05	5.923e-13	2.066e-07	3.070e-07	5.923e-13	5.923e-13	1.185e-12
3.00e+04	1.527e-06	7.758e-08	9.394e-06	5.550e-13	1.936e-07	2.877e-07	5.550e-13	5.550e-13	1.110e-12
1.00e+05	1.216e-06	6.177e-08	7.480e-06	4.419e-13	1.541e-07	2.291e-07	4.419e-13	4.419e-13	8.838e-13
3.00e+05	5.242e-07	3.722e-08	3.992e-06	2.365e-13	8.241e-08	1.195e-07	2.365e-13	2.365e-13	4.612e-13
1.00e+06	5.560e-08	3.303e-09	3.999e-07	2.363e-14	8.241e-09	1.225e-08	2.363e-14	2.362e-14	4.725e-14

Table 2-4. Columbia River base-case calculation of potential dose to a worst-situated individual with an average diet and lifestyle (rem) for fission products inventory type (Group II): SRP glass waste (curies/canister).[15]

time	body equiv	body	gi - lli	thyroid	bone	liver	lung	kidney	skin
0.	2.187e+00	3.591e+00	5.688e-01	2.139e-03	1.243e+01	1.147e+00	2.142e-03	4.861e-01	2.512e-03
1.0	2.415e+00	3.956e+00	6.341e-01	7.859e-03	1.391e+01	1.128e+00	7.863e-03	4.825e-01	8.256e-03
3.0	2.691e+00	4.396e+00	7.267e-01	1.593e-02	1.572e+01	1.098e+00	1.593e-02	3.948e-01	1.861e-02
10.	2.762e+00	4.498e+00	7.757e-01	3.837e-02	1.628e+01	9.624e-01	3.837e-02	3.643e-01	4.481e-02
30.	1.812e+00	2.925e+00	5.326e-01	5.775e-02	1.051e+01	6.539e-01	5.775e-02	2.688e-01	6.747e-02
1.00e+02	3.398e-01	5.412e-01	1.861e-01	2.113e-02	1.894e+00	1.438e-01	2.113e-02	6.441e-02	2.478e-02
3.00e+02	2.672e-03	4.289e-03	9.262e-04	2.526e-04	1.488e-02	1.494e-03	2.561e-04	6.937e-04	3.417e-04
1.00e+03	3.614e-06	2.191e-06	5.887e-06	1.824e-06	4.876e-06	6.387e-06	4.595e-06	5.885e-06	1.455e-06
3.00e+03	3.466e-06	2.095e-06	4.699e-06	9.388e-07	4.782e-06	5.168e-06	4.585e-06	5.630e-06	1.831e-06
1.00e+04	3.489e-06	2.861e-06	4.646e-06	9.334e-07	4.764e-06	4.991e-06	4.486e-06	5.333e-06	1.826e-06
3.00e+04	3.264e-06	1.973e-06	4.587e-06	9.266e-07	4.713e-06	4.549e-06	4.435e-06	4.596e-06	1.812e-06
1.00e+05	2.985e-06	1.758e-06	4.135e-06	8.769e-07	4.541e-06	3.543e-06	4.268e-06	2.948e-06	9.643e-07
3.00e+05	2.421e-06	1.475e-06	3.518e-06	7.633e-07	4.086e-06	2.598e-06	3.881e-06	1.552e-06	8.394e-07
1.00e+06	1.636e-06	1.026e-06	2.264e-06	4.697e-07	2.857e-06	1.873e-06	2.577e-06	1.847e-06	5.165e-07

Table 2-5. Columbia River base-case calculation of potential dose to a worst-situated individual with an average diet and lifestyle (rem) for actinide inventory type (Group III): SRP glass waste (curies/canister).[15]

time	body equiv	body	gi - lli	thyroid	bone	liver	lung	kidney	skin
0.	1.444e-03	5.171e-04	2.693e-03	4.599e-06	1.486e-02	3.289e-03	4.599e-06	2.989e-03	1.315e-05
1.0	1.438e-03	5.158e-04	2.678e-03	5.153e-06	1.398e-02	3.279e-03	5.153e-06	2.981e-03	1.418e-05
3.0	1.425e-03	5.132e-04	2.649e-03	6.252e-06	1.383e-02	3.258e-03	6.252e-06	2.966e-03	1.688e-05
10.	1.383e-03	5.039e-04	2.549e-03	1.882e-05	1.332e-02	3.185e-03	1.882e-05	2.911e-03	2.242e-05
30.	1.268e-03	4.775e-04	2.285e-03	2.882e-05	1.194e-02	2.977e-03	2.882e-05	2.758e-03	3.983e-05
1.00e+02	9.574e-04	4.811e-04	1.596e-03	4.655e-05	8.337e-03	2.369e-03	4.655e-05	2.259e-03	8.886e-05
3.00e+02	5.484e-04	2.868e-04	7.539e-04	7.565e-05	3.985e-03	1.457e-03	7.565e-05	1.473e-03	1.198e-04
1.00e+03	2.224e-04	1.574e-04	2.583e-04	4.357e-05	1.415e-03	4.987e-04	4.357e-05	5.286e-04	7.478e-05
3.00e+03	2.848e-04	3.158e-04	7.655e-05	8.384e-06	1.182e-03	8.838e-05	8.384e-06	9.559e-05	2.239e-05
1.00e+04	9.231e-04	1.698e-03	8.278e-05	2.866e-05	3.868e-03	1.786e-04	2.866e-05	8.226e-05	3.556e-05
3.00e+04	2.888e-03	5.396e-03	1.348e-04	5.541e-05	1.147e-02	4.773e-04	5.541e-05	1.842e-04	7.465e-05
1.00e+05	6.841e-03	1.288e-02	2.586e-04	1.263e-04	2.697e-02	1.022e-03	1.263e-04	3.485e-04	1.514e-04
3.00e+05	7.368e-03	1.387e-02	2.785e-04	1.372e-04	2.918e-02	1.026e-03	1.372e-04	1.572e-04	1.633e-04
1.00e+06	1.266e-03	2.353e-03	7.652e-05	2.928e-05	5.223e-03	1.686e-04	2.928e-05	3.375e-05	3.459e-05

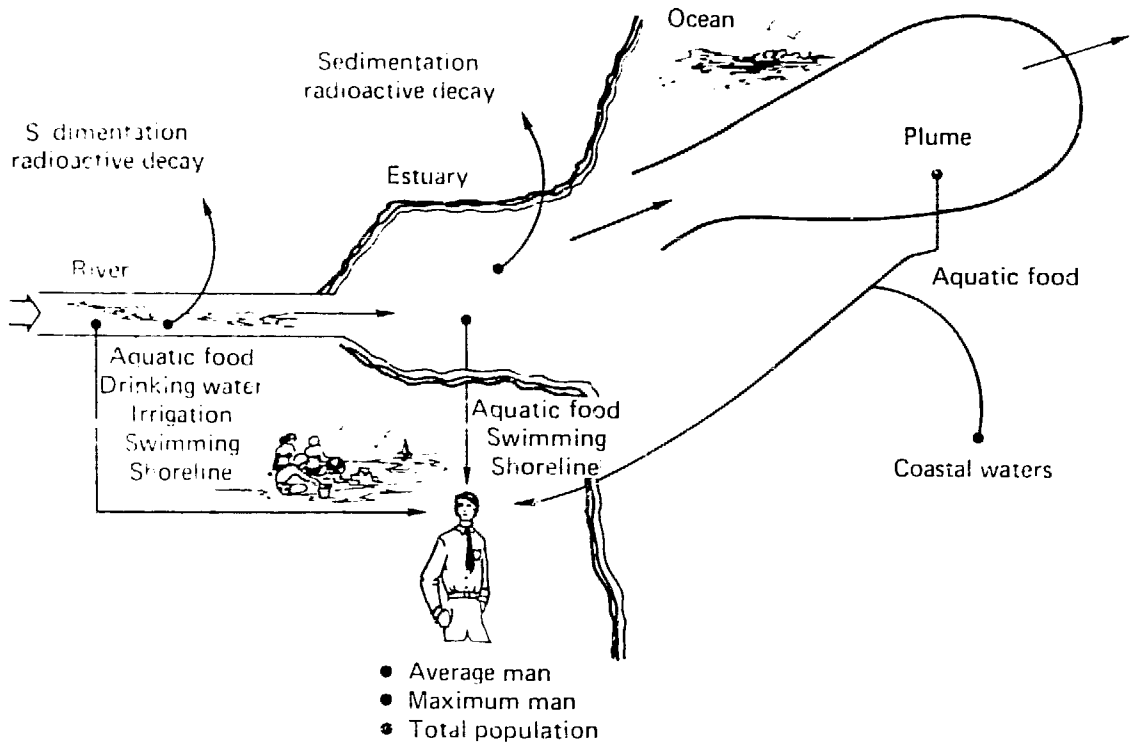

Figure 2-9. Pathways modeled in BIODOSE.

cal demography. Population doses were, therefore, based on estimates of the usage rates of the water system rather than on population.

Tables 2-3 through 2-5 show dose values, based on the Columbia River system of usage, for the 53 significant nuclides per canister of Savannah River defense waste. Figures 2-10 through 2-13 are time-dependent plots of dose to the liver of an individual using surface water.

Well-Release Scenario Dose-To-Man Model. The dose-to-man model is intended to display a performance measure sensitive to engineered features (including waste-form performance) in high-level nuclear waste repositories. This obviously precludes a long transport scenario that masks the effects of design factors.

We would also like to choose a performance measure that has been used traditionally in the regulation of the nuclear fuel cycle, i.e., individual dose. Acceptable population doses have been achieved by regulating the maximum dose to the public and to individuals in the nuclear work force.

Our measure of repository design performance is the standard man who drinks 2.2 litres of water per day from a well located just downstream from the shaft of our repository. Depending on the placement of the well and shaft relative to the repository, the standard man will receive dose from the flow of radioactivity from the shaft or through the barrier media, or both. The shaft radioactivity will be diluted during the flow from the shaft to the well. The amount of dilution depends on the distance of travel, as well as on the relative amounts of water flow in the shaft and aquifer.

We consider a "sampling well" whose diameter is smaller than that of the shaft and assume that the withdrawal rate is slow enough to ensure that the magnitude and direction of aquifer water velocity are unaffected by well operation. Piezometric heads in the aquifer also remain unchanged, and we assume that the well samples the aquifer water uniformly with respect to depths. Further, to study the "worst-case" dose to man, we assume that both the well and shaft are placed on the centerline of the repository.

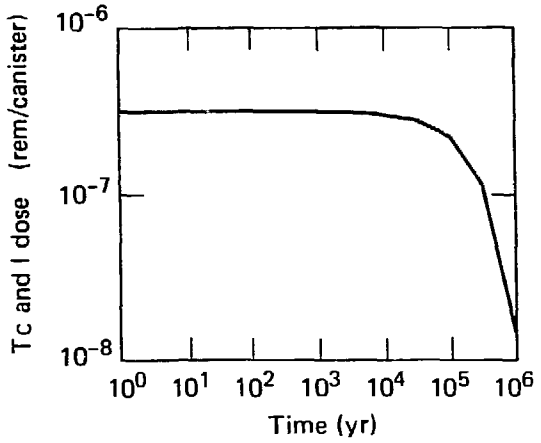

Figure 2-10. Group I dose to liver (from Table 2-1).

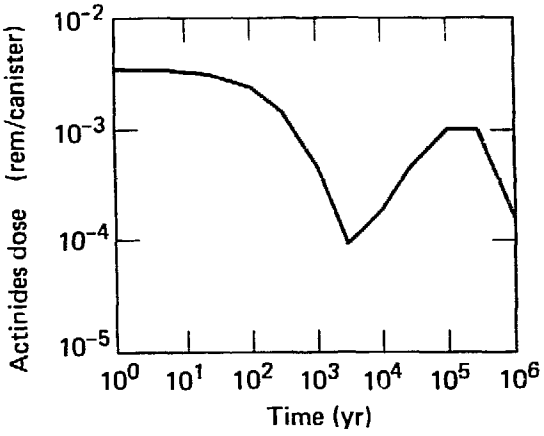

Figure 2-12. Group III dose to liver (from Table 2-3).

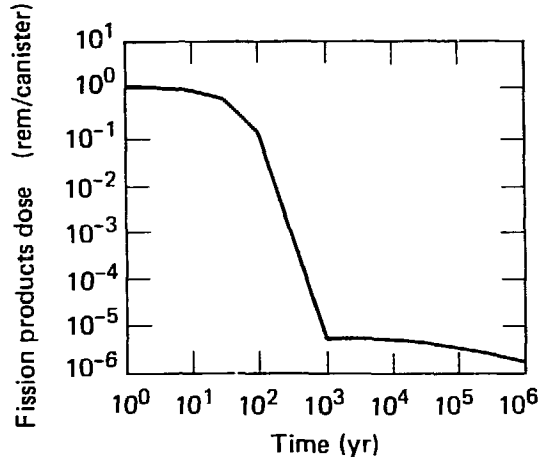

Figure 2-11. Group II dose to liver (from Table 2-2).

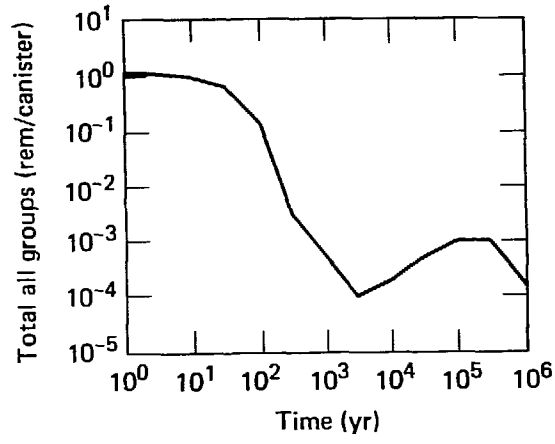

Figure 2-13. Summation of all group doses to liver (from Tables 2-1 through 2-3).

Appendix F of Ref. 22 shows that, on the centerline, the concentration in the aquifer, from a continuous source f, can be approximated by

$$C \approx \frac{f}{4\eta_a b\, q_a [\pi(\alpha - 2\mu)x]^{1/2}} \quad , \tag{22}$$

where

η_a is the effective porosity
b is the thickness of the aquifer
q_a is the actual water velocity
$\alpha - 2\mu$ is the lateral dispersion constant

and x is the distance from the source, f. Clearly, we must restrict x so that the denominator is greater than or equal to 1.

Let x be the distance from the shaft to the well. Then, if

$$F_S \equiv 4\eta_a q_a b [\pi(\alpha - 2\mu)\, x]^{1/2} < 1 \quad , \tag{23}$$

we consider an approximation based on Fig. 2-14. Here we assume that there are no effects from lateral dispersion and that a well will mix the water in the vertical direction.

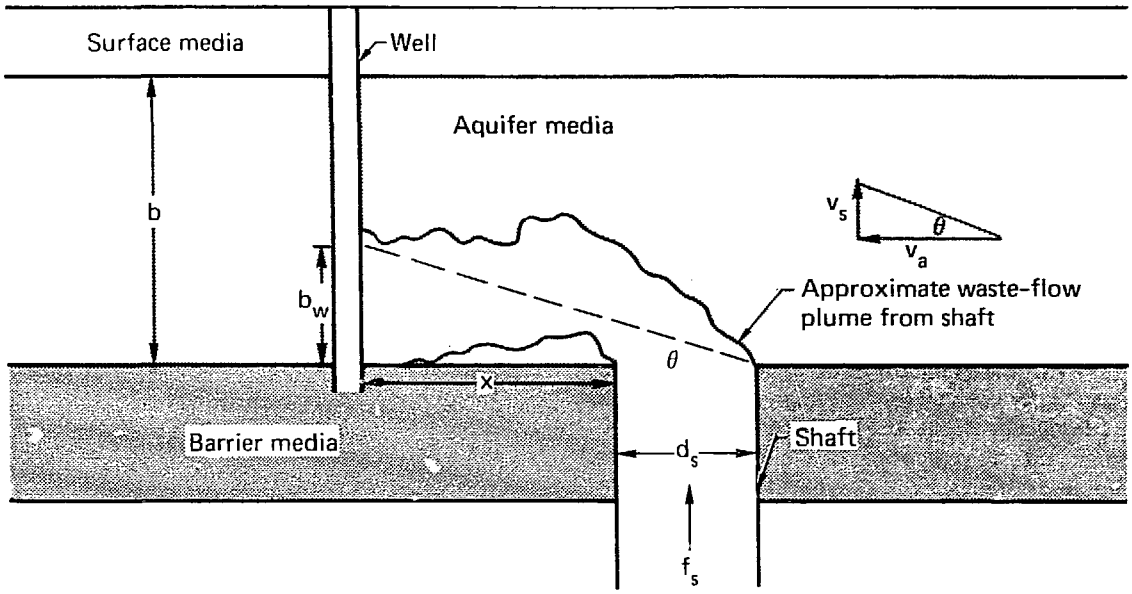

Figure 2-14. Schematic for close-to-shaft well-concentration calculation, with $b_w = (x + d_s) \tan \theta$.

We assume a circular shaft for which we have input the cross-sectional area A_s so that its diameter is

$$d_S = 2(A_S/\pi)^{1/2} \quad .$$

Then, from the figure, we compute

$$F_{NS} = Q_S \min\left[1, \frac{(d_S + x)\, v_s}{b\, v_a}\right] \quad , \tag{24}$$

where $v = q\eta$ is the D'Arcy velocity in the shaft or aquifer and Q_S is the D'Arcy flux in the shaft.

For flow through the media to the aquifer, we compute the dilution factor by

$$F_M = a\, b\, q_a\, \eta_a \quad , \tag{25}$$

where

a is the width of the repository
b is the thickness of the aquifer
$q_a\eta_a$ is the water velocity in the aquifer.

In each case, F_S, F_{NS}, and F_m are in cubic metres per year.

In our transport and release models, we have computed the release function at observation point k to give $J_r^k(\sigma_r,\tau_r;T)$ in units of initial inventory per year, e.g., canisters/year or MWe-year/year, at the discretized time points T_i for nuclide-retardation group r. We then note that

$$C_r^k \equiv \frac{J_r^k}{F_m}$$

for m = S, NS, or M gives us concentration of a nuclide group r, e.g., canisters per cubic metre.

We assume that our standard man consumes all his water from the well at the rate of 2.2 litres per day. Then, for example,

$$C_r^k \frac{\text{canisters}}{\text{m}^3} \times \frac{2.2 \text{ litres}}{\text{day}} \times \frac{365 \text{ days}}{\text{year}} \times \frac{0.001 \text{ m}^3}{\text{litre}}$$

gives

$$\bar{C}_r^k = 0.803\, J_r^k/F_m \frac{\text{canisters}}{\text{year}} \tag{26}$$

of nuclide group r at observation point k with well scenario m = S, NS, or M.

If we use the potential hazard tables produced by the ORIGEN code in the same manner as we did in the "Waste Package" section, then

$$\bar{D}_r^k(T_i) = H_r(T_i)\,\bar{C}_r(T_i)$$

$$= 0.803\,\frac{J_r^k(T_i)}{F}\,H_r(T_i)\,\frac{C_i}{\text{year}} \qquad (27)$$

is a potential hazard measure.

The equivalent whole-body dose, 50-year commitment discussed in Ref. 25, provides a rational method for combining doses to different organs from different radionuclides into a single dose measure. This dose measure can then be used to analyze repository-engineered features.

The basic quantity used for such a combination is the "annual limit of intake" (ALI) for each radionuclide. If an ALI for nuclide n is ingested, then the 50-year dose commitment is 5 rem. Table 2-6 is a listing of ALI for numerous nuclides in becquerels (Bq); we note that one curie = 3.7 $\times 10^{10}$ Bq.

Under our assumptions, we may write the effective annual whole-body dose from nuclide n by

$$D_n^k(T_i) = 3.7 \times 10^{12}\,\bar{D}_r^k(T_i)/\text{ALI}_n\,\frac{\text{rem}}{\text{yr}} \quad , \qquad (28)$$

where $D_r^k(T_i)$ is from Eq. (27), with r chosen so that nuclide n is a member of retardation group r and ALI_n (in Bq), the annual limit of intake, is from Table 2-6.

Then, the final dose is obtained by summation so that

$$D^k(T_i) = \sum_n D_n^k(T_i)\,\frac{\text{rem}}{\text{yr}} \quad . \qquad (29)$$

Uncertainty in the Biological Impact Models. A dosimetry subprogram is used to compute hazards on the basis of length of exposure and period of dose commitment. Doses are computed for the whole body and seven body organs. In addition, an effective "whole-body-equivalent" dose commitment is computed by aggregating doses according to their contribution to cancer risk.

There is no uncertainty in the biological impact models as used in this work and elsewhere. Conceptually, they are used as a monitoring device to obtain relative information. The population model is really extremely uncertain. If these uncertainties were incorporated in the analysis, the dose results recorded would be much more scattered than they are.

A population model is necessary to provide a method of cost/benefit analysis. Since we are mainly concerned with the effects of the physical parameters, and how these uncertainties affect the long-term hazard, fixing the population model does not seem unreasonable. If population dose becomes the accepted measure of future risk, using a probabilistic population model would be appropriate, and much larger fluctuations in the results would be expected due to population uncertainties.

Table 2-6. Annual limits of intake for nuclear industry workers.

Nuclide	ALI (Bq)	Nuclide	ALI (Bq)
^{243}Am	8×10^4	^{93m}Nb	5×10^8
^{241}Am	8×10^4	^{93}Zr	2×10^8
^{240}Pu	4×10^5	^{90}Sr	2×10^6
^{239}Pu	4×10^5	^{79}Se	7×10^7
^{238}Pu	5×10^5	^{59}Ni	1×10^9
^{237}Np	5×10^3	^{126}Sn	2×10^7
^{238}U	7×10^5	^{239}Np	5×10^7
^{235}U	6×10^5	^{225}Ac	2×10^6
^{234}U	6×10^5	^{225}Ra	5×10^5
^{233}U	6×10^5	^{223}Ra	3×10^5
^{231}Pa	1×10^3	^{126}Sb	2×10^7
^{232}Th	7×10^3	^{90}Y	2×10^7
^{230}Th	4×10^5	^{244}Cm	2×10^5
^{229}Th	5×10^4	^{242}Cm	3×10^6
^{227}Ac	1×10^5	^{241}Pu	2×10^7
^{228}Ra	2×10^5	^{147}Pm	2×10^8
^{226}Ra	1×10^5	^{144}Ce	9×10^6
^{210}Po	1×10^5	^{134}Cs	3×10^6
^{210}Pb	5×10^4	^{106}Ru	9×10^6
^{154}Eu	3×10^7	^{95}Nb	8×10^7
^{151}Sm	6×10^8	^{95}Zr	5×10^7
^{137}Cs	4×10^6	^{91}Y	2×10^7
^{135}Cs	3×10^7	^{89}Sr	2×10^7
^{129}I	5×10^5	^{242m}Am	7×10^4
^{107}Pd	1×10^9	^{242}Pu	5×10^5
^{99}Tc	2×10^8	^{236}U	6×10^5

Monte Carlo Procedure. Uncertainty analysis with MISER is accomplished using a simple Monte Carlo approach. At each trial a full set of input parameters is generated and a peak dose and time of peak dose are computed. The input parameter selection may involve correlations and/or constraints. The computed outputs are counted as "hits" in the bins of a discretized output space to form frequency histograms and probability curves. A detailed discussion of the procedure as implemented in MISER follows.

Nested Loops and Order of Selection. The Monte Carlo is written as a set of nested do-loops

in the code. The outermost loop involves the network solution of the hydrology and selection of heads (boundary conditions), path lengths, areas, and permeabilities. The second loop involves water flow speed and dispersion using effective porosity and longitudinal dispersivity. The third loop computes nuclide transport time and involves the geochemical retardation factors. The innermost loop computes the waste release from the canister breach time and waste release rate. The user may specify the number of trials at each level.

Selection of Parameter Values. The analyst may specify any parameter as certain or uncertain. If uncertain, the parameter is selected from a specified distribution using a pseudo-random number generator which chooses a number, r, from the interval [0,1]. For normal or log-normal distributions we then compute x by linear interpolation in the normal (0,1) probability table so that prob (x) = r. if no correlations or constraints are involved, then we choose the parameter, p, by

$p = \mu + \sigma x$ if p is from normal (μ,σ)
$p = \mu\sigma^{x}$ if p is from log-normal (μ,σ)
$p = a + r\,(b - a)$ if p is uniform [a,b].

Constraints. In some cases the distribution specification and random selection procedure may choose parameters that violate physical or model constraints. In these cases we either rechoose or modify the selected parameter. In particular we rechoose parameters whenever

Hydraulic head < 0
Canister breach time ≤ 0
Waste dissolution time ≤ 0.

And, for each path, whenever

Length ≤ 0
Area ≤ 0
Permeability ≤ 0
Effective porosity ≤ 0 or ≥ 1
Longitudinal dispersivity ≤ 1
Retardation < 1.

We modify parameters as follows:

If actinide retardation (R_3) $\leq$ cation fission product retardation, (R_2), then $R_3 = R_2(1 + r)$.

If longitudinal dispersivity (α) > path length/10, then α = path length/10.

All but the last of these constraints are physical. The final constraint is discussed in the section, "Nuclide Transport Submodel."

The analyst may also specify that the upper and lower horizontal gradients are to be chosen in a manner such that they are equal. If, for example, only four heads are specified as boundary conditions (e.g., H_{UL}, H_{UR}, H_{LL}, H_{LR}), then the upper horizontal gradient is a function of $H_{UL} - H_{UR}$. The vertical gradient is chosen as a function of $H_{LL} - H_{UR}$. Then H_{LI} is computed so that the lower horizontal gradient is equal to the upper horizontal gradient.

Correlations. When the uncertain parameters are specified by normal or log-normal distributions, the analyst may also specify pairwise correlations. Although these correlations may not be well known in every case, there may be reasonable relationships based on measurement or model considerations. For example, if we assume that a given layered medium is homogeneous, then there is a perfect correlation between hydrogeologic parameters for each path in that medium. Golder Associates[26] have also reviewed numerous measurements of permeability and effective porosity. In some cases they have derived empirical relationships of correlations. Our procedure is for a sequential string of pair-by-pair correlations in the order of choices with no feedback. We use the covariance matrix methodology of Oplinger.*[27]

In particular, suppose ρ_1 and ρ_2 are both normal (μ_1,σ_1) and (μ_2,σ_2), respectively, with correlation coefficient ρ. Then, choosing two pseudo random numbers, x_1 and x_2 from normal (0,1), compute

$$\rho_1 = \sigma_1 x_1 + \mu_1$$

$$\rho_2 = \rho_2^{\sigma} x_1 + \sigma_2 x_2 \sqrt{1 - \rho^2} + \mu_2 \quad .$$

Appropriate use of logarithmic values extends this methodology to log-normal correlations. Figure 2-15 is a plot of normalized choices of two parameters chosen with correlation coefficient of 0.7. Figure 2-16 compares normalized choices for uncorrelated parameters. Both plots are ordered by decreasing values of the solid line parameter, not by order of Monte Carlo trial. The reader may easily observe the effects of correlations.

*Oplinger's methodology is written for an arbitrary number of parameters; however, there is currently no real justification for implementation in MISER.

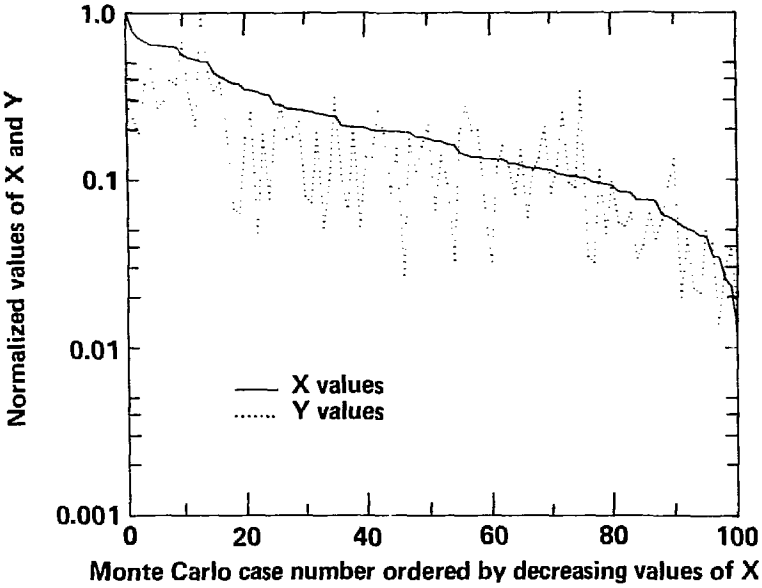

Figure 2-15. Plot of normalized choices of two parameters chosen with correlation coefficient of 0.7.

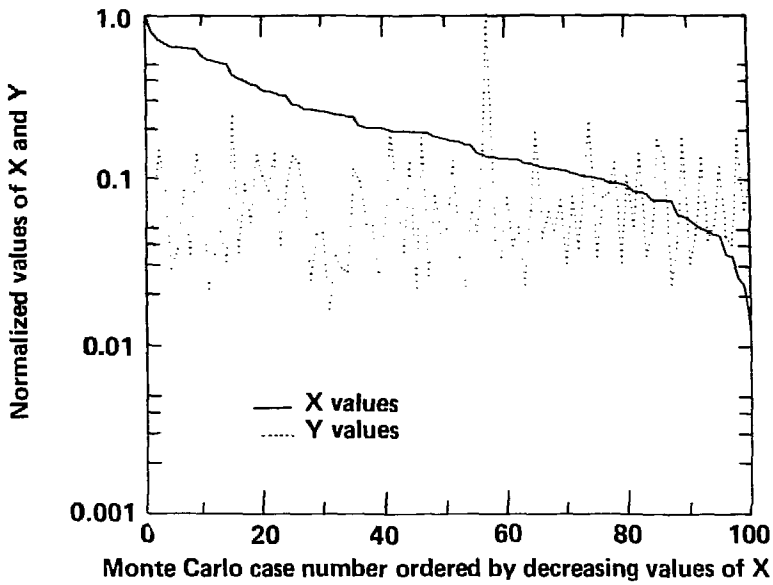

Figure 2-16. Comparison of normalized choices for uncorrelated parameters (both plots are ordered by decreasing values of solid line parameter, not by order of Monte Carlo trial).

Monte Carlo Output. The output space for peak dose and time of peak dose is a jointly distributed frequency distribution. The space is discretized by $D_i = 10^{i/I}$ and $T_i = 10^{i/j}$, i,j = 0, ±1, ±2,..., where I and J are the numbers per decade specified by the user. If, for trial, n, we compute peak dose, $\hat{d}_n$ occurring at time $\hat{t}_n$, and if

$$D_i \leq \hat{d}_n < D_{i+1}, \; T_j \leq \hat{t}_n < T_{j+1}$$

we set $H_{i,j} = H_{i,j} + 1$ (i.e., a "hit" in this bin at trial n). Extraction of marginal frequency distributions e.g., $(\sum_j H_{i,j} = h_i)$, produces a histogram prob $(D_i) = h_i/N$, of peak dose which, for N trials, may be converted to the risk curves of the following section.

References

1. T. F. Harvey, *Suggested Technical Scheme to Help Resolve Regulatory Issues*, Lawrence Livermore National Laboratory, Livermore, Calif., UCID-17858 (1978).
2. *Earth Science Technical Plan for Disposal of Radioactive Waste in a Mined Repository* (draft), Office of Nuclear Waste Management, U.S. Department of Energy and Geological Survey, DOE/TIC-4033 (1980).
3. L. L. Edwards, *MACRO1: A Code to Test a Methodology for Analyzing Nuclear Waste Management Systems*, Lawrence Livermore National Laboratory, Livermore, Calif., UCRL-52736 (1979).
4. B. I. Ross et al., *NUTRAN: A Computer Model of Long-Term Hazards from Waste Repositories*, The Analytical Sciences Corporation, Reading, Mass. (1979).
5. J. E. Campbell, P. C. Kaestner, B. S. Langkopf, and R. B. Lantz, *Risk Methodology for Geologic Disposal of Radioactive Waste: The Network Flow and Transport (NWFT) Model*, Sandia National Laboratory, Albuquerque, N.M., NUREG/CR-1190, SAND 79-1920 (1980).
6. A. M. Kaufman, L. L. Edwards, and W. F. O'Connell, "A Repository Post-Sealing Risk Analysis Using MACRO," in *Proc. Symp. Waste Mgmt., Tuscon, Arizona, 1980*, 109.
7. H. Cheung, L. L. Edwards, T. F. Harvey, D. D. Jackson, and M. A. Revelli, *Nuclear Waste Form Risk Assessment for U.S. Defense Waste at Savannah River Plant—Annual Report FY 1981*, Lawrence Livermore National Laboratory, Livermore, Calif. (1981).
8. R. Heckman, D. Towse, D. Isherwood, T. Harvey, and T. Holdsworth, *High Level Waste Repository Site Suitability Study--Status Report*, Lawrence Livermore National Laboratory, Livermore, Calif., UCRL-52633, NUREG/CR-0578 (1979).
9. T. G. Naymik and L. D. Thorson, *Numerical Simulation of Transport in a Regional Groundwater Flow System*, Lawrence Livermore National Laboratory, Livermore, Calif., UCRL-52556 (1978).
10. G. E. Raines, "Development of Reference Repository Conditions," in *Proceedings of the 1980 National Waste Terminal Storage Program Information Meeting*, Office of Nuclear Waste Isolation, Columbus, Ohio, ONWI-212 (1980), pp. 310–315.
11. *Nuclear Waste Isolation Activities Report*, Office of Nuclear Waste Isolation, Columbus, Ohio (1979).
12. L. L. Edwards and T. F. Harvey, *A High-Level Waste-Repository Excavation Model and Limiting Individual Dose*, Lawrence Livermore National Laboratory, Livermore, Calif., UCRL-86849 (1981).
13. T. Harvey, R. A. Heckman, D. F. Towse, D. Isherwood, and T. Holdsworth, *Site Suitability Criteria for Solidified High Level Waste Repositories*, Lawrence Livermore National Laboratory, Livermore, Calif., UCRL-52633 (1977).
14. Arthur D. Little, Inc., *Assessment of Accidental Pathways*, Draft Subtask D Report, Vol. I, C-80560 (1978).
15. T. H. Gould, Savannah River Laboratory, Aiken, S.C., private communication (May 23, 1980).
16. M. J. Bell, *ORIGEN - The ORNL Isotope Generation and Depletion Code*, Oak Ridge National Laboratory, Oak Ridge, Tenn., ORNL-462ℓ (1973).
17. T. H. Gould, Savannah River Laboratory, Aiken, S.C., private communication (January 22, 1982).
18. P. F. DuBois and R. C. Basinger, *MATHLIB*, Lawrence Livermore National Laboratory, Livermore, Calif., LCSD-442, Rev. 0 (1980).

19. A. M. Kaufman, *Waste Pipe Calculus*, Lawrence Livermore National Laboratory, Livermore, Calif., UCID-17953 (1978).
20. W. J. O'Connell, *Waste Pipe Calculus Extensions*, Lawrence Livermore National Laboratory, Livermore, Calif., UCID-18136 (1979).
21. M. J. Bell, *ORIGEN—The ORNL Isotope Generation and Depletion Code*, Oak Ridge National Laboratory, Oak Ridge, Tenn., ORNL-4628 (1973).
22. L. E. Berman et al., *Analysis of Some Nuclear Waste Management Options*, Lawrence Livermore National Laboratory, Livermore, Calif., UCRL-13917, Vols. I and II (1978).
23. S. G. Oston, *Finite Medium Green's Functions Solutions to Nuclide Transport in Porous Media*, The Analytical Sciences Corporation, Reading, Mass., TR-1485-2 (1979).
24. N. A. Bonner and Y. C. Ng, *BIODOSE: A Code for Predicting the Dose to Man from Radionuclides Released from Underground Nuclear Waste Repositories*, Lawrence Livermore National Laboratory, Livermore, Calif., UCID-18652 (1980).
25. Committee 2, International Commission on Radiological Protection, "Limits for Intakes of Radionuclides by Workers," *Radiation Protection*, ICRP 30, Part 1 (Pergamon Press, N.Y., 1978).
26. *Second Report: Development of Site Suitability Criteria for the High-Level Waste Repository for Lawrence Livermore National Laboratory*, Golder Associates, Kirkland, Wash., Lawrence Livermore National Laboratory, Livermore, Calif., UCRL-13755-2 (1977).
27. J. L. Oplinger, *Generation of Correlated Pseudo-Random Numbers for Monte Carlo Simulations*, M.S. thesis, University of Pennsylvania, Moore School of Electrical Engineering, Philadelphia, Penn. (May 1971).

3. Analytical Results

Our approach to predicting the consequences of defense high-level waste disposal is twofold. First, we construct a method that relies on data and is representative of a repository site with a credible excavation design. This requires calculation of the effects of system uncertainties and excavation detail. Secondly, we focus on a "basecase" (normal), uneventful, bedded-salt scenario with only SRP defense HLW in the repository.* The basecase doses are compared with other doses from representative scenarios, including disruptive events and different waste form release rates. We explored the effects of mine design features upon doses.

The bedded-salt repository with a simple yet realistic excavation design is studied in the next subsection "Basecase Repository—Uneventful Layered Salt." In "Alternative Waste Forms," the effects of a lower waste form release rate are given as functions of different sites and designs, and the effects of different health standards and future disruptive events are discussed. The way in which understanding waste form behavior affects our results is studied in the subsection "Release Rates and Uncertainties" by using ranges of median release rates and uncertainties. The effects of mine design features were studied additionally under the subsection "Point-Source and Extended-Source Models" in which the limitations of the point-source model (PSM) are discussed and the results from PSM analyses are compared with those from the extended-source model (ESM). We make a comparison study with Sandia's NWFT and SWIFT codes in the subsection entitled "Comparison of MISER and Other Models." In the subsection called "Sensitivity and Uncertainty Analyses" we look at the deterministic sensitivity of various parameters, the statistical correlations with some important parameters, and the effects of the selection of the number of trials have on the precision of our statistical results. We also look at extrapolations to higher confidence levels using lognormal distributions.

*An alternative design scenario would be to intersperse defense HLW with commercial waste in a licensed repository.

Basecase Repository – Uneventful Layered Salt

Generic Layered-Salt Repository

Our generic, layered-salt repository model includes general features of sedimentary basins containing bedded salt. We do not attempt to include specific details of any particular basin. It is intended as a model with the data characteristics of a real basin that has had a moderate amount of exploration.

For our basecase, we follow the generic, layered-salt basin developed by Naymik and Thorson.[1] This basin contains a locally extensive bedded-salt layer that is discontinuous over the entire basin. Figure 3-1A shows its cross section, together with the assumed location of the repository. The basin consists of five layers. The central repository layer is bedded salt. It is the least permeable and is sandwiched between two essentially identical shale layers. There are two outer layers of sandstone. These are identical to each other except for thickness. The horizontal distance from the repository to the river is 20 km. The distance to the well at the edge of the accessible environment is 1.6 km. A vertical head drop of approximately 5.75 m between the aquifers and a horizontal gradient of 0.001 m/m are assumed.

The repository is situated in a local area of high integrity where the salt bed is quite extensive. On the regional scale, there will be interconnections of the aquifer layers through the barrier rock and salt layers, possibly including joints, faults, and breccia pipes. The rock parameters in the local area around the repository will differ from the regional averages because variability over the region is to be expected. Site exploration will ensure that the repository is placed in a local area with extra competent rock.

Horizontal motion of waste in this study will assume less importance than in Naymik and Thorsen's study because the ratio of vertical to horizontal gradient has been conservatively chosen here as approximately 10 times greater than it is in their work. The lower horizontal gradient leads to conservative near-field doses because: 1) the high ratio of vertical-to-horizontal gradient leads to more trials with waste migrating up the shafts, and 2) the low dilution factor in the upper aquifer leads to greater individual doses in the near field.

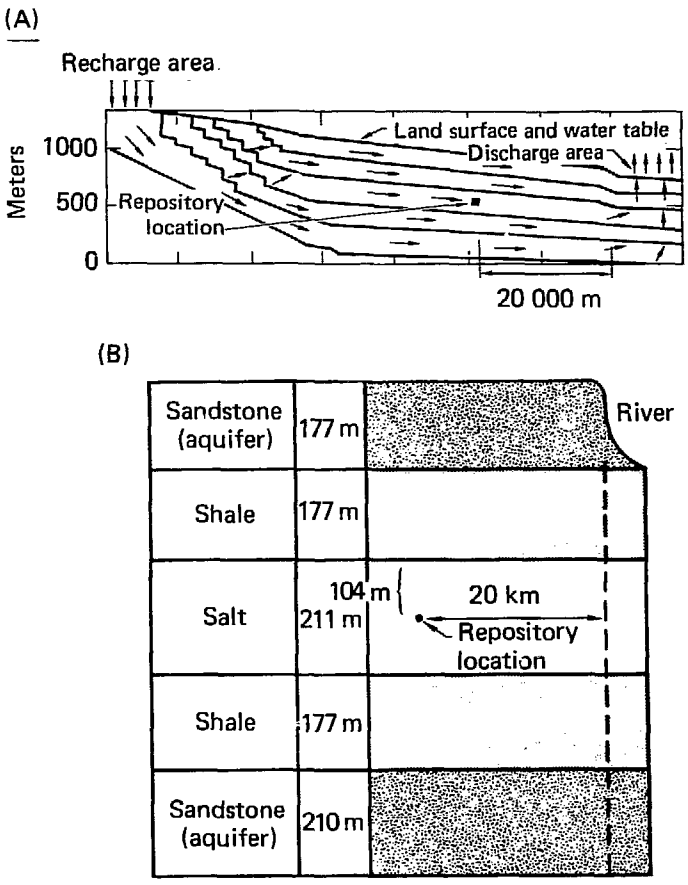

Figure 3-1. Cross sections of far-field and near-field layered-salt repository.

In some of our scenarios, the local area is assumed to contain isolated pathways, such as faults or fractures. These allow extra water and waste migration. (This is discussed in "Disruptive Events.")

Generic Geologic Data

The values of the hydrologic parameters chosen to characterize the repository region have been adopted from the LLNL Bedded Salt Report,[2] which, in turn, is supported by several authoritative sources, including studies by Geotechnical Engineering, Inc.,[3] Golder Associates, Inc.,[4-6] the LLNL Earth Sciences Department,[7] and U.S. Geological Survey.[8] Parameters for the five layers (shown in Fig. 3-1B) are tabulated in Table 2-1. Each entry is comprised of a median value (μ) and, where appropriate, a geometric standard deviation (σ).

Several correlations, constraints, and assumptions apply to the utilization of this data by the MISER code for any given analysis of a repository siting scenario in bedded salt. The values selected as input parameters to characterize the geohydrology of each flow path within a given layer are constant (i.e., there is no spatial variability of geologic parameters within a layer for a given trial run). Within each layer, the porosity, η, (constrained such that $0.0 < \eta \leq 1.0$) is correlated to the permeability, k, (constrained such that $k > 0.0$) by a factor of 0.8. The following correlations apply to the permeabilities associated with the various flow paths:

- Lower salt to upper salt with correlation coefficient of 0.8.
- Upper shale to upper salt with correlation coefficient of 0.7.

- Between storage rooms to upper salt with correlation coefficient of 0.8.
- Along storage rooms to tunnels/shafts with correlation coefficient of 0.8.

The dispersivity along any flow path is constrained to be less than or equal to 1/10 of the path length. Failure to impose this constraint would allow the physically unreal case of material exiting a flow path instantaneously upon entering. Nuclide retardation is assumed to occur only in the aquifer; absorption along other flow paths is considered negligible because of the high concentration of dissolved solids naturally present in the ground water. Retardation factors along the aquifer are as shown in Table 2-1 and are constrained such that 1.0 $\leq$ Group II retardation factor $\leq$ Group III retardation factor.

Flow Simulation

The defense HLW migration is simulated here with convective flow.[9] Some believe that salt and shale interbeds may not allow convection unless flawed. Migration in layered salt has been calculated[9] for both Brownian diffusion and convective flow. For the uneventful (unflawed) case, the doses from the diffusion simulation were orders of magnitude below those from the convective approach. Considering uncertainties of permeability of layered-salt basins, we have chosen the conservative convection simulation. Also, if there is an undetected flaw that would allow convective flow, the convective flow simulation of the unflawed scenario seems to provide a conservative probabilistic estimate of dose. If this convective flow assumption ultimately proves to be wrong, the appropriate diffusion calculation could lower results substantially. If our conservative forecasts are within acceptable standards, the diffusion approach would only lead to even more acceptable doses.[10]

Monte Carlo Results

A scenario trial requires a Monte Carlo sample be taken from each of the scenario's stochastic parameters. The samples are then used in a deterministic "process" calculation. The deterministic result is binned in the result space.* A distribution of the sampled results can be plotted as shown in Fig. 3-2, which displays our basecase results for the peak AEI dose.

*Only the computed outputs are binned. All uncertain parameters for each Monte Carlo trial are chosen from equivalent continuous parent distributions.

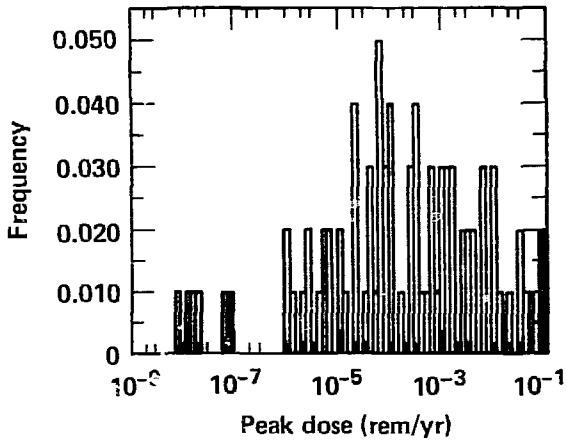

Figure 3-2. Frequency distribution of AEI peak dose rate for 100-trial Monte Carlo run for layered-salt (basecase) repository with REFERENCE waste form.

A 100-trial Monte Carlo run was made for the uneventful salt repository with basecase design and borosilicate glass waste form.* A "best estimate" (BE) of 0.06 mrem/yr AEI dose was obtained and is indicated in Fig. 3-2. The 90th percentile value in Fig. 3-2 is 10 mrem/yr and will be referred to as the 90%-confidence level (90CL) dose. This means that we have at least (because of our many conservative assumptions) 90% confidence that the future repository behavior will cause an AEI dose of less than 10 mrem/yr. This dose value is more than 100 times greater than the BE. To be extra conservative, we could use the 90CL as our performance measures.

Figure 3-3A shows the same result as Fig. 3-2, except the curve in Fig. 3-3A has been integrated to produce a cumulative curve. Although Fig. 3-3A doesn't show the detailed structure of Fig. 3-2, many who are using probabilistic risk information prefer it. In this report, the cumulative form is used to display our probabilistic results.

*The dose measures are binned with 10 bins/decade. We have compared the results of 5 independent runs of 100 trials each, as well as those of a 500-trial run. Generally, the statistics fall within ± 2 bins and the probability-dose-is-exceeded accumulant plots essentially lie over each other. In the counting process for percentiles, we choose the first bin in which the count exceeds the percentile. For example, the accumulant of bin n may contain 89% whereas bin n + 1 may contain 97%. In this case, the 90th percentile is associated with bin n + 1 dose values. We make no attempt to interpolate. This implies that, in general, the reported percentiles are on the conservative side. See also "Sensitivity and Uncertainty Analyses" below.

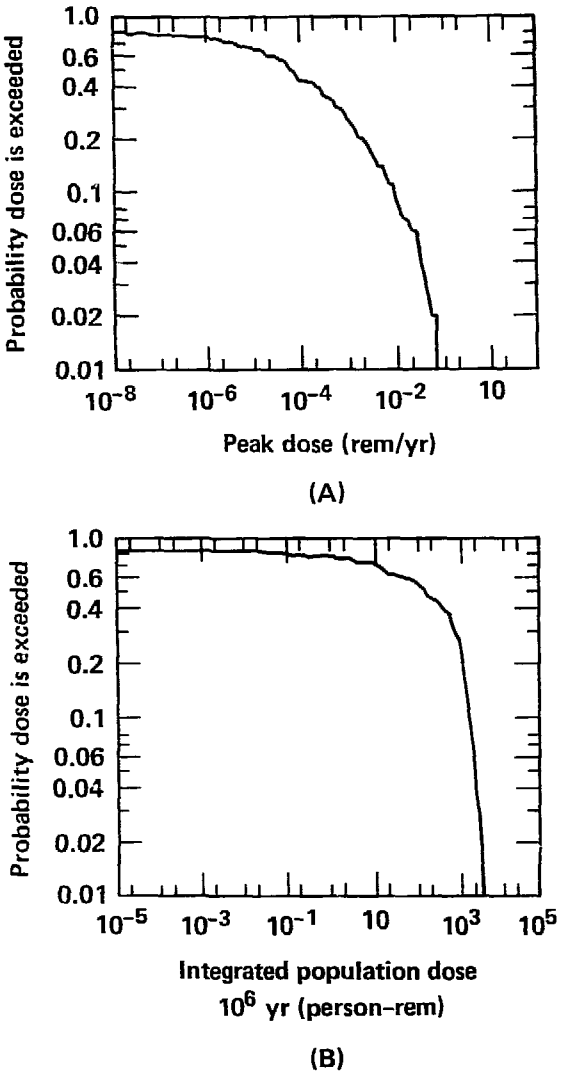

Figure 3-3. Cumulative distributions for layered-salt (basecase) repository: (A) same results as Fig. 3-2; (B) probabilistic results for million-year integrated population dose.

Note in Fig. 3-3A that 16% of the results was below 10^{-8} rem/yr. For these results radionuclides did not flow up the shaft. Thus, radionuclides had to migrate slowly through the upper aquitard to reach the biosphere. This either caused: 1) sufficient delay so that no dose was seen in one million years, or 2) dilution in the upper aquifer so great (due to the slow leakage of radionuclides from the upper aquitard into the aquifer) that 16% of the time, the peak dose in the first million years was below the lowest value on the scale. For population dose, our basecase results are integrated for one million years. Figure 3-3B shows our basecase population dose.

Table 3-1 is the expanded set of results for the uneventful scenario. Here, we have included performance measures of peak individual dose rate (rem/yr), integrated population dose (person-rem), and peak individual radioactivity ingested per year (Ci/yr). Across the top of Table 3-1 we see the 25th, 50th, 75th, 90th percentiles, and the maximum value of the dose obtained in 100 trials. The 50th percentile is our best-estimate result, and in most cases is similar to the result we would obtain if we used all median values to describe a scenario. The various performance measures are

- Limiting individual (LI): this individual has located his well about 0.25 km directly downstream from the shafts.
- Accessible environment individual (AEI): he is located 1.6 km downstream from the repository.
- Columbia River average individual (CRI)*: this individual is located 20 km away from the repository and is part of a community that uses the Columbia River water system. He has an average use pattern, but eats only contaminated foods.
- CRP dose rate: this is the dose per year to the population using the Columbia River water system.
- CRP for 10^4 yr (CRP4): this is the time-integrated population dose for the first 10,000 years after closure of the repository.
- CRP for 10^5 yr (CRP5): same as above, except time integration is for 100,000 years.
- CRP for 10^6 yr (CRP6): same as above, except time integration is for one million years.

Tables similar to this one, showing the expanded set of performance measures, are included in Appendix B. For our purposes here, we use only the most relevant output, i.e., peak AEI and CRP for 10^6 yr (CRP6) doses as our primary displays. In "Alternative Criteria," we discuss the effects of using other performance measures.

As shown in Table 3-1, the AEI best-estimate dose is 3 orders of magnitude below background radiation for a layered-salt repository with simple design and REFERENCE waste form. The 90CL dose is an order of magnitude below background.

*We recognize that, strictly speaking, the Columbia River use system is appropriate only for the repository located in basalt. There are no salt regions of interest in the Pacific Northwest. However, for comparison, we will use the same river/population system for both media.

Table 3-1. Expanded basecase tabular results.

A.		Peak dose rate percentiles				
		25	50	75	90	Max
Limiting individual	rem/yr	3×10^{-7}	2×10^{-3}	5×10^{-2}	2×10^{-1}	3×10^{0}
(above repository)	Ci/yr	2×10^{-10}	2×10^{-7}	3×10^{-6}	3×10^{-5}	1×10^{-3}
Accessible environment individual	rem/yr	1×10^{-9}	6×10^{-5}	1×10^{-3}	1×10^{-2}	8×10^{-2}
(1.6 km from repository)	Ci/yr	1×10^{-9}	8×10^{-5}	1×10^{-6}	8×10^{-6}	1×10^{-4}
Columbia River average individual	rem/yr	5×10^{-11}	3×10^{-9}	3×10^{-8}	2×10^{-7}	1×10^{-6}
Population dose rate	person-rem/yr	8×10^{-6}	6×10^{-4}	6×10^{-3}	5×10^{-2}	3×10^{-1}

B.		Integrated dose percentiles				
		25	50	75	90	Max
CRP for 10^4 yr	person-rem	2×10^{-5}	2×10^{-3}	1×10^{-1}	2×10^{0}	2×10^{2}
CRP for 10^5 yr	person-rem	4×10^{-5}	9×10^{-3}	1×10^{0}	9×10^{2}	3×10^{3}
CRP for 10^6 yr	person-rem	3×10^{-4}	2×10^{-2}	1×10^{1}	2×10^{3}	4×10^{3}

The population dose—even at the 90CL—is trivially small (about 2000 person-rem in a million years). These results should be biased on the high side, because the release rates were not solubility limited, and Darcian flow in unflawed salt was conservatively assumed.

Alternative Waste Forms

In this section we discuss the effects of improving the waste form's release rate by comparing the results from a baseline release rate and a generic "improved" release rate. Improved release rates would likely result from modeling the detailed chemical interactions of the waste elements. Also, improved release rates would result from using a more durable waste form, such as ceramic-like SYNROC-D.[11] There are many possible scenarios for which release comparisons can be made. In this section, we choose a representative set of alternative scenarios, for example, a repository design with bypass. We compare scenario forecasts for the two release rates using these representative scenarios.

We compare system performance for the two release rates, REFERENCE and ALTERNATIVE: 1) in layered salt; 2) in basalt; 3) with better design; and 4) for alternative criteria. We also look at how disruptive events might change our results. For each scenario we tabulate the peak AEI dose and the integrated CRP population dose for 10^6 yr. For both ALTERNATIVE and REFERENCE, we present computer overlay comparisons of results with the basecase site and design.

Figure 3-4 shows representative 100-trial histograms and parent populations for REFERENCE (solid line) and ALTERNATIVE (dotted line) release durations. The REFERENCE geometric mean release duration is 2×10^5 yr. For ALTERNATIVE it is 2×10^6 yr. The geometric standard deviations are 10 and 15 for REFERENCE and ALTERNATIVE, respectively. Although it does not occur in Fig. 3-4, low-probability, high-release-rate samples for both waste forms could be quite similar.

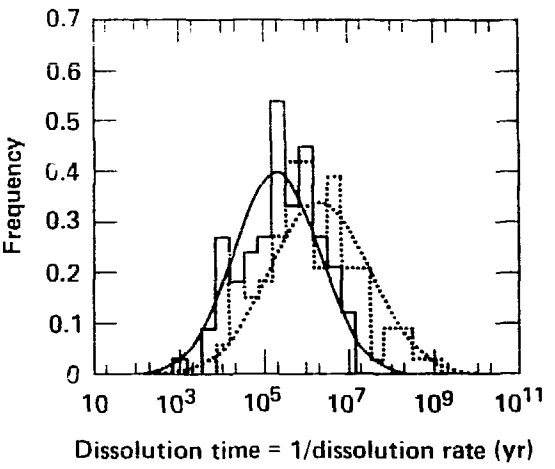

Figure 3-4. Histogram comparison of selections of median leach durations for REFERENCE (solid line) and ALTERNATIVE (dotted line) for sample Monte Carlo run (parent populations are also displayed).

Numerically, the samples chosen from the distributions are truncated at 3.4 standard deviations. The waste form probability distribution functions are not presently correlated with other parameters, such as the flow rates past the canisters. We chose not to correlate the release rate in this work because their relationships with other parameters are not sufficiently known to justify this added model complexity.

Our knowledge of the release rates is very limited. Thus, the geometric mean and standard deviation representing release may also be taken as uncertain. Therefore, we have examined the sensitivity of our results to these choices (see "Release Rates and Uncertainties"). The analysis in the aforementioned subsection is actually a second-order uncertainty analysis, i.e., a study that examines the effects of uncertainty on parameters representing first-order uncertainty.

Basecase

Figures 3-5A and 3-5B, respectively, show AEI and CRP6 doses for the layered-salt site. Table 3-2 summarizes the effects of using ALTERNATIVE rather than REFERENCE. Expanded tabular results for the basecase with ALTERNATIVE are given in Table B1 of Appendix B. Figure 3-5A shows that the improvement of ALTERNATIVE/AEI* dose over REFERENCE/AEI dose is better than a factor of 10 for probabilities below the 95CL. A general tendency, however, for the probabilistic curves to converge at high doses appears throughout our results. This indicates that there are other processes tending to dominate the dose when release rates are sampled at sufficiently high levels.

Figure 3-5B shows that ALTERNATIVE/CRP6 and REFERENCE/CRP6 doses are nearly the same at the high side of the curve. Only below the 70CL does the lower release rate improve the doses by an order of magnitude. Above the 90CL, the predictions are almost identical.

A comparison of AEI/BE doses with accepted risk standards shows them to be orders of magnitude below the standards. The REFERENCE/90CL/AEI dose is a factor of 50 below the 500-mrem/yr level (used in 10CFR20 for operating nuclear facilities). ALTERNATIVE/90CL/AEI dose is a factor of 10 better than REFERENCE/90CL/AEI dose.

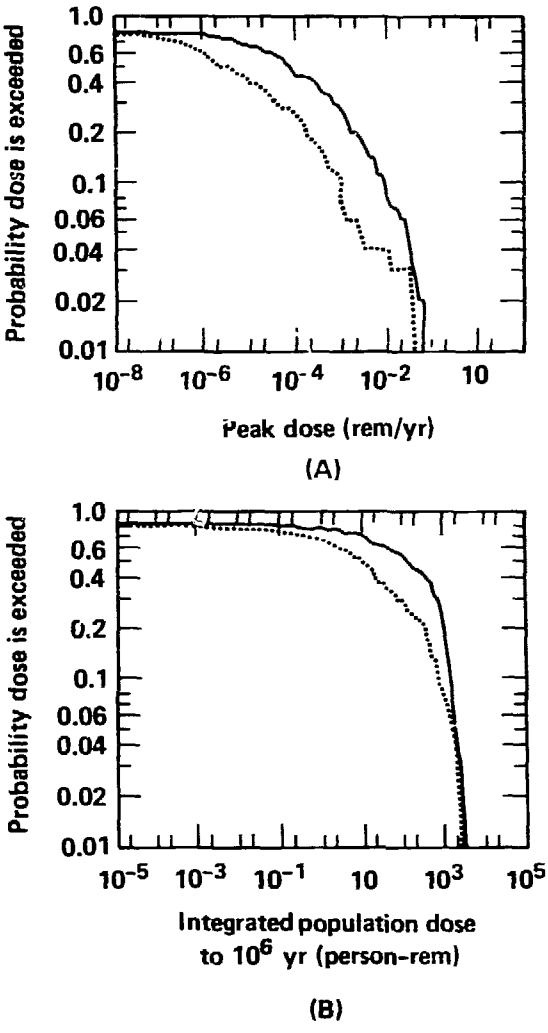

Figure 3-5. Comparison of REFERENCE (solid line) and ALTERNATIVE (dotted line) for basecase layered-salt and basecase design: (A) probabilistic results for AEI dose rate; (B) million-year integrated population dose.

The population doses for the worst case shown in Table 3-2, i.e., REFERENCE/90CL, indicate that in the first million years there might be one premature cancer.† The improvement of ALTERNATIVE over REFERENCE for the 90CL/CRP6 is only a factor of about 2. ALTERNATIVE produces a net reduction of about 1200

*We will use a string of system characteristics (e.g., REFERENCE/CRP6/SALT/90CL) to specify a particular case. This string refers to the REFERENCE waste form, the 10^6 yr population dose, the salt site, and the 90% confidence level. It is much briefer and, once it becomes familiar, provides a better mental picture than a string of phrases. There will be no preferred ordering in the string of system characteristics.

†We use the BEIR recommendations on biological effects as the conversion factor from person-rem to premature cancers.

Table 3-2. Comparison of REFERENCE and ALTERNATIVE waste package release for basecase site and design.

Case	AEI (rem/yr)		CRP6 (person-rem)	
	BE	90CL	BE	90CL
REFERENCE	6×10^{-5}	1×10^{-2}	2×10^{2}	2×10^{3}
ALTERNATIVE	2×10^{-6}	1×10^{-3}	1×10^{1}	8×10^{2}

person-rem in a one-million-year period, or only approximately 1 mrem/yr to the population when averaged over one million years.

Alternative Site – Generic Basalt Repository

Another leading candidate medium for a defense waste repository is basalt. The basalt site currently being investigated is at the Hanford Reservation. This is located on the Columbia River Plateau, which is a vast upland built of relatively recent basalt flows. Our description and model of the basalt repository closely follows a description developed by Golder Associates, Inc. (1978).[6]

Typical basalt basins are made up of layered, extrusive igneous rock caused by multiple flows of hot, low-viscosity molten rock. Individual basalt flows generally range from a few feet to tens of feet thick, but with some flows exceeding 200 ft in thickness.

The source of the Columbia River Plateau basalt was not from a single central vent or series of them, but from a series of fissures, each of which was several miles long. An individual flow was probably fed by several fissures erupting simultaneously. The flows spread almost like water for great distances.

These flows sought the lowest places, filling the old valleys and encroaching on the flanks of hills and mountains. In time, the original topography was buried and a relatively flat basalt plain was constructed. As the flows spread over a region, they interrupted the drainage, damming streams, and giving rise to local lakes and swamps in which sediments accumulated. Because the Miocene climate was considerably more moist than at present, the processes of weathering, erosion, and deposition could rapidly transform an initially barren flow into one of rich soil and abundant vegetation. The landscape that was developed on the top of one lava flow was buried beneath the next flow, creating interlayers of various thickness between basalt flows. When successive eruptions were close in time, the buried surface was relatively smooth and barren, consisting only of a slightly weathered treeless surface from the preceding flow.

Thus, thick basalt sequences consist of complex interlayering of dense but strongly jointed basalts, clays, sands, and gravels. The basalts may be expected to have fracture permeability and the sands and clays interstitial permeability. Some layers of basalt are significantly less fractured and the repository would presumably be placed in one of these. Some of the clay layers can also be of low permeability. A complex flow regime can result. Figure 3-6A shows a generic basalt basin.

In basalt basins, sources of fresh water are likely to be tapped by wells. Aquifers within sequences examined to date tend to contain fresh water. The basalts studied are located in a desert environment. Thus, the potential release of waste through wells is a critical factor in the suitability of basalts for defense HLW repositories.

It is not practical, at this time, to model each of the numerous, rather thin, basalt flows and interbeds found within a thick basalt sequence. Instead, equivalent thicknesses of rock layers are used. These equivalent thicknesses are based on the estimated percentages of five types of layers existing in basalt sequences. They are

- Dense, relatively unfractured basalt.
- Fractured and weathered basalt.
- Coarse-grained interbeds and volcanic rubble.
- Fine-grained interbeds.
- Very dense basalt.

Our generic basalt model includes general features of flood basalt basins. It is not a simulation of any particular site, but rather it is modeled to have characteristics similar to those of a real site with moderate exploration. The basin modeled includes an extra-competent layer of very dense basalt in which the repository is placed. The design of the repository is the same as the design used in layered salt and is shown in Fig. 2-4. The basin is simulated by six layers shown in Fig. 3-6B. Because of their similar permeabilities, the fine interbeds and dense basalt layers have been

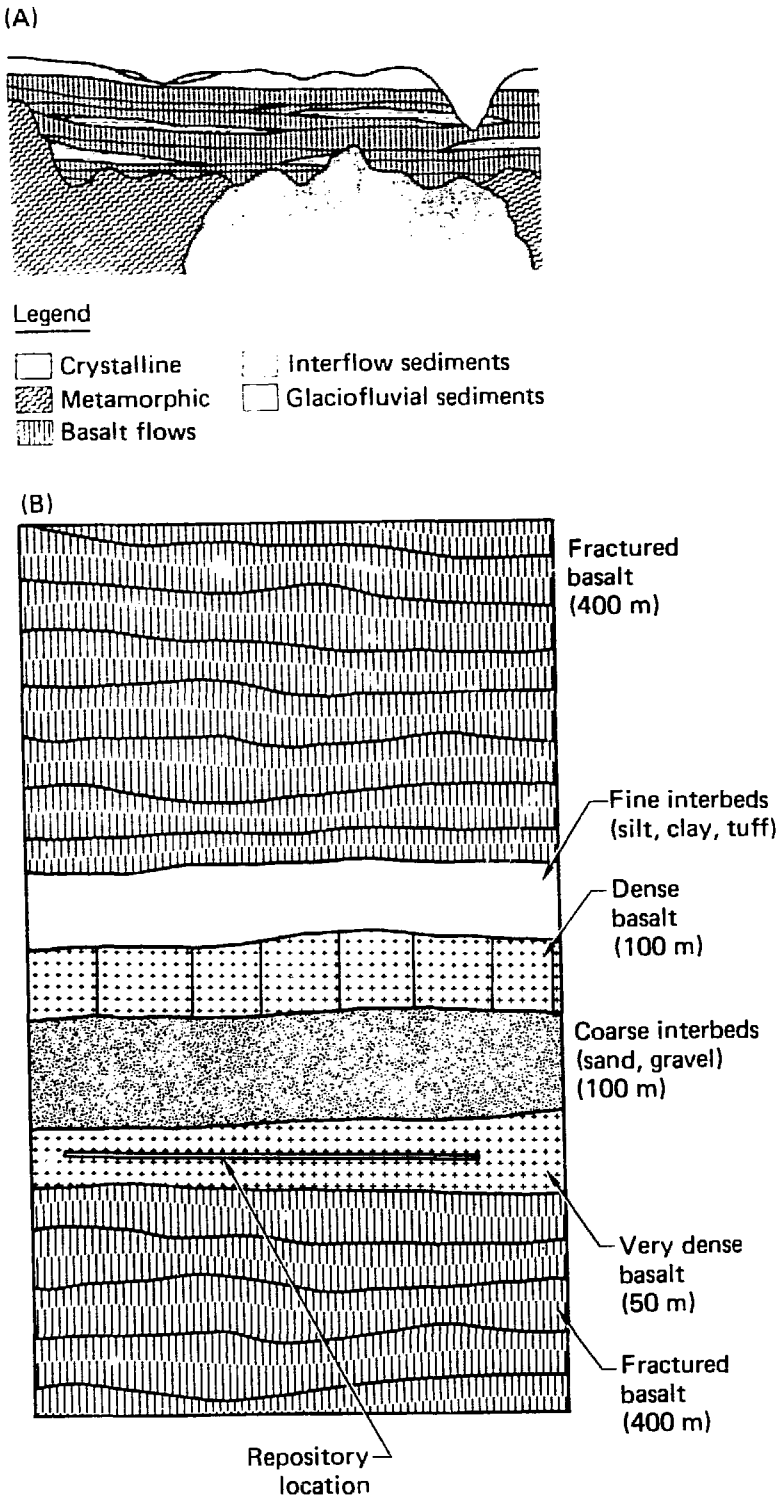

Figure 3-6. Near-field and far-field cross sections of layered-basalt basin: (A) regional configuration; (B) near-field configuration used in this study.

modeled as a single hydrologic element. Directly above the very dense basalt layer is a permeable layer of sand and gravel. This provides a highly conductive pathway where the waste can move horizontally towards any vertical pathway to the upper aquifer. The very dense basalt, coarse interbeds, fine interbeds, and dense basalt layers are sandwiched between two aquifers consisting mainly of fractured basalt. These two layers are essentially identical to one another.

As in the layered-salt repository scenario, the well is assumed to be located 1.6 km from the edge of the repository. The river is assumed to be located 20 km away.

Generic Basalt Repository Geologic Data. The values of the hydrologic parameters chosen to characterize this region have been adapted from those reported by Golder Associates, Inc.[6] Table 3-3 summarizes these parameters for the six layers shown in Fig. 3-6. Each entry consists of a median value (μ) and, where appropriate, a geometric standard deviation (σ). The vertical artesian head between the two aquifers is taken as 5 m, and the horizontal gradient is chosen as 0.001 m/m.

The selection of input parameters from the basalt data base is subject to a set of correlations, constraints, and assumptions similar to those previously described for bedded salt. Again, the MISER code assigns only one set of values, randomly chosen from the appropriate distributions, to all the hydrologic input parameters used to characterize the flow paths within a single layer for a given trial run. Within each layer, the porosity (η) is correlated to the permeability (k) by a factor of 0.8; however, no correlations are assumed between media layers. All choices of permeability are constrained to be greater than zero, and all porosity choices are greater than zero but less than or equal to one. The distribution of aquifer porosity values is truncated at 0.4 to preserve the reported range (i.e., minimum = 0.01, preferred = 0.25, maximum = 0.4). Again, the dispersivity along any flow path is constrained to be less than or equal to 1/10 of the path length. Retardation factors along all flow paths are constrained such that 1.0 = Group I $\leq$ Group II $\leq$ Group III.

Results. Figures 3-7A and 3-7B show the probabilistic results comparing doses from the basalt and salt sites for the AEI and CRP6 doses. The layered-salt curves are labeled "S" and the basalt site predictions are labeled "Ba." First we notice for AEI and CRP6 that the basalt doses are generally higher than the salt doses. Also, the difference in the doses for basalt and salt becomes smaller, the higher the dose. For the CRP6 dose, the difference nearly disappears at about the 70CL. This is true for either the alternative site or the alternative waste form. This implies that for high doses, there is very little sensitivity of CRP6 to alternative sites or, for that matter, alternative waste forms.

Table 3-3. Hydrologic parameters—unflawed basalt.

	Vertical permeability		Porosity	
	μ (cm/s)	σ	μ	σ
Aquifer (upper and lower)	5×10^{-4}	7.63	0.2	2.4
Fine interbeds and dense basalt	10^{-7}	3.87	0.05	1.7
Coarse interbeds	10^{-3}	3.87	0.25	1.13
Very dense basalt	5×10^{-8}	3.6	0.002	1.6
Fracture zones, Tunnels, shafts	5×10^{-6}	3.87	0.002	1.6

	μ	σ
Vertical gradient	0.02 m/m	2.0
Horizontal gradient	0.001 m/m	2.0
Dispersivity	50 m	2.5
Horizontal permeability of dense basalt (between rooms)	5×10^{-8} cm/s	3.16

	Group I		Group II		Group III	
Retardation factor (along all media paths)	μ	σ	μ	σ	μ	σ
	1.0	Certain	10^2	3.87	10^4	3.87

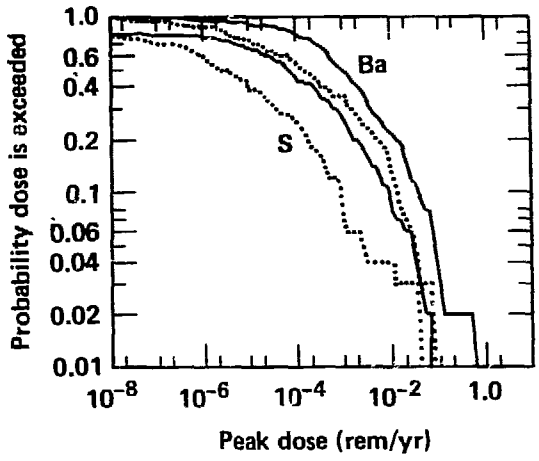

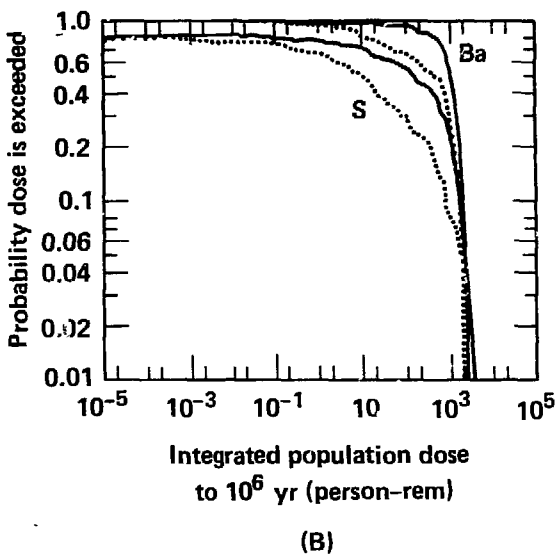

Figure 3-7. Comparison of ALTERNATIVE (dotted lines) and REFERENCE (solid lines) risks for basalt (Ba) and layered-salt (S) repositories: (A) AEI peak dose rate; (B) CRP6 dose.

The second item of note is that the alternative waste form release rate makes a bigger difference when used in the salt repository than when it is used in a basalt repository. For example, at 50CL, the waste form difference in salt is a factor of approximately 30 and a factor of 10 in basalt. At 90CL, it is 10 for salt and 4 for basalt. This again points out, the higher the predicted dose, the less effect a change of waste form has in reducing it. This result is due to other physical attributes of the excavation and transport which cause low dose rates, even when high release rates have been sampled.

In Table 3-4, the AEI dose is a maximum of 1 mrem/yr for REFERENCE/BASALT/BE. This dose increases to a value of 40 mrem/yr for REFERENCE/BASALT/90CL. For ALTERNATIVE/BASALT/90CL, there is an improvement to 10 mrem/yr, a factor of 4, due to waste form improvement. All AEI doses shown in Table 3-4 are at least a factor of 10 below natural background radiation.

The largest best-estimate population dose in Table 3-4 is for BASALT/REFERENCE. It is 1000 person-rem accumulated in one million years. The largest 90CL dose in the table is 2000 person-rem. This occurs for SALT/REFERENCE, BASALT/REFERENCE, and BASALT/ALTERNATIVE. SALT/ALTERNATIVE is 800 person-rem.

It is estimated that 2000 rem to the population creates less than 40% probability that a single premature cancer will occur. If a salt repository is chosen, our prediction at the 90CL is that the ALTERNATIVE waste form will improve the system performance by reducing population dose about 1000 person-rem in one million years. This leads to about 20% reduction in the probability of the repository causing a single premature cancer in a million years.

Contrary to the trend for the AEI dose, the LI dose for basalt is substantially lower than that for salt (see Fig. 3-8). A BASALT/LI/90CL dose reduction 4 orders of magnitude (from about 200

Table 3-4. Comparison of waste form release rates for alternative sites.

Waste form	Site	AEI (rem/yr)		CRP6 (person-rem)	
		BE	90CL	BE	90CL
REFERENCE	SALT	6×10^{-5}	1×10^{-2}	2×10^{2}	2×10^{3}
	BASALT	1×10^{-3}	4×10^{-2}	1×10^{3}	2×10^{3}
ALTERNATIVE	SALT	2×10^{-6}	1×10^{-3}	1×10^{1}	8×10^{2}
	BASALT	1×10^{-4}	1×10^{-2}	5×10^{2}	2×10^{3}

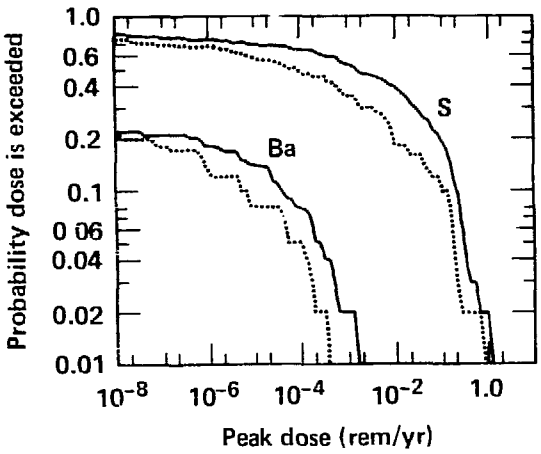

Figure 3-8. Comparison of LI peak dose rates for basalt (Ba) and layered-salt (S) repositories.

mrem/yr at the 90CL/SALT to 0.04 mrem/yr for 90CL/BASALT) in basalt is due to slower migration of much of the waste and water through the rock above the storage area. Hence, in the case of basalt, less radioactivity flows up the shafts and, in many more cases, water flows down the shafts. Thus, we get substantially lower LI/BASALT doses.

Expanded tabular results for basalt with REFERENCE and ALTERNATIVE waste forms are given in Appendix B in Tables B2 and B3, respectively.

Alternative Design

In situations where the waste forms dissolve fairly rapidly, it has been shown that design features can have a strong effect on near-field doses.[12] To analyze the possible effects of design on predicted doses, we have calculated the doses with a hydraulic bypass as shown in Fig. 3-9. The development of an optimum design was not completed for this analysis. The effects of the bypass on the AEI and CRP6 doses were relatively large (see Table 3-5). It also had major effects on some other performance measures. For example, it drastically changed the flow patterns in the system.

We chose a bypass just below the salt layer as shown in Fig. 3-9. The mined configuration is shown in the plane view of the bypass horizon. It consists of 23 storage-like drifts running along the direction of the horizontal regional flow gradient. The side view shows that the upstream side of the bypass starts to the left of the return air shaft and is located 120 m below the storage area. It extends for 100 m beyond the storage area and discharges into seven vertical shafts with an area of 100 m^2 each.

For water originally in the storage room to get to the bypass requires that it flow through at least 100 m of salt barrier, either horizontally out the

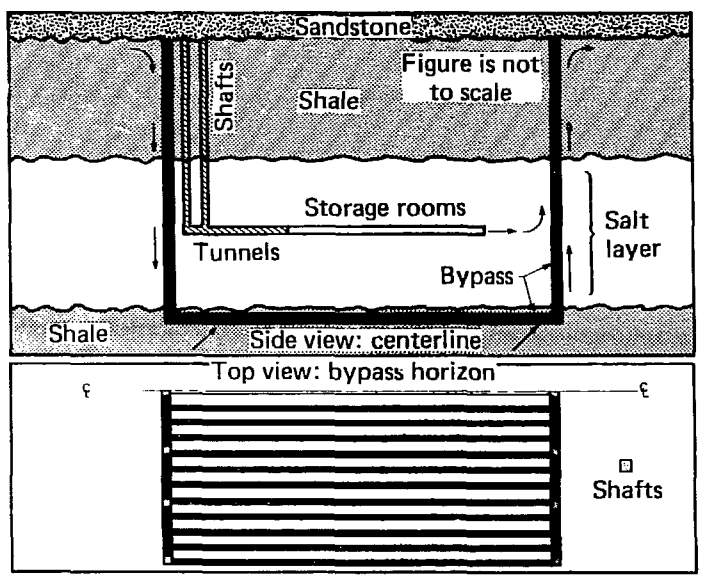

Figure 3-9. Layout of hydraulic bypass used in alternative design scenario (arrows indicate direction of flow when bypass is used; flows are significantly different from those shown in Fig. 2-2).

Table 3-5. Comparison of REFERENCE and ALTERNATIVE waste form for alternative designs.

Waste form	Design	AEI (rem/yr)		CRP6 (person-rem)	
		BE	90CL	BE	90CL
REFERENCE	w/o BYPASS	6×10^{-5}	1×10^{-2}	2×10^{2}	2×10^{3}
	BYPASS	$<1 \times 10^{-15}$	2×10^{-4}	$<1 \times 10^{-7}$	2×10^{1}
ALTERNATIVE	w/o BYPASS	2×10^{-6}	1×10^{-3}	1×10^{1}	8×10^{2}
	BYPASS	$<1 \times 10^{-15}$	3×10^{-5}	$<1 \times 10^{-7}$	2×10^{0}

end of the storage area or downward to the bypass. The bypass width is the same as the storage area shown in Fig. 2-4. Thus, nearly all upward flow from the lower aquifer will be intercepted by the bypass before it gets to the defense HLW storage area.

The permeability and effective porosity of the bypass is that of gravel. This choice effectively eliminates all upward flow of nuclides in the shafts. It causes a downward or horizontal (left-to-right) flow through the repository to the bypass for all Monte Carlo trials. This increases the time of initial radionuclide emergence at the AEI well from 6700 to about one million years for the median value case, thus, keeping hazardous material confined to the repository for much longer times. The flow patterns observed when the bypass is included are roughly shown by arrows in Fig. 3-9. The flows in the shafts for the basecase (without BYPASS) are nearly always in the opposite direction.

Results. In Figs. 3-10A and 3-10B, we see that the dose is reduced by a factor of at least 10 for all confidence levels below 95CL when the hydraulic bypass is in place. AEI and CRP6 doses were observed only in 30 to 35% of the trials when the bypass was included in the repository design. Thus, the "best-estimate" dose for both REFERENCE and ALTERNATIVE is zero.

With the bypass, there is a reduction of about a factor of 50 in individual dose at the high-dose side of the curve for AEI/REFERENCE. Changing to ALTERNATIVE does not improve the predicted AEI dose at the 50CL when the bypass is used. It improves the AEI dose rate by 0.2 mrem/yr at the 90CL. As one moves to lower confidence levels, the percentage of reduction in dose over the basecase (without BYPASS) becomes very large. For example, at the 50%-confidence level, this factor is unbounded.

The BYPASS-without-ALTERNATIVE design improves the basecase performance, both for AEI and CRP6, by a factor of better than 5 more than the ALTERNATIVE-without-BYPASS design.

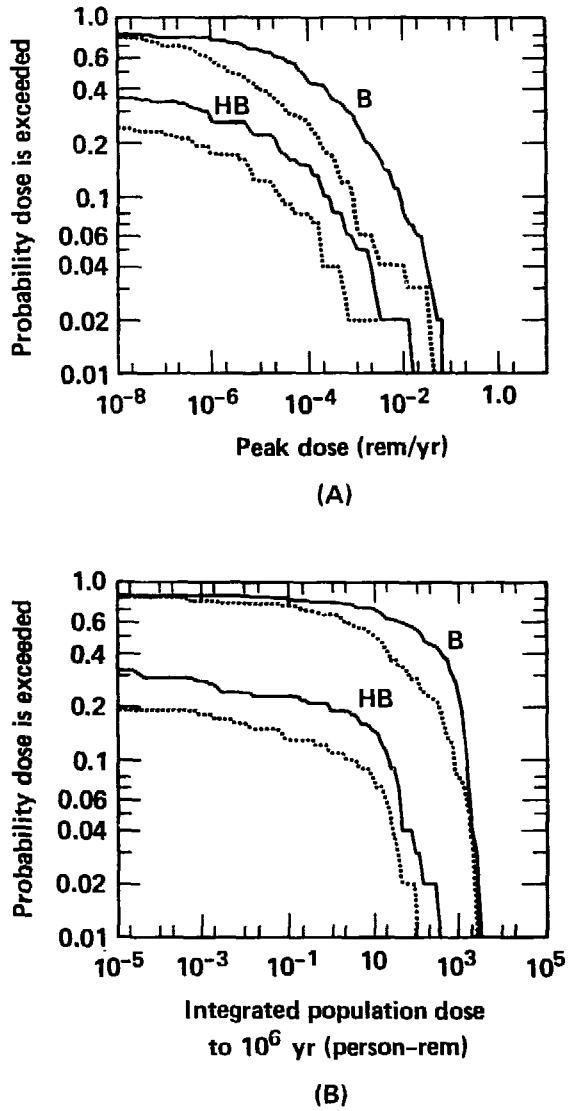

Figure 3-10. Comparison of REFERENCE (solid line) and ALTERNATIVE (dotted line) for basecase (B) and hydraulic bypass (HB) designs in bedded-salt repository: (A) AEI peak dose rate; (B) CRP6 dose.

Including both the BYPASS and improved waste form (i.e., BYPASS/ALTERNATIVE) decreases the BYPASS/REFERENCE dose at the high-confidence levels by about a factor of 5.

Improvements in the population dose integrated for one million years are substantial. At 50CL, the improvement is at least a factor of 10^8 for both waste forms. At the 90CL, it is an improvement of 100 for REFERENCE and 400 for ALTERNATIVE. This can be compared with a reduction in CRP6/90CL dose by a factor of only 2 when the improved waste form is used without a bypass.

The derived population dose benefit obtained from changing to ALTERNATIVE is zero at 50CL and only 18 person-rem at 90CL when there is a bypass.

Another interesting observation, which is not strongly sensitive to model assumptions, is that the LI dose was zero for all trials when there was a bypass. This is caused by water flowing down the shafts for every Monte Carlo trial when the bypass was part of the design. Upward flow in the shafts occurs about 80% of the time for the basecase. When the flow is downward, LI receives no dose because the LI well is downstream of the shafts, but upstream of the storage areas.

Expanded tabular results for the bypass studies appear in Tables B4 and B5 in Appendix B.

Disruptive Events

To determine the magnitude of the hazard if future disruptive events occur, we have examined events in our basecase salt repository, which we consider both sufficiently probable and also likely to lead to high doses. These events must disrupt the flow system enough to cause significantly higher doses than those of the uneventful scenario. There are, of course, very low probability scenarios that could lead to high consequences. There is, for example, a meteorite direct hit. This, however, has such a low probability of occurrence, i.e., a 0.1% chance during a time period approximating the age of the earth, that its risk is considered negligible.[13] Another type of uninteresting scenario, for example, is the repository site receiving a substantially large rainfall, say twice seasonal average in the next 10,000 yr. This has a high probability of occurrence, but its impact on the long-term hydrology would be insignificant. Thus, the consequences will lead to no effective change in the results from the uneventful scenario. Numerically, we handle this as an uneventful scenario.

Scenarios. The scenarios we feel are important in our first-order uncertainty analysis are a fault, a failed (i.e., a future drilling or undetected) borehole,* deteriorated backfill, and breccia pipe formation.

Our approach has been to choose what we consider to be conservative assumptions to make the scenarios consistent with our modeling approximations, i.e., the event occurs early by 1000 yr after closure. This should lead to worse consequences than if the event were to occur at late times. The second assumption is that we have chosen the event to occur at a particularly bad location in the repository, i.e., at the downstream edge of the repository (see Fig. 3-11). This produces flow so that recharge is more likely from both the lower aquifer and the shaft into the excavation. On the average, this should lead to larger flow speeds and more radionuclides moving through the flow path than at upstream locations. There will, however, be sets of parameters that might lead to individual trials with worse results for upstream locations and different event times. Analyzing these possibilities is beyond the scope of this work. A third assumption is that if a flaw occurs at more than 10,000 yr after closure, its effect on waste migration is insignificant. This assumption is useful numerically, and is consistent with the 10,000-yr period of interest dictated by EPA and NRC draft policy statements.

Figure 3-12 shows the cumulative distribution functions for the disruptive event scenarios for the AEI dose. Table 3-6 summarizes these results. We see that, at the 90% level of confidence, the maximum increase in dose to AEI/REFERENCE is no more than an order of magnitude above the uneventful case. This occurs for fault slippage, which has a fairly low probability of occurrence.

For the 90CL, the deteriorated backfill and the breccia pipe consequences lead to doses about the same as the uneventful case for the REFERENCE waste form and AEI individual. This is due to the higher effective porosities for the deteriorated backfill, which lead to slower migration rates than the uneventful case, even though the permeability is higher. The borehole produces high velocities and is recharged by large amounts of water in the system.

In Tables 3-6 and 3-7, the largest BE/AEI/EVENTFUL dose is only 6 mrem/yr. This is over

*Undetected-flaw scenarios are defined as eventful scenarios. In our steady-state flow model, flaws caused by future events and undetected flaws are treated in the same manner, i.e., as though they existed from the time of closure.

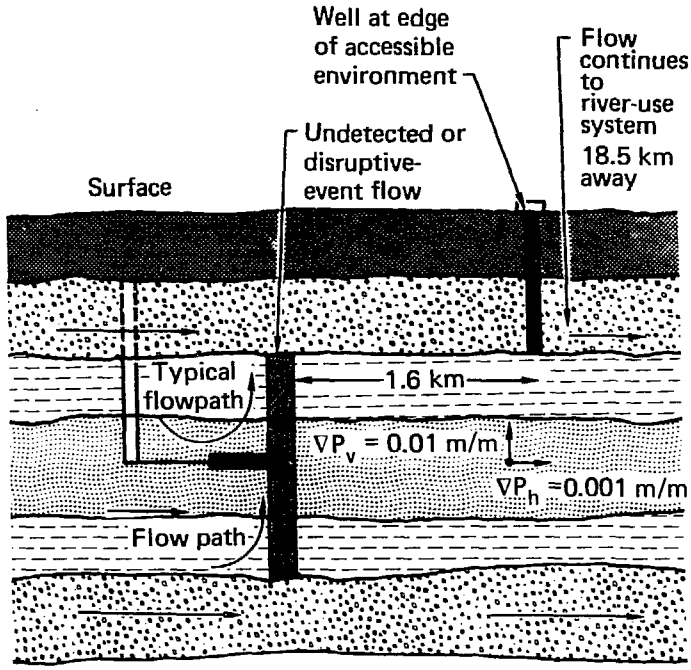

Figure 3-11. Disruptive event scenario (flaw is located at downstream edge of repository, thus providing easy flow path to aquifer).

Table 3-6. Eventful scenario "best-estimate" doses.

		Uneventful	Fault	Borehole	Deteriorated backfill	Breccia pipe
AEI	REFERENCE	6×10^{-5}	6×10^{-3}	5×10^{-3}	6×10^{-4}	3×10^{-4}
(rem/yr)	ALTERNATIVE	2×10^{-6}	4×10^{-4}	6×10^{-4}	3×10^{-5}	4×10^{-5}
CRP6	REFERENCE	2×10^{2}	2×10^{3}	1×10^{3}	1×10^{3}	3×10^{2}
(person-rem)	ALTERNATIVE	1×10^{1}	4×10^{2}	4×10^{2}	9×10^{1}	5×10^{1}

Table 3-7. Eventful scenario 90% confidence level doses.

		Uneventful	Fault	Borehole	Deteriorated backfill	Breccia pipe
AEI	REFERENCE	1×10^{-2}	1×10^{-1}	8×10^{-2}	1×10^{-2}	1×10^{-2}
(rem/yr)	ALTERNATIVE	1×10^{-3}	6×10^{-2}	4×10^{-2}	2×10^{-3}	5×10^{-3}
CRP6	REFERENCE	2×10^{3}	3×10^{3}	3×10^{3}	2×10^{3}	2×10^{3}
(person-rem)	ALTERNATIVE	8×10^{2}	2×10^{3}	3×10^{3}	2×10^{3}	9×10^{2}

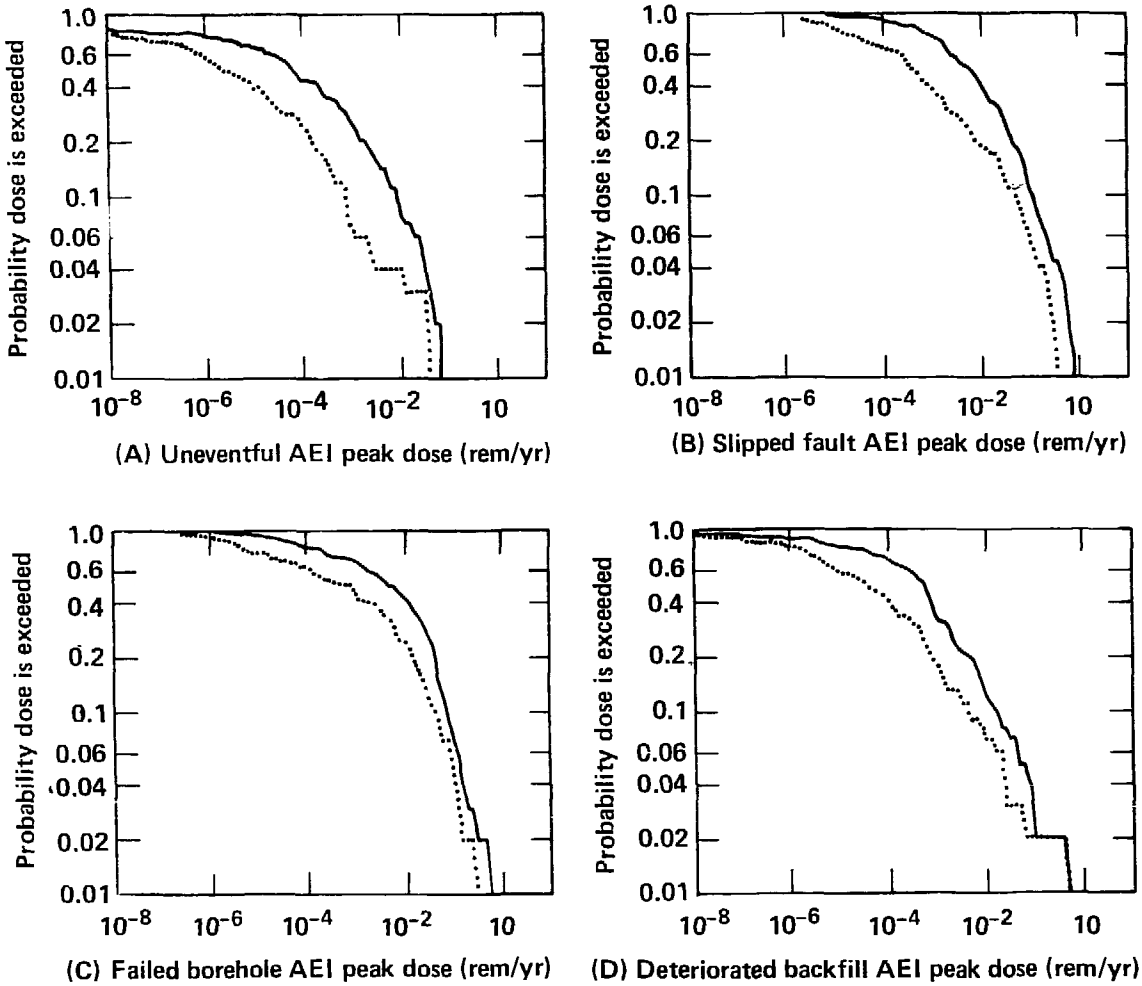

Figure 3-12. Comparison of eventful and uneventful AEI risk curves (REFERENCE and ALTERNATIVE waste forms are solid and dotted lines, respectively). Results from scenarios: (A) uneventful; (B) slipped fault; (C) failed borehole; (D) deteriorated backfill; (E) breccia pipe formation.

an order of magnitude below background. Our highest 90CL dose is only about background radiation. This occurs for a low probability event, i.e., fault slippage. For the borehole case, we have conservatively assumed that it intersects a storage room and not a pillar. The storage room penetration leads to a higher dose but the likelihood of its intercepting a storage room is only 1/3 as high as that for a pillar.

The largest population dose (90CL/REFERENCE) is 3000 person-rem from a slipped-fault scenario. This is only 150% of the uneventful case dose. It is an insignificant population dose when compared with any other measure of risk. Over a one-million-year disposal period, the repository has about a 50% probability of producing a single premature cancer, even if fault slippage occurs soon after closure.

Event Probabilities. The risk from all the important scenarios can be incorporated into a single probabilistic curve, which provides a single measure of performance. The information necessary for this curve is the probability for the occurrence of each of the scenarios, an assumption that the probability of two events occurring is much smaller than one, and the choice of a representative disruptive-event set of parameters for each class of scenarios.

Since we are doing a first-order uncertainty study (and we consider the introduction of the disruptive-event scenarios as a first-order correction of the uneventful consequence analysis), we have the probability of the event to occur (e.g., occurrence per year at the site) as our first-order uncertainty associated with that scenario. Incorporating an uncertainty on the rate of occurrence would lead to a second-order uncertainty analysis, which would clearly test our computational capabilities and would be unlikely to change our results significantly.

The disruptive-event scenarios we have considered for bedded salt are deteriorated backfill, failed borehole, fault slippage, and breccia pipe formation.

- For **deteriorated backfill,** we have reviewed the literature and found a large probability of occurrence.[14] Other studies (e.g., Ref. 6) have been less pessimistic and, in fact, have not even considered this event important enough to incorporate in their findings on scenario analysis. We feel that we are being conservative by choosing a probability of occurrence of 0.2 in 10,000 yr.
- For **failed borehole** scenarios, we have used values obtained from Ref. 13. Here we are looking at several physical situations. The first is that of the boreholes, which have been drilled to explore site characteristics. This might lead to seal failure. The second is undetected boreholes from previous exploration for resources. The third is future inadvertent drilling. Reference 13 gives values of 10^{-5} for an undetected borehole. Careful policy should restrict site exploration damage to zero. Under loss of administrative control Arthur D. Little, Inc., has given a probability of 10^{-2} during the first 200 yr for future drilling. If one assumes this rate as constant for 10^4 yr, the probability of at least one drill hole occurring in a bedded salt repository is 0.4. Since the analysis[13] was for a repository area several times larger, we have chosen 0.1 as our estimate of a failed borehole (i.e., a future drilling).
- **Faulting** is given by various studies[6,14] as having a probability in 10,000 yr from a high of 5×10^{-3} to 10^{-6}. We choose a conservative order-of-magnitude estimate of 10^{-3}. We also assume that once the fault opens, it remains open for the duration. This is probably not the case, but it is conservative and allows the computation to be done with a steady-state model.
- **Breccia pipe** formation is estimated[13] to occur in bedded salt with a frequency of about 10^{-8}/yr. Thus, for 10,000 yr, we get approximately a 10^{-4} probability of occurrence. Expanded tabular results for the breccia pipe formation analyses are given in Tables B12 and B13 of Appendix B.

Table 3-8 summarizes the rates used in calculating the probability of seeing a particular scenario in the next 10,000 yr. These lead to the curves shown in Fig. 3-13. The curve can be read, for example, as a model prediction that there is a 0.01% chance of seeing a dose greater than 130 mrem/yr from a fault slippage at the site for a REFERENCE waste form. Thus, we believe with 99.99% confidence level that not more than 130 mrem/yr will be received by AEI from a future fault-slippage scenario with REFERENCE waste form.

When we sum the effects of all the scenarios, we get the curves for REFERENCE and ALTERNATIVE shown as total risk. We predict with 90%

Table 3-8. Scenario probabilities.

Scenario	Rate of occurrence
Deteriorated backfill	2×10^{-5}/yr
Failed borehole	1×10^{-5}/yr
Faulting	10^{-3}/yr
Breccia pipe formation	10^{-8}/yr

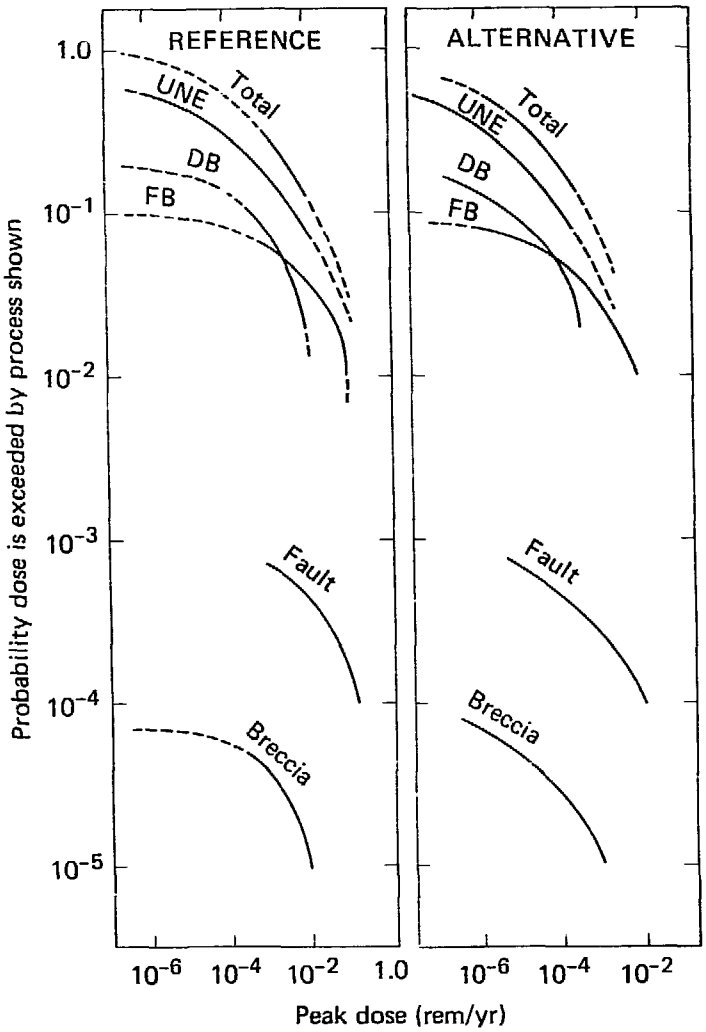

Figure 3-13. Scenario of normalized eventful AEI risk curves and total risk for REFERENCE (LHS) and ALTERNATIVE (RHS). (DB, deteriorated backfill; FB, failed borehole; UNE, uneventful.)

confidence that the future AEI/ALTERNATIVE dose will be below 3 mrem/yr. This is a factor of 30 below background radiation.

Finally, Fig. 3-14 compares the total risk curve with the curve we would get if we assumed that all future disruptive events lead to insignificant changes in the system hydrology. Table 3-9 is extracted from Fig. 3-14 to compare BE and 90CL AEI doses for both waste forms for the disruptive-event and basecase scenarios. One can see for a given confidence level that there is very little change in the cumulative distributions. This implies that the major risk sensitivities in a permeable layered-salt system are due to inability to measure and predict the process of a given scenario, not the effects of disruptive events. Thus, we could have arrived at excellent approximations without a very careful scenario analysis. Excavation parameters and dynamic processes are the most important considerations in our forecasts.

Expanded tabular results for disruptive event scenarios with REFERENCE and ALTERNATIVE waste forms are presented in Appendix B in Tables B6 through B13.

Alternative Criteria

The curve labeled 10^4 in Fig. 3-15B shows the population dose accumulated to 10,000 yr after closure (the time frame of interest to NRC and EPA). For this performance measure, only 29% of the samples had sufficient transport velocity to lead to a measurable population dose. The best-estimate dose is zero. The 90th-percentile dose is

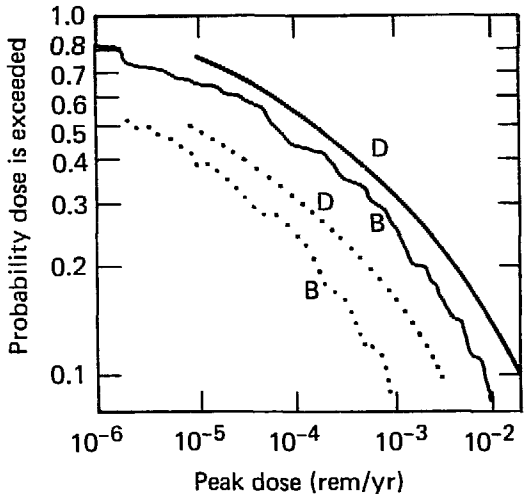

Figure 3-14. Comparison of basecase (B) and disruptive-event (D) risk curves for REFERENCE (solid line) and ALTERNATIVE (dotted line).

an extremely small 0.2 person-rem in 10^4 yr. This population dose is about what one person receives from natural background radiation in one year.

The 10^4 curve is but one of many different performance measures that can be devised for a repository system. No definitive national standard exists with which forecasts can be unequivocally compared. Traditional standards have been cast into two types: the first protects the individual, and thus the local environment; the second type protects the population and is more global in nature. In developing our capability, we have considered both types of results.

There are several locations where it seems reasonable to forecast the individual dose. In our scenario, fresh water is available from the upper aquifer. We thus chose three different locations leading to the LI, AEI, and CRI doses. The first dose is from a well just downstream from the

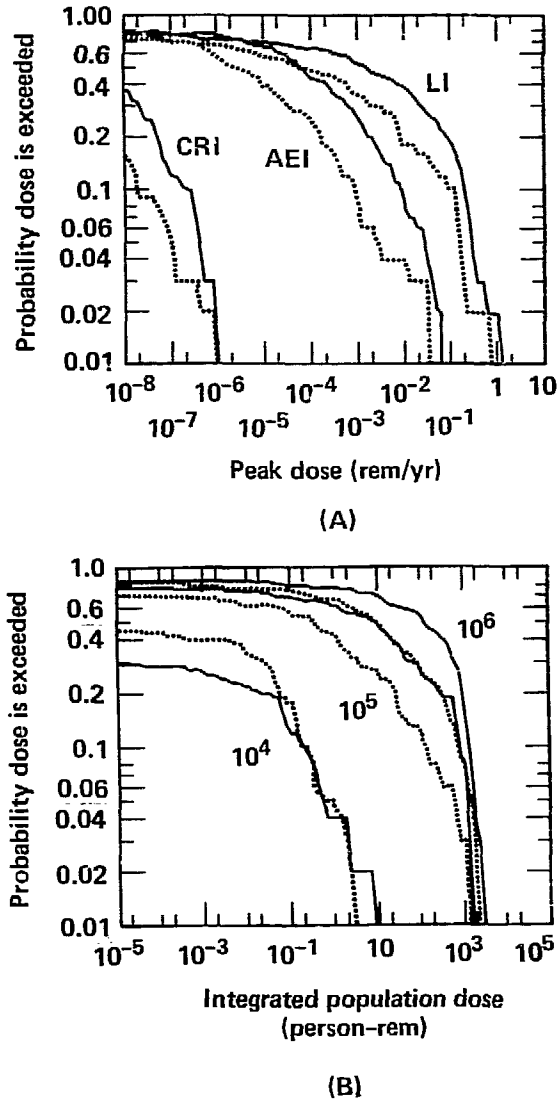

Figure 3-15. Comparison of effects on risk curves of different potential safety standards: (A) effects on individual peak dose of locating "observation" point at different places; (B) effects of changing period over which population dose is integrated.

Table 3-9. AEI dose comparison of waste forms for eventful and uneventful scenarios (rem/yr).

	Uneventful		Eventful	
Waste form	BE	90CL	BE	90CL
REFERENCE	6×10^{-5}	1×10^{-2}	2×10^{-4}	2×10^{-2}
ALTERNATIVE	2×10^{-6}	1×10^{-3}	6×10^{-6}	3×10^{-3}

shafts. The second is a well 1.6 km from the repository edge and the third (CRI) is an average individual who lives in the Columbia River water use system. Figure 3-15A compares these individual REFERENCE and ALTERNATIVE doses for our basecase.

From Fig. 3-15A, it is obvious that the choice of performance measure can greatly influence the predicted level of dose. The peak dose ranges from 5 to 6 orders of magnitude, between the CRI and LI doses. For comparison, the difference between using different waste forms is only about a factor of 10 for LI. It is reassuring to note that the largest BE peak individual dose using any of the performance measures is only 2 mrem/yr. At the 90% confidence level, the LI dose rate is 200 mrem/yr. For the ALTERNATIVE/AEI/90CL case, we have 1 mrem/yr. For REFERENCE/CRI/90CL, we forecast 2×10^{-4} mrem/yr (about one-millionth of background radiation).

We see for the highest doses that the ALTERNATIVE waste form is not especially effective in lowering dose rate (cf. the LI/90CL dose rates). ALTERNATIVE does, however, reduce doses by about a factor of 10 for all the performance measures below the 80CL. If we introduce a bypass in the design, the LI dose rate becomes zero and the AEI/90CL dose rate is reduced by a factor of 50. Since the AEI dose rate is less sensitive than the LI dose to alternatives like the bypass, it is the more robust performance measure. It also is closer to the prescription for performance assessment given in draft 40CFR191 than the LI performance measure.

Choosing a population risk measure is as difficult as picking an individual dose measure. Figure 3-15B shows three integrated dose periods. The 10^4-yr dose curve is the one apparently favored by EPA. With our system parameters, the 10^4-yr integrated population dose only measures the unreliable front end of the radioactive pulse. This results in CRP4 doses being 4 orders of magnitude below the 10^5- and 10^6-yr doses. CRP4 is essentially dealing with model noise. Thus, we have used the more reliable 10^6-yr integrated dose as our conservative population dose performance measure.

In Fig. 3-15B, we note that there is little difference at 90CL for the 10^5- and 10^6-yr integration periods. There is also no major improvement in the 10^6-yr integrated dose if ALTERNATIVE is used instead of REFERENCE. The dose is more sensitive to waste form at 90CL if a 10^5-yr integration period is used. The largest integrated dose in Table 3-10 is below the dose that would be expected to lead to one premature cancer death, whether REFERENCE or ALTERNATIVE is used.

Release Rates and Uncertainties

Our choice of release rates and their uncertainties (as represented by the median and geometric standard deviation of a lognormal distribution) is an important consideration for the purpose of this work. Thus, we have studied the effects of our choices of these parameters. We use waste form release rates and uncertainties different from our basecase, REFERENCE, and our improved waste form, ALTERNATIVE, to see how they affect repository safety. This takes the form of a sensitivity study over median release rate (U) from 10^{-8}/yr to 10^{-3}/yr, and for geometric standard deviation (S) representing uncertainties of 10 and 100.

For $U = 10^{-6}$/yr and $S = 100$, approximately 98% of the time the sampled release rate would be between 10^{-2}/yr and 10^{-10}/yr. If $S = 10$, then the

Table 3-10. Comparison of REFERENCE and ALTERNATIVE waste forms for alternative criteria.

	Individual dose (rem/yr)					
	Best estimate			90% confidence level		
	LI	AEI	CRI	LI	AEI	CRI
REFERENCE	2×10^{-3}	6×10^{-5}	3×10^{-9}	2×10^{-1}	1×10^{-2}	2×10^{-7}
ALTERNATIVE	1×10^{-4}	2×10^{-6}	1×10^{-10}	1×10^{-1}	1×10^{-3}	2×10^{-8}

	Population dose (person-rem)					
	Best estimate			90% confidence level		
	10^4 yr	10^5 yr	10^6 yr	10^4 yr	10^5 yr	10^6 yr
REFERENCE	$< 2 \times 10^{-6}$	9×10^{0}	2×10^{2}	2×10^{1}	9×10^{2}	2×10^{3}
ALTERNATIVE	$< 10^{-9}$	4×10^{-1}	1×10^{1}	2×10^{-1}	2×10^{2}	8×10^{2}

same percentage of samples would be chosen between 10^{-4}/yr and 10^{-8}/yr.

In Table 3-11, we compare our basecase REFERENCE release rate model with one with a factor of 10 larger uncertainty, as modeled by a log-normal distribution with a geometric standard deviation of 100. For the basecase, S is 10. The basecase median release rate is $U = 5 \times 10^{-6}$/yr. We see for this U that the 90CL doses are identical for S = 10 and S = 100.

For the BE doses, the ratios of basecase doses to "larger uncertainty" doses range from 2 to 10. Thus, for this comparison, we see that the doses are sensitive to uncertainty at the 50CL (BE), but not at the higher confidence level of 90%.

Figures 3-16 and 3-17 show how the 90CL, BE, and 25CL change with respect to median release rates. The S = 10 curves are represented by solid lines and S = 100 doses by dashed lines. Figure 3-16 displays LI and AEI doses. Figure 3-17 shows the CRP6 doses. The dotted lines show curves where the percent change of peak dose is equal to the percent change of median release rate, i.e., if the release rate changes by a factor of 10, so will the peak dose.

Figure 3-16 shows that, for the 25CL and BE curves, the percent change in dose nearly equals the percent change in median release rate for $U = 10^{-8}$/yr to 10^{-3}/yr. For CRP6, this is true only for median release rates less than 10^{-4}/yr.

For low-dose levels, as depicted by the 25CL curve in Figs. 3-16 and 3-17, the doses are consistent with a model linearly proportional to release rate. Thus, if we were to know the 25CL dose at, say, $U = 10^{-8}$/yr and the proportionality constant, we could predict within an order of magnitude, the 25CL dose at median release rates as high as 10^{-3}/yr. This is true for the BE and 25CL levels for the individual dose curves. It is also true for the CRP6/25CL and BE curves with $U < 10^{-4}$/yr.

For the more important high doses, e.g., the 90CL dose, the linearity of the doses with respect to median release rate does not occur for $U > 5 \times 10^{-7}$/yr. This is best exemplified by the LI/90CL dose shown in Fig. 3-16. Above $U = 5 \times 10^{-7}$/yr median release rate, the curve is almost flat. Thus, the sensitivity to U is nearly zero in this domain. The sensitivity to S is also nearly zero in this domain, as the 90CL dashed and solid curves are almost identical.

The same nonlinear effect that occurs for LI/90CL occurs for all the curves. This effect is nearly as pronounced for the CRP6/90CL (shown in Fig. 3-17) as it is for LI/90CL. Physically, it is due to dilution factors other than the release rate in the system. These factors are primarily the spacial extension of the repository for the LI doses and the dispersion and retardation for the CRP6 doses. The BE dose is nearly insensitive to uncertainties for all cases over the full range of U.

Improving the median release rate by a factor of 10 tends to improve all doses at each confidence level ($\leq$90CL) by about a factor of 10 for release rates less than 10^{-7}/yr. Doses for confidence levels greater than 90% will require even lower U's to show dose linearity with respect to U. For median release rates of less than 10^{-6}/yr, the uncertainty of the release rate impacts the 90CL dose, leading to higher dose levels the larger the uncertainty. For sufficiently high confidence levels, or sufficiently high median release rates, the dose is insensitive to uncertainty of the release rate.

Some specific points are

- Improving the median release rate improves doses linearly if the median release rate is less than 5×10^{-7}/yr and the confidence level is less than 90%.
- Reducing release rate uncertainty provides lowered dose at high confidence levels (~90CL) if the median release rate is less than about 10^{-7}/yr.
- High dose results cannot be driven higher than those shown in Figs. 3-16 and 3-17 by choices of medians and geometric standard devi-

Table 3-11. Comparison of larger release rate uncertainty with basecase.

Release rate uncertainty	LI (rem/yr)		AEI (rem/yr)		CRP6 (person-rem)	
	BE	90CL	BE	90CL	BE	90CL
Basecase (S = 10)	2×10^{-3}	2×10^{-1}	6×10^{-5}	1×10^{-2}	2×10^{2}	2×10^{3}
Larger uncertainty (S = 100)	2×10^{-4}	2×10^{-1}	3×10^{-5}	1×10^{-2}	5×10^{1}	2×10^{3}

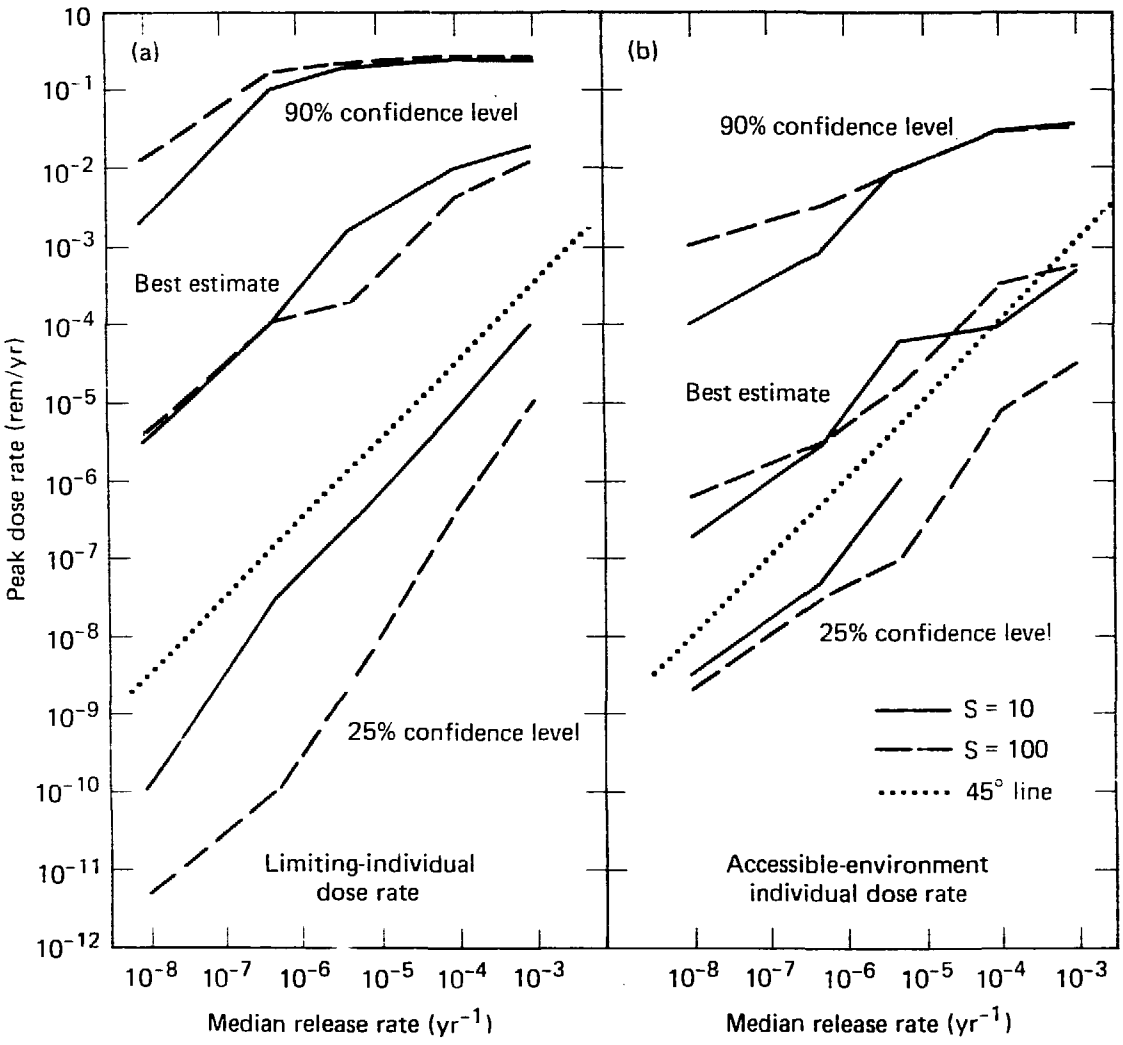

Figure 3-16. Individual peak dose comparison of varying waste form technology. (The technology improves with lower median release rate and reduced uncertainty on that release rate.) Curves show effects on 90%, 50%, and 25% confidence levels as release rate is lowered from 10^{-3}/yr to 10 ^{8}/yr (dashed curve: release rate geometric standard deviation of 100 indicating poor understanding of leaching process; solid curve: geometric standard deviation of 10, which represents much better understanding of release rate; dotted line: slope where percent change in release rate leads to equal percent change in dose.)

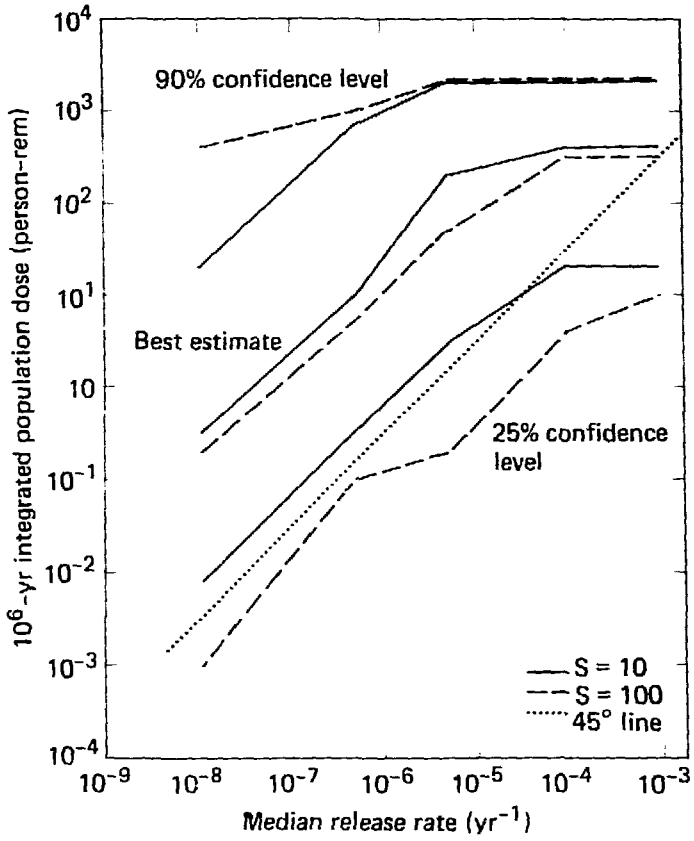

Figure 3-17. Population dose comparison of varying waste form technology (see Fig. 3-16).

ations representing a worse state of waste form technology. For example, a choice of 1000 for the geometric standard deviation would lead to no more than approximately 30 mrem/yr AEI dose, the same result obtained when S = 10. This is independent of the median release rate chosen. Better designs or better sites could, however, reduce the 30 mrem/yr AEI dose.

For REFERENCE and ALTERNATIVE, and U's of 5×10^{-6}/yr and 5×10^{-7}/yr, the 90CL shows almost no sensitivity to uncertainty. For the 25CL, the ratio of doses with S = 10 and 100 can be over 100 (as shown in the LI case). These large sensitivities to the choice of uncertainty are, however, always for low doses, e.g., 10^{-8} to 10^{-10} rem/yr.

In summary, where the doses are sensitive to the choice of uncertainty, the doses are orders of magnitude below background. Where the doses are significant fractions of background, the sensitivity to release rate uncertainty is nearly zero. Thus, the decision on repository safety should be relatively insensitive with respect to uncertainty on release rate.*

Expanded tabular results for the cases analyzed in this subsection are given in Tables B14 through B22 in Appendix B.

Point-Source and Extended-Source Repository Models

Introduction

The U.S. Nuclear Regulatory Commission in its proposed rulemaking 10 CFR Part 60[15] has drafted performance objectives for the disposal of

*Another interesting aside on appropriately choosing performance measures would be the case where we use "mean dose" as our measure of performance. If the mean dose were used as a measure of safety, a higher uncertainty on release rates would lead to lower mean doses if U was above 10^{-6}/yr. Such a choice of performance measure could be misleading to decision makers; i.e., it would imply larger uncertainty leads to better repository performance.

high-level radioactive wastes in geologic repositories.

"In the course of the Commission's deliberation, it becomes evident that in order to have confidence in the ability of a geologic repository to contain and isolate the wastes for an extended period of time, the repository must consist of multiple barriers. In view of the uncertainties that attach to reliance on the geologic setting alone, the Commission believes that a repository should consist of two major engineered barriers (waste package and underground facility) in addition to the natural barrier provided by the geologic setting."

Extensive research has been reported on both the waste package and the thermal, thermomechanical, and radiation effects in the disturbed zone. Analyses of the natural barriers of the geologic setting have also been reported extensively.[16-26] Little effort has gone into understanding the effect of a spatially extended mine design.

The U.S. Department of Energy, in its waste confidence rulemaking[27] has stated that performance analysis must predict the combined effects of all credible phenomena. Further, if ". . .the analysis identifies any effects that could release radionuclides and deliver doses to people, it must estimate the magnitude of those doses."

In this work we explore the effects of the hydrology of the mine design features of the underground facility. We find in the event of failure of the waste package, particularly for high release rates of radionuclides, that models using a point-source repository assumption may predict doses to a worst-situated "limiting individual" that vary by orders of magnitude. We also show that these doses may be lowered substantially if some mine design features are included in an extended-source repository model.

Choice of System Parameters and Scenario. In this section, we use a set of parameters different from that in the basecase salt repository in the previous sections.

We had two motives in mind when we chose the system parameters for this study: to define a system that could calculate the dose to the "limiting individual," and to choose a system that could test the underground facility (mine) design. The fact that we chose the limiting-individual dose as an appropriate performance measure is actually consistent with the second motive, to test the mine design. Near-field dose is most sensitive to mine design. Far-field population doses are less sensitive to mine-design details and are essentially, if integrated over time, sensitive only to the biosphere emergence time of the radionuclides.[19-23] Thus, if we want to measure the effectiveness of mine designs as barriers; we must concentrate primarily on near-field effects.

That waste-package parameters can mask the effects of mine design as a migration barrier is obvious. For example, if the waste package never fails (i.e., the breach time is infinite or the leach rate is zero), the limiting- individual dose is always zero. Consequently, mine-design changes will not lead to changes in the calculated dose for this type of scenario. Another set of parameters that can lead to zero is hydraulic gradients. If the gradients in the system are zero and remain zero, there will be no radionuclide migration from the system.

To test the sensitivity of individual dose to mine design, we have selected a model that is sensitive to mine-design parameters. In effect, we have chosen waste-package parameters and hydraulic gradients that lead to mine-design sensitivity in the predictions, making the mine-design barrier the only effective barrier in the model. To do this, we have chosen 1000 yrs as the point at which to initiate the transport so as not to influence the results unduly with very short-lived fission products. At 1000 yrs the canisters are considered breached, and the waste is leached out at an average leach rate of 1%/yr. These values are considerably higher than we would expect in a repository. However, we are considering the case of failure of the other barriers; i.e., a low-probability event scenario. Under these circumstances, the major effect reducing the dose is the mine layout. Finally, we have chosen hydraulic gradients that are large enough to cause fairly high flows. The vertical gradient is 0.1 m of water head/m.

In all scenarios for this study, we have distributed one canister of typical defense waste, with radionuclides as shown in Table 3-12. If a point-source model is used, all the waste is in one canister at a designated location. If a distributed source of 25 canisters is used, for example, each model canister has 1/25th of the waste that is in one canister of defense waste. Thus, each scenario is normalized to the same number of initial curies of waste.

Schematic to Describe MISER Runs. To help differentiate between our underground facility models, we have developed a schematic shorthand. Schematics of two cases are shown in Fig. 3-18. The left schematic, consisting of both a top and a side view, shows a one-cell hydraulic flow

Table 3-12. Repository and media parameters at 1000 years.

Upper and lower aquifers

- Depth to upper aquifer = 100 m
- Depth to lower aquifer = 900 m
- Rock type = sandstone
- Hydraulic conductivity = 10^{-4} cm/s
- Length = 3.14 km
- Thickness = 200 m
- Effective porosity = 0.1

Rock barrier

- Depth to aquitard = 300 m
- Vertical pressure gradient = 0.1 m/m
- Rock type = shale
- Hydraulic conductivity = 10^{-8} cm/s
- Length = 3.14 km
- Thickness = 600 m
- Effective porosity = 0.05

Repository

- Depth = 600 m

Storage area

- Length = 2.5 km
- Width = 2.0 km

Tunnel

- Length = 440 m
- Area = 150 m^2

Shaft

- Length = 300 m
- Area = 64 m^2
- Thickness = 6 m

Fracture zone

- Hydraulic conductivity = 10^{-4} cm/s
- Effective porosity = 0.01

Comments

- Steady-state hydrology
- Deteriorated backfill and shaft seals
- Regional hydraulic pressure gradient = 0.005 m/m

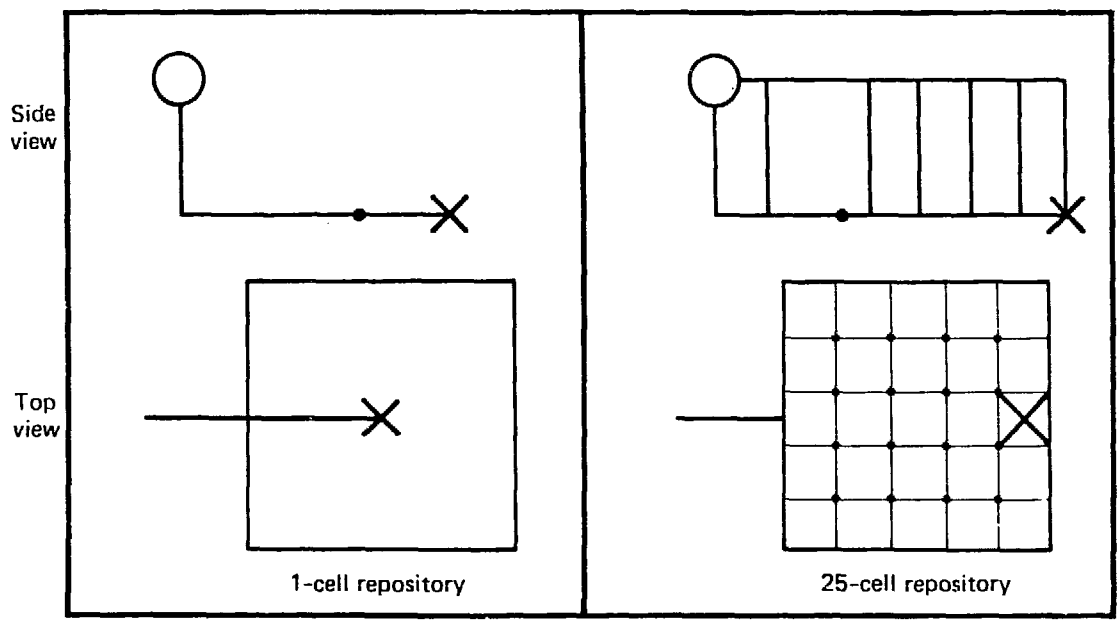

Figure 3-18. Two examples of schematic devised to help describe computer scenarios.

model of a repository storage area. The schematic at right shows a 25-cell flow model of the same storage area. The flow cells for each are depicted by rectangular segments, as seen in the top views.

The "X" in each schematic shows where the waste is emplaced originally, and "O" shows the location of the limiting individual (observer). The dot, seen in the side view, is where the tunnel meets the storage area.

Note that the top and side views are not drawn to scale. Thus the schematic features, unlike those in a mechanical drafting diagram, do not line up. The main purpose of the top view is not alignment, but to show where the waste is located in the storage area. The side view is meant to show the flow paths that waste must travel to reach the observer.

1-Cell Model. The 1-cell case depicted in Fig. 3-18 shows a single series pathway from the waste to the observer. For this case, all waste first migrates from the center of the storage area where it was originally emplaced to the edge of the storage area where it enters the tunnel. Because of the large cross-sectional area in the storage area, compared to that of the tunnel, there is a convergence of streamlines at the tunnel entrance. Thus, there is a large increase in flow rate as the waste enters the tunnel. The time required for the waste to transit the tunnel and shaft to the observer is short compared to the transition time in the storage area. The schematic shows that the waste goes through the storage area to the tunnel, through the tunnel to the shaft, and then up the shaft to the observation point. This is a series pathway.

25-Cell Model. Our more-realistic hydraulic model of the repository storage area (shown at right in Fig. 3-18) has seven parallel paths by which waste traverses to the observer. Where two or more downstream flow tubes leave a node in the schematic, the radioactive waste splits into two or more pulses.

By using centerline symmetry in the model, we can actually model the hydrology of the storage area with 88 flow cells. Without symmetry, the system would require 141 flow cells. The only flow cells shown in the schematic are those on the centerline that have waste flowing through them. The upstream flow cells, which contain uncontaminated water, and the off-centerline flow cells are not shown.

A detailed discussion of the flow in the 25-cell case should prove enlightening. The leftmost vertical line, depicting the shaft in the 25-cell repository, is 300 m long and encompasses an area of 64 m^2. The next vertical line to the right is a schematic of the flow path taken by the waste that leaks out of the tunnel and then flows through the aquitard barrier to the upper aquifer and from there to the observer. The vertical lines to the right of the dot are flow pathways from the storage area to the upper aquifer. The five lines shown represent the five centerline cells. Each of the cells is 0.2 km^2 in cross-sectional area. Because of the large area of these vertical cells, compared to the horizontal flow cells, most of the waste flows upward through the aquitard barrier even though its permeability is much less than the deteriorated backfill permeability of the storage area and tunnel.

If we follow the waste from its source to the observer, as indicated in the side view of the 25-cell repository, we see it starts its journey by splitting into two parts. At the initial node, most of the waste moves upward through the rightmost flow path of the aquitard to the upper aquifer. Once in the upper aquifer the waste does not split again, but proceeds in its entirety to disperse, advect, and mix with other waste as it moves along the upper aquifer until it reaches "O." The remaining portion of waste at "X" starts its journey by moving left along the centerline of the storage area, splitting (leaking) within each of the four flow cells it must traverse as it moves toward the connecting tunnel. Each time it crosses a cell, it leaks radioactivity to the surrounding rock. The leaked waste slowly moves vertically through the barrier rock to the upper aquifer. The unleaked waste that finally reaches the tunnel moves into the tunnel entrance and through it to the shaft. Even as it moves along the tunnel, the waste can leak into the rock barrier. The waste remaining at the end of the tunnel moves up the shaft to the observer, causing his peak dose.

Conservatism of Point-Source Model

In this section we analyze different point-source repository models to establish how their assumptions affect predictions of individual dose. Figure 3-19 shows ten separate point-source models, each of which simulates the same physical system. The ten cases differ in that they use different modeling strategies. By comparing schematics, one can see that Cases 1, 2, 3, 5, and 8 are one-cell-storage-area hydrology models. The other five cases are 25-cell-storage-area hydrology models.

The two relative peak annual dose curves shown in Fig. 3-19 are represented by a thin line and a thick line. The thin line is the peak annual

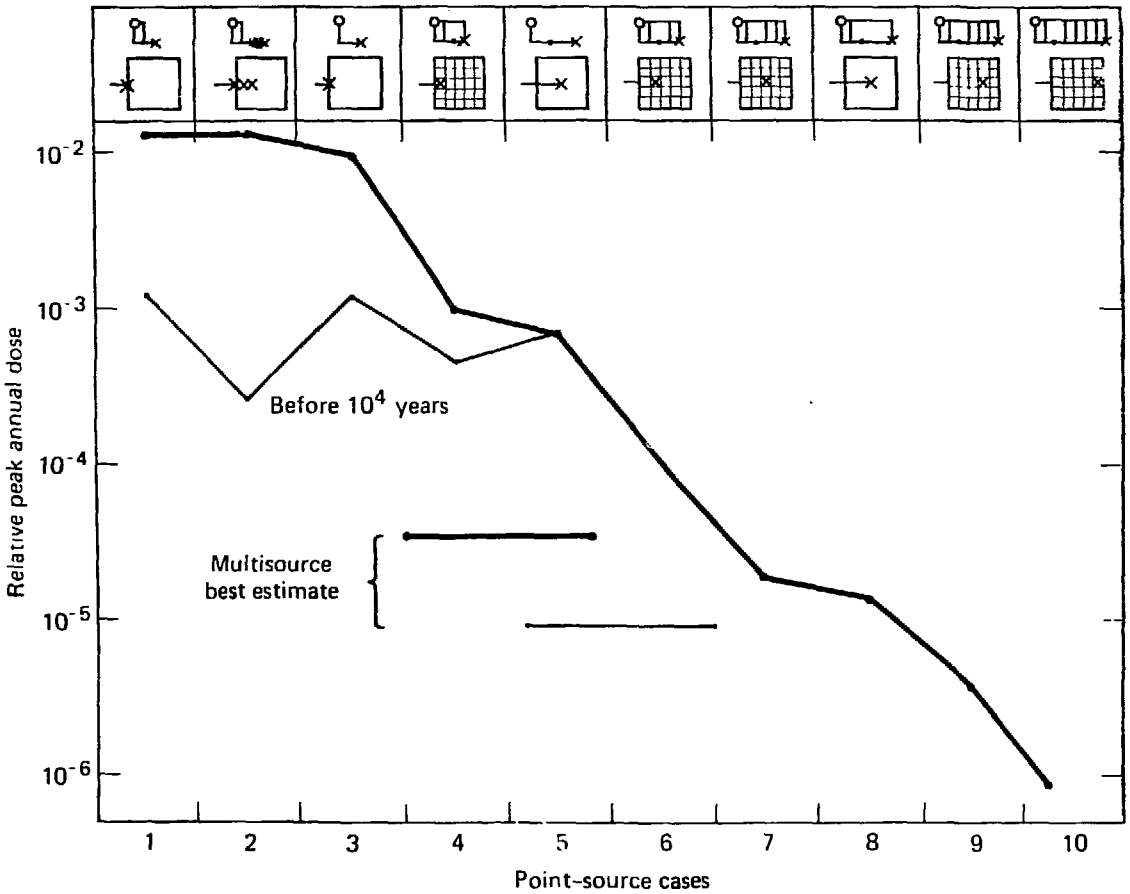

Figure 3-19. Results, arranged in descending order of peak 10^6-yr dose, showing discrepancies among various point-source models of physical waste repository.

dose occurring in the first 10^4 yrs. The thick line is the peak in the first 10^6 yrs. Where the lines coincide, the peak occurs before 10^4 yrs. This occurs for Cases 5–10. We have reported the doses as relative because this is a generic site study and because we have chosen a scenario with many system barrier failures.

For Cases 1–4, the retarded fission products and actinides move through the system quickly enough to be counted before they decay away or before 10^6 yrs have passed. In Cases 1–3, all the waste is at the boundary of the tunnel and the storage area. For Case 4, it is barely inside the storage area. Thus, these cases do not have enough flow within the storage area to realistically detain the retarded radionuclides; therefore, the retarded radionuclides cause the peak dose after 10^4 yrs. In Cases 5–10, unretarded anion fission products cause the peak dose.

Canister Breaching. All cases except Case 2 have initial release of the waste pulse at 1000 yrs. Case 2, however, has 25 canisters of waste that are initially released at times randomly chosen between 1000 and 2000 yrs. Each of the 25 canisters is assumed to have 1/25th of the waste of a real canister, which normalizes Case 2 to the same amount of waste as the other 9 cases. Although, for Case 2, there is no effect on the peak dose for 10^6 yrs, the 10^4-yr dose is reduced several fold. Real repositories will have canisters breaching at different times. Depending on breach-time parameter values, they can have a major effect on near-field individual doses.

Waste-Pulse Branching. In Fig. 3-19, we have arranged the results in descending order of peak 10^6-yr dose. Cases 3 and 5 are single-pathway models. As shown in their schematics, they have only one path from "X" to "O." Case 1, on the

other hand, has two pathways along which waste migrates to the observer. Thus, for every pulse of waste released from "X" in Case 1, there will be two pulses reaching "O." For Cases 3 and 5, there is only one pulse reaching "O" for each pulse released from "X." For Case 10, there are seven pulses reaching "O" for each pulse released.

Branching occurs at each node in the model. Thus, for each of the nodes on the centerline in the schematic of Case 10, the pulse splits into two parts. Most of the waste flows into the vertical path following the major portion of the water; the remaining waste and water flow down the centerline of the storage area toward the tunnel. The result is that seven pulses, each moving along a different path, arrive at "O" for Case 10.

Comparison With Best Estimate. Additional results (horizontal lines) plotted on the figure are from our best-effort model; i.e., one with 25 cells and 1000 canisters. We compare the results from point-source models with these results. For our best-estimate model, we see that the 10^6-yr dose is about a factor of four greater than the 10^4-yr dose. This is not predicted by the point-source models.

The more-conservative point-source cases predict a value that is about a factor of 400 greater than our best estimate. If we use a point-source strategy that minimizes the peak-dose prediction, the results for the 10^6-yr dose are about a factor of 100 smaller than our best estimate.

The peak doses from the point-source model for Cases 5–10 are due to unretarded ^{99}Tc. For the best-estimate case, the peak dose is due to retarded actinides that reach the observer at about 75,000 yrs, not from ^{99}Tc. Thus, even the radionuclides that cause the peak dose can be predicted incorrectly by the point-source models.

The difference in the predicted radionuclides that cause the peak dose is due mainly to the fact that our best-estimate model is a 1000-canister model, each canister of which has a different initial release time. They breach between 1000 and 2000 yrs. The point-source models, however, have only one canister that breaches at 1000 yrs. This leads to a single pulse from the nearest storage cell of relatively nondiluted ^{99}Tc, which causes the peak dose. In the best-estimate model, the ^{99}Tc is diluted by the many canisters releasing at different times and locations. Thus, the peak dose for the best estimate is due to retarded cations, not to ^{99}Tc, which migrates as an anion.

In summary, point-source models can lead to very misleading predictions of individual dose. An apparently conservative strategy might not lead to a conservative result. For example, Cases 7 and 8, which appear heuristically conservative, do not predict a dose that is as high as the best estimate. Alternatively, ultraconservative models (i.e., Case 1) can produce results that are actually two or three orders of magnitude too high. Besides being substantially too high or too low, point-source models can predict the wrong radionuclides as the main cause of peak dose.

We conclude that the choices in a point-source model are quite arbitrary and can lead to poor or misleading predictions of near-field individual doses. Also, predictions from point-source models of curies released to the near field must be considered very questionable. To adequately predict repository releases in the local vicinity will require more-sophisticated models of the repository than point-source models.

Point-Source and Extended-Source Comparisons

Figure 3-20 shows the results generated to test the effect of smearing-out the same amount of waste over different fractional areas of a repository. In each case, the amount of smeared-out waste totals a single canister. The observed reduction of calculated dose (the more reduction, the greater the spatial separation of the canisters) will tend to reduce the significance of lower leach-rate waste forms. In fact, where the permeabilities are quite low, the individual's dose could be very insensitive to the choice of waste form.

The relative peak annual dose to a limiting individual is shown on the ordinate of the figure. On the abscissa, we have labeled the cases by the areal fraction of the repository that has been used to store the waste. The top view of the schematic shows the location and areal coverage of the waste in the repository.

Other cases, shown to the right of the 0/25 case, have more detail and spatial coverage of the repository. The 0/25 case is a point-source repository. To its right is a model that covers 1/25 of the repository area. The next four cases cover 2/25, 4/25, 9/25, and 25/25 of the area of the repository. Each of these cases has one canister per cell. The rightmost case is a model of a 1000-canister repository.

We have plotted two curves in Fig. 3-20. The first curve, depicted by a thick line, shows the peak dose to the limiting individual, which occurs in the first million years. The second curve, the thin line, is the maximum dose reached in the first 10,000 yrs. For these cases, we notice that the peak dose always occurs after 10,000 yrs. This is espe-

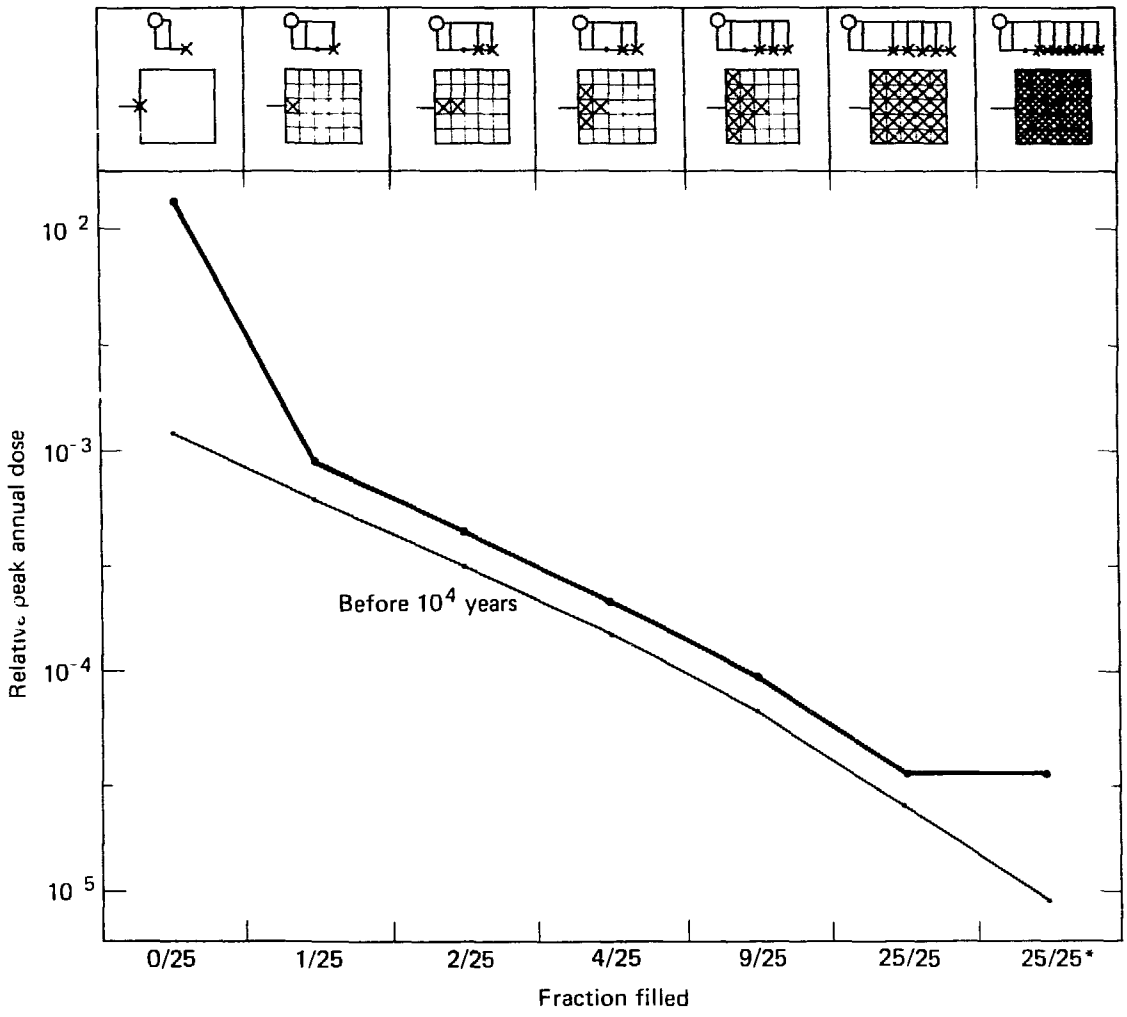

Figure 3-20. Results generated to test effect of smearing-out same amount of waste over different fractional areas of repository, showing dose sensitivity to spatial distribution of source term.

cially true of the point-source repository case, which has an order-of-magnitude difference between the thick and thin lines. The difference is caused by retarded actinides contributing to the dose before one million years. Note that in the point-source model the nuclides do not have to travel through the media and storage rooms of the repository. For retarded nuclides, this travel time is significant in predicting which nuclides cause the peak dose.

A large difference between the thick and thin lines results for the 1000-canister case, i.e., the 25/25* case. Here the initial leach time occurs between 1000 and 2000 yrs. In all other cases, all canisters leach simultaneously at 1000 yrs. This produces a large effect on the anion pulses because they have no retardation. Its effect on the retarded fission products and actinides is insignificant because their release into the upper aquifers covers tens of thousands of years.

In conclusion, we see that the difference between a conservative point-source model, the 0/25 case, and a detailed 1000-canister model is about two orders of magnitude. Besides these differences, the radionuclide causing the peak dose also changes from the 0/25 case to the 25/25* case.

Some Engineering Features of Repositories

Some simple engineering of the hydraulic parameters of a repository can reduce the dose to future individuals living close to a repository. In this section, we examine some simple engineered considerations that show potential for reducing near-field doses. To save computer costs, a 9-cell repository model was used instead of a 25-cell one. Comparison shows that results from the 9-cell model are consistently about 15% below those from the 25-cell model. Since the range of doses for the engineered-features cases we have examined is two orders of magnitude (see Fig. 3-21), the 9-cell-model approximation appears adequate for a relative comparison of repositories with different design features.

The curve shown in Fig. 3-21 is peak individual dose in the first 10^6 years. The cases we have analyzed are referred to as standard case, upstream-shaft, off-tunnel storage, and hydraulic bypass, each of which is discussed below.

Standard Case. For our standard case, we chose a downstream shaft with a repository storage area that is uniformly filled over its entire area. This is shown as Case 1 in Fig. 3-20. The limiting individual's peak annual dose is 3.0×10^{-3} units. Given enough time, all standard-case radioactivity from each of the nine cells of the repository migrates to the observer. This is shown for centerline cells by the side view of the schematic.

Upstream-Shaft. If we specify flow from the left by changing our model boundary conditions, the observer finds himself upstream with respect to the horizontal regional gradients. The solution of the hydrology equations for the upstream-shaft system, however, shows water flows in the tunnel to the left, actually against the regional horizontal gradient. This is driven by the stronger vertical gradient. Because the vertical gradient is large and the permeability of the tunnel and shaft is much greater than the aquitard barrier, some radioactivity in the repository migrates from the repository, through the tunnel, and up the shaft to the observer. This is the path of least resistance for a portion of the repository waste. The migration through the tunnel is shown in the Case 2 schematic for waste nearest the tunnel. The side-view schematic for Case 2 shows that two-thirds of the radioactivity on the centerline moves up through the aquitard barrier and down the aquifer to the right. This waste is never seen by our observer at "O."

The upstream-shaft dose to the limiting individual is reduced by about a factor of two over that for the base case. The conclusion, however, is sensitive to the hydrology parameters chosen for this study. More horizontal gradient and less vertical gradient could result in zero observed dose at the observation point, which means that the limiting dose would be at a different point in the system.

Off-Tunnel Storage. Returning to the downstream-shaft case (our standard case), we design a system so that there is a waste-exclusion area along the centerline of the repository. We model this area as no waste in the three centerline cells, shown in the Case 3 schematic. Unlike Case 2, waste from all the cells ultimately migrates to the downstream observation point. The fact that it is delayed by the exclusion zone, however, reduces the limiting individual's dose about a factor of 10 below the standard-case value.

Hydraulic Bypass. The final case is for a hydraulic bypass design which differs from the study presented earlier in that this study is deterministic and uses a very rapid release rate. The engineered bypass encircles the repository by 50 m. The dashed lines in the schematic indicate portions of the bypass where water flows but waste does not, while the solid lines show where waste flows from its storage location to the observation point. Arrows show the direction of waste flow when the direction is other than toward the observation point.

The 10-m-high bypass runs below the 2-km width of the repository, and its permeability is the same as that of the aquifer. Thus, the bypass can be conceptualized as another horizon to the repository, with 10-m-high ceilings and a 2-km width. It is filled with very permeable material. This 20,000-m^2 hydraulic conduit runs under the tunnel and shaft and connects into vertical conduits that have the same permeabilities as the aquifer, 20,000-m^2 areas, and are located at both ends of the repository.

Our limiting individual's dose for this repository design is reduced by two orders of magnitude from the standard-case value. One might ask what dose the limiting individual would receive if he moved his well 50 m to the left, where it would then be downstream of the bypass discharge into the upper aquifer. Since the dilution in the bypass is greater than that in the tunnel and shaft, the limiting individual's dose should still be lower than our standard-case results. In other words, the hydraulic bypass can effectively reduce the limiting individual's dose whether he is at the well or at the bypass discharge.

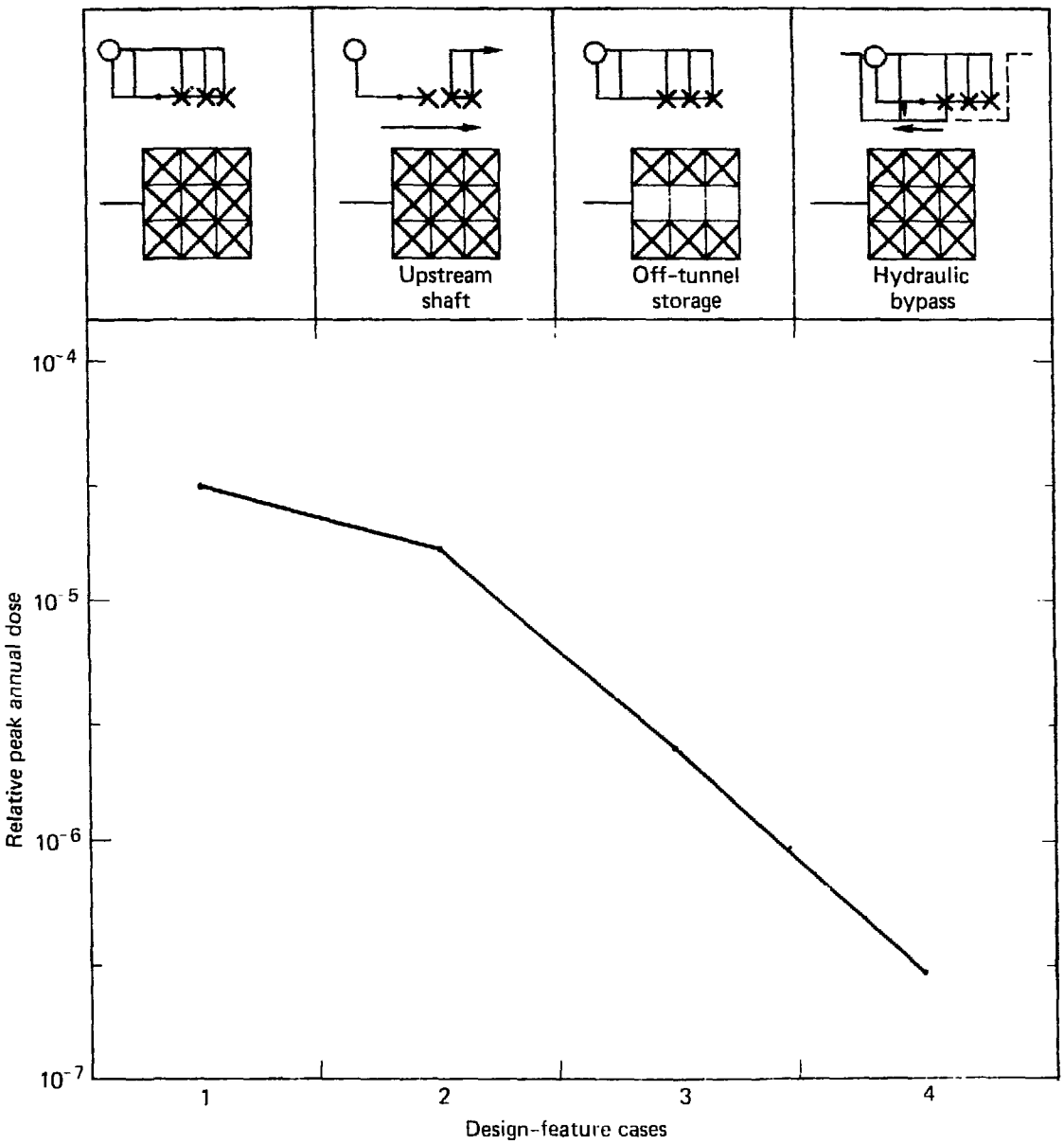

Figure 3-21. Peak individual dose in first 10^6 yr, showing dose sensitivity to various design features.

We conclude that engineered features could be integrated into a repository design that would lead to substantial reductions in forecasts of near-field doses to individuals. We suspect that a reduction of over four orders of magnitude in a deterministic study can be obtained by combining the features examined here for a specific site. Searching for optimum results and expanding the features could improve the near-field individual dose even further. Such site-specific numerical studies would be relatively inexpensive and would certainly help attain an ALARA-designed repository.

Comparison of MISER and Other Models

Comparison calculations were made with MISER and NWFT, a network code developed by Sandia. The release of two radionuclides, ^{240}Pu and ^{236}U, from a sealed nuclear waste repository using the MISER model is compared with that reported by Sandia. We find that when we use the same waste release model, a step-function, the results are in agreement. In Figs 3-22 and 3-23 the dotted lines are NWFT results, the solid lines are those from MISER.

Reference 25 shows that the results from NWFT are in close agreement with those obtained using the three-dimensional finite difference model SWIFT; therefore, we conclude that MISER is also in agreement with SWIFT. Although such agreement does not prove validation of any of the models, it may lend credibility to peer acceptance.

From previous studies, we know that if the pulse spread due to dispersion is relatively small, (9.4×10^3 in this case), the pulse shape is strongly dependent on the shape of the release function. Figures 3-24 and 3-25 compare the MISER Green's function release form with the step-function release of NWFT. The MISER release is truncated at $\pm 2\sigma$. Using Fig. 3-26, the undecayed nuclide flux at the release point, we conclude from Fig. 3-24 that when the relatively short half-life (6.76×10^3 yrs) of ^{240}Pu is folded into the flux, the decay is more rapid than the build-up of flux. In the case of ^{236}U (half-life = 2.39×10^7 yrs), the decay has little effect on the pulse, and the peak release is larger (4.4×10^{-5} Ci/day as compared to 2.7×10^{-5} Ci/day) for the Green's function release, as shown on Fig. 3-25.

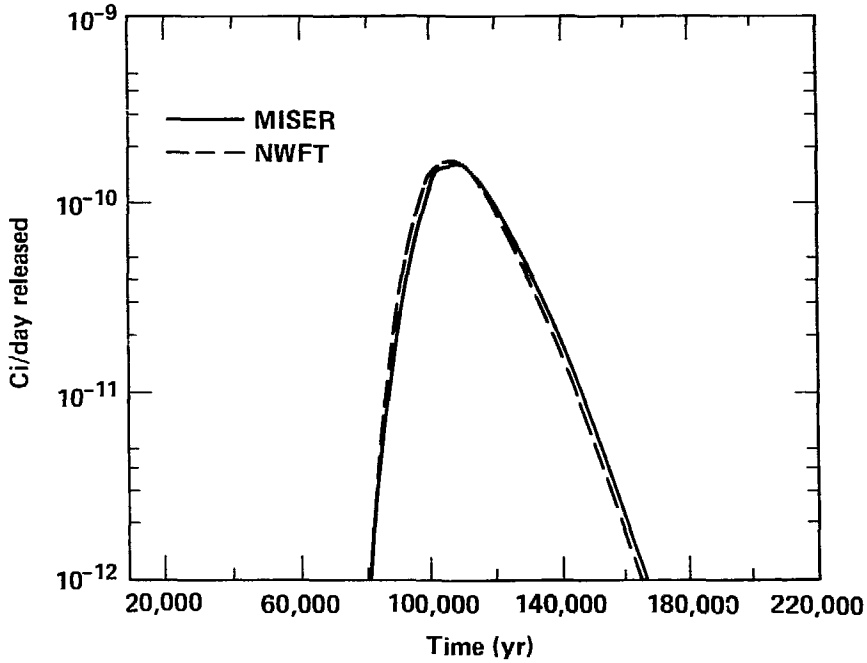

Figure 3-22. Release (Ci/day) of ^{240}Pu as a function of time, step release.

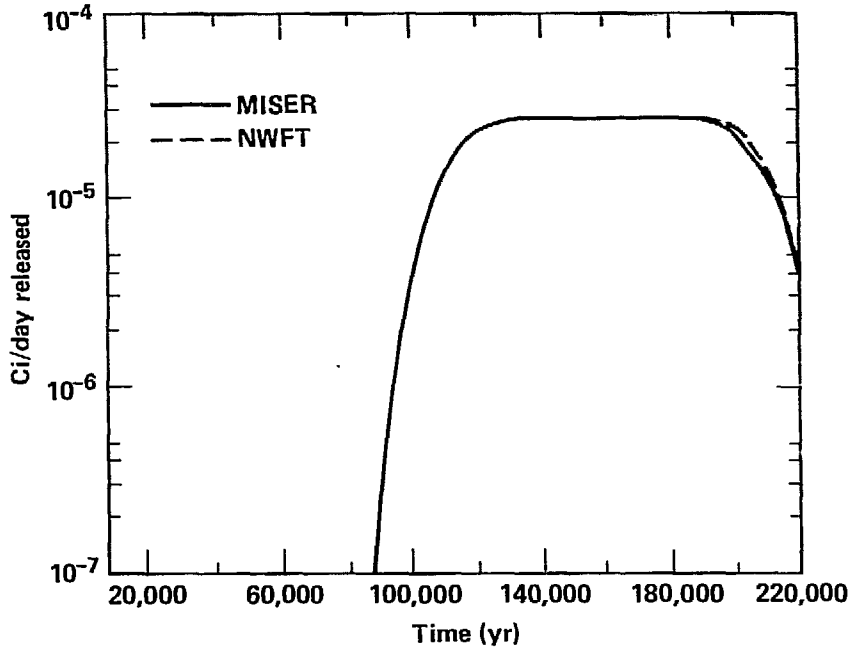

Figure 3-23. Release (Ci/day) of ^{236}U as a function of time, step release.

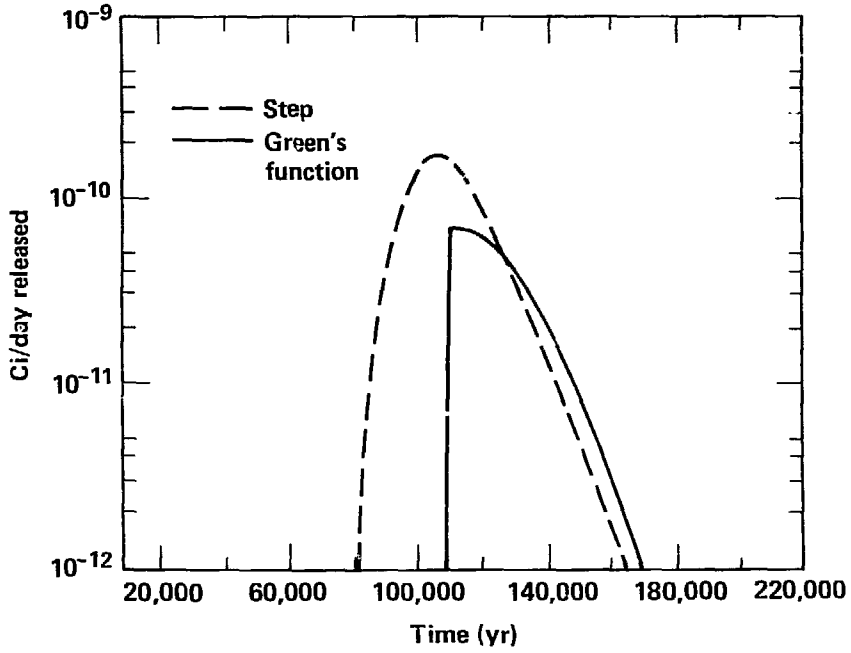

Figure 3-24. Release (Ci/day) of ^{240}Pu as a function of time for step release and Green's function releases truncated at $\pm 2\sigma$.

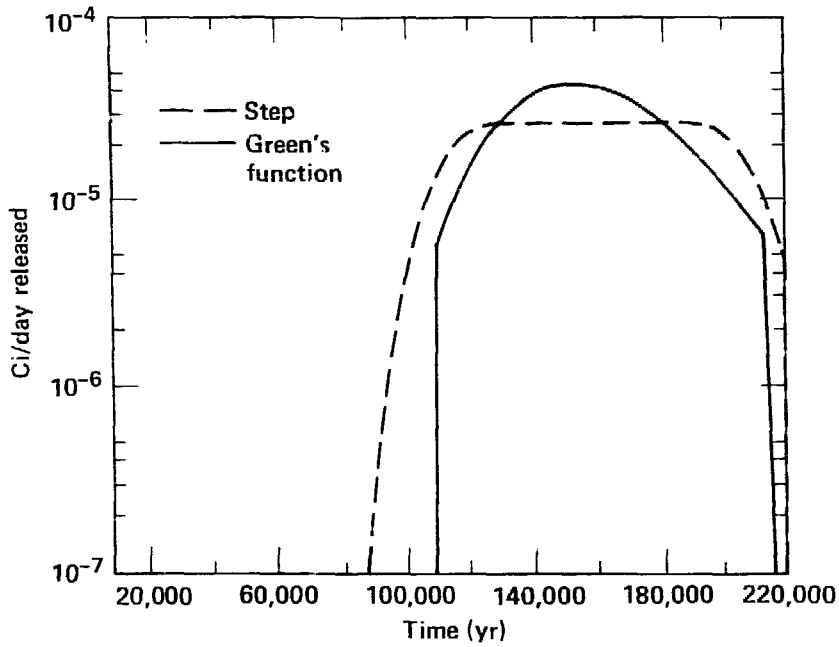

Figure 3-25. Release (Ci/day) of ^{236}U as a function of time for step release and Green's function releases truncated at $\pm 2\sigma$.

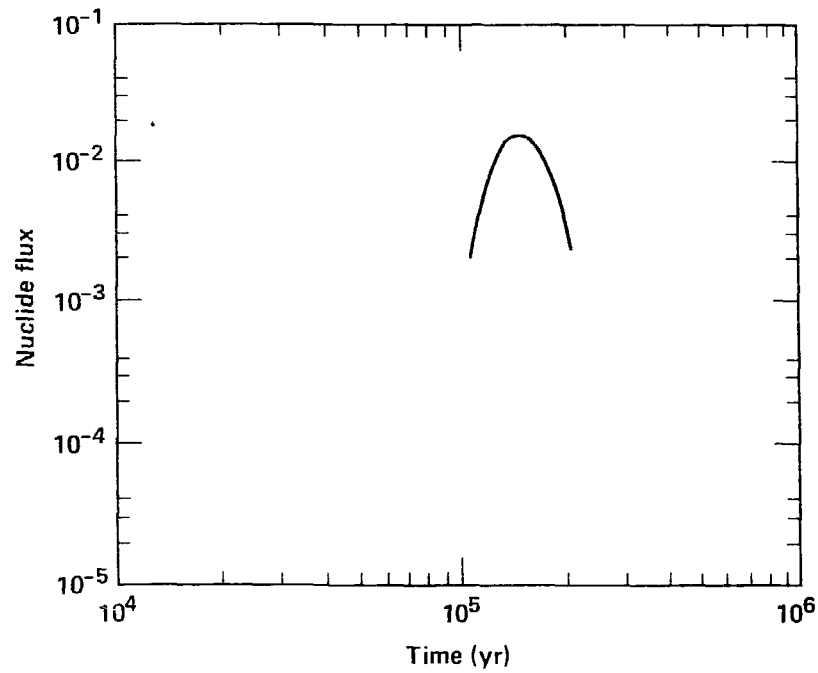

Figure 3-26. Undecayed nuclide flux as a function of time for Green's function releases truncated at $\pm 2\sigma$.

Figure 3-27 shows a comparison of the undecayed flux due to the step-release and Green's function releases truncated at $\pm 2\sigma$ and $\pm 3\sigma$. The flatter pulse is from the step release. Except for leading and trailing edges and a slight difference at the peak, the two Green's function releases essentially agree.

Figures 3-28 and 3-29 compare the step release with a Green's function release truncated at $\pm 3\sigma$. For the case of ^{240}Pu the leading edge build-up is in closer agreement than when truncated at $\pm 2\sigma$. The peak release for the $\pm 3\sigma$ is 6.84×10^{-11} Ci/day, for the $\pm 2\sigma$ is 7.13×10^{-11} and for the step is 1.68×10^{-10}. The choice of truncation can be arbitrary in the model. If peak nuclide release is the measure, then $\pm 2\sigma$ is slightly conservative for a single nuclide pulse.

Based on these results one cannot conclude that one model is better than the other. However, for peak doses exhibited by long-lived nuclides, the Green's function release would be more conservative. We also know that if one does a more realistic model of the repository, the resulting dose is due to many pulses arriving at the release point. In this case the resultant nuclide flux is quite insensitive to the shape of any particular pulse as discussed earlier.

One can conclude from these results that even for a long aquifer run-out, the dose due to any single nuclide is dependent on the shape of the release function. Generalizing this concept to the total repository, since the shape of the release function is also dependent on repository design, the design must be adequately accounted for to obtain a reliable model dose, even if there is a long geosphere run-out.

Sensitivity and Uncertainty Analyses

Selected Sensitivity Studies

In Ref. 28 we reported numerous parametric analyses based on a single path model. In those analyses we considered the impact of generic waste form properties under a range of geologic conditions. In the section "Release Rates and Uncertainties," we performed an uncertainty-sensitivity study on waste dissolution properties in a network model of the basecase salt repository. In this section we report results of additional sensitivity studies, two dealing with the hydraulic gradients and two dealing with model choices. In all these cases we use the 89-pathway network of the basecase salt repository.

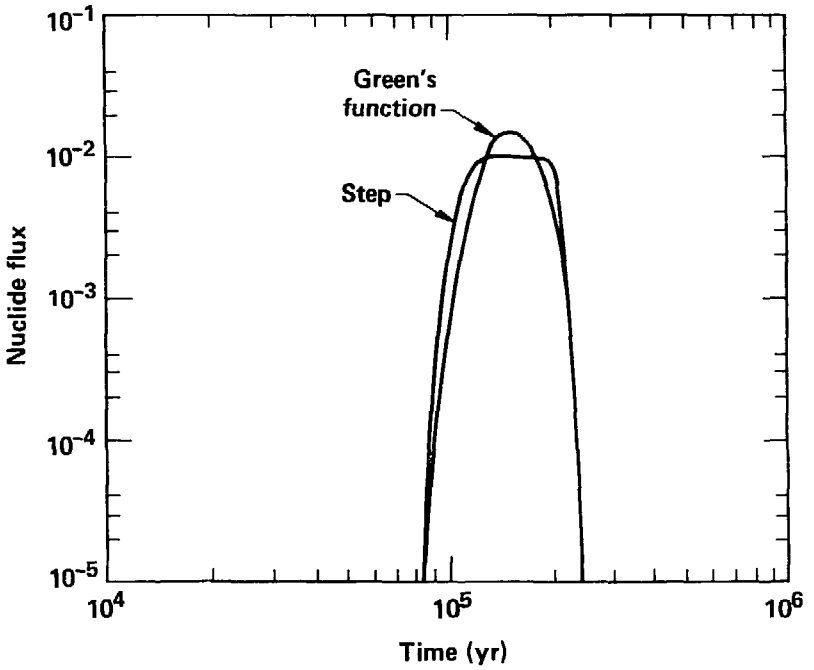

Figure 3-27. Comparison of undecayed nuclide flux as a function of time for step release, and Green's function releases truncated at $\pm 3\sigma$.

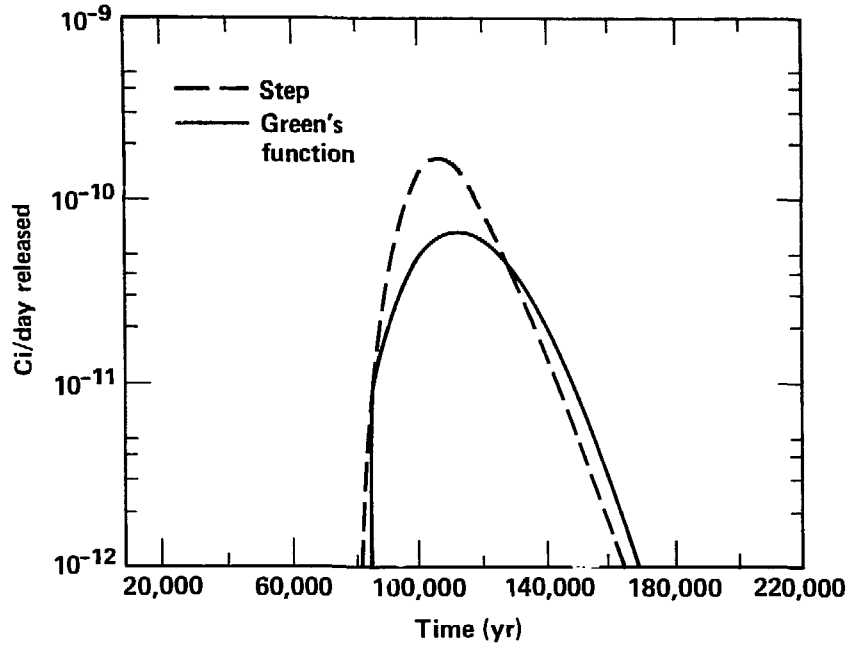

Figure 3-28. Release (Ci/day) of ^{240}Pu as a function of time for step release and Green's function releases truncated at $\pm 3\sigma$.

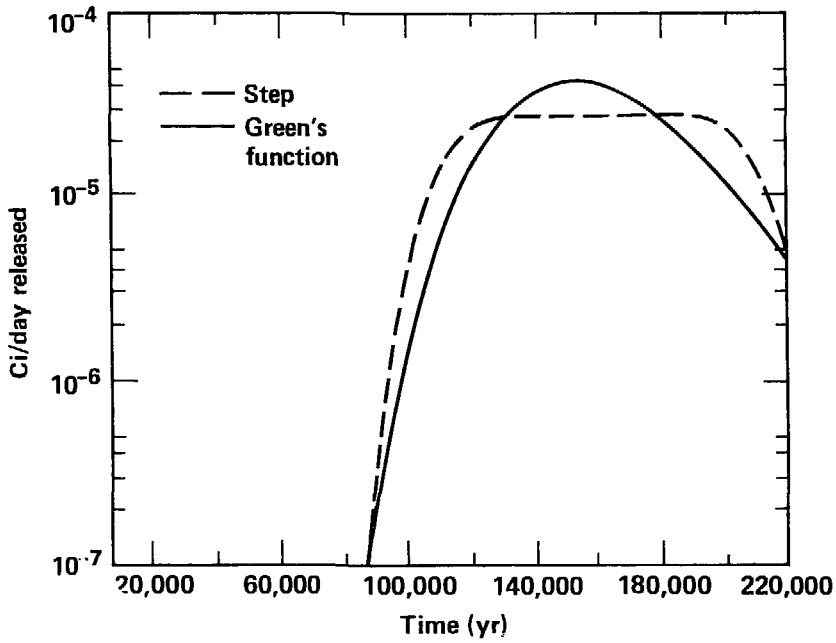

Figure 3-29. Release (Ci/day) of ^{236}U as a function of time for step release and Green's function releases truncated at $\pm 3\sigma$.

Horizontal Gradient. In this study we fix all parameters of the network at their median values (see Table 3-13) and vary the horizontal gradient of the system from 10^{-6} m/m to 10^{-2} m/m. The vertical gradient is fixed at 0.01 m/m. Figure 3-30 is a plot of water speeds in the air shaft, main shaft and upper aquifer. We observe a linear dependence of upper aquifer speed with horizontal gradient as expected. We further observe a near independence of shaft speeds until the gradient reaches 10^{-3} m/m. At this point we observe a rapid fall off in shaft speed and by 5×10^{-2} m/m the flow in the shafts has reversed; i.e., shaft flow is downward.

Table 3-13 gives the peak and time of peak dose for the limiting individual (LI) 237 m downstream of the shafts, the accessible environment individual (AEI) 1.58 km downstream of the repository, and an individual using the Columbia River (CRI) 20 km downstream of the repository. Figure 3-31 is a plot of the peak doses as a function of horizontal gradient.

For the LI peak dose we observe a linear dropoff as long as the dose is all due to the unretarded Group I. As expected this is due to the shaft dilution factor which is directly related to the linear aquifer speed and near constant shaft speed. Above 10^{-4} m/m the retarded Groups II

Table 3-13. Peak doses (rem/yr) and time of peak (yr) for varying horizontal gradients (all CRI beyond 10^6 yr are extrapolated values).

Horizontal gradient	Total		Peak dose (rem/yr) and time (yr)					
			Group I		Group II		Group III	
m/m	Peak	Time	Peak	Time	Peak	Time	Peak	Time
A. Limiting Individual (LI)								
10^{-6}	6.36×10^{-1}	2.06×10^{5}	6.36×10^{-1}	2.06×10^{5}	6.84×10^{-4}	1.39×10^{6}	~0	1.48×10^{8}
10^{-5}	1.23×10^{-1}	1.07×10^{5}	1.23×10^{-1}	1.07×10^{5}	7.54×10^{-3}	1.14×10^{6}	5.90×10^{-12}	1.58×10^{7}
5×10^{-5}	2.57×10^{-2}	1.14×10^{5}	2.51×10^{-2}	1.00×10^{5}	1.20×10^{-2}	3.49×10^{5}	7.99×10^{-4}	2.20×10^{6}
10^{-4}	1.56×10^{-2}	1.14×10^{5}	1.23×10^{-2}	9.36×10^{4}	1.04×10^{-2}	2.20×10^{5}	1.89×10^{-3}	1.58×10^{6}
5×10^{-4}	1.33×10^{-2}	7.69×10^{5}	2.23×10^{-3}	9.36×10^{4}	2.89×10^{-3}	1.30×10^{5}	1.33×10^{-3}	7.69×10^{5}
10^{-3}	2.72×10^{-2}	8.21×10^{5}	9.41×10^{-4}	1.00×10^{5}	1.26×10^{-3}	1.14×10^{5}	2.72×10^{-2}	8.21×10^{5}
2.5×10^{-3}	2.58×10^{-2}	5.53×10^{5}	1.65×10^{-4}	1.00×10^{5}	2.22×10^{-4}	1.07×10^{5}	2.58×10^{-2}	5.53×10^{5}
$5. \times 10^{-3}$	0	–	0	–	0	–	0	–
10^{-2}	0	–	0	–	0	–	0	–
B. Accessible Environment Individual (AEI)								
10^{-6}	2.23×10^{-3}	1.14×10^{6}	2.23×10^{-3}	1.14×10^{6}	7.92×10^{21}	5.91×10^{7}	0	–
10^{-5}	2.61×10^{-2}	2.20×10^{5}	2.61×10^{-2}	2.20×10^{5}	1.33×10^{-6}	9.36×10^{6}	~0	–
5×10^{-5}	7.47×10^{-3}	1.22×10^{5}	7.47×10^{-3}	1.22×10^{5}	2.55×10^{-4}	2.51×10^{6}	~0	–
10^{-4}	3.79×10^{-3}	1.14×10^{5}	3.79×10^{-3}	1.14×10^{5}	5.25×10^{-4}	1.30×10^{6}	~0	–
5×10^{-4}	7.02×10^{-4}	1.00×10^{5}	7.02×10^{-4}	1.00×10^{5}	5.92×10^{-4}	3.49×10^{5}	1.55×10^{-3}	1.69×10^{7}
10^{-3}	3.25×10^{-4}	1.30×10^{5}	2.96×10^{-4}	1.00×10^{5}	3.29×10^{-4}	2.20×10^{5}	2.24×10^{-8}	8.21×10^{6}
2.5×10^{-3}	1.03×10^{-4}	1.30×10^{5}	5.20×10^{-5}	1.00×10^{5}	6.59×10^{-5}	1.58×10^{5}	6.75×10^{-6}	4.25×10^{6}
$5. \times 10^{-3}$	8.70×10^{-6}	3.98×10^{6}	1.63×10^{-9}	1.93×10^{6}	3.76×10^{-7}	3.27×10^{6}	8.38×10^{-6}	3.98×10^{6}
10^{-2}	4.59×10^{-5}	1.93×10^{6}	1.69×10^{-8}	1.14×10^{6}	6.31×10^{-7}	2.20×10^{6}	4.53×10^{-5}	1.93×10^{6}
C. Columbia River Individual (CRI)								
10^{-6}	~0	–	~0	–	0	–	0	–
10^{-5}	5.52×10^{-10}	1.14×10^{6}	5.52×10^{-10}	1.14×10^{6}	0	–	0	–
5×10^{-5}	1.37×10^{-8}	3.06×10^{5}	1.37×10^{-8}	3.06×10^{5}	3.20×10^{-14}	1.93×10^{7}	~0	–
10^{-4}	2.04×10^{-8}	1.93×10^{5}	2.04×10^{-8}	1.93×10^{5}	1.23×10^{-11}	1.07×10^{7}	~0	–
5×10^{-4}	2.34×10^{-8}	1.22×10^{5}	2.34×10^{-8}	1.22×10^{5}	5.79×10^{-9}	2.20×10^{6}	~0	–
10^{-3}	2.03×10^{-8}	1.07×10^{5}	2.03×10^{-8}	1.07×10^{5}	1.52×10^{-8}	1.14×10^{6}	~0	–
2.5×10^{-3}	1.41×10^{-8}	5.18×10^{5}	9.01×10^{-9}	1.07×10^{5}	1.41×10^{-8}	5.18×10^{5}	~0	–
5×10^{-3}	6.18×10^{-11}	2.51×10^{6}	1.28×10^{-13}	1.93×10^{6}	6.17×10^{-4}	2.51×10^{6}	~0	–
10^{-2}	2.12×10^{-10}	2.68×10^{6}	2.66×10^{-12}	1.14×10^{6}	2.12×10^{-10}	2.68×10^{6}	~0	–

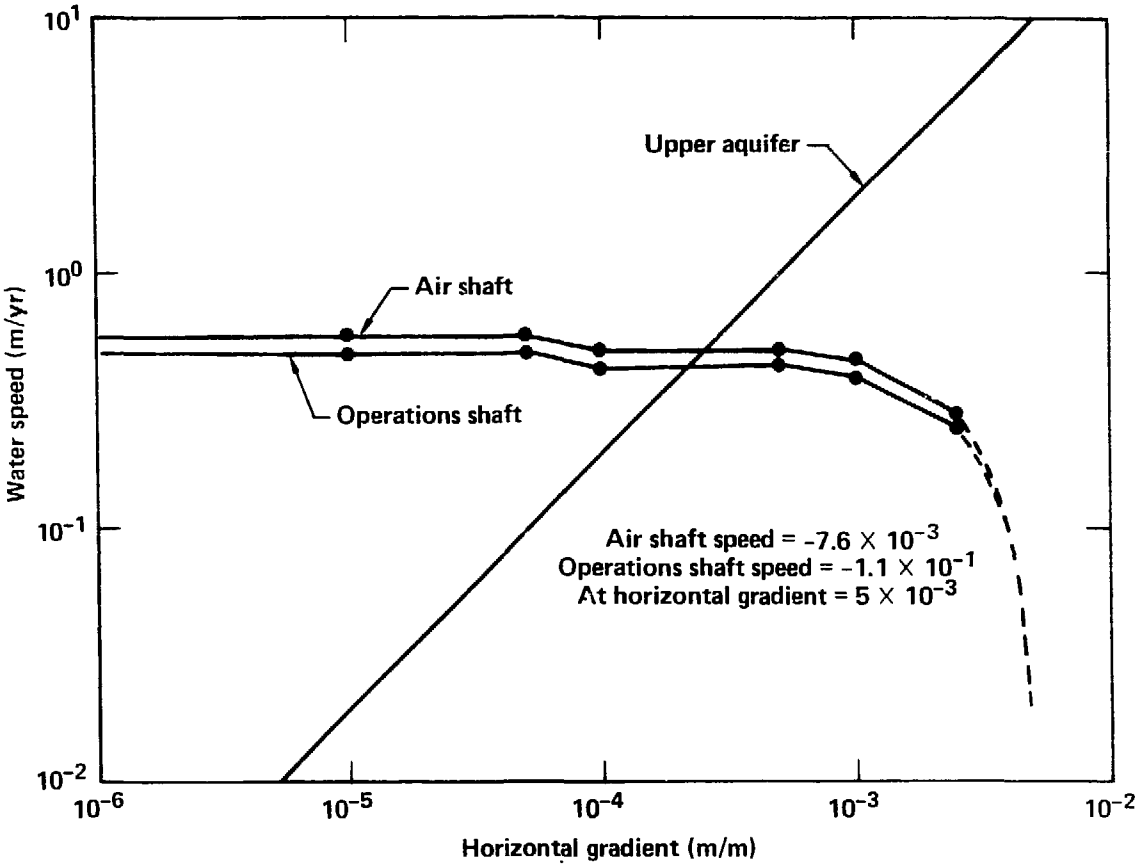

Figure 3-30. Water speeds in upper aquifer, air shaft, and operations shaft as a function of horizontal pressure gradient; vertical pressure gradient is fixed at 0.01 m/m. Note flow reverses in shafts between 2.5×10^{-3} and 5×10^{-3}.

and III with higher toxicity dominate. When the shaft flow reverses the LI dose goes to zero.

The AEI dose exhibits similar attributes with two exceptions. The difference between 10^{-6} and 10^{-5} m/m is due to the decay of Group I over about 9×10^5 yrs; i.e., the slow transit time from the shafts to the observation point. The increase in dose between 5×10^{-3} and 10^{-2} m/m is caused by the arrival of the actinides in much shorter transit time after flow up through the media.

The CRI doses are relatively constant when the peak occurs in 10^6 or less years. The extrapolated values for horizontal gradients less than 5×10^{-5} indicate such a slow transit time that decay dominates. The CRI behaves much like AEI for high gradient flow.

Vertical Gradient. With the horizontal gradient fixed at 10^{-3} m/m, we computed peak doses for 10^{-1} m/m and 10^{-3} m/m vertical gradient. These results are shown in Table 3-14.

These data indicate that the LI and AEI doses are not nearly as sensitive to the vertical gradient as they are to the horizontal gradient.

Five and Twenty-Five Canisters per Cell. Our network model has three cells representing the repository storage rooms. The MISER model allows an arbitrary number of canisters to be placed in each cell. Each canister may have differing "across the cell" transit times as discussed in Section 2 under the subsection, "Transport Green's Function." Since each canister produces a waste pulse that must be followed to the observation

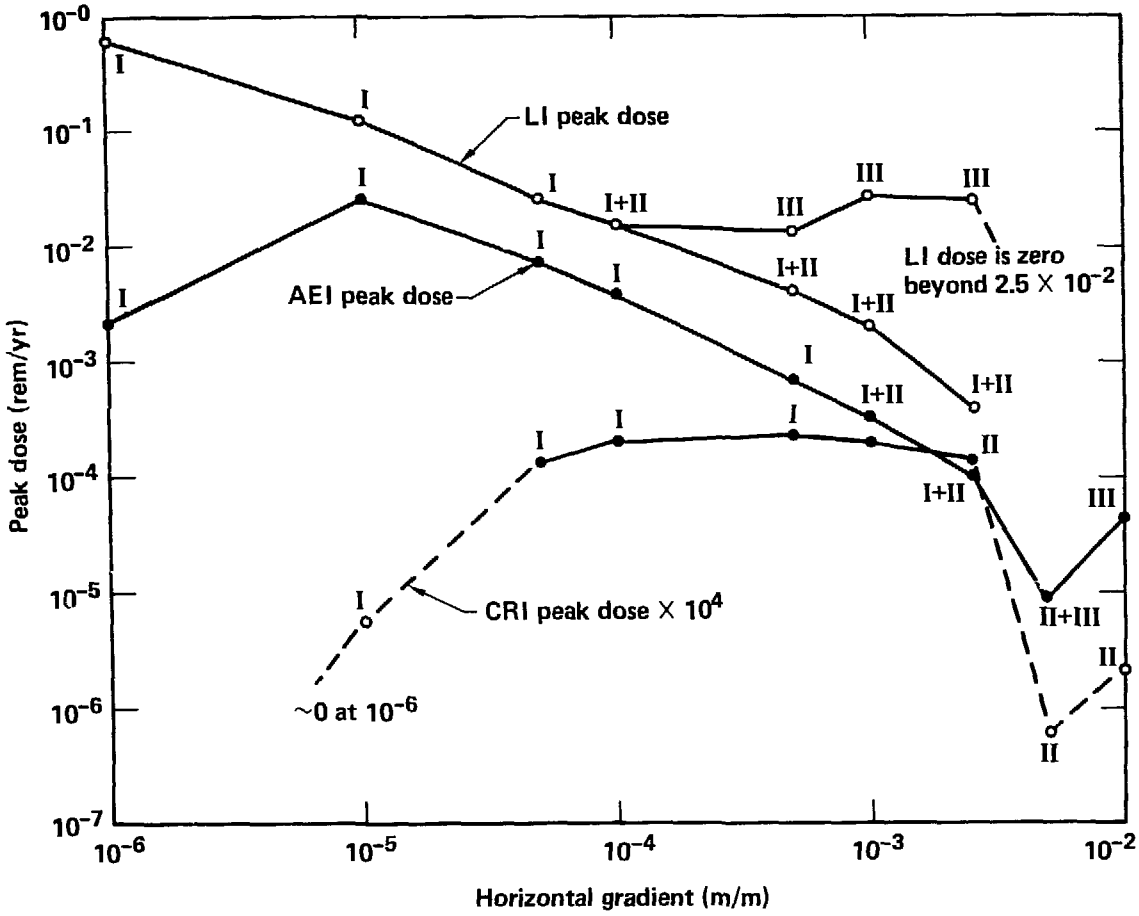

Figure 3-31. Peak dose as a function of horizontal gradient (numbers indicate dominant contributor to peak dose).

Table 3-14. Sensitivity of calculated doses to vertical gradient.

Vertical gradient m/m	Peak dose, rem/yr (at time, yr)		
	LI	AEI	CRI
10^{-1}	3.72×10^{-2} (8.21×10^{5})	4.85×10^{-5} (1.93×10^{5})	2.88×10^{-8} (1.07×10^{5})
10^{-2}	2.72×10^{-2} (8.21×10^{5})	2.96×10^{-4} (1.0×10^{5})	2.03×10^{-8} (1.07×10^{5})
10^{-3}	0	4.3×10^{-10} (1.14×10^{7})	3.2×10^{-14} (1.14×10^{7})

point, computer time increases as the number of canisters increases.

In our analyses we used five canisters per cell. For comparison, Figures 3-32 through 3-35 show the 100-trial probability curves for LI, AEI, CRI, and CRP6, respectively. One observes only minor differences and can conclude that the five-canister case is a reasonable representation.

Transport and Release Functions. We have stated that with the extended source repository (see "Point-Source and Extended-Source Comparisons") many waste pulses are generated. At an observation point these many pulses overlap and only the envelope is important; i.e., the model becomes insensitive to the particular shape of any single pulse.

Figures 3-36 through 3-39 compare LI, AEI, CRI and CRP6 doses for 100-trial cases using a Gaussian

$$g(\sigma, \tau, t) = \frac{1}{(2\pi)^{1/2}\sigma} \exp\left[-\frac{(t-\tau)^2}{2\sigma^2}\right]$$

and an approximate Green's Function

$$G(\sigma, \tau, t) = \frac{1}{(2\pi)^{1/2}\sigma}\left(\frac{\tau}{t}\right)^{3/2} \exp\left[-\frac{(t-\tau)^2 t}{2\sigma^2 t}\right]$$

release and transport models.

Figures 3-40 and 3-41 compare AEI and CRI doses for the Gaussian release and transport with a simple flat pulse release and transport. That is,

$$F(\sigma, \tau, t) = \begin{cases} f/4\sigma & \text{for } \tau - 2\sigma \le t \le \tau + 2\sigma \\ 0 & \text{otherwise} \end{cases}$$

where f is the fraction of waste in the given path.

Since the statistical curves are nearly identical we conclude that when many pulses are involved, the final dose computed is essentially independent of individual pulse shapes.

Statistical Parameter Sensitivities

A major uncertainty in calculated repository performance is caused by uncertainty in model input parameters. Such performance uncertainty can be calculated using Monte Carlo techniques. To obtain a feeling for repository performance sensitivity to various input and intermediate parameters, correlation of these parameters with their corresponding dose can be calculated.

Because of the form of our data, we have chosen to represent many of our input parameters as lognormal distributions. We also have included correlations where appropriate between input parameter distributions. We know that groups of parameters operate together to enhance the dose, thus a systematic multiparameter correlations study would be useful but is beyond the scope of this work.

The calculated correlation coefficients for the intermediate parameters are shown in Table 3-15. The most significant correlations are for the Group I dose rate, the peak dose rate time-of-arrival, and the Group II dose rate. Of lesser importance, but still of significance, are the water velocity in the upper aquifer, the water velocity in the tunnel which connects the repository storage area to the operations shafts, and the horizontal gradient across the repository, which, of course, influences the aquifer water velocity.*

Another concern is that correlations are calculated over the total number of samples. As will be discussed below, when regulatory standards and background radiation levels are important to establish the actual desirability of a particular configuration, the correlations at the lower dose levels can be misleading because their influence on the correlation coefficient can be weighted unduly high.

A cursory inspection of calculated repository dose rates shows distributions which look unimodal and somewhat symmetrical about the mode when the logarithm of the dose rate is plotted. Because the input and results are lognormal and lognormal-like, respectively, we calculate the correlation coefficient of the logarithm of the normalized parameters and dose rates. The normalized values are obtained by dividing all values of a distribution by the largest value in the distribution. We also order the peak doses from highest to lowest. This requires a corresponding reordering of their input and intermediate parameters as well.

*The gradient does not, however, directly determine the aquifer water velocity since the velocity also requires selection of permeability and effective porosity for its calculation. Thus, the gradient is expected to have less influence on calculated dose than water velocity. This is borne out, since we had a calculated horizontal gradient correlation coefficient of 0.10, and a water velocity correlation coefficient of 0.18.

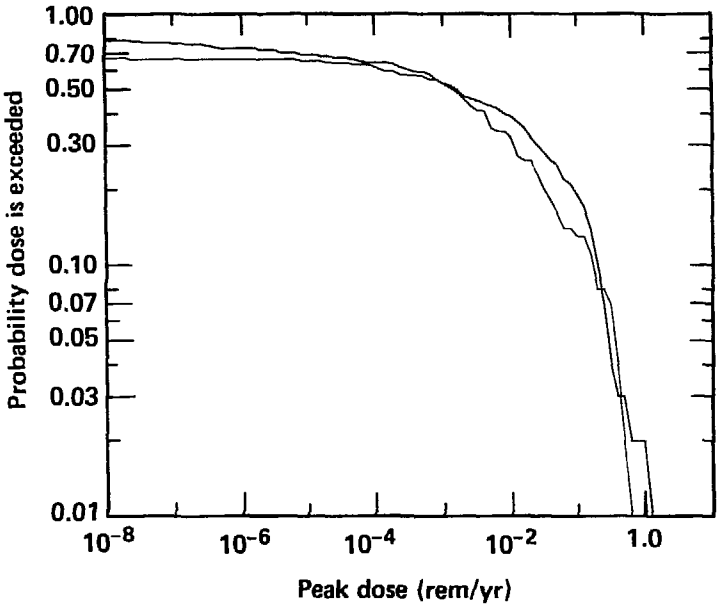

Figure 3-32. LI dose for 5 and 25 canisters per cell.

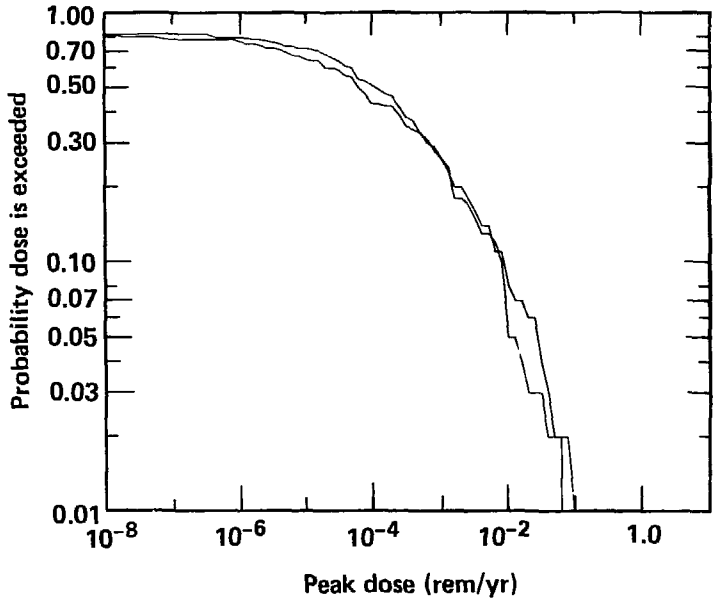

Figure 3-33. AEI dose for 5 and 25 canisters per cell.

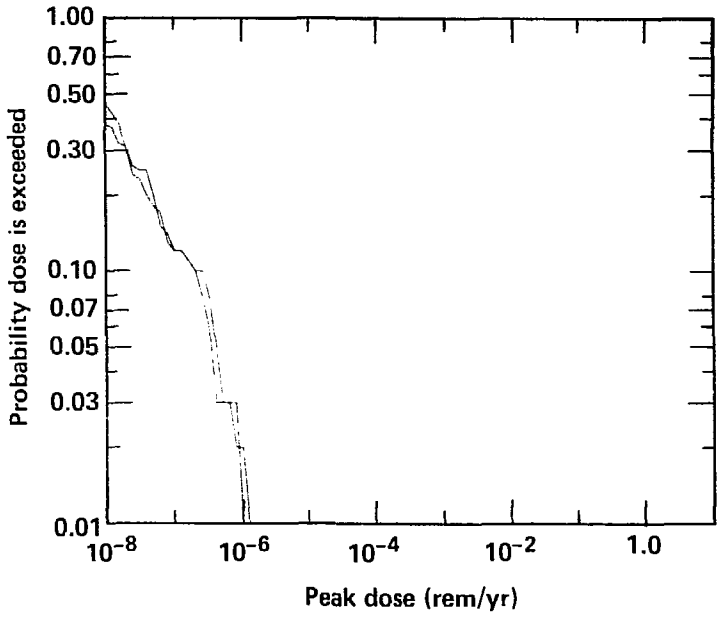

Figure 3-34. CRI dose for 5 and 25 canisters per cell.

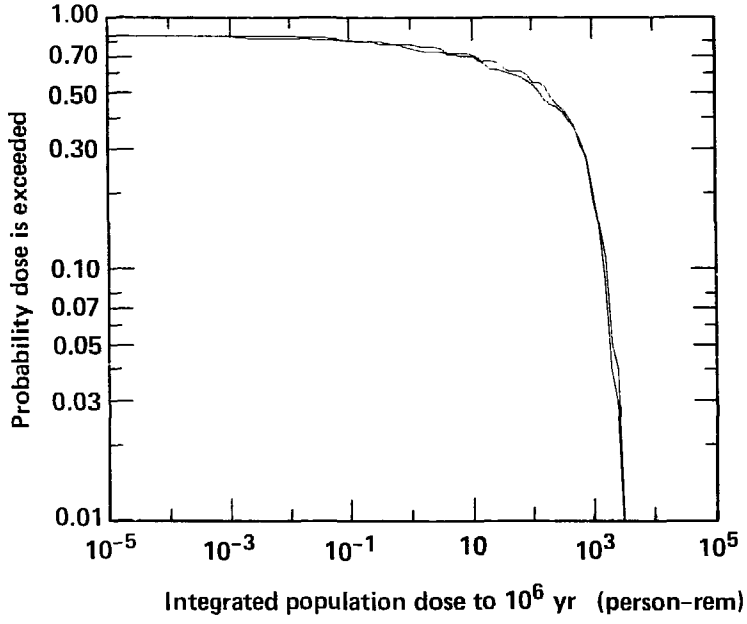

Figure 3-35. CRP6 dose for 5 and 25 canisters per cell.

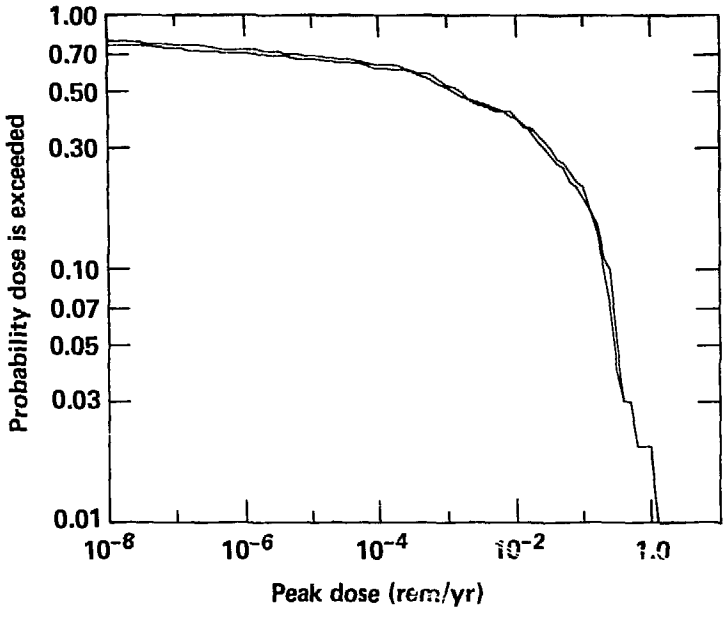

Figure 3-36. LI dose for Gaussian and Green's Function release and transport.

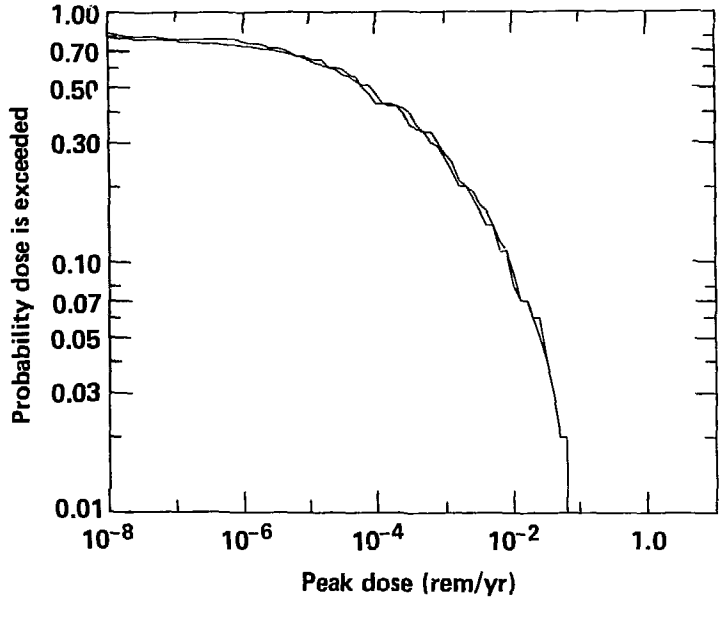

Figure 3-37. AEI dose for Gaussian and Green's Function release and transport.

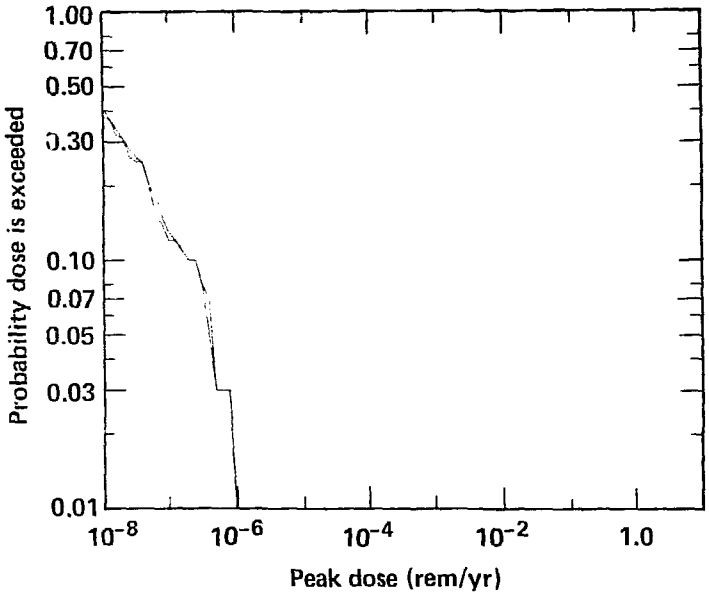

Figure 3-38. CRI dose for Gaussian and Green's Function release and transport.

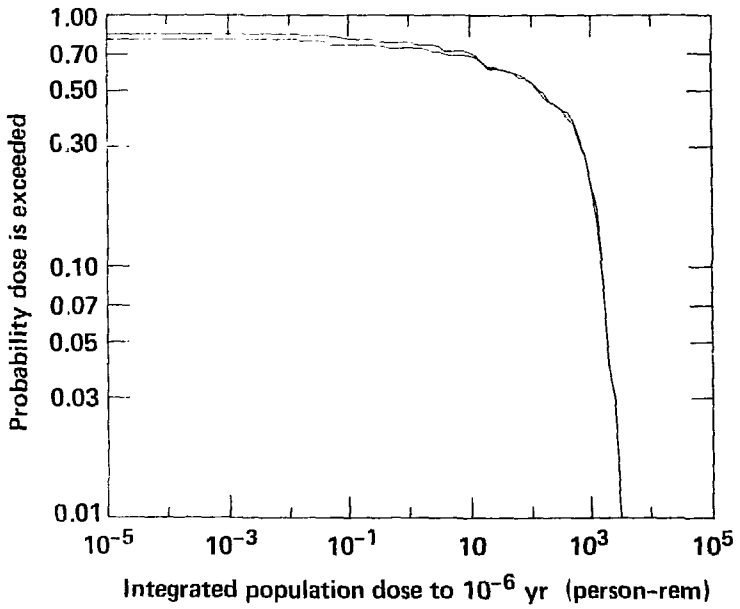

Figure 3-39. CRP6 dose for Gaussian and Green's Function release and transport.

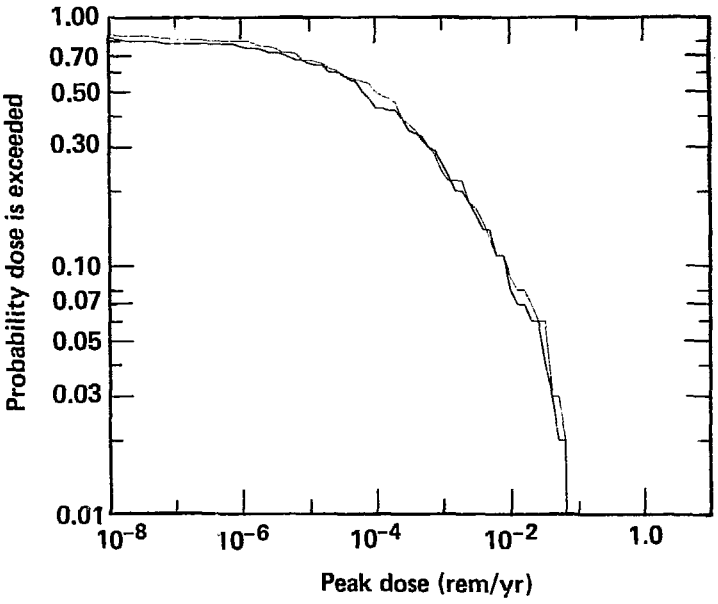

Figure 3-40. AEI dose for Gaussian and flat pulse release and transport.

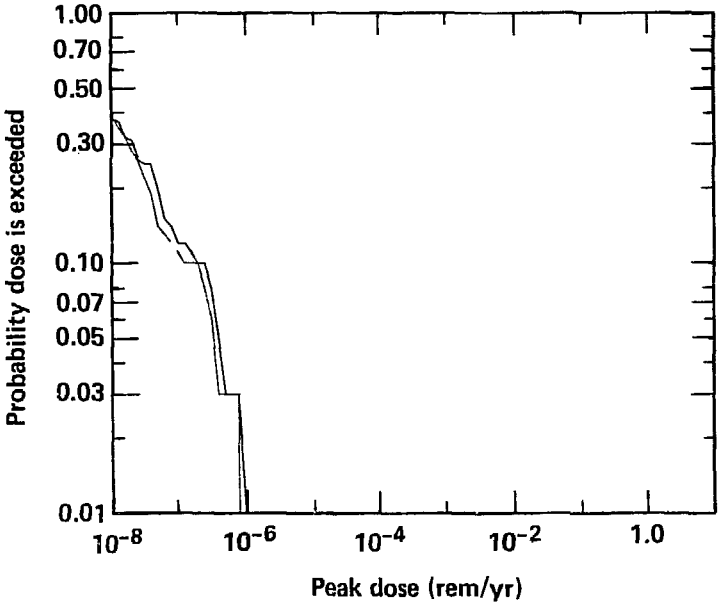

Figure 3-41. CRI dose for Gaussian and flat pulse release and transport.

Table 3-15. Correlation coefficient for log of intermediate parameters with log of dose.

Parameter description	*Correlation coefficient*
Group I dose	0.62
Peak dose time of arrival	−0.61
Group II dose	0.52
Aquifer water velocity	0.18
Tunnel velocity	0.15
Horizontal gradient	0.10
Group III dose	−0.07
Operations shaft velocity	−0.07
Air shaft velocity	−0.07
Vertical gradient	−0.06

The correlation coefficient is given by

$$\rho = \frac{\frac{1}{100}\sum_{i=1}^{100}(\log_{10} v_i - \log_{10} \bar{V})(\log_{10} d_i - \log_{10} \bar{D})}{\log_{10} \Sigma_v \cdot \log_{10} \Sigma_d} ,$$

where $\bar{V} = 10^{\bar{v}}$, $\bar{D} = 10^{\bar{d}}$, $\Sigma_v = 10^{\sigma_v}$, and $\Sigma_d = 10^{\sigma_d}$. The variances are defined as

$$\sigma_v^2 = \frac{1}{100}\sum_{i=1}^{100}(\log_{10} v_i - \log_{10} \bar{V})^2 ,$$

and

$$\sigma_d^2 = \frac{1}{100}\sum_{i=1}^{100}(\log_{10} d_i - \log_{10} \bar{D})^2 .$$

The means are given by

$$\bar{d} = \frac{1}{100}\sum_{i=1}^{100}\log_{10} d_i ,$$

and

$$\bar{v} = \frac{1}{100}\sum_{i=1}^{100}\log_{10} v_i .$$

The peak dose time-of-arrival has a high correlation, $\rho = -0.61$. A graphical representation of this correlation is shown in Fig. 3-42. This figure also shows a large variation in time-of-arrival (about a factor of ten) for doses that are nearly the same. This trend agrees with our intuition; a long containment time tends to lead to lower peak dose rates; however, there are more complex considerations as manifested by large fluctuations of arrival times for nearly the same doses. The arrival time goes to greater than one million years for twenty-six of our samples resulting in the vertical line at sample number 74.

The largest ρ calculated was for the Group I dose rate, $\rho = 0.62$. Figure 3-43 compares the ordered, normalized Group I, Group II, and Group III dose rates, at time of peak dose rate, with the calculated AEI normalized peak dose rate. We see that Group I is not only highly correlated with the AEI peak dose rate, but generally speaking the Group I doses do not fluctuate much from the ith to the i + 1st sample, which indicates that the total peak dose rate is caused mostly by Group I radionuclides.

The behavior of Group I can be contrasted with Group II by comparing Figs. 3-43A and 3-43B. Although the correlation coefficient for Group II is almost as high as Group I's ($\rho = 0.52$), Group II does not contribute as much to the peak dose as Group I. We see large fluctuations (an order of magnitude or more) in Group II's behavior for nearby AEI peak doses. By contrast much smaller fluctuations occur in Group I behavior.

There are four or five very high AEI dose levels that are caused by Group III actinides. The three highest dose results are caused by actinides, causing the Group I dose curve to fluctuate greatly in the 0–10 sample number domain. Except for these few highest-dose cases, the actinides do not correlate well with, nor contribute much to, the calculated peak dose rate at its time-of-arrival. Thus, their correlation coefficient is nearly zero.

If we look only at input parameters (not intermediate parameters), we obtain correlation coefficients shown in Table 3-16. The dissolution time has the highest correlation with $\rho = 0.45$. This can be contrasted with the time-of-arrival of the peak dose rate in that the dissolution time is more of a dilution effect, whereas the time-of-arrival tends to be more a containment effect. If one simply states that the dissolution time is the most important parameter based on correlating it with the calculated peak dose rate, one must remember that the sensitivity to dissolution time for the highest dose rates calculated was near zero (see Fig. 3-16). This demonstrates that care must be exercised in using correlation coefficients to establish important sensitivities. For safety considerations, too much weight is put on low peak dose rates when calculating the correlation coefficient, thus leading to a large ρ for the dissolution time.

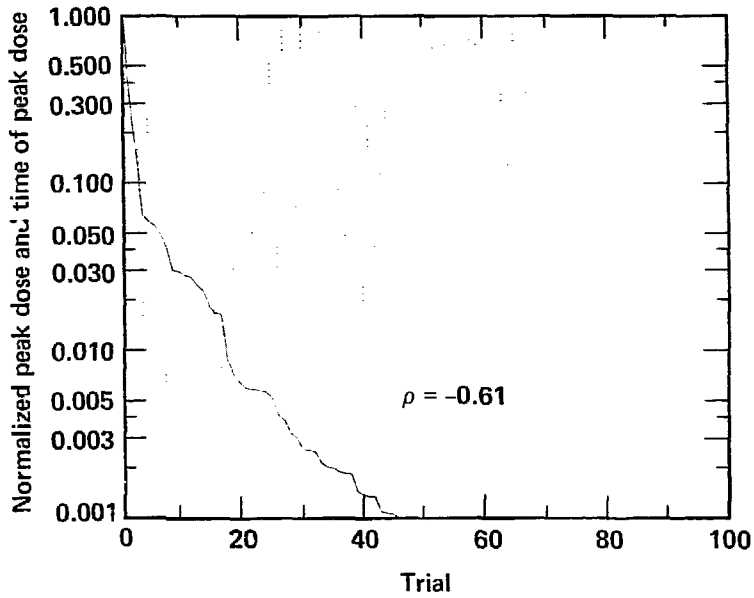

Figure 3-42. Comparison of normalized AEI peak dose rate (solid line) with normalized time of arrival of peak dose rate (dotted line).

Figure 3-44 shows the ordered pairs of peak dose rate and dissolution time for 100 trials. Other input parameters that show significant correlations in Table 3-16 are the retardation factors in the upper aquifer (see Fig. 3-45 for Group III retardations) and the parameters that affect the water velocity in the connecting tunnel (i.e., the tunnel's permeability and effective porosity). Note also that the heads at the lower left and upper left which determine the horizontal gradient both have $\rho = 0.10$, the same correlation coefficient as for the horizontal gradient, an expected result because little else has any effect on the calculation of the horizontal gradient. Another expected result is that breach time, as has been noted by many risk assessments, has a very low correlation coefficient.

Trials and Extrapolations

In doing a probabilistic analysis using Monte Carlo techniques, there is always the question of how many trials should be in a Monte Carlo run. To establish the approximate precision of our results at different confidence levels, we have run our basecase for five 100-trial runs, starting the random number generator at differing values for each run. This procedure provides us with a sample range of results for each of our confidence levels. Also, if we combine the results of the 500 trials, we have a 500-trial frequency distribution, which should provide a fairly precise estimate of the 99th-percentile confidence level. This allows us to test the use of the lognormal distribution to extrapolate our results from the 100-trial case to the 500-trial case.

The results for the five 100-trial runs are tabulated for our AEI and CRI peak dose rates in Tables 3-17 and 3-18, respectively. Also shown are the 100-trial percentile means as well as the values of the 500-trial case. For the fiftieth to ninetieth percentiles, the results for the five 100-trial

Table 3-16. Correlation coefficient for log of input parameters with log of dose.

Parameter description	Correlation coefficient
Dissolution time	−0.45
Effective porosity of tunnel	0.24
Group II retardation factor	0.23
Tunnel permeability	0.19
Group III retardation factor	−0.17
Upper aquifer effective porosity	−0.15
Permeability of lower aquifer	−0.15
Storage room effective porosity	0.12
Head at lower left	0.10
Head at upper left	0.10
Permeability of lower shale	0.09
Breach time	0.08

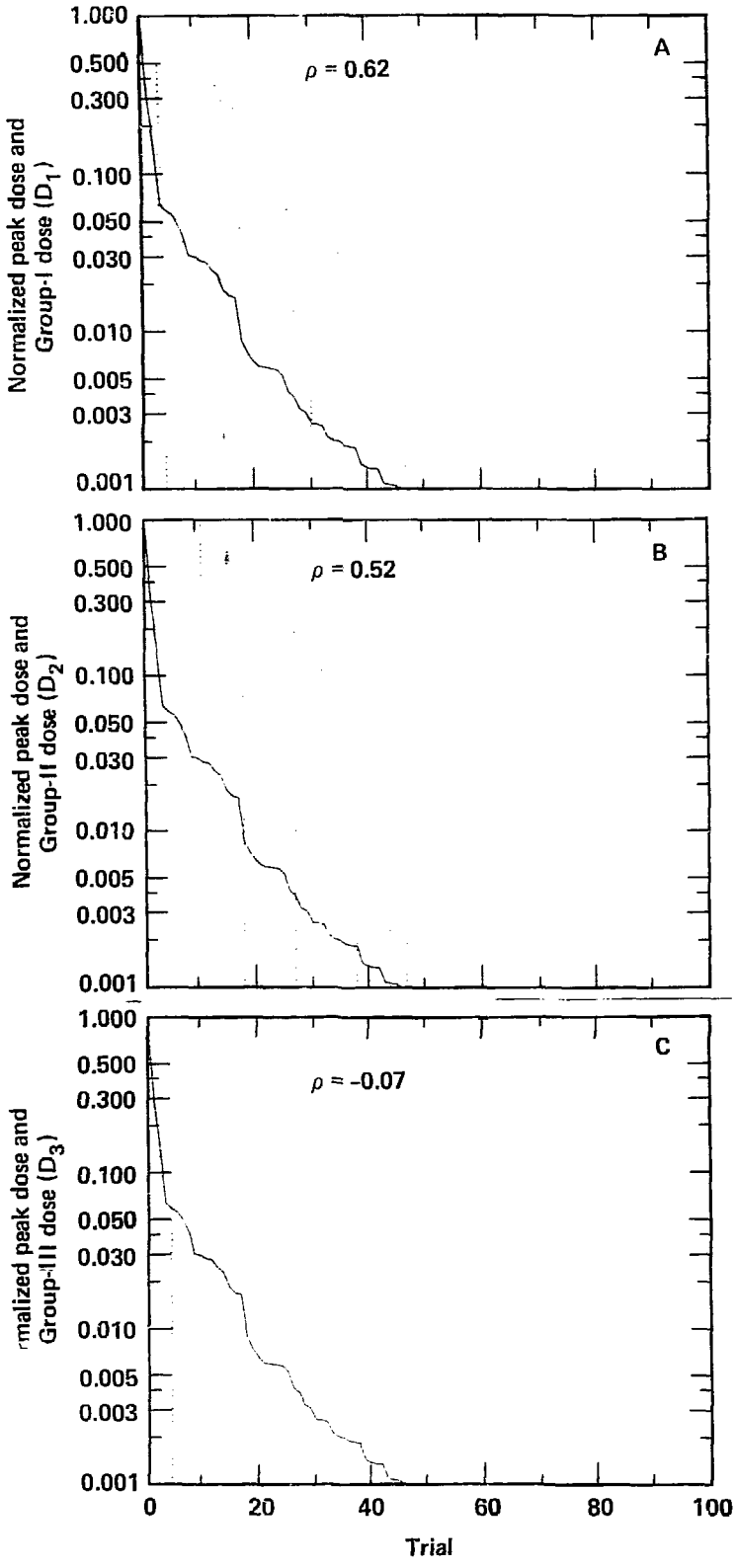

Figure 3-43. Comparison of normalized AEI peak dose rate (solid lines) with normalized AEI (A) Group I dose rate, (B) Group II dose rate, and (C) Group III dose rate at time of arrival of peak dose rate.

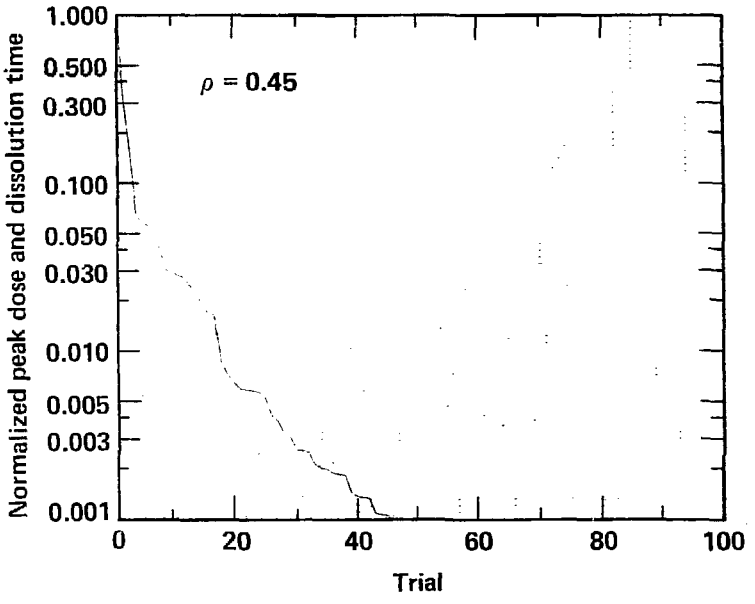

Figure 3-44. Comparison of normalized AEI peak dose rate (solid line) with normalized dissolution time (dotted line).

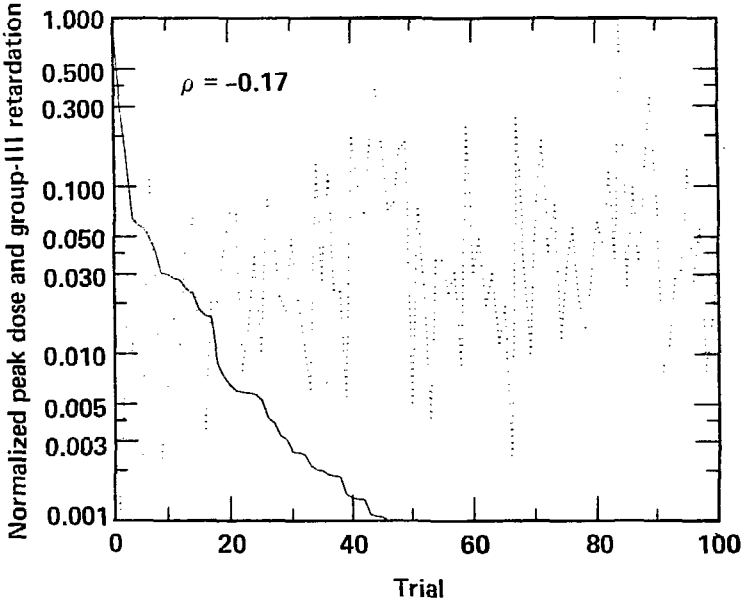

Figure 3-45. Comparison of normalized AEI peak dose rate (solid line) with normalized Group III retardation factor (dotted line).

Table 3-17. Peak AEI dose rate (rem/yr).

Trials	Percentiles				Maximum
	X_{25}	Median	X_{75}	X_{90}	
1-100	1.3×10^{-6}	6.3×10^{-5}	1.3×10^{-3}	1.0×10^{-2}	8.0×10^{-2}
101-200	1.3×10^{-6}	1.3×10^{-4}	1.6×10^{-3}	6.3×10^{-3}	3.2×10^{-2}
201-300	2.5×10^{-6}	7.9×10^{-5}	7.9×10^{-4}	5.0×10^{-3}	6.3×10^{-2}
301-400	2.5×10^{-6}	2.0×10^{-4}	2.0×10^{-3}	1.3×10^{-2}	4.0×10^{-1}
401-500	4.0×10^{-6}	2.5×10^{-4}	1.3×10^{-3}	6.3×10^{-3}	5.0×10^{-2}
Mean	2.3×10^{-6}	1.4×10^{-4}	1.4×10^{-3}	8.1×10^{-3}	
Trials					
1-500	2.5×10^{-6}	1.3×10^{-4}	1.3×10^{-3}	7.9×10^{-3}	3.9×10^{-1}

Table 3-18. Peak CRI dose rate (rem/yr).

Trials	Percentiles				Maximum
	X_{25}	Median	X_{75}	X_{90}	
1-100	5.0×10^{-11}	3.2×10^{-9}	3.2×10^{-8}	2.0×10^{-7}	1.3×10^{-6}
101-200	1.3×10^{-11}	4.0×10^{-9}	4.0×10^{-8}	1.6×10^{-7}	2.0×10^{-6}
201-300	7.9×10^{-11}	6.3×10^{-9}	4.0×10^{-8}	1.6×10^{-7}	1.6×10^{-6}
301-400	1.3×10^{-10}	4.0×10^{-9}	5.0×10^{-8}	2.5×10^{-7}	1.0×10^{-6}
401-500	2.5×10^{-10}	7.9×10^{-9}	6.3×10^{-8}	1.6×10^{-7}	7.9×10^{-7}
Mean	1.0×10^{-10}	5.1×10^{-9}	4.5×10^{-8}	1.9×10^{-7}	
Trials					
1-500	7.9×10^{-11}	5.0×10^{-9}	5.0×10^{-8}	2.0×10^{-7}	2.0×10^{-6}

cases fall within a factor of two of the mean for both the CRI and AEI peak dose rates. A comparison of mean values for the 100-trial cases shows them to be within 10% of the dose obtained for the 500-trial case.

Figure 3-46 overlays the five 100-trial cases. Figure 3-46A displays the AEI doses, and Fig. 3-46B, the CRI doses. It is apparent the statistics break down at high confidence levels, as indicated by the jaggedness of the curves. We see at the 99%-confidence level that there is a factor of approximately 4 difference between the mean and the smallest dose calculated using only 100 trials.

The CRI 100-trial comparison shown in Fig. 3-46B has much less dispersion, which simply implies that a river-use system with a river 20 km from the repository has smaller sensitivity to parameters describing the repository than one that is 1.6 km away, a fact that many studies have already noted. The nearer to the repository that the peak dose rate is determined, the more sensitive the results will be to repository design and local measurement and forecasting uncertainties.

In Figs. 3-47A and 3-47B we compare the first 100-trial case with the 500-trial case. The 500-trial case is the smoother of the two curves. The 100-trial curve is vertical when the ordinate is below 10^{-2} because each trial has a statistical weight of 0.01. In contrast, there is structure in the 500-trial curve below 10^{-2} because each trial has a statistical weight of 0.002. Thus, with the 500-trial case we can forecast the 99th-percentile dose to within about a factor of two. It is 5.0×10^{-2} rem/yr for the AEI peak dose rate.

We see that the 100-trial curve is a good approximation to the 500-trial curve over nearly the entire figure. Unless very high confidence levels are required, say greater than 95%, a 100-trial Monte Carlo run should be sufficiently accurate.

This brings up the question of extrapolating to higher confidence levels. It has been suggested that extrapolation by using a lognormal distribution would be appropriate. Figure 3-48 demonstrates how good a lognormal extrapolation would be if used to extrapolate our doses to higher confidence levels. Here we have plotted the first 100-

trial case and the 500-trial case on log-statistical paper. A lognormal distribution,

$$f(x) = \frac{1}{\sqrt{2\pi}\,\log_{10}\sigma\,x^{\alpha}} e^{-1/2\left(\frac{\log_{10}x - \log_{10}\bar{x}}{\log_{10}\sigma}\right)^2},$$

where $\alpha = 1$, σ is the geometric standard deviation, and $\bar{x}$ is the median, will plot as a straight line on this paper. Thus, plotting any two points from Table 3-17 and drawing a straight line through them provides an inexpensive way of fitting a lognormal distribution and extrapolating it to very high confidence levels.

We have done this using the median with the 75CL, the median with the 90CL, and the 75CL with the 90CL. These extrapolations give 99CL's of 2.0 rem/yr, 0.55 rem/yr, and 0.3 rem/yr, respectively. Using the 500-trial value as "the correct value," however, we arrive at only 0.05 rem/yr.

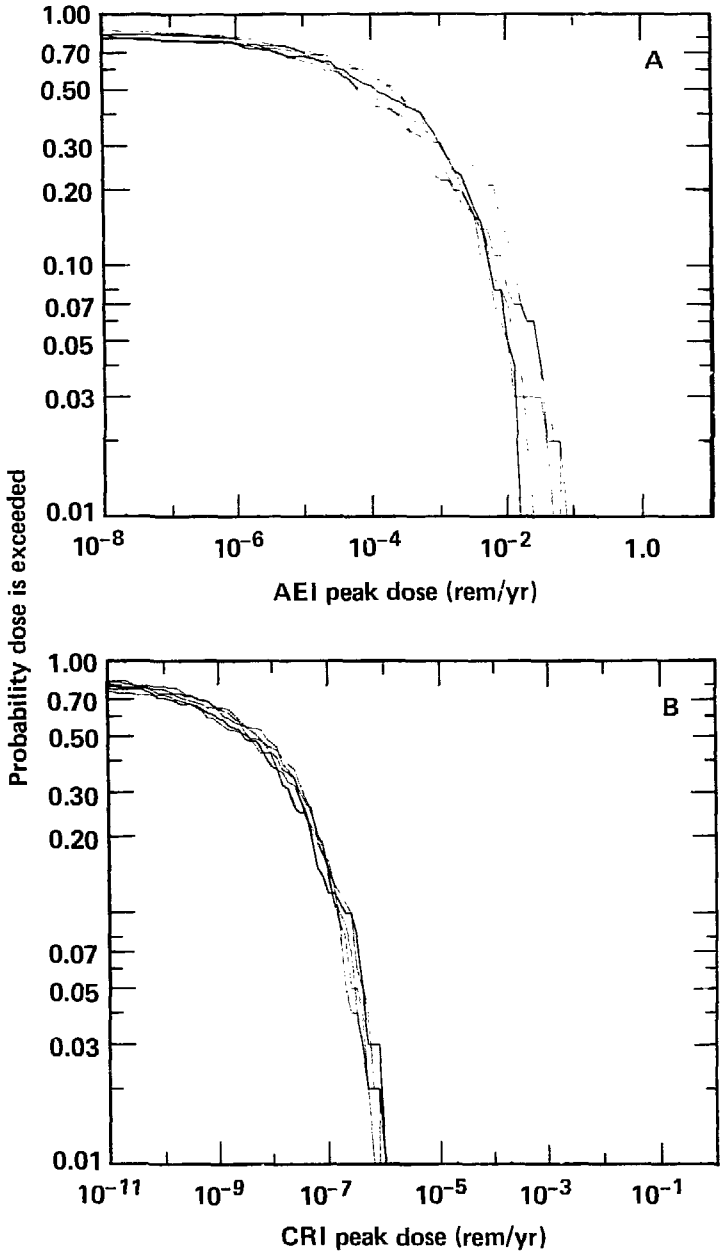

Figure 3-46. Comparison of five independent Monte Carlo runs of 100 trials each. Cumulative distributions of (A) AEI peak dose rate and (B) CRI peak dose rate.

This is a factor of 6 to 40 below that estimated using a lognormal distribution for the extrapolation. If a more sophisticated regression analysis with a lognormal distribution were used (instead of using two points and a straight line on statistical graph paper), the results would be similar, gross over-estimates. If, on the other hand, a nonlinear regression analysis with a better model were used (with $\alpha > 1$, for example) a much better fit could be obtained.

To conclude, we believe that a lognormal extrapolation is unrealistically conservative, that a more sophisticated approach must be used if extrapolated results are desired within an order of magnitude. Our opinion is that the "true" curve, when plotted on log-statistical paper, will continue to accelerate to the right, producing worse lognormal approximations as the confidence level increases, causing orders-of-magnitude overestimates if simplistic lognormal extrapolations

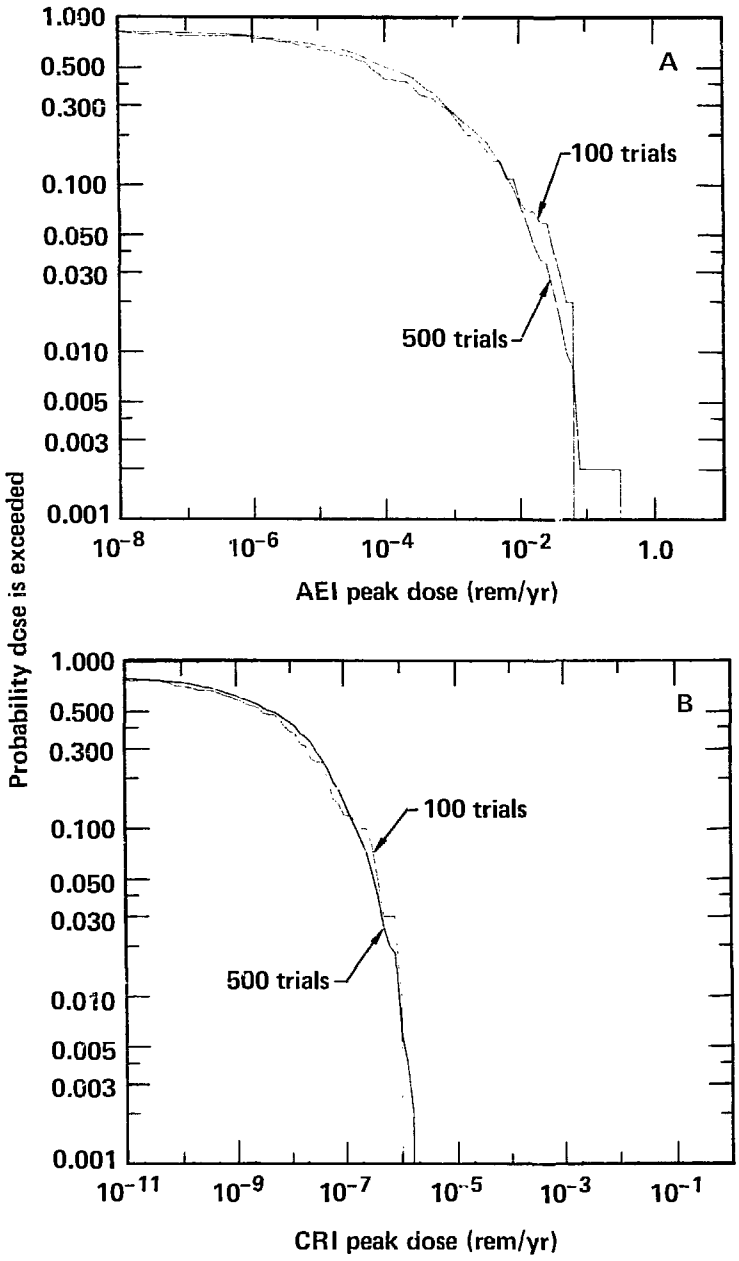

Figure 3-47. Comparison of 100-trial and 500-trial cumulative distributions for (A) AEI peak dose rate and (B) CRI peak dose rate.

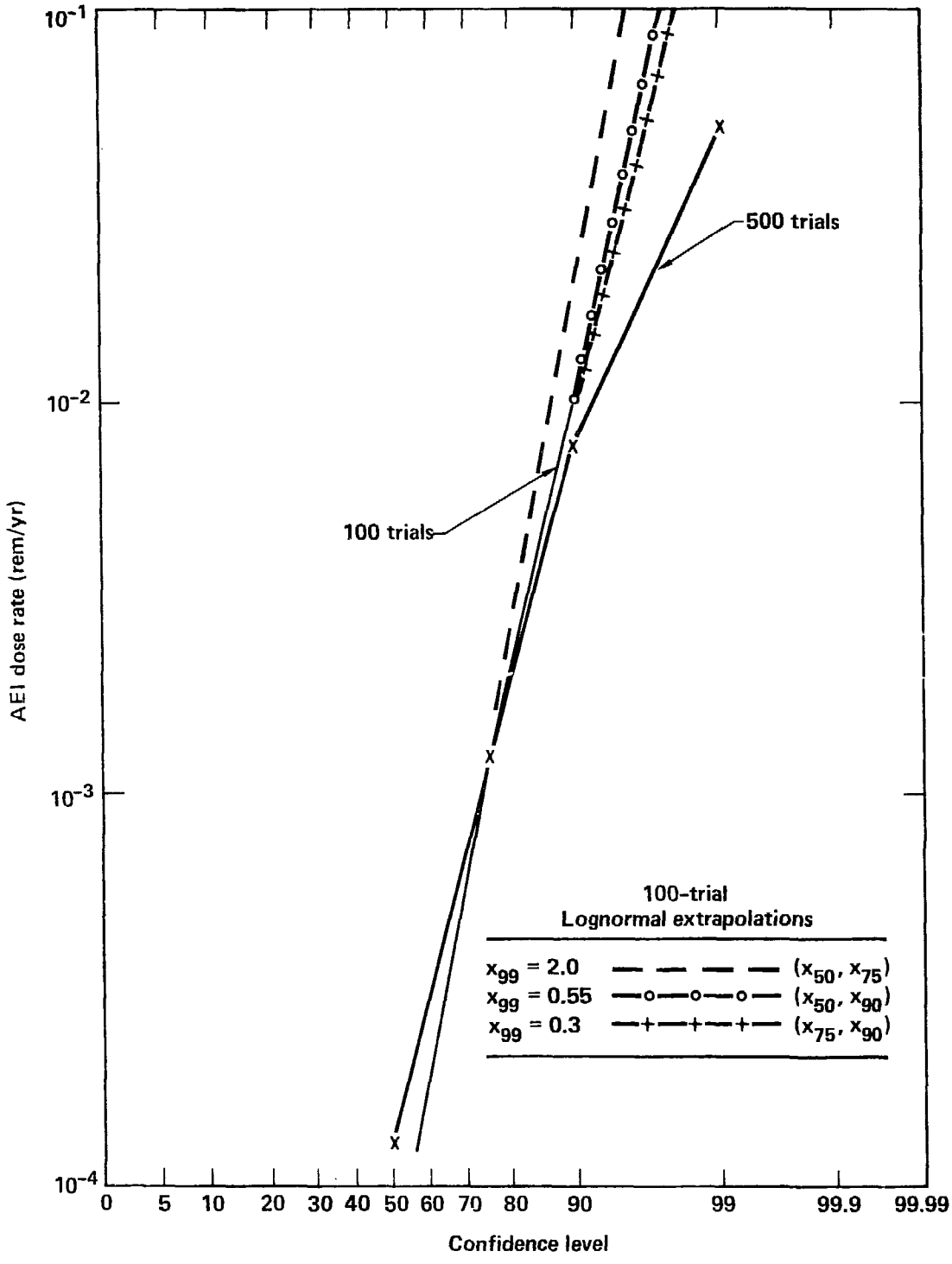

Figure 3-48. Comparison of 100-trial lognormal extrapolation schemes with 500-trial results (key in lower right corner gives result of extrapolation to X_{99} using X_{50} and X_{75} of 100-trial run, for example, as 2.0 rem/yr; other values for X_{99} were 0.55 and 0.3 rem/yr—see text for further discussion).

are used. Of course, a lognormal extrapolation, even though a very bad extrapolation, would be a conservative extrapolation, and, thus, appropriate for many risk assessments where the standard is sufficiently above the calculated risks. Where this is not the case, however, a larger number of Monte Carlo trials and/or more sophisticated nonlinear regression analysis should be used.

References

1. T. G. Naymik and L. D. Thorson, *Numerical Simulation of Transport in a Regional Groundwater Flow System*, Lawrence Livermore National Laboratory, Livermore, Calif., UCRL-52556 (1978).
2. F. R. Kovar and T. L. Steinborn, *The Bedded Salt Report*, Lawrence Livermore National Laboratory, Livermore, Calif., UCRL-52737 (1980).
3. *Final Report on Geological Studies Pertinent to Site Suitability Criteria for High Level Waste Repositories*, (Geotechnical Engineers, Inc., Winchester, Mass.) Lawrence Livermore National Laboratory, Livermore, Calif., UCRL-13741 (1977).
4. *Development of Site Suitability Criteria for the High Level Waste Repository for Lawrence Livermore Laboratory*, (Golder Associates, Kirkland, Wash.), Lawrence Livermore National Laboratory, Livermore, Calif., UCRL-13755 (1977).
5. *Second Report: Development of Site Suitability Criteria for the High Level Nuclear Waste Repository for Lawrence Livermore Laboratory*, (Golder Associates, Kirkland, Wash.), Lawrence Livermore National Laboratory, Livermore, Calif., UCRL-13793 (1977).
6. *Third Report: Development of Site Suitability and Design Performance Data Base for a High Level Nuclear Waste Repository for Lawrence Livermore Laboratory*, (Golder Associates, Kirkland, Wash.), Lawrence Livermore National Laboratory, Livermore, Calif., UCRL-13856 (1978).
7. D. Isherwood, *Geoscience Data Base Handbook for Modeling a Nuclear Waste Repository*, Vol. 1, Lawrence Livermore National Laboratory, Livermore, Calif., UCRL-52719 (1980).
8. E. B. Ekren, G. A. Dinwiddie, J. W. Mytton, W. Thordarson, J. E. Wein, Jr., E. N. Henrichs, and L. J. Schroeder, *Geologic and Hydrologic Considerations for Various Concepts of High-Level Radioactive Waste Disposal in the Conterminous U.S.*, U.S. Geological Survey Open-File Report 74-158 (1974).
9. M. S. Giufre, M. F. Kaplan, D. A. Ensminger, S. G. Oston, J. Y. Nalbandian, *Bedded Salt Repository Analysis: Final Report*, Lawrence Livermore National Laboratory, Livermore, Calif., UCRL-15236 (1980).
10. I. Remson, S. J. Dreiss, and A. G. Journel, "Radioactive-Waste Disposal—An Application of Predictive Geology," in *Predictive Geology with Emphasis on Nuclear Waste Disposal*, C. De Marsily and D. F. Merriam, Eds. (Pergamon Press, NY, 1982) pp. 25–32.
11. J. H. Campbell, "SYNROC: Permanent Radioactive-Waste Storage," *Energy and Technology Review*, Lawrence Livermore National Laboratory, Livermore, Calif. (Dec. 1981).
12. L. L. Edwards and T. F. Harvey, *A High Level Waste-Repository Excavation Model and Limiting Individual Dose*, Lawrence Livermore National Laboratory, Livermore, Calif., UCRL-86849 (1981).
13. Arthur D. Little, Inc., *Assessment of Accidental Pathways*, Draft Subtask D Report, Vol. I, C-80560 (1978).
14. H. C. Burkholder, "The Development of Release Scenarios for Geologic Nuclear Waste Repositories: Where Have We Been? Where Should We Be Going," *Proceedings of the NEA Workshop*, Paris (September 1980) pp. 13–26.
15. U.S. Nuclear Regulatory Commission, "10 CFR, Part 60, Disposal of High-Level Radioactive Wastes in Geologic Repositories," *Fed Reg.* **46** (130), July 8, 1981.
16. C. Klingsberg and J. Duguid, *Status of Technology for Isolating High-Level Radioactive Wastes in Geologic Repositories*, DOE/TIC-11207 (draft), October, 1980.
17. U.S. Department of Energy, *Proceedings of the 1981 National Waste Terminal Storage Program Information Meeting*, DOE/NWTS-15, November 1981.

18. W. V. De Mier, M. O. Cloninger, H. C. Burkholder, and P. S. Liddall, *GETOUT—A Computer Program for Predicting Radionuclide Decay Chain Transport Through Geologic Media*, Pacific Northwest Laboratory, Richland, Wash., PNL-2970, 1979.
19. B. J. Wood, "The Use of Simple Transport Equations to Estimate Waste Package Performance Requirements," *Waste Management '81*, American Nuclear Society, R. G. Post, Ed., Vol. 2, pp. 911–947, 1981.
20. M. D. Hill and P. D. Grimwood, *Preliminary Assessment of the Radiological Protection Aspects of Disposal of High-Level Waste in Geologic Formations*, NRPD-469, 1978.
21. M. D. Hill, "The Effect of Variations in Parameter Values on the Predicted Radiological Consequences of Geologic Disposal of High-Level Waste," *Scientific Basis for Nuclear Waste Management*, Vol. 2, p. 753, 1980.
22. M. O. Cloninger, C. R. Cole, and J. F. Washburn, *An Analysis of the Use of Engineered Barriers for Geologic Isolation of Spent Fuel in a Reference Salt Site Repository*, Battelle Pacific Northwest Laboratory, Richland, Wash., PNL-3356, 1980.
23. G. S. Barney and B. J. Wood, *Identification of Key Radionuclides in a Nuclear Waste Repository in Basalt*, Rockwell Hanford Operations, Richland, Wash., RHO-BWT-ST-9, 1980.
24. J. R. Raymond, F. W. Bond, C. R. Cole, R. W. Nelson, A. E. Reisenauer, J. F. Washburn, N. A. Norman, P. A. Mote, and G. Segal, *Test Case Release Consequences Analysis for a Spent Fuel Repository in Bedded Salt*, Pacific Northwest Laboratory, Richland, Wash., PNL-2782, 1980.
25. J. E. Campbell, P. C. Kaestner, B. S. Langkopp, and R. B. Lantz, *Risk Methodology for Geologic Disposal of Radioactive Waste: The Network Flow and Transport (NWFT) Model*, Sandia National Laboratories, Albuquerque, New Mex., NUREG/CR-1190, SAND-79-1920, 1980.
26. A. M. Kaufman, L. L. Edwards, and W. J. O'Connell, "A Repository Post Sealing Risk Analysis Using MACRO," *Proceedings of the Waste Management Symposium, Tucson, Arizona, 1980* (University of Arizona, College of Engineering, Tucson, Ariz., 1980), p. 109.
27. U.S. Department of Energy, *Statement of Position of the U.S. Department of Energy Waste Confidence Rulemaking*, DOE/NE-0007, PR-50, 51 (44FR61372) (1980).
28. H. Cheung, L. L. Edwards, I. F. Harvey, D. D. Jackson, M. A. Revelli, *Nuclear Waste-Form Risk Assessment for U.S. Defense Waste at Savannah River Plant: Annual Report FY 1981*, Lawrence Livermore National Laboratory, Livermore, Calif., UCRL-53188-81 (1982).

4. Technical Conclusions

Unless otherwise indicated, our results are best estimates. In our probabilistic approach, "best estimate" means calculated median dose. In general, we found median dose rates far below natural background radiation levels for peak individual doses and nearly trivial results for integrated population doses.

The reduction of these small doses by using an improved ALTERNATIVE waste form instead of REFERENCE (borosilicate glass) is consequently small, even though the reduction at times was greater than an order of magnitude. Where the doses were large in the probabilistic analysis (i.e., at high confidence levels) the effect of changing the waste form to ALTERNATIVE was small. Thus, ironically, for the repository layout chosen where one would hope to gain the most from a better waste form, there seems to be little effect. This indicates that there are other contributing factors for the high confidence level doses which vitiate the effect of release rate.

Some other highlights of the study relevant to a waste form decision are described below.

Basecase Peak Individual Dose

- For the layered-salt repository with REFERENCE waste form, our "best estimate" of peak-equivalent-whole-body dose to an individual using a well located one mile downstream from a repository (the "accessible environment individual"), is about 3 orders of magnitude below background radiation. If the individual puts his well at nearly the worst location possible, right above the repository, he will receive about 1/50 background radiation. If, however, the individual is part of the Columbia River water-use system with an average diet of only contaminated food, he will receive approximately one ten-millionth background radiation. If we wish to increase our confidence level (from 50% to 90%) that the estimated dose will not be exceeded, then the AEI peak dose increases to 10 mrem/yr—still an order of magnitude below background. The 90% dose to the average individual in the CRP system would still be orders of magnitude below background.
- The lower-release-rate ALTERNATIVE waste form improves the peak dose obtained form a well one mile downstream over a factor of 10 for doses below the 70% confidence level. Above the 90% confidence level, there is little or no improvement.

Basecase Integrated Population Dose

- Integrated population dose over the first million years results in a 200 person-rem total dose, less than 1/10 of the dose considered to lead to a single additional premature cancer in the population. This is our 50% confidence level estimate. If we wish to improve our confidence level from 50% to 90%, we increase the integrated population dose to 2000 person-rem.
- Changing to the improved waste form (ALTERNATIVE) has essentially no effect on the best-estmate integrated population dose; i.e., it reduces the CRP dose by only 190 person-rem in one million years.

Site Alternative

- The basalt repository was a poorer performer by a factor of approximately 5–50 than the layered-salt repository for the integrated population dose and the peak AEI dose. It was a better performer by about a factor of 10,000 for the individual with his well above the repository (LI dose). Including the bypass in the design reduces the well-above-repository peak dose rate to zero.
- Using the improved waste form (ALTERNATIVE) produces no significant effect on basalt repository performance; i.e., it reduces the AEI dose by 1 mrem/yr and the integrated population dose by 500 person-rem.

Design Alternative

- The bypass increases containment time of initial pulse from 6700 yrs to approximately one million years for the median-value parameters case. Also, at the 90% confidence level, BYPASS reduces the AEI dose by about a factor of 50.
- Changing to ALTERNATIVE does not improve the performance of the repository with BYPASS at the 50% confidence level. Even at the 90% confidence level improvement in performance is insignificant (AEI dose by 0.2 mrem/yr and integrated population dose by 18 person-rem).

Release Rates and Uncertainties

- The low-dose ends of the dose vs release rate curves are sensitive to both release rate and release rate uncerainty. Also, the high-release-rate ends of these curves for high (~90%) confidence levels are insensitive to release rate and release rate uncertainty. This is true for release rates greater than approximately 5×10^{-7}/yr.
- The choice of waste form should not be affected by the uncertainty of the waste form release rate. Where the doses are sensitive to uncertainty, the doses are orders of magnitude below background. Where the doses are significant fractions of background, they are insensitive to uncertainty of the waste form release rate.

Point-Source and Extended-Source Repository Models

Most studies have been examinations of far-field release points, while we have developed a technique to examine close-in effects. As a result we are able to assess the limitations of the point-source model, to determine the effects of extended sources, and to evaluate the advantages of certain simple design features:

- We have found that orders-of-magnitude variations in limiting individual dose can be contrived on the basis of different point-source modeling assumptions.
- The difference between a conservative point-source model and a detailed 1000-canister extended-source model is about two orders of magnitude.
- Combined engineered features may be integrated into a repository design that could lead to reduction of four orders of magnitude in limiting individual dose.

Other Conclusions

- Changing the location of the calculation of peak dose rate can lead to a change of several orders of magnitude in calculated risk.
- Incorporating possible flaws or disruptive events into the analysis changed the best estimates of the peak individual dose rate by a factor of 3. This is a small change since the factor between the 50% and the 90% confidence level is 100.
- The BYPASSS-without-ALTERNATIVE design is a better performer than the ALTERNATIVE-without-BYPASS design by a factor of more than 5.

Appendix A. Radioactivity vs Time.

The ORIGEN[A1] code uses the matrix exponential method to solve the linear differential equations for nuclear transmutation and decay that can be expressed as:

$$\dot{X} = A\,X(t), \tag{A1}$$

where

A	=	$(B - I)\Lambda + (T - I)\sum\phi$
B	=	decay transition matrix with b_{ij} = fraction of decays of nuclide j that produce nuclide i
I	=	identity matrix
T	=	transmutation matrix with t_{ij} = fraction of neutron captures with j to produce i
Λ and Σ	=	diagonal matrices whose ith elements are λ_i and σ_i, respectively with
λ_i	=	decay constant (s^{-1}) and
σ_i	=	capture cross sections (cm^2/atom)
$\dot{X}(t)$	=	dx/dt
ϕ	=	scalar flux (n/cm^2-s)

The solution is given by

$$X(t) = X(0)\exp(-At), \tag{A2}$$

using numerical techniques presented by Bell.[A1]

From the ORIGEN output, we obtain a table of activity (curies) for each nuclide either in the original inventory or produced by decay as a function of time at selected time points. Table A1 is an example based on Savannah River Defense Waste Inventory. For three nuclide groups based on retardation factors, MISER sums the activities,

$$\left.\begin{aligned} H_1(t_j) &= a_{129_I}(t_j) + a_{99_{Tc}}(t_j) + a_{14_C}(t_j) \\ H_2(t_j) &= \sum a_k(t_j) \\ &\quad \{k: \text{other fission products}\} \\ H_3(t_j) &= \sum a_k(t_j) \\ &\quad \{k: \text{actinides}\} \end{aligned}\right\} \tag{A3}$$

to produce the potential hazard functions.

Reference

A1. M. J. Bell, *ORIGEN—The ORNL Isotope Generation and Depletion Code*, Oak Ridge National Laboratory, Oak Ridge, Tenn., ORNL-4628 (1973).

Table A1. Savannah River Laboratory defense waste (curies/canister). The first set is the 14 timesteps for the calculations. Remaining sets are the activity of the particular nuclide as a function of the 14 timesteps.

```
   87   14
 srl defense waste-87 nuclides(5/23/80 memo-table 5)ci/canister
 0.00000000e+00   1.00000000e+00   3.00000000e+00   1.00000000e+01   3.00000000e+01
 1.00000000e+02   3.00000000e+02   1.00000000e+03   3.00000000e+03   1.00000000e+04
 3.00000000e+04   1.00000000e+05   3.00000000e+05   1.00000000e+06
am243
 5.92283000e-03   5.92227000e-03   5.92116000e-03   5.91726000e-03   5.90614000e-03
 5.86738000e-03   5.75804000e-03   5.39117000e-03   4.46674000e-03   2.31243000e-03
 3.52490000e-04   4.87439000e-07   3.30132000e-15   8.44149000e-44
am241
 3.59835000e+01   3.59814000e+01   3.59696000e+01   3.59609000e+01   3.51803000e+01
 3.17039000e+01   2.30107000e+01   7.48601000e+00   3.02609000e-01   4.01873000e-06
 4.68187000e-20   7.98934000e-69   0.               0.
pu240
 4.59196000e+00   4.59148000e+00   4.59050000e+00   4.58711000e+00   4.57741000e+00
 4.54363000e+00   4.44847000e+00   4.13085000e+00   3.34288000e+00   1.59370000e+00
 1.91965000e-01   1.64325000e-04   7.48523000e-14   5.04335000e-46
pu239
 7.30713000e+00   7.30692000e+00   7.30650000e+00   7.30502000e+00   7.30082000e+00
 7.28611000e+00   7.24426000e+00   7.09966000e+00   6.70222000e+00   5.47841000e+00
 3.07942000e+00   4.10036000e-01   1.29113000e-03   2.26201000e-12
pu238
 4.41611000e+02   4.38136000e+02   4.31269000e+02   4.08070000e+02   3.48436000e+02
 2.00441000e+02   4.12944000e+01   1.64053000e-01   4.64206000e-08   3.26814000e-22
 8.02210000e-62   0.               0.               0.
np237
 9.38728000e-03   9.39083000e-03   9.39796000e-03   9.42320000e-03   9.49635000e-03
 9.74329000e-03   1.03180000e-02   1.13419000e-02   1.18092000e-02   1.18025000e-02
 1.17262000e-02   1.14634000e-02   1.07443000e-02   8.56462000e-03
u236
 3.00959000e-04   3.00959000e-04   3.00959000e-04   3.00959000e-04   3.00959000e-04
 3.00959000e-04   3.00959000e-04   3.00959000e-04   3.00958000e-04   3.00958000e-04
 3.00957000e-04   3.00954000e-04   3.00944000e-04   3.00912000e-04
u235
 5.46370000e-05   5.46370000e-05   5.46370000e-05   5.46370000e-05   5.46370000e-05
 5.46370000e-05   5.46370000e-05   5.46370000e-05   5.46369000e-05   5.46365000e-05
 5.46355000e-05   5.46317000e-05   5.46209000e-05   5.45833000e-05
u234
 1.37144000e-01   1.38390000e-01   1.40853000e-01   1.49173000e-01   1.70557000e-01
 2.23611000e-01   2.80558000e-01   2.94734000e-01   2.93130000e-01   2.87384000e-01
 2.71582000e-01   2.22824000e-01   1.26680000e-01   1.79458000e-02
u233
 2.02711000e-06   2.06799000e-06   2.14979000e-06   2.43657000e-06   3.26019000e-06
 6.19165000e-06   1.49317000e-05   4.81353000e-05   1.49046000e-04   4.99256000e-04
 1.43880000e-03   4.10536000e-03   8.14232000e-03   9.08846000e-03
pa231
 5.79563000e-08   5.91187000e-08   6.14437000e-08   6.95864000e-08   9.28858000e-08
 1.74835000e-07   4.12395000e-07   1.28304000e-06   4.08875000e-06   1.69921000e-05
 6.81662000e-05   2.23556000e-04   3.03158000e-04   3.04570000e-04
th232
 2.94324000e-12   3.00211000e-12   3.11984000e-12   3.53189000e-12   4.70919000e-12
 8.82972000e-12   2.06026000e-11   6.18072000e-11   1.79530000e-10   5.91505000e-10
 1.76810000e-09   5.88070000e-09   1.75841000e-08   5.80036000e-08
th230
 4.36755000e-05   4.50687000e-05   4.74873000e-05   5.62809000e-05   8.40179000e-05
 2.04932000e-04   6.53515000e-04   2.41760000e-03   7.42560000e-03   2.40658000e-02
 6.46498000e-02   1.4 15900e-01   1.55198000e-01   2.60252000e-02
th229
 4.76598000e-09   4.95697000e-09   5.34662000e-09   6.85835000e-09   1.22173000e-08
 4.32437000e-08   2.39530000e-07   2.23726000e-06   1.90562000e-05   1.76340000e-04
```

Table A1. (Continued)

9.7363800e-04	3.7478000e-03	8.0147500e-03	9.1123600e-03	
ac227				
3.2817000e-08	3.3869200e-08	3.5998300e-08	4.3684800e-08	6.7158400e-08
1.5691900e-07	4.2511200e-07	1.4095200e-06	4.5836100e-06	1.9196700e-05
7.7215100e-05	2.5350600e-04	3.4384000e-04	3.4544300e-04	
ra228				
4.9132900e-12	5.0309900e-12	5.2665200e-12	6.0917700e-12	8.4531600e-12
1.6743700e-11	4.0612400e-11	1.2617300e-10	3.8628900e-10	1.4287900e-09
4.8773800e-09	1.7548700e-08	5.3679300e-08	1.7846200e-07	
ra226				
4.1271000e-07	4.3179600e-07	4.7149900e-07	6.2708100e-07	1.2244700e-06
5.4337800e-06	4.0233000e-05	4.4207600e-04	3.2510400e-03	1.8736600e-02
6.0391900e-02	1.4456700e-01	1.5576600e-01	2.6193500e-02	
po210				
1.3419400e-07	1.4406300e-07	1.6192900e-07	2.3359200e-07	5.2852100e-07
2.5747200e-06	1.9152700e-05	1.9164500e-04	1.5453700e-03	6.8491100e-03
2.0437600e-02	3.5603200e-02	2.6098200e-02	3.6423100e-04	
pb210				
1.4211400e-07	1.5068600e-07	1.6880800e-07	2.4332300e-07	5.6372800e-07
3.3282500e-06	3.1331600e-05	4.0726100e-04	3.1916800e-03	1.8655000e-02
6.0308000e-02	1.4447500e-01	1.5564100e-01	2.5946200e-02	
eu154				
3.3868400e+00	3.1244000e+00	2.6589600e+00	1.5118900e+00	3.0128100e-01
1.0642800e-03	1.0509400e-10	3.1797300e-35	0.	0.
0.	0.	0.	0.	
sm151				
1.4267800e+02	1.4161700e+02	1.3952100e+02	1.3242400e+02	1.1407300e+02
6.7678700e+01	1.5228100e+01	8.2284200e-02	2.7360100e-08	5.8072500e-31
0.	0.	0.	0.	
cs137				
6.5723000e+03	6.4226900e+03	6.1335900e+03	5.2204500e+03	3.2937300e+03
6.5758200e+02	6.5678300e+00	6.5573400e-07	6.5277000e-27	0.
0.	0.	0.	0.	
cs135				
6.1875500e-02	6.1875500e-02	6.1875400e-02	6.1875300e-02	6.1874900e-02
6.1873600e-02	6.1869900e-02	6.1856800e-02	6.1819500e-02	6.1689200e-02
6.1318200e-02	6.0037400e-02	5.6523200e-02	4.5766400e-02	
i129				
2.0505100e-21	2.0505100e-21	2.0505100e-21	2.0505100e-21	2.0505000e-21
2.0505000e-21	2.0504800e-21	2.0504200e-21	2.0502400e-21	2.0496100e-21
2.0478200e-21	2.0415800e-21	2.0238500e-21	1.9629800e-21	
sn126				
1.5608200e-02	1.5608200e-02	1.5608200e-02	1.5608100e-02	1.5607900e-02
1.5607100e-02	1.5605000e-02	1.5597400e-02	1.5575800e-02	1.5500300e-02
1.5286800e-02	1.4562300e-02	1.2676000e-02	7.8004000e-03	
pd107				
9.4534000e-03	9.4533900e-03	9.4533900e-03	9.4533900e-03	9.4533700e-03
9.4532900e-03	9.4531000e-03	9.4523900e-03	9.4503700e-03	9.4433100e-03
9.4231800e-03	9.3530500e-03	9.1555500e-03	8.4965600e-03	
tc99				
2.5454500e+00	2.5454400e+00	2.5454200e+00	2.5453600e+00	2.5452000e+00
2.5446200e+00	2.5429600e+00	2.5371800e+00	2.5207100e+00	2.4639400e+00
2.3686900e+00	1.8383800e+00	9.5891100e-01	9.8282900e-02	
zr93				
1.8786100e+00	1.8786100e+00	1.8786000e+00	1.8786000e+00	1.8785700e+00
1.8784700e+00	1.8782000e+00	1.8772400e+00	1.8745000e+00	1.8649400e+00
1.8379100e+00	1.7463300e+00	1.5090700e+00	9.0519800e-01	
sr90				
5.6130500e+03	5.4762900e+03	5.2126800e+03	4.3860300e+03	2.6780300e+03
4.7634400e+02	3.4305200e+00	1.0874200e-07	4.0813500e-29	0.
0.	0.	0.	0.	
se79				
1.4059500e-01	1.4059400e-01	1.4059100e-01	1.4058000e-01	1.4055000e-01
1.4044500e-01	1.4014600e-01	1.3910300e-01	1.3616500e-01	1.2636500e-01
1.0207900e-01	4.8363900e-02	5.7229700e-03	3.2619500e-06	

Table A1. (Continued)

ac225				
4.747290Ø0e-Ø9	4.9382400e-Ø9	5.3275100e-Ø9	6.8358800e-Ø9	1.2187300e-Ø8
4.3102400e-Ø8	2.3770000e-Ø7	2.1933500e-Ø6	1.8838100e-Ø5	1.7619900e-Ø4
9.7363400e-Ø4	3.7478000e-Ø3	8.Ø147400e-Ø3	9.1123600e-Ø3	
ra225				
4.7548200e-Ø9	4.9457900e-Ø9	5.3352100e-Ø9	6.8449400e-Ø9	1.2199400e-Ø8
4.3208600e-Ø8	2.3944700e-Ø7	2.2370000e-Ø6	1.9055500e-Ø5	1.7633800e-Ø4
9.7363600e-Ø4	3.7478000e-Ø3	8.Ø147500e-Ø3	9.1123600e-Ø3	
ra223				
3.2701700e-Ø8	3.3753000e-Ø8	3.5880300e-Ø8	4.3561400e-Ø8	6.7Ø19100e-Ø8
1.5660300e-Ø7	4.2274900e-Ø7	1.3760600e-Ø6	4.3070100e-Ø6	1.6185800e-Ø5
6.Ø8332Ø0e-Ø5	1.9984700e-Ø4	3.3051800e-Ø4	3.4539900e-Ø4	
sb126				
2.1851500e-Ø3	2.1851500e-Ø3	2.1851400e-Ø3	2.1851300e-Ø3	2.1851000e-Ø3
2.1850000e-Ø3	2.1846900e-Ø3	2.1836300e-Ø3	2.1806100e-Ø3	2.1700400e-Ø3
2.1401500e-Ø3	2.Ø3872Ø0e-Ø3	1.7746400e-Ø3	1.Ø920600e-Ø3	
y90				
5.6145200e+Ø3	5.4777200e+Ø3	5.2140400e+Ø3	4.3871700e+Ø3	2.6787300e+Ø3
4.7646800e+Ø2	3.4314100e+ØØ	1.Ø877000e-Ø7	4.Ø824100e-29	Ø.
Ø.	Ø.	Ø.	Ø.	
cm244				
1.2162900e-Ø2	1.1705300e-Ø2	1.Ø842700e-Ø2	8.2942500e-Ø3	3.8576600e-Ø3
2.6469100e-Ø4	1.2537400e-Ø7	2.8996600e-19	1.6483700e-52	Ø.
Ø.	Ø.	Ø.	Ø.	
cm242				
8.8179000e-Ø3	8.7777800e-Ø3	8.6980900e-Ø3	8.4248100e-Ø3	7.6904200e-Ø3
5.5887500e-Ø3	2.2449900e-Ø3	9.2227800e-Ø5	1.ØØ892ØØe-Ø8	1.3814300e-22
3.3909200e-62	Ø.	Ø.	Ø.	
pu241				
3.5496900e+Ø1	3.3862000e+Ø1	3.Ø8145ØØe+Ø1	2.2151600e+Ø1	8.6265000e+ØØ
3.1793600e-Ø1	2.5505600e-Ø5	1.1794100e-19	1.3Ø21ØØØe-60	Ø.
Ø.	Ø.	Ø.	Ø.	
pm147				
6.2224600e-Ø3	4.7774500e-Ø3	2.8162100e-Ø3	4.4290100e-Ø4	2.2438700e-Ø6
2.Ø769400e-14	2.3138200e-37	Ø.	Ø.	Ø.
Ø.	Ø.	Ø.	Ø.	
ce144				
4.8190400e-17	1.9785800e-17	3.3353300e-18	6.5597800e-21	1.2154900e-28
1.Ø526800e-55	Ø.	Ø.	Ø.	Ø.
Ø.	Ø.	Ø.	Ø.	
cs134				
2.1732100e-Ø5	1.5522900e-Ø5	7.9197200e-Ø6	7.5126500e-Ø7	8.9778900e-10
5.2969100e-20	3.1465600e-49	Ø.	Ø.	Ø.
Ø.	Ø.	Ø.	Ø.	
ru106				
2.ØØ956ØØe-13	1.Ø118800e-13	2.5656000e-14	2.1Ø568ØØe-16	2.3119600e-22
3.2ØØ7300e-43	Ø.	Ø.	Ø.	Ø.
Ø.	Ø.	Ø.	Ø.	
am242m				
5.Ø8583ØØe-Ø5	5.Ø626900e-Ø5	5.Ø1673ØØe-Ø5	4.8591100e-Ø5	4.4355400e-Ø5
3.2233800e-Ø5	1.2948300e-Ø5	5.3193500e-Ø7	5.8190700e-11	7.9675700e-25
1.9557500e-64	Ø.	Ø.	Ø.	
pu242				
6.1650200e-Ø3	6.1650200e-Ø3	6.1650100e-Ø3	6.1649500e-Ø3	6.1647900e-Ø3
6.1641800e-Ø3	6.1622500e-Ø3	6.1547100e-Ø3	6.1327100e-Ø3	6.Ø5629ØØe-Ø3
5.8431800e-Ø3	5.1546400e-Ø3	3.6Ø2660Ø0e-Ø3	1.Ø2828ØØe-Ø3	
u236				
1.1949400e-Ø3	1.1950700e-Ø3	1.1953500e-Ø3	1.1963000e-Ø3	1.1990100e-Ø3
1.2084600e-Ø3	1.2350700e-Ø3	1.3238900e-Ø3	1.5442300e-Ø3	2.Ø331700e-Ø3
2.4239300e-Ø3	2.4724800e-Ø3	2.4579200e-Ø3	2.4075100e-Ø3	
co60				
5.Ø1804ØØe-Ø2	4.3931000e-Ø2	3.3705200e-Ø2	1.3422700e-Ø2	9.6040400e-Ø4
9.4103300e-Ø8	3.3093100e-19	2.6989500e-59	Ø.	Ø.
Ø.	Ø.	Ø.	Ø.	
rb87				
9.3369700e-Ø6	9.3369700e-Ø6	9.3369700e-Ø6	9.3369700e-Ø6	9.3369700e-Ø6
9.3369700e-Ø6	9.3369700e-Ø6	9.3369700e-Ø6	9.3369700e-Ø6	9.3369700e-Ø6
9.3369700e-Ø6	9.3369500e-Ø6	9.3369300e-Ø6	9.3368300e-Ø6	

Table A1. (Continued)

ag110				
2.0165100e-22	7.3839700e-23	9.9007700e-24	8.7396900e-27	1.6416800e-35
4.7163300e-66	0.	0.	0.	0.
0.	0.	0.	0.	
in115				
2.3181100e-26	2.3181100e-26	2.3181100e-26	2.3181100e-26	2.3181100e-26
2.3181100e-26	2.3181100e-26	2.3181100e-26	2.3181100e-26	2.3181100e-26
2.3181100e-26	2.3181100e-26	2.3181100e-26	2.3181100e-26	
sn121m				
1.2620200e-02	1.2454200e-02	1.2113400e-02	1.0992400e-02	8.3291200e-03
3.1540500e-03	1.9675500e-04	1.1929400e-08	1.0645900e-20	7.1470200e-63
0.	0.	0.	0.	
sn123				
6.6644500e-45	9.3639800e-46	1.8486400e-47	1.9985900e-53	0.
0.	0.	0.	0.	0.
0.	0.	0.	0.	
sb128				
3.7291000e-04	2.8929200e-04	1.7410100e-04	2.[illegible]394000e-05	1.8347700e-07
3.5065000e-15	3.1002200e-37	0.	0	0.
0.	0.	0.	0	
sb126m				
1.5608200e-02	1.5608200e-02	1.5608200e-02	1.5608100e-02	1.5607900e-02
1.5607100e-02	1.5605000e-02	1.3413800e-02	1.3395200e-02	1.3330300e-02
1.3146600e-02	1.2523600e-02	1.0901400e-02	7.7934600e-03	
te125m				
9.1066400e-05	7.0646500e-05	4.2516300e-[illegible]	7.1892500e-06	4.4805900e-08
8.5630200e-16	7.5708700e-38	0.	0.	0.
0.	0.	0.	0.	
ce142				
9.8580800e-06	9.8580800e-06	9.8580800e-06	9.8580800e-06	9.8580800e-06
9.8580800e-06	9.8580800e-06	9.8580800e-06	9.8580800e-06	9.8580800e-06
9.8580800e-06	9.8580700e-06	9.8580600e-06	9.8580200e-06	
nd144				
5.0069000e-10	5.0069000e-10	5.0069000e-10	5.0069000e-10	5.0069000e-10
5.0069000e-10	5.0069000e-10	5.0069000e-10	5.0069000e-10	5.0069000e-10
5.0069000e-10	5.0069000e-10	5.0069000e-10	5.0069000e-10	
sm147				
2.5860700e-06	2.5860700e-06	2.5860700e-06	2.5860700e-06	2.5860700e-06
2.5860700e-06	2.5860700e-06	2.5860700e-06	2.5860700e-06	2.5860700e-06
2.5860700e-06	2.5860700e-06	2.5860700e-06	2.5860600e-06	
sm143				
5.8107300e-12	5.8107300e-12	5.8107300e-12	5.8107300e-12	5.8107300e-12
5.8107300e-12	5.8107300e-12	5.8107300e-12	5.8107300e-12	5.8107300e-12
5.8107300e-12	5.8107300e-12	5.8107300e-12	5.8107300e-12	
sm149				
1.8011600e-12	1.8011600e-12	1.8011600e-12	1.8011600e-12	1.8011600e-12
1.8011600e-12	1.8011600e-12	1.8011600e-12	1.8011600e-12	1.8011600e-12
1.8011600e-12	1.8011600e-12	1.8011600e-12	1.8011600e-12	
eu152				
1.0839400e-01	1.0276200e-01	9.2361500e-02	6.3575100e-02	2.1870000e-02
5.2217000e-04	1.2118200e-08	7.2963800e-25	0.	0.
0.	0.	0.	0.	
eu155				
7.2241700e-02	6.2521600e-02	4.6828800e-02	1.7029500e-02	9.4629900e-04
3.8276100e-08	1.0744700e-20	1.2592900e-64	0.	0.
0.	0.	0.	0.	
bi210				
1.4052900e-07	1.4900800e-07	1.6693600e-07	2.4065600e-07	5.5769200e-07
3.2938000e-06	3.1014000e-05	4.0317300e-04	3.1597300e-03	1.8468400e-02
5.9704900e-02	1.4303000e-01	1.5408500e-01	2.5686800e-02	
bi210m				
4.0201200e-15	4.3529300e-15	5.0775600e-15	8.3324400e-15	2.5819200e-14
2.6824900e-13	5.3835500e-12	1.9141900e-10	5.0701000e-09	1.0014900e-07
1.0922800e-06	8.8537800e-06	3.9754300e-05	7.0205600e-05	

Table A1. (Continued)

rn222				
4.12426ØØe-Ø7	4.3150400e-Ø7	4.7119200e-Ø7	6.2671700e-Ø7	1.2239300e-Ø6
5.4324700e-Ø5	4.Ø229ØØØe-Ø5	4.4286300e-Ø4	3.2510100e-Ø3	1.8736400e-Ø2
6.Ø3908ØØe-Ø2	1.4455400e-Ø1	1.5569400e-Ø1	2.5954ØØØe-Ø2	
ra224				
4.1Ø541ØØe-Ø3	4.Ø6591ØØe-Ø3	3.9880600e-Ø3	3.7271100e-Ø3	3.Ø7186ØØe-Ø3
1.5613600e-Ø3	2.2583700e-Ø4	2.6160800e-Ø7	1.9423Ø9ØØe-Ø9	2.8359ØØe-Ø9
5.9509400e-Ø9	1.8266700e-Ø8	5.3940200e-Ø8	1.7846600e-Ø7	
th227				
2.8756100e-Ø8	2.9679700e-Ø8	3.1548800e-Ø8	3.8296800e-Ø8	5.8908200e-Ø8
1.3774100e-Ø7	3.7330000e-Ø7	1.2379300e-Ø6	4.Ø258100e-Ø6	1.6860900e-Ø5
6.7820000e-Ø5	2.2266200e-Ø4	3.Ø2ØØ5ØØe-Ø4	3.Ø341300e-Ø4	
th228				
4.1Ø483ØØe-Ø3	4.Ø653400e-Ø3	3.9875ØØØe-Ø3	3.7265900e-Ø3	3.Ø7143ØØe-Ø3
1.5611400e-Ø3	2.2580500e-Ø4	2.6157300e-Ø7	1.9532800e-Ø9	2.9309500e-Ø9
6.2088400e-Ø9	1.8421600e-Ø8	5.3940500e-Ø8	1.7846600e-Ø7	
th231				
5.4997100e-Ø5	5.5ØØ43ØØe-Ø5	5.5Ø187ØØe-Ø5	5.5Ø691ØØe-Ø5	5.5212900e-Ø5
5.5715700e-Ø5	5.7145800e-Ø5	6.2991ØØØe-Ø5	7.5680200e-Ø5	1.1752500e-Ø4
1.9955ØØØe-Ø4	2.9Ø8Ø5ØØe-Ø4	3.Ø4722ØØe-Ø4	3.Ø4556ØØe-Ø4	
th234				
3.ØØ959ØØe-Ø4	3.ØØ959ØØe-Ø4	3.ØØ959ØØe-Ø4	3.ØØ959ØØe-Ø4	3.ØØ959ØØe-Ø4
3.ØØ959ØØe-Ø4	3.ØØ959ØØe-Ø4	3.ØØ959ØØe-Ø4	3.ØØ961ØØe-Ø4	3.ØØ967ØØe-Ø4
3.ØØ985ØØe-Ø4	3.Ø1Ø41ØØe-Ø4	3.Ø1166ØØe-Ø4	3.Ø1357ØØe-Ø4	
pa233				
9.3872600e-Ø3	9.3998100e-Ø3	9.3979400e-Ø3	9.4231700e-Ø3	9.4963300e-Ø3
9.7432800e-Ø3	1.Ø318ØØØe-Ø2	1.1341900e-Ø2	1.1899200e-Ø2	1.1825ØØe-Ø2
1.1726200e-Ø2	1.1463400e-Ø2	1.Ø7443ØØe-Ø2	8.5646209e-Ø3	
u232				
3.9953100e-Ø3	3.9568800e-Ø3	3.8811100e-Ø3	3.6271500e-Ø3	2.9894700e-Ø3
1.5194900e-Ø3	2.1978ØØØe-Ø4	2.5451400e-Ø7	1.5673400e-Ø9	1.5Ø258ØØe-Ø9
1.3319400e-Ø9	8.7346100e-1Ø	2.6163700e-1Ø	3.8486ØØØe-12	
np236				
1.7920200e-Ø8	1.7920100e-Ø8	1.7919900e-Ø8	1.7919100e-Ø8	1.7917ØØØe-Ø8
1.7909400e-Ø8	1.7887ØØØe-Ø8	1.7812500e-Ø8	1.7599100e-Ø8	1.6872ØØØe-Ø8
1.4955900e-Ø8	9.8078ØØØe-Ø9	2.9378400e-Ø9	4.3214600e-11	
pu236				
4.9966500e-Ø8	3.9526500e-Ø8	2.4919900e-Ø8	5.8478100e-Ø9	1.6275300e-Ø9
1.5939300e-Ø9	1.5920600e-Ø9	1.5853500e-Ø9	1.5663600e-Ø9	1.5Ø164ØØe-Ø9
1.3311100e-Ø9	8.7291600e-1Ø	2.6147400e-1Ø	3.8462ØØØe-12	
am242				
1.Ø6312ØØe-Ø2	1.Ø5829ØØe-Ø2	1.Ø4868ØØe-Ø2	1.Ø1573ØØe-Ø2	9.2718900e-Ø3
6.7380300e-Ø3	2.7Ø665ØØe-Ø3	1.1119400e-Ø4	1.2164ØØØe-Ø8	1.6655100e-22
4.Ø882300e-62	Ø.	Ø.	Ø.	
cm243				
1.Ø461400e-Ø3	1.Ø21Ø100e-Ø3	9.7253ØØØe-Ø4	8.2Ø284ØØe-Ø4	5.Ø4325ØØe-Ø4
9.1901700e-Ø5	7.Ø922900e-Ø7	2.8635500e-14	2.1455900e-35	Ø.
Ø.	Ø.	Ø.	Ø.	
cm245				
6.8313900e-Ø6	6.8308400e-Ø6	6.8297200e-Ø6	6.8258100e-Ø6	6.8146500e-Ø6
6.7757500e-Ø6	6.6658100e-Ø6	6.2949ØØØe-Ø6	5.3450000e-Ø6	3.Ø1512ØØe-Ø6
5.8734800e-Ø7	1.9162800e-Ø9	1.5Ø782ØØe-16	2.Ø6Ø62ØØe-41	
cm246				
5.4274100e-Ø7	5.4266200e-Ø7	5.4250300e-Ø7	5.4194600e-Ø7	5.4Ø36ØØØe-Ø7
5.3484500e-Ø7	5.1939700e-Ø7	4.6875800e-Ø7	3.4967100e-Ø7	1.2535800e-Ø7
6.6875800e-Ø9	2.3451900e-13	4.3785ØØØe-26	1.2314400e-7Ø	
cm247				
6.7431800e-13	6.7431800e-13	6.7431800e-13	6.7431800e-13	6.7431700e-13
6.7431500e-13	6.7431000e-13	6.7428800e-13	6.7422900e-13	6.7401900e-13
6.7342000e-13	6.7132900e-13	6.6538900e-13	6.4501200e-13	
cm248				
7.Ø408500e-13	7.Ø4083ØØe-13	7.Ø4Ø8ØØØe-13	7.Ø4Ø7ØØØe-13	7.Ø4Ø4100e-13
7.Ø394100e-13	7.Ø3654ØØe-13	7.Ø2649ØØe-13	6.9978800e-13	6.8986300e-13
6.6227700e-13	5.7412500e-13	3.8174200e-13	9.1504500e-14	

Appendix B. Results of Analyses.

This appendix consists of a compilation of expanded tabular results of the analyses.

Table B-1. Expanded tabular results for basecase with ALTERNATIVE waste form.

A.		Peak dose rate percentiles				
		25	50	75	90	Max
Limiting individual (above repository)	rem/yr	5.0×10^{-9}	1.0×10^{-4}	7.9×10^{-3}	1.0×10^{-1}	7.9×10^{-1}
	Ci/yr	2.5×10^{-12}	5.0×10^{-9}	2.5×10^{-7}	3.9×10^{-6}	7.9×10^{-4}
Accessible environment individual (1.6 km from repository)	rem/yr	5.0×10^{-8}	1.9×10^{-6}	1.3×10^{-4}	1.0×10^{-3}	6.3×10^{-2}
	Ci/yr	3.9×10^{-11}	2.0×10^{-9}	1.0×10^{-7}	1.0×10^{-6}	1.0×10^{-4}
Columbia River average individual, rem/yr		1.6×10^{-12}	1.3×10^{-10}	3.2×10^{-9}	2.0×10^{-8}	1.3×10^{-6}
Population dose rate, person-rem/yr		3.2×10^{-7}	2.5×10^{-5}	6.3×10^{-4}	5.0×10^{-3}	2.5×10^{-1}

B.	Integrated dose percentiles				
	25	50	75	90	Max
CRP for 10^4 yr, person-rem	$<1 \times 10^{-9}$	$<1 \times 10^{-9}$	4.3×10^{-2}	1.7×10^{-1}	1.1×10^{1}
CRP for 10^5 yr, person-rem	$<2 \times 10^{-7}$	3.6×10^{-1}	1.1×10^{1}	1.8×10^{2}	1.8×10^{3}
CRP for 10^6 yr, person-rem	1.6×10^{-1}	1.3×10^{1}	2.0×10^{2}	8.0×10^{2}	3.2×10^{3}

Table B-2. Expanded tabular results for basalt with REFERENCE waste form.

A.		Peak dose rate percentiles				
		25	50	75	90	Max
Limiting individual (above repository)	rem/yr	$<1 \times 10^{-10}$	$<1 \times 10^{-10}$	$<1 \times 10^{-10}$	4.0×10^{-5}	6.3×10^{-2}
	Ci/yr	$<1 \times 10^{-15}$	$<1 \times 10^{-15}$	$<1 \times 10^{-15}$	5.0×10^{-8}	1.0×10^{-4}
Accessible environment individual (1.6 km from repository)	rem/yr	1.6×10^{-4}	1.0×10^{-3}	6.3×10^{-3}	4.0×10^{-2}	1.3×10^{0}
	Ci/yr	2.5×10^{-7}	1.6×10^{-6}	7.9×10^{-6}	5.0×10^{-5}	1.6×10^{-3}
Columbia River average individual, rem/yr		7.9×10^{-9}	3.2×10^{-8}	7.9×10^{-8}	2.5×10^{-7}	1.0×10^{-6}
Population dose rate, person-rem/yr		1.6×10^{-3}	7.9×10^{-3}	2.0×10^{-2}	6.3×10^{-2}	2.0×10^{-1}

B.	Integrated dose percentiles				
	25	50	75	90	Max
CRP for 10^4 yr, person-rem	$<8 \times 10^{-9}$	$<8 \times 10^{-9}$	$<8 \times 10^{-9}$	$<8 \times 10^{-9}$	7.9×10^{1}
CRP for 10^5 yr, person-rem	$<2.5 \times 10^{-7}$	3.6×10^{1}	5.8×10^{2}	1.8×10^{3}	2.3×10^{3}
CRP for 10^6 yr, person-rem	7.5×10^{-2}	1.2×10^{3}	1.5×10^{3}	1.9×10^{3}	3.0×10^{3}

Table B-3. Expanded tabular results for basalt with ALTERNATIVE waste form.

A.		Peak dose rate percentiles				
		25	50	75	90	Max
Limiting individual (above repository)	rem/yr	$<1 \times 10^{-15}$	$<1 \times 10^{-15}$	$<1 \times 10^{-15}$	5.0×10^{-6}	6.3×10^{-2}
	Ci/yr	$<1 \times 10^{-15}$	$<1 \times 10^{-15}$	$<1 \times 10^{-15}$	7.9×10^{-9}	7.9×10^{-5}
Accessible environment individual (1.6 km from repository)	rem/yr	5.0×10^{-6}	1.3×10^{-4}	2.5×10^{-3}	1.3×10^{-2}	2.0×10^{-1}
	Ci/yr	7.9×10^{-9}	2.0×10^{-7}	3.2×10^{-6}	2.0×10^{-5}	2.5×10^{-4}
Columbia River average individual, rem/yr		2.0×10^{-10}	5.0×10^{-9}	3.2×10^{-8}	1.6×10^{-7}	5.0×10^{-7}
Population dose rate, person-rem/yr		5.0×10^{-5}	1.0×10^{-3}	6.3×10^{-3}	3.2×10^{-2}	1.3×10^{-1}

B.	Integrated dose percentiles				
	25	50	75	90	Max
CRP for 10^4 yr, person-rem	$<3 \times 10^{-10}$	$<3 \times 10^{-10}$	1.9×10^{-2}	1.5×10^{-1}	3.0×10^{0}
CRP for 10^5 yr, person-rem	9.0×10^{-2}	2.3×10^{0}	2.3×10^{1}	1.4×10^{3}	2.3×10^{3}
CRP for 10^6 yr, person-rem	3.0×10^{1}	4.7×10^{2}	1.2×10^{3}	1.9×10^{3}	2.3×10^{3}

Table B-4. Expanded tabular results for basalt with bypass and REFERENCE waste form.

A.		Peak dose rate percentiles 25	50	75	90	Max
Limiting individual (above repository)	rem/yr	0	0	0	0	0
	Ci/yr	0	0	0	0	0
Accessible environment individual (1.6 km from repository)	rem/yr	$<1 \times 10^{-15}$	$<1 \times 10^{-15}$	6.3×10^{-9}	2.5×10^{-5}	5.0×10^{-2}
	Ci/yr	$<1 \times 10^{-15}$	$<1 \times 10^{-15}$	2.5×10^{-12}	3.2×10^{-8}	7.9×10^{-7}
Columbia River average individual, rem/yr		$<1 \times 10^{-15}$	$<1 \times 10^{-15}$	$<1 \times 10^{-15}$	5.0×10^{-11}	1.3×10^{-8}
Population dose rate, person-rem/yr		$<1 \times 10^{-15}$	$<1 \times 10^{-15}$	$<1 \times 10^{-15}$	1.0×10^{-5}	3.2×10^{-3}

B.	Integrated dose percentiles 25	50	75	90	Max
CRP for 10^4 yr, person-rem	0	0	0	0	0
CRP for 10^5 yr, person-rem	$<5 \times 10^{-9}$	$<5 \times 10^{-9}$	$<5 \times 10^{-9}$	$<5 \times 10^{-9}$	5.0×10^{1}
CRP for 10^6 yr, person-rem	$<7 \times 10^{-8}$	$<7 \times 10^{-8}$	$<7 \times 10^{-8}$	2.1×10^{0}	6.8×10^{2}

Table B-5. Expanded tabular results for basalt with bypass and ALTERNATIVE waste form.

A.		Peak dose rate percentiles 25	50	75	90	Max
Limiting individual (above repository)	rem/yr	0	0	0	0	0
	Ci/yr	0	0	0	0	0
Accessible environment individual (1.6 km from repository)	rem/yr	$<1 \times 10^{-15}$	$<1 \times 10^{-15}$	6.3×10^{-6}	2.0×10^{-4}	5.0×10^{-2}
	Ci/yr	$<1 \times 10^{-15}$	$<1 \times 10^{-15}$	2.0×10^{-9}	1.6×10^{-7}	2.5×10^{-6}
Columbia River average individual, rem/yr		$<1 \times 10^{-15}$	$<1 \times 10^{-15}$	7.9×10^{-14}	4.0×10^{-10}	2.0×10^{-8}
Population dose rate, person-rem/yr		$<1 \times 10^{-15}$	$<1 \times 10^{-15}$	1.6×10^{-8}	7.9×10^{-5}	4.0×10^{-3}

B.	Integrated dose percentiles 25	50	75	90	Max
CRP for 10^4 yr, person-rem	0	0	0	0	0
CRP for 10^5 yr, person-rem	$<1.7 \times 10^{-8}$	$<1.7 \times 10^{-8}$	$<1.7 \times 10^{-8}$	$<1.7 \times 10^{-8}$	1.7×10^{2}
CRP for 10^6 yr, person-rem	$<7.4 \times 10^{-8}$	$<7.4 \times 10^{-8}$	2.9×10^{-3}	2.3×10^{1}	7.4×10^{2}

Table B-6. Expanded tabular results for deteriorated backfill with REFERENCE waste form.

A.		Peak dose rate percentiles 25	50	75	90	Max
Limiting individual (above repository)	rem/yr	2.0×10^{-3}	2.0×10^{-2}	1.0×10^{-1}	5.0×10^{-1}	7.9×10^{0}
	Ci/yr	2.0×10^{-7}	3.2×10^{-6}	1.6×10^{-5}	4.0×10^{-5}	2.0×10^{-4}
Accessible environment individual (1.6 km from repository)	rem/yr	5.0×10^{-5}	6.3×10^{-4}	3.2×10^{-3}	1.0×10^{-2}	2.0×10^{0}
	Ci/yr	5.0×10^{-8}	7.9×10^{-7}	3.2×10^{-6}	1.0×10^{-5}	6.3×10^{-5}
Columbia River average individual, rem/yr		3.2×10^{-9}	2.5×10^{-8}	1.6×10^{-7}	3.2×10^{-7}	1.9×10^{-6}
Population dose rate, person-rem/yr		5.0×10^{-4}	5.0×10^{-3}	3.2×10^{-2}	6.3×10^{-2}	2.0×10^{-1}

B.	Integrated dose percentiles 25	50	75	90	Max
CRP for 10^4 yr, person-rem	$<1 \times 10^{-8}$	$<1 \times 10^{-8}$	$<1 \times 10^{-8}$	5.2×10^{-1}	1.0×10^{2}
CRP for 10^5 yr, person-rem	7.1×10^{0}	1.1×10^{2}	1.1×10^{3}	1.8×10^{3}	3.5×10^{3}
CRP for 10^6 yr, person-rem	3.1×10^{2}	9.7×10^{2}	1.9×10^{3}	2.4×10^{3}	3.9×10^{3}

Table B-7. Expanded tabular results for deteriorated backfill ALTERNATIVE waste form.

A.		Peak dose rate percentiles 25	50	75	90	Max
Limiting individual (above repository)	rem/yr	1.6×10^{-4}	3.2×10^{-3}	2.0×10^{-2}	2.0×10^{-1}	1.0×10^{0}
	Ci/yr	6.3×10^{-9}	1.6×10^{-7}	2.0×10^{-6}	6.3×10^{-6}	1.6×10^{-4}
Accessible environment individual (1.6 km from repository)	rem/yr	1.3×10^{-6}	3.2×10^{-5}	5.0×10^{-4}	1.6×10^{-3}	6.3×10^{-2}
	Ci/yr	1.3×10^{-9}	4.0×10^{-8}	5.0×10^{-7}	2.0×10^{-6}	5.0×10^{-5}
Columbia River average individual, rem/yr		1.0×10^{-10}	6.3×10^{-10}	2.0×10^{-8}	7.9×10^{-8}	6.3×10^{-7}
Population dose rate, person-rem/yr		1.3×10^{-5}	1.3×10^{-4}	3.2×10^{-3}	1.6×10^{-2}	1.6×10^{-1}

B.	Integrated dose percentiles 25	50	75	90	Max
CRP for 10^4 yr, person-rem	$<7 \times 10^{-10}$	$<7 \times 10^{-10}$	9.8×10^{-2}	3.1×10^{-1}	7.8×10^{0}
CRP for 10^5 yr, person-rem	3.0×10^{-1}	4.8×10^{0}	7.6×10^{1}	6.0×10^{2}	1.9×10^{3}
CRP for 10^6 yr, person-rem	9.5×10^{0}	9.5×10^{1}	7.5×10^{2}	1.5×10^{3}	3.0×10^{3}

Table B-8. Expanded tabular results for failed borehole with REFERENCE waste form.

A.		Peak dose rate percentiles 25	50	75	90	Max
Limiting individual (above repository)	rem/yr	$<1 \times 10^{-15}$	$<1 \times 10^{-15}$	1×10^{-15}	1.0×10^{-2}	5.0×10^{-1}
	Ci/yr	$<1 \times 10^{-15}$	$<1 \times 10^{-15}$	$<1 \times 10^{-15}$	6.3×10^{-7}	4.0×10^{-5}
Accessible environment individual (1.6 km from repository)	rem/yr	3.2×10^{-4}	5.0×10^{-3}	4×10^{-2}	8×10^{-2}	3.2×10^{0}
	Ci/yr	2.0×10^{-7}	3.2×10^{-6}	2.5×10^{-5}	6.3×10^{-5}	7.9×10^{-4}
Columbia River average individual, rem/yr		1.6×10^{-9}	4.0×10^{-8}	2.0×10^{-7}	5.0×10^{-7}	1.6×10^{-6}
Population dose rate, person-rem/yr		2.5×10^{-4}	7.9×10^{-3}	5.0×10^{-2}	1.3×10^{-1}	3.2×10^{-1}

B.	Integrated dose percentiles 25	50	75	90	Max
CRP for 10^4 yr, person-rem	$<1 \times 10^{-7}$	4.2×10^{-2}	4.2×10^{-1}	5.3×10^{0}	1.1×10^{3}
CRP for 10^5 yr, person-rem	8.0×10^{0}	2.0×10^{2}	1.3×10^{3}	1.6×10^{3}	4.0×10^{3}
CRP for 10^6 yr, person-rem	1.8×10^{2}	1.1×10^{3}	2.2×10^{3}	2.8×10^{3}	1.1×10^{4}

Table B-9. Expanded tabular results for failed borehole with ALTERNATIVE waste form.

A.		Peak dose rate percentiles 25	50	75	90	Max
Limiting individual (above repository)	rem/yr	$<1 \times 10^{-15}$	$<1 \times 10^{-15}$	$<1 \times 10^{-15}$	7.9×10^{-4}	3.2×10^{-2}
	Ci/yr	$<1 \times 10^{-15}$	$<1 \times 10^{-15}$	$<1 \times 10^{-15}$	5.0×10^{-8}	1.0×10^{-5}
Accessible environment individual (1.6 km from repository)	rem/yr	7.9×10^{-6}	6.3×10^{-4}	7.9×10^{-3}	4.0×10^{-2}	2.5×10^{0}
	Ci/yr	6.3×10^{-9}	2.5×10^{-7}	5.0×10^{-6}	2.5×10^{-5}	4.0×10^{-4}
Columbia River average individual, rem/yr		3.2×10^{-11}	4.0×10^{-9}	4.0×10^{-8}	2.0×10^{-7}	1.0×10^{-6}
Population dose rate, person-rem/yr		6.3×10^{-6}	5.0×10^{-4}	7.9×10^{-3}	4.0×10^{-2}	2.0×10^{-1}

B.	Integrated dose percentiles 25	50	75	90	Max
CRP for 10^4 yr, person-rem	$<1 \times 10^{-8}$	4.0×10^{-2}	2.5×10^{-1}	1.6×10^{0}	1.0×10^{2}
CRP for 10^5 yr, person-rem	5.2×10^{-1}	1.6×10^{1}	2.1×10^{2}	1.3×10^{3}	4.2×10^{3}
CRP for 10^6 yr, person-rem	3.5×10^{0}	3.5×10^{2}	1.4×10^{3}	2.8×10^{3}	1.1×10^{4}

Table B-10. Expanded tabular results for faulting with REFERENCE waste form.

A.		Peak dose rate percentiles 25	50	75	90	Max
Limiting individual (above repository)	rem/yr	4.0×10^{-5}	2.5×10^{-3}	1.6×10^{-2}	2.0×10^{-1}	2.5×10^{0}
	Ci/yr	5.0×10^{-9}	4.0×10^{-7}	4.0×10^{-6}	1.6×10^{-5}	2.5×10^{-4}
Accessible environment individual (1.6 km from repository)	rem/yr	1.0×10^{-3}	6.3×10^{-3}	3.2×10^{-2}	1.3×10^{-1}	1.0×10^{0}
	Ci/yr	7.9×10^{-7}	4.0×10^{-6}	1.6×10^{-5}	6.3×10^{-5}	1.0×10^{-3}
Columbia River average individual, rem/yr		1.0×10^{-8}	7.9×10^{-8}	3.2×10^{-7}	6.3×10^{-7}	3.2×10^{-6}
Population dose rate, person-rem/yr		1.3×10^{-3}	1.3×10^{-2}	6.3×10^{-2}	1.6×10^{-1}	7.9×10^{-1}

B.	Integrated dose percentiles 25	50	75	90	Max
CRP for 10^4 yr, person-rem	$<2 \times 10^{-7}$	5.3×10^{-1}	4.2×10^{0}	2.1×10^{2}	2.1×10^{3}
CRP for 10^5 yr, person-rem	4.2×10^{1}	6.7×10^{2}	1.3×10^{3}	1.7×10^{3}	4.2×10^{3}
CRP for 10^6 yr, person-rem	6.1×10^{2}	1.5×10^{3}	2.4×10^{3}	3.0×10^{3}	4.8×10^{3}

Table B-11. Expanded tabular results for faulting with ALTERNATE waste form.

A.		Peak dose rate percentiles 25	50	75	90	Max
Limiting individual (above repository)	rem/yr	1.0×10^{-6}	1.6×10^{-4}	4.0×10^{-3}	6.3×10^{-2}	2.5×10^{0}
	Ci/yr	7.9×10^{-11}	1.0×10^{-8}	4.0×10^{-7}	3.2×10^{-6}	6.3×10^{-5}
Accessible environment individual (1.6 km from repository)	rem/yr	2.0×10^{-5}	4.0×10^{-4}	5.0×10^{-3}	6.3×10^{-2}	7.9×10^{-1}
	Ci/yr	1.6×10^{-8}	4.0×10^{-7}	2.0×10^{-6}	1.0×10^{-5}	1.6×10^{-4}
Columbia River average individual, rem/yr		1.6×10^{-10}	3.2×10^{-9}	4.0×10^{-8}	1.6×10^{-7}	1.6×10^{-6}
Population dose rate, person-rem/yr		2.5×10^{-5}	6.3×10^{-4}	6.3×10^{-3}	3.2×10^{-2}	2.0×10^{-1}

B.	Integrated dose percentiles 25	50	75	90	Max
CRP for 10^4 yr, person-rem	4.6×10^{-3}	1.5×10^{-1}	1.2×10^{0}	1.5×10^{1}	4.5×10^{2}
CRP for 10^5 yr, person-rem	1.4×10^{0}	2.2×10^{1}	3.4×10^{2}	1.1×10^{3}	4.3×10^{3}
CRP for 10^6 yr, person-rem	1.8×10^{1}	3.6×10^{2}	1.1×10^{3}	2.3×10^{3}	4.5×10^{3}

Table B-12. Expanded tabular results for breccia pipe formation with REFERENCE waste form.

A.		Peak dose rate percentiles 25	50	75	90	Max
Limiting individual (above repository)	rem/yr	7.9×10^{-5}	4.0×10^{-3}	3.2×10^{-2}	2.5×10^{-1}	1.3×10^{1}
	Ci/yr	2.5×10^{-8}	6.3×10^{-7}	5.0×10^{-6}	3.2×10^{-5}	5.0×10^{-4}
Accessible environment individual (1.6 km from repository)	rem/yr	$<1 \times 10^{-15}$	2.5×10^{-4}	1.6×10^{-3}	1.0×10^{-2}	7.9×10^{-1}
	Ci/yr	4.0×10^{-9}	3.2×10^{-7}	1.6×10^{-6}	1.0×10^{-5}	1.3×10^{-4}
Columbia River average individual, rem/yr		$<1 \times 10^{-15}$	1.0×10^{-8}	5.0×10^{-8}	1.6×10^{-7}	7.9×10^{-7}
Population dose rate, person-rem/yr		7.9×10^{-7}	2.0×10^{-3}	1.0×10^{-2}	3.2×10^{-2}	2.0×10^{-1}

B.	Integrated dose percentiles 25	50	75	90	Max
CRP for 10^4 yr, person-rem	$<1 \times 10^{-7}$	$<1 \times 10^{-7}$	3.0×10^{-1}	2.4×10^{0}	9.5×10^{2}
CRP for 10^5 yr, person-rem	3.5×10^{0}	5.5×10^{1}	3.5×10^{2}	1.1×10^{3}	1.7×10^{3}
CRP for 10^6 yr, person-rem	8.5×10^{1}	3.4×10^{2}	1.1×10^{3}	2.1×10^{3}	3.4×10^{3}

Table B-13. Expanded tabular results for breccia pipe formation with ALTERNATIVE waste form.

A.		Peak dose rate percentiles 25	50	75	90	Max
Limiting individual (above repository)	rem/yr	1.6×10^{-5}	5.0×10^{-6}	6.3×10^{-3}	4.0×10^{-2}	7.9×10^{0}
	Ci/yr	1.6×10^{-9}	4.0×10^{-8}	5.0×10^{-7}	4.0×10^{-6}	1.3×10^{-4}
Accessible environment individual (1.6 km from repository)	rem/yr	2.5×10^{-6}	4.0×10^{-5}	5.0×10^{-4}	5.0×10^{-3}	6.3×10^{-1}
	Ci/yr	1.6×10^{-9}	1.6×10^{-8}	2.5×10^{-7}	1.6×10^{-6}	3.2×10^{-5}
Columbia River average individual, rem/yr		2.5×10^{-11}	6.3×10^{-10}	7.9×10^{-9}	4.0×10^{-8}	7.9×10^{-7}
Population dose rate, person-rem/yr		5.0×10^{-6}	1.0×10^{-4}	1.6×10^{-3}	5.0×10^{-3}	1.6×10^{-1}

B.	Integrated dose percentiles 25	50	75	90	Max
CRP for 10^4 yr, person-rem	$<6 \times 10^{-8}$	4.9×10^{-3}	9.8×10^{-2}	9.8×10^{-1}	6.2×10^{2}
CRP for 10^5 yr, person-rem	1.0×10^{-1}	2.1×10^{0}	2.6×10^{1}	1.7×10^{2}	1.7×10^{3}
CRP for 10^6 yr, person-rem	2.9×10^{0}	4.6×10^{1}	3.6×10^{2}	9.3×10^{2}	2.9×10^{3}

Table B-14. Expanded tabular results for S = 100 and median is 10^{-8}/yr.

A.		Peak dose rate percentiles 25	50	75	90	Max
Limiting individual (above repository)	rem/yr	5.0×10^{-12}	4.0×10^{-6}	4.0×10^{-4}	1.3×10^{-2}	7.9×10^{-1}
	Ci/yr	2.5×10^{-15}	5.0×10^{-11}	3.2×10^{-9}	5.0×10^{-7}	1.0×10^{-3}
Accessible environment individual (1.6 km from repository)	rem/yr	2.0×10^{-9}	7.9×10^{-7}	6.3×10^{-5}	1.0×10^{-3}	7.9×10^{-2}
	Ci/yr	1.6×10^{-12}	1.0×10^{-10}	1.6×10^{-9}	2.0×10^{-7}	1.0×10^{-4}
Columbia River average individual, rem/yr		2.5×10^{-14}	2.0×10^{-12}	2.5×10^{-10}	4.0×10^{-9}	1.3×10^{-6}
Population dose rate, person-rem/yr		6.3×10^{-9}	4.0×10^{-7}	6.3×10^{-5}	7.9×10^{-4}	2.5×10^{-1}

B.	Integrated dose percentiles 25	50	75	90	Max
CRP for 10^4 yr, person-rem	$<1 \times 10^{-10}$	4.1×10^{-4}	1.0×10^{-2}	6.5×10^{-2}	1.3×10^{0}
CRP for 10^5 yr, person-rem	9.1×10^{-5}	2.3×10^{-2}	7.2×10^{-1}	2.9×10^{1}	1.8×10^{3}
CRP for 10^6 yr, person-rem	1.4×10^{-3}	1.8×10^{-1}	1.8×10^{1}	3.5×10^{2}	2.8×10^{3}

Table B15. Expanded tabular results for S = 100 and median is 5×10^{-7}/yr.

A.		Peak dose rate percentiles 25	50	75	90	Max
Limiting individual (above repository)	rem/yr	1.0×10^{-10}	1.0×10^{-4}	1.0×10^{-2}	1.6×10^{-1}	1.3×10^{0}
	Ci/yr	1.3×10^{-13}	2.5×10^{-9}	3.2×10^{-7}	1.6×10^{-5}	1.0×10^{-3}
Accessible environment individual (1.6 km from repository)	rem/yr	3.2×10^{-8}	2.5×10^{-6}	1.6×10^{-4}	3.2×10^{-3}	7.9×10^{-2}
	Ci/yr	3.2×10^{-11}	1.6×10^{-9}	1.0×10^{-7}	5.0×10^{-6}	1.0×10^{-4}
Columbia River average individual, rem/yr		1.3×10^{-12}	5.0×10^{-11}	5.0×10^{-9}	1.0×10^{-7}	1.3×10^{-6}
Population dose rate, person-rem/yr		2.0×10^{-7}	7.9×10^{-6}	1.0×10^{-3}	2.0×10^{-2}	2.5×10^{-1}

B.	Integrated dose percentiles 25	50	75	90	Max
CRP for 10^4 yr, person-rem	$<1 \times 10^{-7}$	$<1 \times 10^{-7}$	2.3×10^{-2}	1.2×10^{-1}	4.6×10^{2}
CRP for 10^5 yr, person-rem	3.0×10^{-6}	2.4×10^{-1}	1.5×10^{1}	7.5×10^{2}	1.9×10^{3}
CRP for 10^6 yr, person-rem	9.7×10^{-2}	4.9×10^{0}	2.4×10^{2}	1.2×10^{3}	3.9×10^{3}

Table B16. Expanded tabular results for S = 100 and median is 5×10^{-6}/yr.

A.		Peak dose rate percentiles 25	50	75	90	Max
Limiting individual (above repository)	rem/yr	3.2×10^{-9}	2.0×10^{-4}	3.2×10^{-2}	2.0×10^{-1}	1.3×10^{0}
	Ci/yr	4.0×10^{-12}	4.0×10^{-8}	3.2×10^{-6}	6.3×10^{-5}	1.0×10^{-3}
Accessible environment individual (1.6 km from repository)	rem/yr	1.3×10^{-7}	2.5×10^{-5}	1.3×10^{-3}	1.0×10^{-2}	7.9×10^{-2}
	Ci/yr	6.3×10^{-11}	2.5×10^{-8}	7.9×10^{-7}	1.3×10^{-5}	1.0×10^{-4}
Columbia River average individual, rem/yr		1.6×10^{-12}	1.0×10^{-9}	4.0×10^{-8}	3.2×10^{-7}	2.0×10^{-6}
Population dose rate, person-rem/yr		2.0×10^{-7}	2.0×10^{-4}	7.9×10^{-3}	7.9×10^{-2}	4.0×10^{-1}

B.	Integrated dose percentiles 25	50	75	90	Max
CRP for 10^4 yr, person-rem	$<1 \times 10^{-7}$	$<1 \times 10^{-7}$	2.3×10^{-2}	4.7×10^{-1}	5.9×10^{2}
CRP for 10^5 yr, person-rem	3.1×10^{-5}	3.1×10^{0}	9.8×10^{1}	9.8×10^{2}	3.1×10^{3}
CRP for 10^6 yr, person-rem	1.6×10^{-1}	5.2×10^{1}	8.2×10^{2}	1.6×10^{3}	4.1×10^{3}

Table B-17. Expanded tabular results for S = 100 and median is 10^{-4}/yr.

A.		Peak dose rate percentiles 25	50	75	90	Max
Limiting individual (above repository)	rem/yr	4.0×10^{-7}	4.0×10^{-3}	1.0×10^{-1}	2.5×10^{-1}	1.0×10^{1}
	Ci/yr	4.0×10^{-11}	7.9×10^{-7}	2.0×10^{-5}	1.3×10^{-4}	1.0×10^{-3}
Accessible environment individual (1.6 km from repository)	rem/yr	7.9×10^{-6}	3.2×10^{-4}	5.0×10^{-3}	3.2×10^{-2}	1.6×10^{-1}
	Ci/yr	4.0×10^{-9}	3.2×10^{-7}	5.0×10^{-6}	3.2×10^{-5}	1.0×10^{-4}
Columbia River average individual, rem/yr		7.9×10^{-11}	1.6×10^{-8}	1.6×10^{-7}	6.3×10^{-7}	2.0×10^{-6}
Population dose rate, person-rem/yr		1.3×10^{-5}	2.5×10^{-3}	4.0×10^{-2}	1.3×10^{-1}	4.0×10^{-1}

B.	Integrated dose percentiles 25	50	75	90	Max
CRP for 10^4 yr, person-rem	$<7 \times 10^{-8}$	$<7 \times 10^{-8}$	2.3×10^{-4}	1.4×10^{0}	7.3×10^{2}
CRP for 10^5 yr, person-rem	5.4×10^{-3}	5.1×10^{1}	8.2×10^{2}	1.6×10^{3}	3.2×10^{3}
CRP for 10^6 yr, person-rem	4.2×10^{0}	2.6×10^{2}	1.3×10^{3}	2.1×10^{3}	4.2×10^{3}

Table B-18. Expanded tabular results for S = 100 and median is 10^{-3}/yr.

A.		Peak dose rate percentiles 25	50	75	90	Max
Limiting individual (above repository)	rem/yr	1.0×10^{-5}	1.3×10^{-2}	1.3×10^{-1}	2.5×10^{-1}	1.3×10^{1}
	Ci/yr	1.3×10^{-9}	3.5×10^{-6}	4.0×10^{-5}	2.0×10^{-4}	1.0×10^{-3}
Accessible environment individual (1.6 km from repository)	rem/yr	3.2×10^{-5}	6.3×10^{-4}	1.3×10^{-2}	4.0×10^{-2}	2.0×10^{1}
	Ci/yr	3.2×10^{-8}	7.9×10^{-7}	1.0×10^{-5}	5.0×10^{-5}	1.3×10^{-4}
Columbia River average individual, rem/yr		5.0×10^{-10}	3.2×10^{-8}	4.0×10^{-7}	7.9×10^{-7}	2.0×10^{-6}
Population dose rate, person-rem/yr		7.9×10^{-5}	7.9×10^{-3}	7.9×10^{-2}	2.0×10^{-1}	4.0×10^{0}

B.	Integrated dose percentiles 25	50	75	90	Max
CRP for 10^4 yr, person-rem	$<1 \times 10^{-7}$	$<1 \times 10^{-7}$	$<1 \times 10^{-7}$	6.3×10^{0}	8.0×10^{2}
CRP for 10^5 yr, person-rem	6.5×10^{-2}	8.1×10^{1}	1.0×10^{3}	1.6×10^{3}	3.2×10^{3}
CRP for 10^6 yr, person-rem	1.3×10^{1}	3.3×10^{2}	1.3×10^{3}	2.1×10^{3}	4.2×10^{3}

Table B-19. Expanded tabular results for S = 10 and median is 10^{-8}/yr.

A.		Peak dose rate percentiles 25	50	75	90	Max
Limiting individual (above repository)	rem/yr	1.3×10^{-10}	3.2×10^{-6}	2.0×10^{-4}	2.0×10^{-3}	1.6×10^{-1}
	Ci/yr	1.0×10^{-13}	3.2×10^{-11}	2.5×10^{-9}	1.3×10^{-8}	5.0×10^{-5}
Accessible environment individual (1.6 km from repository)	rem/yr	3.2×10^{-9}	1.6×10^{-7}	4.0×10^{-6}	1.0×10^{-4}	6.3×10^{-3}
	Ci/yr	4.0×10^{-12}	1.0×10^{-10}	1.0×10^{-9}	4.0×10^{-9}	7.9×10^{-6}
Columbia River average individual, rem/yr		1.3×10^{-13}	3.2×10^{-12}	3.2×10^{-11}	1.3×10^{-10}	2.5×10^{-7}
Population dose rate, person-rem/yr		2.5×10^{-8}	6.3×10^{-7}	5.0×10^{-6}	3.2×10^{-5}	6.3×10^{-2}

B.	Integrated dose percentiles 25	50	75	90	Max
CRP for 10^4 yr, person-rem	$<2 \times 10^{-11}$	1.2×10^{-3}	1.2×10^{-2}	4.9×10^{-2}	1.6×10^{-1}
CRP for 10^5 yr, person-rem	2.9×10^{-4}	2.3×10^{-2}	2.9×10^{-1}	1.4×10^{0}	1.4×10^{3}
CRP for 10^6 yr, person-rem	8.3×10^{-3}	2.6×10^{-1}	2.6×10^{0}	2.1×10^{1}	2.6×10^{3}

Table B-20. Expanded tabular results for S = 10 and median is 5×10^{-7}/yr.

A.		Peak dose rate percentiles 25	50	75	90	Max
Limiting individual (above repository)	rem/yr	3.2×10^{-8}	1.0×10^{-4}	7.9×10^{-3}	1.0×10^{-1}	6.3×10^{-1}
	Ci/yr	1.3×10^{-11}	6.3×10^{-9}	2.5×10^{-7}	2.5×10^{-6}	3.2×10^{-4}
Accessible environment individual (1.6 km from repository)	rem/yr	5.0×10^{-8}	2.5×10^{-6}	1.0×10^{-4}	7.9×10^{-4}	6.3×10^{-2}
	Ci/yr	6.3×10^{-11}	2.5×10^{-9}	1.0×10^{-7}	7.9×10^{-7}	7.9×10^{-5}
Columbia River average individual, rem/yr		4.0×10^{-12}	1.6×10^{-10}	3.2×10^{-9}	1.6×10^{-8}	1.3×10^{-6}
Population dose rate, person-rem/yr		6.3×10^{-7}	2.5×10^{-5}	5.0×10^{-4}	3.2×10^{-3}	2.5×10^{-1}

B.	Integrated dose percentiles 25	50	75	90	Max
CRP for 10^4 yr, person-rem	$<6 \times 10^{-10}$	1.4×10^{-4}	5.5×10^{-2}	2.2×10^{-1}	5.5×10^{0}
CRP for 10^5 yr, person-rem	2.8×10^{-5}	5.7×10^{-1}	1.1×10^{1}	1.1×10^{2}	1.8×10^{3}
CRP for 10^6 yr, person-rem	2.9×10^{-1}	1.5×10^{1}	2.3×10^{2}	7.3×10^{2}	2.9×10^{3}

Table B-21. Expanded tabular results for S = 100 and median is 5×10^{-6}/yr.

A.		Peak dose rate percentiles 25	50	75	90	Max
Limiting individual (above repository)	rem/yr	3.2×10^{-7}	1.6×10^{-3}	5.0×10^{-2}	2.0×10^{-1}	3.2×10^{0}
	Ci/yr	1.6×10^{-10}	1.6×10^{-7}	3.2×10^{-6}	2.5×10^{-5}	1.0×10^{-3}
Accessible environment individual (1.6 km from repository)	rem/yr	1.3×10^{-6}	6.3×10^{-5}	1.3×10^{-3}	1.0×10^{-2}	7.9×10^{-2}
	Ci/yr	1.0×10^{-9}	7.9×10^{-8}	1.0×10^{-6}	7.9×10^{-6}	1.0×10^{-4}
Columbia River average individual, rem/yr		5.0×10^{-11}	3.2×10^{-9}	3.2×10^{-8}	2.0×10^{-7}	1.3×10^{-6}
Population dose rate, person-rem/yr		7.9×10^{-6}	6.3×10^{-4}	6.3×10^{-3}	5.0×10^{-2}	2.5×10^{-1}

B.	Integrated dose percentiles 25	50	75	90	Max
CRP for 10^4 yr, person-rem	$<2 \times 10^{-8}$	$<2 \times 10^{-8}$	1.4×10^{-3}	2.2×10^{-1}	1.7×10^{2}
CRP for 10^5 yr, person-rem	3.7×10^{-3}	9.3×10^{0}	1.2×10^{2}	9.3×10^{2}	3.0×10^{3}
CRP for 10^6 yr, person-rem	3.2×10^{0}	1.6×10^{2}	1.0×10^{3}	1.6×10^{3}	4.0×10^{3}

Table B-22. Expanded tabular results for S = 100 and median is 10^{-4}/yr.

A.		Peak dose rate percentiles 25	50	75	90	Max
Limiting individual (above repository)	rem/yr	$<1 \times 10^{-15}$	1.0×10^{-2}	1.0×10^{-1}	2.5×10^{-1}	1.0×10^{-1}
	Ci/yr	4.0×10^{-8}	3.2×10^{-6}	5.0×10^{-5}	2.0×10^{-4}	1.3×10^{-3}
Accessible environment individual (1.6 km from repository)	rem/yr	$<1 \times 10^{-15}$	1.3×10^{-4}	5.0×10^{-3}	3.2×10^{-2}	7.9×10^{-2}
	Ci/yr	3.2×10^{-8}	1.0×10^{-6}	1.6×10^{-5}	5.0×10^{-5}	4.0×10^{-4}
Columbia River average individual, rem/yr		2.0×10^{-10}	4.0×10^{-8}	2.0×10^{-7}	6.3×10^{-7}	2.0×10^{-6}
Population dose rate, person-rem/yr		3.2×10^{-4}	1.3×10^{-2}	1.0×10^{-1}	2.0×10^{-1}	4.0×10^{-1}

B.	Integrated dose percentiles 25	50	75	90	Max
CRP for 10^4 yr, person-rem	$<1 \times 10^{-8}$	$<1 \times 10^{-8}$	$<1 \times 10^{-8}$	1.9×10^{1}	7.7×10^{2}
CRP for 10^5 yr, person-rem	8.4×10^{-1}	1.3×10^{2}	1.1×10^{3}	1.7×10^{3}	4.2×10^{3}
CRP for 10^6 yr, person-rem	2.1×10^{1}	4.3×10^{2}	1.4×10^{3}	2.1×10^{3}	4.3×10^{3}

Table B-23. Expanded tabular results for S = 100 and median is 10^{-3}/yr.

A.		Peak dose rate percentiles 25	50	75	90	Max
Limiting individual (above repository)	rem/yr	1.3×10^{-4}	2.0×10^{-2}	1.6×10^{-1}	2.5×10^{-1}	1.3×10^{1}
	Ci/yr	4.0×10^{-8}	3.2×10^{-6}	5.0×10^{-5}	2.0×10^{-4}	1.3×10^{-3}
Accessible environment individual (1.6 km from repository)	rem/yr	$<1 \times 10^{-15}$	5.0×10^{-4}	1.3×10^{-2}	4.0×10^{-2}	2.5×10^{-1}
	Ci/yr	3.2×10^{-8}	1.0×10^{-6}	1.6×10^{-5}	5.0×10^{-5}	4.0×10^{-4}
Columbia River average individual, rem/yr		1.3×10^{-9}	6.3×10^{-8}	5.0×10^{-7}	1.0×10^{-6}	2.0×10^{-6}
Population dose rate, person-rem/yr		3.2×10^{-4}	1.3×10^{-2}	1.0×10^{-1}	2.0×10^{-1}	4.0×10^{-1}

B.	Integrated dose percentiles 25	50	75	90	Max
CRP for 10^4 yr, person-rem	$<8 \times 10^{-8}$	$<8 \times 10^{-8}$	$<8 \times 10^{-8}$	1.9×10^{1}	7.7×10^{2}
CRP for 10^5 yr, person-rem	8.4×10^{-1}	1.3×10^{2}	1.1×10^{3}	1.7×10^{3}	4.2×10^{3}
CRP for 10^6 yr, person-rem	2.1×10^{1}	4.3×10^{2}	1.4×10^{3}	2.1×10^{3}	4.3×10^{3}

U. S. Government Printing Office: 1983/9-687-002/8080